10. SITE 695[1]

Shipboard Scientific Party[2]

HOLE 695A

Date occupied: 20 February 1987, 0930 local time

Date departed: 23 February 1987, 1000 local time

Time on hole: 3 days, 30 min

Position: 62°23.476′S, 43°27.095′W

Bottom felt (m, drill pipe): 1311.1

Distance between rig floor and sea level (m): 11

Water depth (drill-pipe measurement from sea level, m): 1300

Penetration (m): 341.1

Number of cores: 36

Total length of cored section (m): 341.1

Total core recovered (m): 254.4

Core recovery (%): 74.6

Oldest sediment cored:
Depth sub-bottom (m): 338.5
Nature: Silty mud
Age: latest Miocene
Measured velocity (km/s): 1.809

Principal results: Site 695 lies on the southeast margin of the South Orkney microcontinent, in the northern Weddell Sea at 1300 m water depth, and is the intermediate of three sites in a depth transect on the northern margin of the Weddell Gyre, drilled to examine history of Antarctic water masses through the Neogene. In addition, a potential gas hydrate bottom-simulating reflector (BSR) at about 600 mbsf on the site survey multichannel seismic profile was to be investigated.

Hole 695A was continuously cored to 341.1 m in 3 days, from 20 to 23 February 1987, and we recovered 254.4 m (74.6%) in 15 advanced hydraulic piston corer (APC) and 21 extended core barrel (XCB) cores. In addition, we took 5 *in-situ* pore water samples and made 8 downhole temperature measurements. Hole 695A was abandoned when the XCB corer sheared, with part in the hole, part jammed in the bit: Hole 695A could not be logged. Three units drilled were: Unit I, 0–190.0 mbsf, Quaternary to lower Pliocene diatom-rich (as much as 80%) oozes and silty, clayey muds; Unit II, 190.0–306.9 mbsf, lower Pliocene diatom-bearing silty and clayey mud (biosiliceous 10%–25%); Unit III, 306.9–341.1 mbsf, lower Pliocene and likely uppermost Miocene silty mud (0%–10% diatoms).

Ice-rafted detritus occurs throughout, but most commonly above 20 mbsf and in Unit II. Volcanic ash beds and glass also occur throughout, but mostly between 50 and 250 mbsf. Illite and chlorite dominate the clay mineral assemblages. Graded beds are rare and the terrigenous component is largely hemipelagic or ice-rafted.

The biogenic component is mainly siliceous: carbonates (foraminifers) are confined to the uppermost 4 mbsf, the limit of the Quaternary. Diatoms dominate, with minor radiolarians and silicoflagellates, and are common to abundant, moderately to well-preserved between 5 and 293 mbsf, but less so elsewhere. Good recovery and low disturbance promise well for magnetostratigraphy, but low remanent intensities defer conclusive determinations to post-cruise investigations. Sedimentation rates were moderate (<30 m/m.y.) in the latest Miocene and earliest Pliocene (early Gilbert), and very high (about 200 m/m.y.) in the late Gilbert, becoming much lower through the Gauss to low rates (2.5–8 m/m.y.) into the Matuyama and Brunhes.

A high early Pliocene biosiliceous productivity was also seen at other Leg 113 sites, and in the Subantarctic (DSDP Site 514), and a parallel calcareous productivity increase is seen in the subtropical Southwest Pacific (DSDP Sites 586–593). The expanded section promises well for high-resolution magneto- and siliceous biostratigraphic correlation, and for paleoceanographic and evolutionary studies. Volcanic glass has a supporting chronostratigraphic potential and will aid correlation between South Orkney transect sites. The determined heat flow value of 1.5 HFU is too high for the 600-m BSR to be a methane hydrate base. No BSR is visible at the now-predicted 310–360-m hydrate base. A sharp methane increase beginning at 250 m is related to depletion of pore water sulfate and indicates an *in-situ* biogenic origin, presumably related to the high biosiliceous accumulation rates. The origin of the 600-m inverse-polarity BSR remains uncertain.

BACKGROUND AND OBJECTIVES

Site 695 (W7) was intended to lie on the southeast margin of the South Orkney microcontinent (SOM), in 1300 m of water near 62°23.5′S, 43°27.1′W (Fig. 1). It is the intermediate site of three (696, 695, and 697) which make up a vertical transect intended to examine the sedimentary record of late Paleogene and Neogene variations in the nature and vertical distribution of the water masses on the northern margin of the Weddell Gyre. The value of this local depth transect will be enhanced by combination and comparison with the results of drilling at other Leg 113 sites (Sites 689–694). Together they provide a transect over a considerable depth range within the circum-Antarctic water-mass structure. The site was of interest also in possessing a potential gas hydrate BSR.

Site 695 was located on multichannel seismic reflection profile AMG845-18 (Fig. 2), which runs north-south across the eastern margin of the SOM (Fig. 3). The SOM underwent pervasive extensional tectonic disruption in the early to middle Oligocene (King and Barker, 1988). In the west, it separated from the northern Antarctic Peninsula with the formation of Powell Basin, and in the east the Jane Arc and trench, which was subducting South American oceanic lithosphere (Barker et al., 1984), separated from the SOM, creating the narrow Jane Basin. These extensional episodes are dated only approximately and indirectly, but apparently occurred between about 35 and 20 Ma ago (King and Barker, 1988; Lawver et al., 1986). They place limits on the time for which the southeastern margin may be used as a paleoceanographic indicator with a largely pelagic sedimentary sequence and fairly predictable paleodepths. At Site 695 the middle Oligocene extension did not lift the site to sea level, so the classic breakup unconformity is not displayed in the reflection profile. Nevertheless, a distinct lithologic change of that age is expected, as the opening of Jane Basin would have cut off the SOM from the direct supply of volcaniclastic turbidites from Jane Arc. Subduction and hence volcanic activity contin-

[1] Barker, P. F., Kennett, J. P., et al., 1988. *Proc. ODP, Init. Repts.*, 113: College Station, TX (Ocean Drilling Program).

[2] Shipboard Scientific Party is as given in the list of Participants preceding the contents.

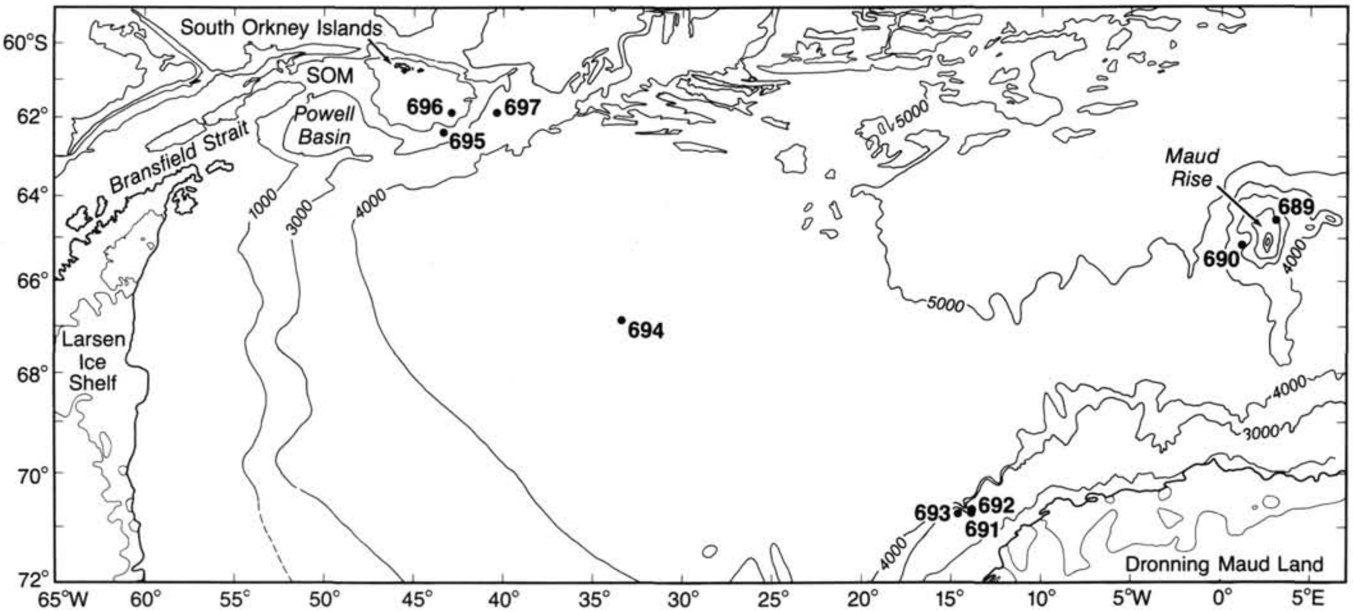

Figure 1. Regional setting of Site 695 (W7) on the southeastern margin of the South Orkney microcontinent (SOM).

ued at Jane Arc until a ridge-crest/trench collision at about 21 Ma (Barker et al., 1984), so airfall ash could provide an additional means of stratigraphic correlation between sites, in the lower part of the sedimentary section.

The site was selected using a more extensive grid of older single-channel seismic data (King and Barker, 1988), to avoid a large component of terrigenous sediment from the landmass of the SOM, which covered a wider area in the past than today. Some terrigenous sediment (other than glacial dropstones) may occur, but the sequence drilled should be largely pelagic. The record of deposition within the shallow to intermediate Antarctic water masses should reflect many of the events proposed on the basis of Subantarctic and more northerly observations, or seen at other sites of Leg 113. Among these events are:

1. A middle Oligocene shallowing of sediment facies related to a proposed global regression (Vail and Hardenbol, 1979), suggested to result from a short-lived glaciation of the Antarctic continent (Miller and Fairbanks, 1985; Murphy and Kennett, 1986).
2. Minor glacial dropstones derived from East Antarctica during the late Oligocene and early Miocene (Site 693), and an indication of glacial or pre-glacial conditions on West Antarctica and the SOM over the same time interval. Given the relative warmth of the early Miocene, the possibility of finding land plants on the SOM cannot be ruled out.
3. A sharp cooling through the middle Miocene, generally supposed (e.g., Shackleton and Kennett, 1975) to involve the growth of the East Antarctic ice-sheet and a distinct cooling of circum-Antarctic deep and intermediate water masses. This is marked by a 6-Ma hiatus at Site 693 on the eastern margin of the Weddell Sea.
4. The suggested (e.g., Ciesielski et al., 1982) late Miocene onset of a West Antarctic ice-sheet and thus, possibly, the glaciation of the SOM. It should be possible to distinguish lithologically the ice-rafted debris derived locally.
5. The shallower equivalent of the thick, coarse sand turbidite sequence (Unit II) of the early Gilbert (C3R4) at Site 694, considered here to result from pronounced growth and instability of a West Antarctic ice-sheet.
6. Evidence for the early Pliocene climatic amelioration (as seen at Subantarctic and more northerly locations) and the possibly related high rate of both siliceous and terrigenous sedimentation seen at Site 693 on the eastern Weddell Sea margin.
7. Renewed climatic deterioration in the late Pliocene and Quaternary, with reductions in siliceous productivity and preservation, and in the supply of ice-rafted detritus (as at all sites previously drilled on Leg 113).

At about 600 mbsf (700 ms) on the reflection profile of Figure 2, a prominent BSR cut the primary sedimentary reflectors. It appeared to have a negative polarity and had been tentatively identified as a gas hydrate BSR. The value of geothermal heat flow that has been calculated under the assumption that this hydrate had a simple methane plus water composition is 35 mW/m^2, a value which is low but not unreasonably so for this tectonic environment. No direct measurements of heat flow had been made to test this interpretation. We were permitted to drill within 50 m of the BSR, following the precautions described in the ODP Safety Manual, and it was intended to make a full suite of measurements of hydrocarbon content, pore water composition (using the *in-situ* sampler), thermal conductivity, and formation temperature. The drilling plan was to use the APC and XCB to the full depth of the hole, which was then intended to be logged.

OPERATIONS

Hole 695A

The ship arrived at this site on the morning of 20 February and the beacon was dropped at 0930 hr at 62°23.476′S 43°27.10′W. We used a recallable beacon that had failed on an earlier site, remodeled by the rig electrician. It reached the sea bottom without incident and began broadcasting properly.

The bit chosen was an RBI C4 number 5695. The bottom-hole assembly was the same as used at Hole 694A.

Site 695 was predicted to contain a possible gas hydrate zone. The Pollution Prevention and Safety Panel (PPSP) had restricted the total depth of the hole to 550 mbsf or 50 m above the calculated base of hydrate stability. Prior to spudding, the depth of

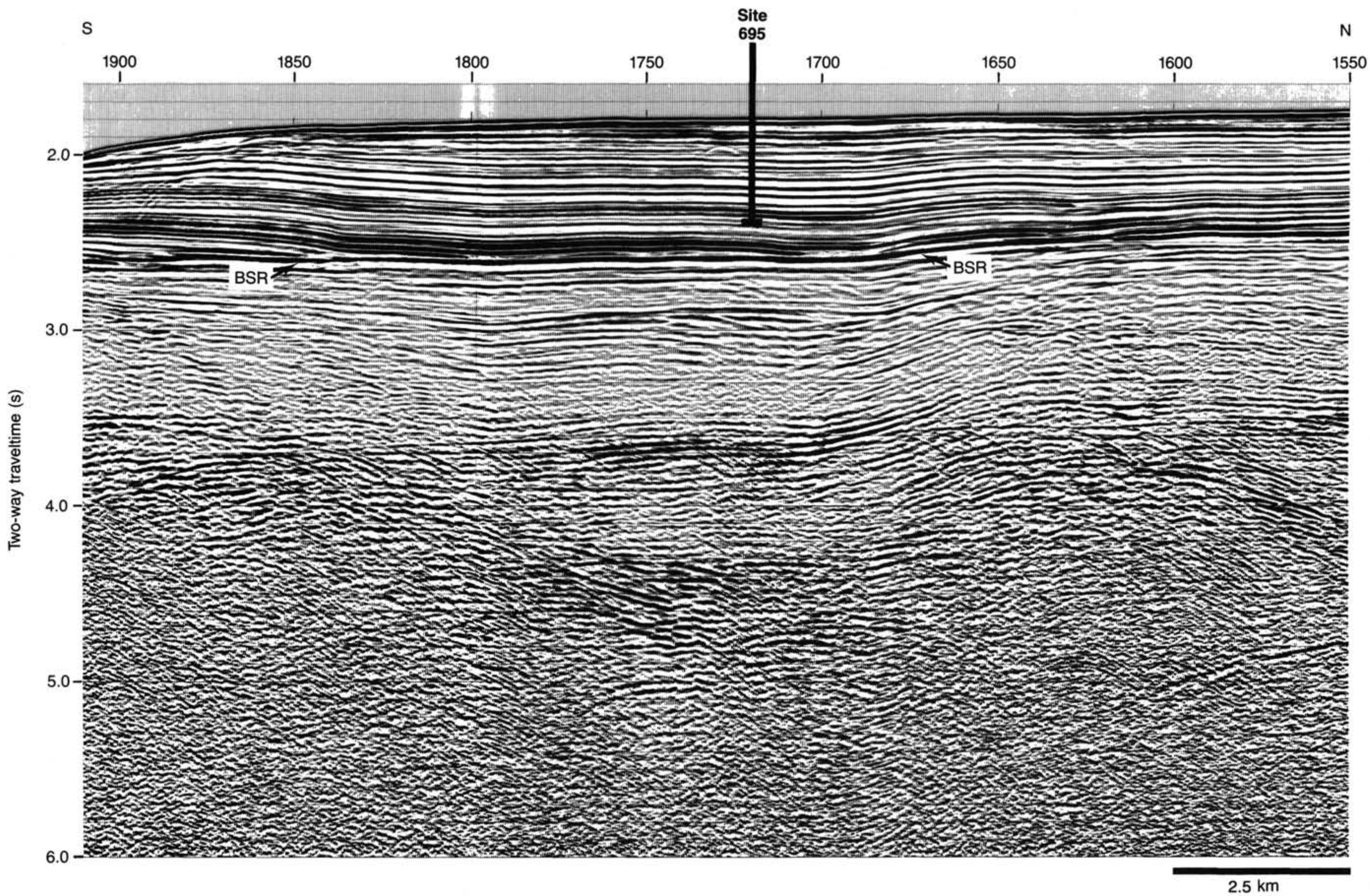

Figure 2. Section of seismic profile AMG845-18, showing location of Site 695 and a prominent bottom-simulating reflector (BSR), considered to be the possible base of a gas hydrate. Location of ship track shown in Figure 3.

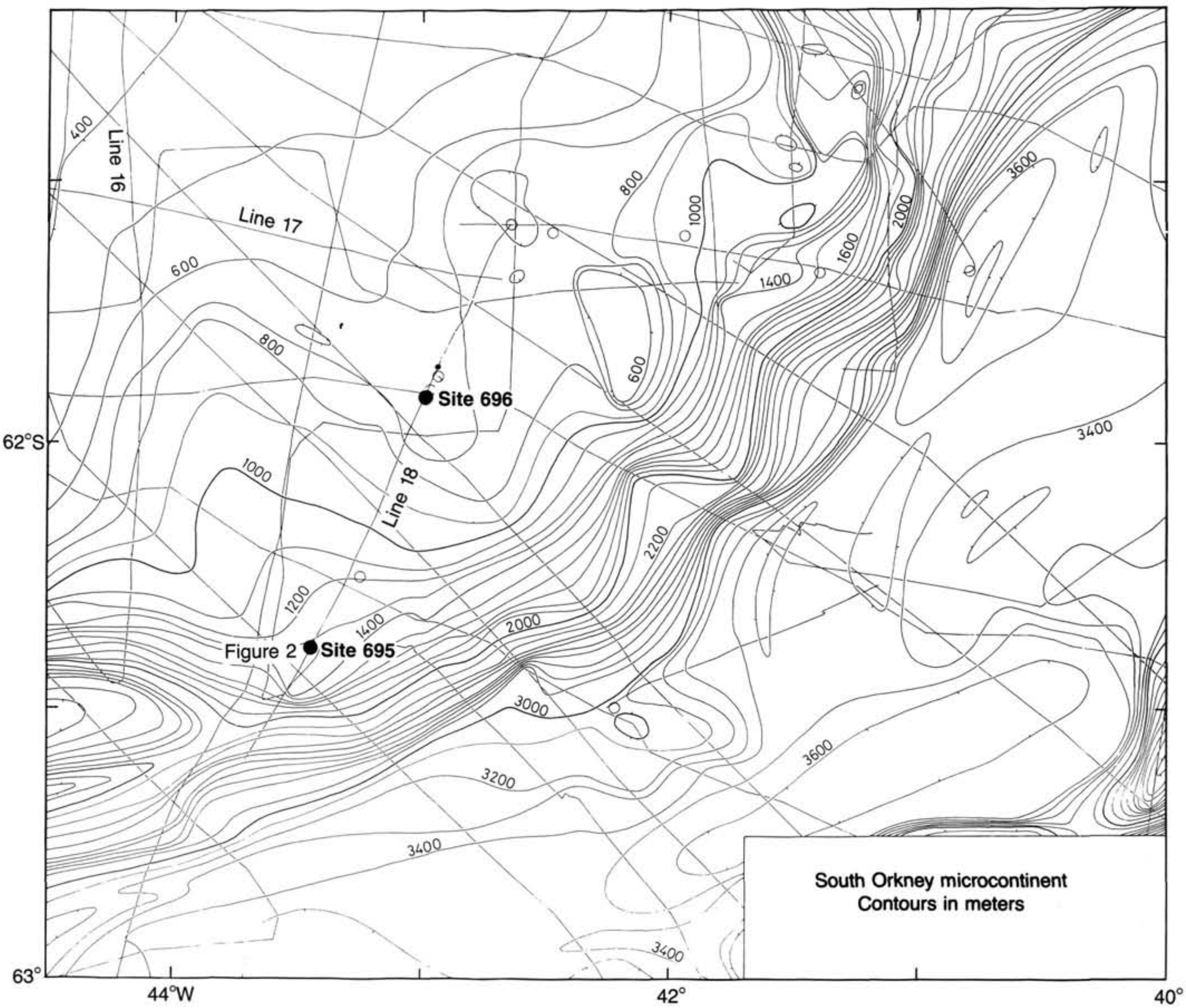

Figure 3. Bathymetry (in meters) of the eastern margin of the South Orkney microcontinent and Jane Basin showing the location of Sites 695 and 696, and of British Antarctic Survey/Birmingham University multichannel seismic line AMG845-16, 17, and 18 and Figure 2.

hydrate stability was calculated (using equation 5, p. 36 of the *JOIDES Journal*, Vol. XII, Special Issue No. 5, March 1986). The depth to the zone of stability was dependent on the thermal gradient. Predictions of thermal gradient ranged from 20° to 100°C/km. The calculations indicated that the depth to the base of hydrate stability would be significantly less than the geophysically derived depth of the BSR unless a gradient near the lowest predicted were used. If a median thermal gradient were used, the calculated depth of hydrate stability would be less than the total depth approved by PPSP.

The precision depth recorder (PDR) corrected water depth was 1316.3 m and the first APC found the seabed at 1311.1 m. Sixteen APC cores were taken to a depth of 137.6 mbsf (Table 1). Cores 113-695A-14H and 113-695A-16H had overpulls of 60,000 and 70,000 lb, which was sufficient reason to convert to the XCB system. Recovery with the APC was 80%.

Four temperature measurements were taken during the APC interval and they produced a thermal gradient of 57°C/km, which yields a calculated base of hydrate stability of 319 mbsf. Geophysical interpretation did not support a hydrate zone at such shallow depths.

A second factor to be considered was the amount of methane in the cores. Methane was in the range of 5–8 ppm which is very small. Because of the high thermal gradient and lack of gas it was considered unlikely that a gas hydrate zone existed. Permission was requested and obtained to continue coring. Coring continued with the XCB system. The only change in the normal drilling parameters was that at 331 mbsf the methane increased by a few parts per million. The percentage change was large but the actual amount of gas present was very small.

At a depth of 341.1 mbsf there was a dramatic decrease in the pump pressure. The core barrel was pulled with the wireline and it was found that the spring stop in the XCB had parted leaving the lower portion of the barrel inside the outer core barrel. This position presented a fishing opportunity. A spear made from a pipe tap welded on to the end of a sinker bar was dropped down the drill pipe. The fish was latched but a pull as high as 10,000 lb was not sufficient to free the barrel. The spear

Table 1. Coring summary, Site 695.

Core no.	Date (Feb. 1988)	Time	Depth (mbsf)	Cored (m)	Recovered (m)	Recovery (%)
113-695A-						
1H	20	1700	0.0-6.4	6.4	6.33	98.9
2H	20	1800	2.9-12.4	9.5	9.81	103.0
3H	20	1900	12.4-22.0	9.6	9.52	99.1
4H	20	1945	22.0-31.6	9.6	9.30	96.9
5H	20	2045	31.6-41.2	9.6	9.03	94.0
6H	20	2130	41.2-50.8	9.6	8.31	86.5
7H	20	2215	50.8-60.4	9.6	3.97	41.3
8H	20	2330	60.4-70.0	9.6	7.56	78.7
9H	21	0015	70.0-79.6	9.6	5.58	58.1
10H	21	0145	79.6-89.2	9.6	7.78	81.0
11I	21	0330	89.2-89.9	0.7	0.00	0.0
12H	21	0430	89.2-98.8	9.6	8.24	85.8
13H	21	0515	98.8-108.5	9.7	5.36	55.2
14H	21	0715	108.5-118.2	9.7	4.52	46.6
15H	21	0815	118.2-127.9	9.7	7.46	76.9
16H	21	0900	127.9-137.6	9.7	7.02	72.4
17I	21	1030	137.6-138.3	0.7	0.00	0.0
18X	21	1230	137.6-147.3	9.7	6.14	63.3
19X	21	1345	147.3-157.0	9.7	9.72	100.0
20X	21	1500	157.0-166.8	9.8	9.32	95.1
21X	21	1600	166.8-176.5	9.7	6.11	63.0
22X	21	1700	176.5-186.2	9.7	7.78	80.2
23X	21	1830	186.2-195.9	9.7	7.78	80.2
24I	21	2015	195.9-196.6	0.7	0.00	0.0
25X	21	2115	195.9-205.6	9.7	9.15	94.3
26X	21	2230	205.6-215.3	9.7	2.74	28.2
27X	21	2315	215.3-225.0	9.7	9.76	100.0
28X	22	0045	225.0-234.7	9.7	3.09	31.8
29X	22	0245	234.7-244.4	9.7	5.37	55.3
30X	22	0430	244.4-254.1	9.7	6.75	69.6
31I	22	0630	254.1-254.8	0.7	0.00	0.0
32X	22	0800	254.1-263.8	9.7	8.63	88.9
33X	22	1000	263.8-273.5	9.7	4.85	50.0
34X	22	1130	273.5-283.1	9.6	8.03	83.6
35X	22	1300	283.1-292.8	9.7	4.90	50.5
36X	22	1415	292.8-302.4	9.6	5.34	55.6
37X	22	1600	302.4-312.0	9.6	9.67	101.0
38I	22	1745	312.0-312.7	0.7	0.00	0.0
39X	22	1915	312.0-321.7	9.7	8.41	86.7
40X	22	2030	321.7-331.4	9.7	3.92	40.4
41X	22	2215	331.4-341.1	9.7	7.14	73.6
42X	22	2330	341.1-345.1	4.0	0.00	0.0
				352.1	254.39	

was jarred free and the wireline pulled from the hole. It was considered risky to place cement in the hole with the inner barrel jammed in the outer barrel; instead 165 barrels of 10 lb/gal mud were pumped into place. The hole was abandoned at 1000 hr 23 February 1987.

LITHOSTRATIGRAPHY

The sediment sequence drilled at Site 695 is of mixed terrigenous, volcanic and pelagic origin. The sediments recovered have been divided into three lithologic units (Fig. 4) mainly based on composition as determined from smear slide analyses (Fig. 5). Abundance of biosiliceous components (mainly diatoms, with silicoflagellates, radiolarians, and sponges) is the most prominent characteristic. Diatom abundance increases with depth from very low percentage at the top of the sediment sequence to a peak of 80% at 45.2 mbsf (113-695A-6H-3, 70 cm) and decreases to 40% at 93.7 mbsf (113-695A-12H-3). It increases again to form a second peak of 70% at 129.9 mbsf (113-695A-16H-2, 50 cm) and drops to less than 30% below 191.2 mbsf (113-695A-23X-4). Below 306.9 mbsf (113-695A-3H) diatoms constitute less than 10% of the sediment or are absent. Silicoflagellates and radiolarians are present only in minor amounts. The calcareous component, exclusively foraminifers, occurs in

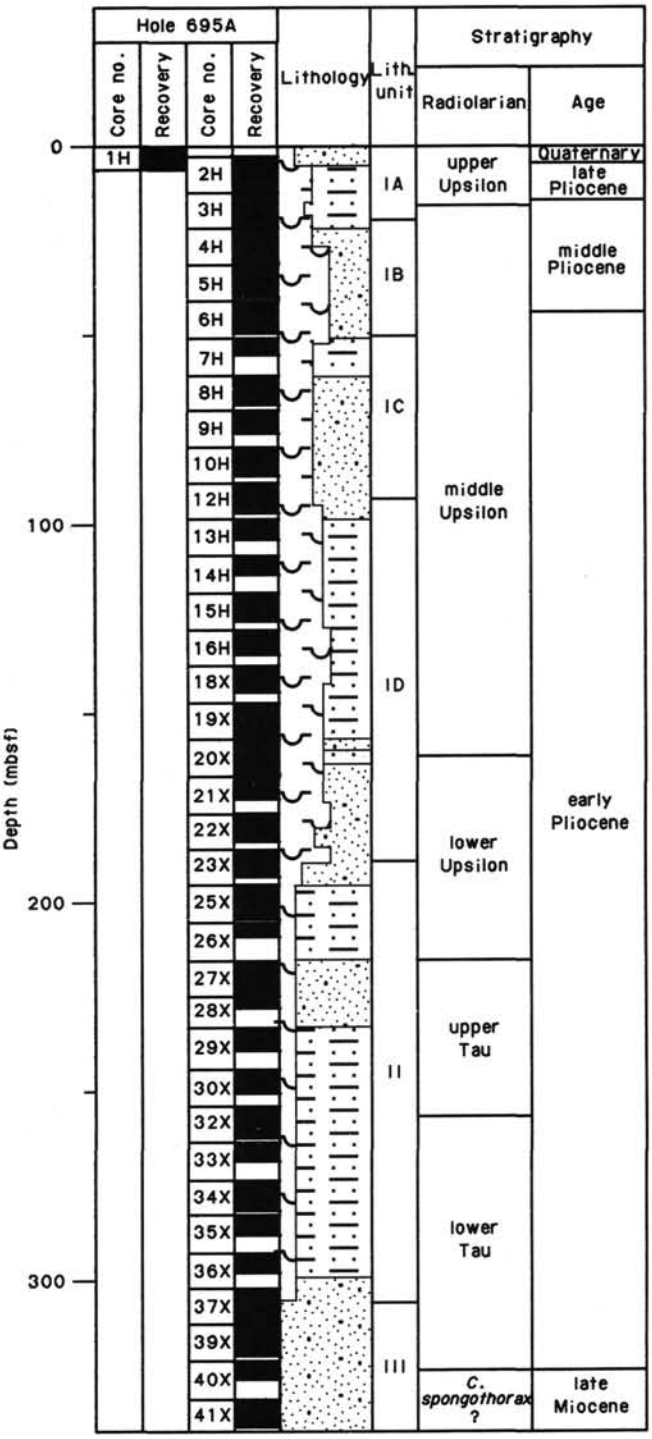

Figure 4. Lithostratigraphic summary, Site 695, South Orkney microcontinent. Included are core type, number, and recovery, lithologic units, and ages.

minor amounts in only the uppermost sections (113-695A-1H-1 to -3).

Lithologic Unit I is composed of diatom-rich sediments. It extends from the mud line to 190.0 mbsf and can be divided into four subunits. Subunit IA, 19.9 m thick and of Quaternary to middle Pliocene age, consists mainly of diatom-bearing silty and clayey muds. Subunit IB, 32.4 m thick, of middle to early

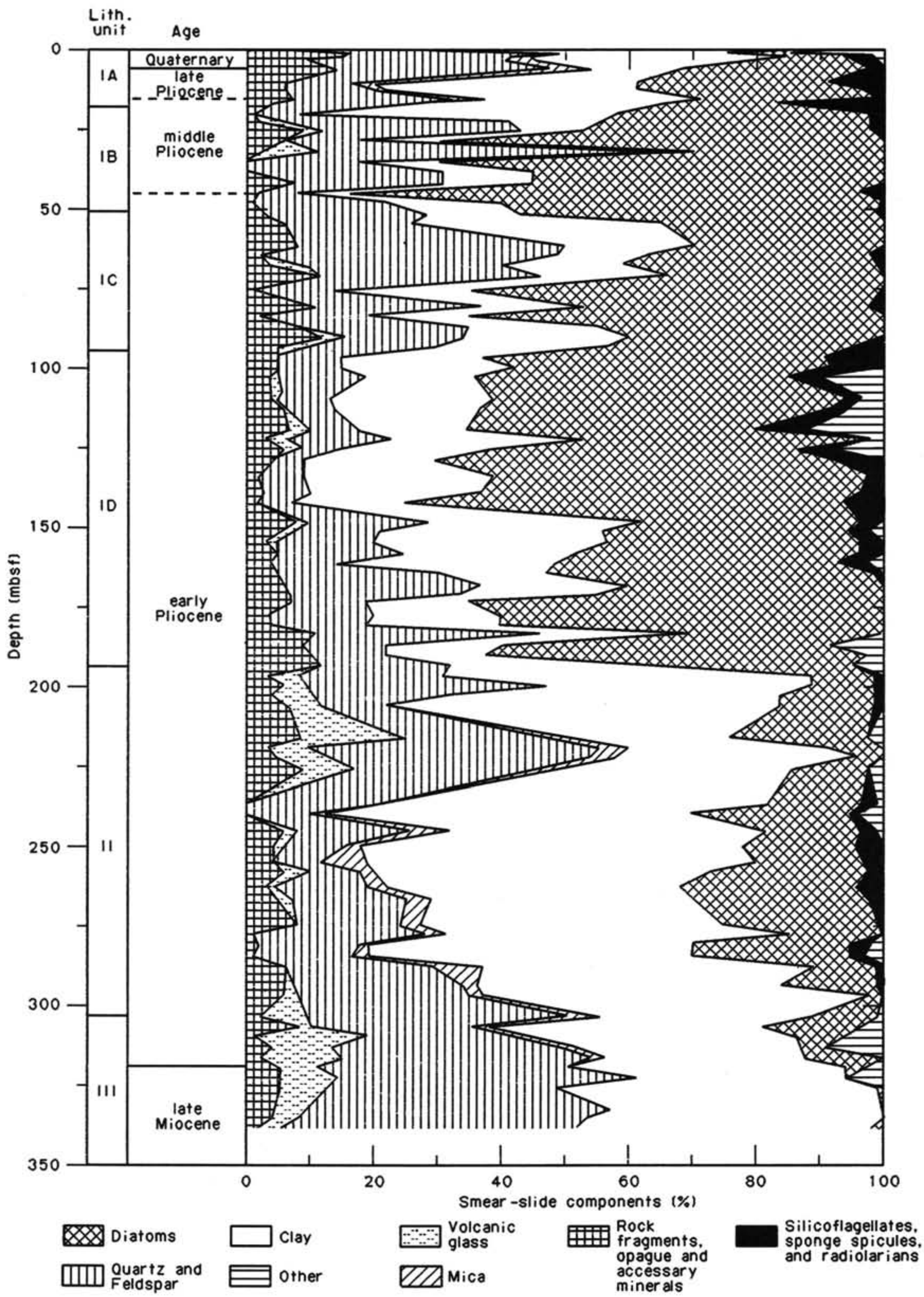

Figure 5. Sediment composition from shipboard smear slide data, Hole 695A, South Orkney microcontinent.

Pliocene age, consists of muddy diatom oozes and diatom-bearing silty muds. Subunit IC, 41.4 m thick, of early Pliocene age, consists predominantly of silty and muddy diatom oozes. Subunit ID, 96.3 m thick, of early Pliocene age, consists of muddy diatom oozes, diatom silty muds and diatom ooze. Lithologic Unit II is characterized by a significant decrease of the biosiliceous component. The unit is 116.9 m thick and of early Pliocene age and consists mainly of diatom-bearing silty and clayey muds. Lithologic Unit III is 34.2 m thick, early Pliocene to late Miocene in age, and consists exclusively of silty mud.

Additionally, the sediment sequence at Site 695 contains variable amounts of volcanic material throughout. Common in all lithologic units are grayish green (5G 5/2) to greenish gray (5G 5/1) beds, 1–5 cm in thickness, which show gradational color contacts at their base and top. These beds are interpreted to represent devitrified volcanic ash layers altered into clay minerals. They are most abundant in lithologic Subunit IC and Unit II and less abundant in Unit III (Fig. 6). Black (5Y 2.5/1) to dark grayish brown (2.5Y 4/2) volcanic-glass-rich beds, 5–10 cm in thickness, occur in Subunits IC and ID as well as in Unit II. The latter unit also contains high amounts of volcanic glass finely dispersed throughout the sediment especially in Cores 113-695A-27X, 113-695A-28X and 113-695A-37X. Fresh pumice pebbles each about 2 cm in diameter were found in Samples 113-695A-1H-1, 50 cm, and 113-695A-8H-1, 50 cm (Fig. 7).

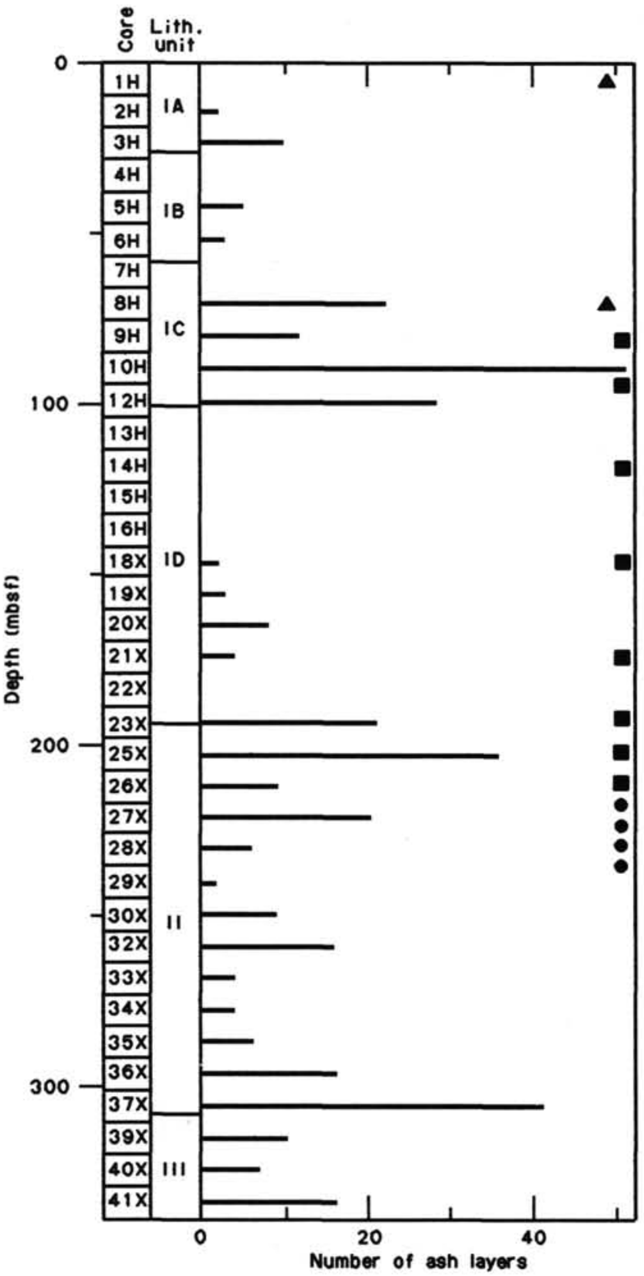

Figure 6. Abundance of grayish green (5G 5/2) devitrified volcanic ash layers in Hole 695A, South Orkney microcontinent. Numbers of layers are not normalized for recovery. Triangles = occurrence of pumice pebbles, squares = thin beds of volcanic glass, dots = high abundance of finely dispersed volcanic glass).

Figure 7. Fresh pumice pebble from lower Pliocene diatom silty mud (2 cm in diameter; lithostratigraphic Subunit IC, Sample 113-695A-8H-1, 50–52 cm).

Ice-rafted detritus (IRD) is common throughout all units and seems to show no significant large scale variations. However, the distribution of dropstones (IRD coarser than about 3 mm) shows remarkable maxima in Cores 113-695A-1H to 113-695A-3H, in Cores 113-695A-19X to 113-695A-20X, and in Cores 113-695A-36X to 113-695A-37X.

Drilling disturbance throughout the recovered sequence, is generally only slight to moderate. Soupy structures are restricted to the mud-line core and to the top of each APC core. Additional disturbance occurs further downhole as drilling biscuits, separated by soft layers, recovered in XCB cores from the more indurated intervals.

Unit I (Depth 0–190.0 mbsf; Age early Pliocene to Quaternary)

Core 113-695A-1H through Sample 113-695A-23X-3, 80 cm; thickness 190.0 m; Quaternary to early Pliocene.

Lithologic Unit I is divided into four subunits mainly on the basis of diatom abundance.

Subunit IA (Depth 0–19.9 mbsf)

Core 113-695A-1H through Section 113-695A-3H-5; thickness 19.9 mbsf; Quaternary to middle Pliocene in age.

The sediments of Subunit IA consist of olive (5Y 5/3) to olive gray (5Y 5/2) diatom-bearing clayey mud, olive gray (5Y 5/2) to gray (5Y 5/1) diatom-bearing silty mud, pale olive (5Y 6/3) to dark greenish gray (5GY 4/1) diatom clayey mud, and greenish gray (5G 5/1) diatom silty mud. A minor lithology, gray (5Y 5/1) foraminifer-bearing clayey mud, is present as a thin veneer in Section 113-695A-1H. Dark greenish gray (5GY 4/1) diatom-bearing clayey mud, silicoflagellate-bearing clayey mud, and clayey diatom ooze occur in Core 113-695A-3H.

A color cyclicity of alternating olive gray (5Y 5/2) and olive (5Y 5/3) beds, each approximately 50–100 cm thick, in Cores 113-695A-1H and 113-695A-2H, is not accompanied by a distinct change in sediment composition. Variable abundance of the biosiliceous components (e.g., diatoms) as well as textural variations in silt and clay content may be responsible for these color changes. The color changes are generally gradational, although sharp color contacts are also observed (Fig. 8).

Numerous greenish gray (5G 5/1) to grayish green (5G 5/2) thin beds (less than 1 cm thick) of altered volcanic ash occur from Section 113-695A-2H-5 through 113-695A-3H-5 (the bottom of this subunit). At the same level, the lithology changes from olive colored silty muds into dark greenish gray (5GY 4/1) diatom-bearing clayey mud and clayey diatom ooze.

An angular, fresh piece of pumice (2 cm in size) occurs in Sample 113-695A-1H-1, 38–40 cm.

Ice-rafted detritus is very common in this subunit. Dropstones are rounded to subangular and show a predominance of sedimentary rocks (sandstones, shales, quartzites) over igneous rocks.

Bioturbation in the sediments of Subunit IA is minor to moderate showing only small vertical structures as a distinct burrow type (Fig. 8).

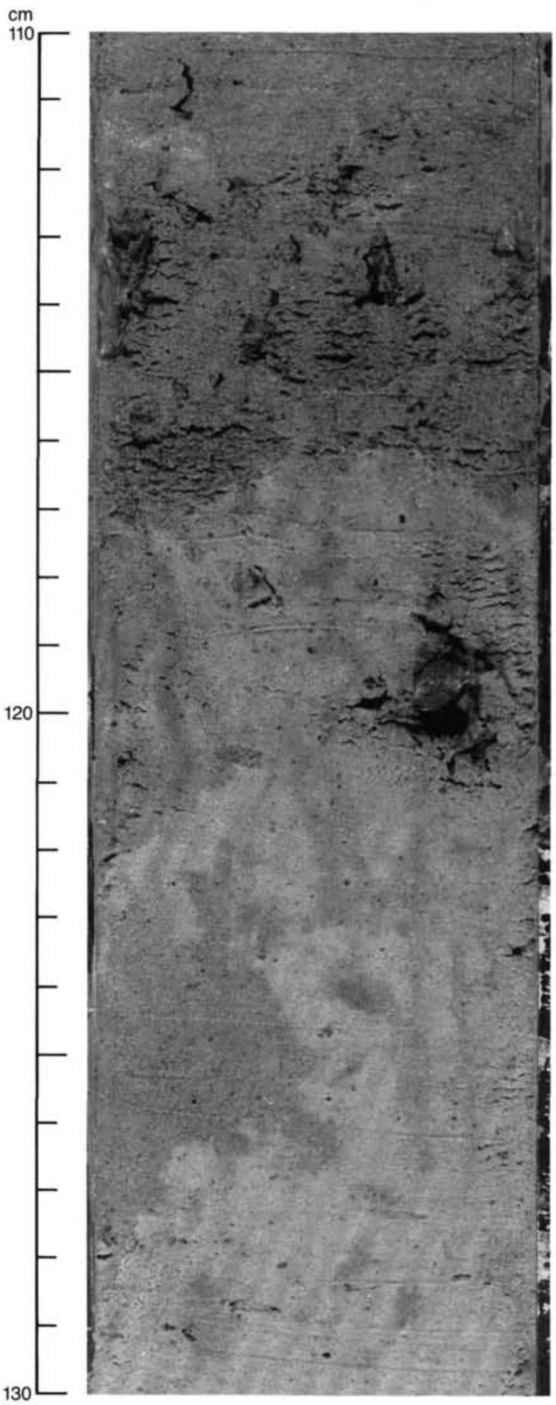

Figure 8. Sharp color contact between pale olive (5Y 6/3) diatom clayey mud (bottom) and olive gray (5Y 5/2) diatom-bearing silty mud (top). The vertical structures below the color contact represent the only burrow type discernible in this sediment. Rounded dropstone is present at 119.3 cm, and smaller fragments of ice-rafted detritus can be observed throughout the photograph. Sample 113-695A-2H-2, 110–130 cm.

Subunit IB (Depth 19.9–52.3 mbsf)

Sections 113-695A-3H-6 through 113-695A-7H-1; thickness 32.4 m; middle Pliocene to early Pliocene in age.

The dominant lithology of Subunit IB is an olive gray (5Y 5/2) to gray (5Y 5/1), muddy diatom ooze. In some intervals it is also greenish gray (5GY 5/1, 5BG 5/1). Greenish gray (5GY 5/1) to dark gray (5Y 4/1) diatom silty muds occur predominantly at the top of this subunit in Cores 113-695A-3H and 113-695A-4H.

The greenish gray (5GY 5/1) muddy diatom ooze occurring in Sections 113-695A-5H-1, 113-695A-6H-1, and 113-695A-6H-2 is associated with the occurrence of grayish green (5G 5/2) beds of altered volcanic ash.

Several thin silty-sandy beds are distributed throughout this subunit and are interpreted to be small turbidites (Fig. 9). Some of the beds contain significant amounts of volcanic glass (e.g., Sample 113-695A-4H-3, 40–43 cm).

Sand-sized IRD is present throughout the sediments of this subunit and seems to be more abundant within the greenish gray (5BG 5/1) than olive gray (5Y 5/2) muddy diatom oozes. Dropstones are significantly less abundant than in Subunit IA; sedimentary, igneous, and metamorphic rocks are present in equal amounts.

Bioturbation in this subunit is minor and no distinct burrow patterns, besides a few faint halo burrows, are recognized.

Subunit IC (52.3–93.7 mbsf)

Sections 113-695A-7H-2 through 113-695A-12H-3; thickness 41.4 m; early Pliocene

Sediments of Subunit IC consist primarily of greenish gray (5GY 5/1, 5G 5/1) to dark greenish gray (5G 4/1, 5GY 4/1) diatom silty mud and gray (5Y 5/1) to olive gray (5Y 5/2) and dark greenish gray (5G 4/1, 5BG 4/1) muddy diatom ooze. A minor lithology, greenish gray (5G 5/1, 5BG 5/1) diatom clayey mud, occurs in Sections 113-695A-7H-2 and 113-695A-7H-3.

Volcanic material is very abundant throughout this subunit (Fig. 6). Numerous grayish green (5G 5/2) beds of volcanic ash altered into clay minerals occur in all cores but show their maximum frequency in Core 113-695A-10H with 51 identifiable beds. Occurrence of these ash beds is always associated with darker colors (dark greenish gray, 5G 4/1, 5GY 4/1) in the surrounding sediment. It is thought that this is an effect of altered volcanic ash material finely dispersed within the darker sediment sequence. It is also possible that the decrease in diatom abundance within Subunit IC is simply an effect of dilution from a high input of volcanogenic detritus.

A striking black (5Y 2.5/1) layer of volcanic glass, 6 cm in thickness, occurs in Sample 113-695A-9H-2, 3–9 cm (Fig. 10). The layer is only slightly blurred by bioturbation. It contains more than 70% sand-sized very fresh and angular glass fragments many of which show fluid inclusion structures and enclosed bubbles.

A fresh pumice pebble, about 2.5 cm in size, was recovered in Sample 113-695A-8H-1, 50 cm (Fig. 7).

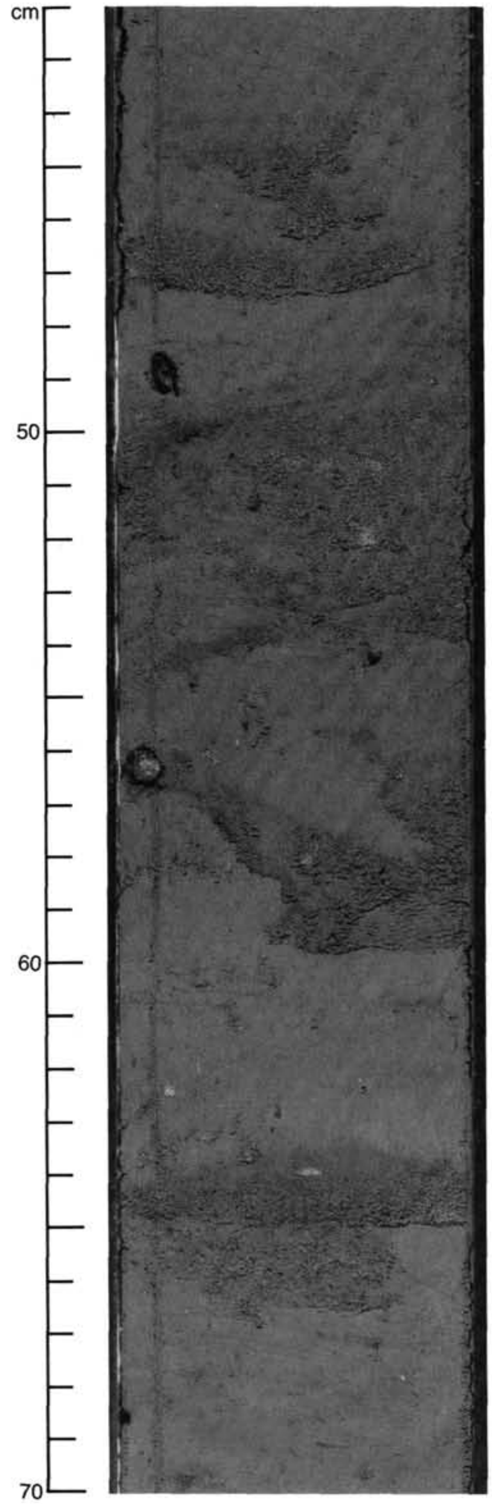

Figure 9. Sequence of silty-sandy turbiditic beds in a muddy diatom ooze partly disturbed by the drilling process. The beds at 47 cm and 65 cm show grading and sharp (erosional?) contacts at the base. Several dropstones are present. Subunit IB; Sample 113-695A-6H-4, 42–70 cm.

Sand-sized IRD occurs in minor amounts throughout this subunit. It is more common at the top of the subunit in Sections 113-695A-7H-2 and 113-695A-7H-3, decreasing in abundance with increasing core depth. Dropstones are present in small numbers and only rarely exceed 1 cm in diameter.

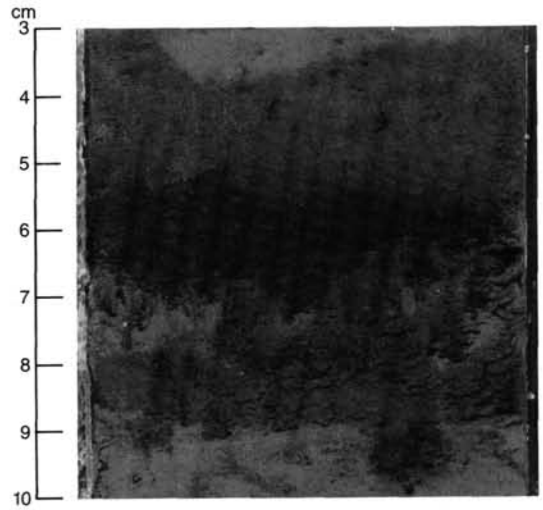

Figure 10. Volcanic ash layer containing a high amount of angular, fresh volcanic glass. The layer is slightly blurred by Planolites-like burrowing. Sample 113-695A-9H-2, 3–10 cm.

Bioturbation in this subunit is minor, and distinct burrows are difficult to recognize.

Subunit ID (Depth 93.7–190.0 mbsf)

Section 113-695A-12H-4 through Sample 113-695A-23X-3, 80 cm; thickness 96.3 m; early Pliocene

Subunit ID consists predominantly of muddy diatom ooze. In the upper part (Cores 113-695A-12H to 113-695A-20X), there is a distinct olive gray (5Y 4/2) and dark gray (5Y 4/1) color cyclicity. Each cycle is 50–100 cm in length. Below Core 113-695A-20X no color cyclicity is recognized, and the color of the muddy diatom ooze changes to greenish gray (5GY 5/1, 5G 5/1).

Other major lithologies present in Subunit ID are dark gray (5Y 4/1), N 4/0), greenish gray (5GY 5/1) to dark greenish gray (5GY 4/1), and grayish green (5G 4/2) diatom silty mud, dark gray (5Y 4/1) to olive gray (5Y 4/2) diatom clayey mud, and olive gray (5Y 4/2) to gray (5Y 5/1) mud-bearing diatom ooze.

As a minor lithology, a very fine silt-sized, light olive gray (5Y 6/2) carbonate ooze occurs in Sample 113-695A-14H-3, 45–60 cm (Fig. 11). Shipboard XRD analysis from this layer shows a mixture of carbonate minerals. Dolomite is the abundant phase, Mg-calcite is common, and siderite is rare.

A light gray (5Y 6/1), 15-cm thick, lithified layer, consisting of dolomite-cemented silty mudstone was recovered in Sample 113-695A-20X, CC, 0–15 cm (Fig. 12). The layer is moderately bioturbated showing some Chondrites type of burrowing.

Several volcanic ash layers are present in Subunit ID. A very dark gray (5Y 3/1), coarse, graded, glass-rich bed occurs in Sample 113-695A-14H, CC, 0–3 cm; a black (5Y 2.5/1) bedded glass-rich layer occurs in Sample 113-695A-18X-4, 120–125 cm; and in Sample 113-695A-21X-2, 68–72 cm, a very dark (5Y 3/1) bed of volcanic glass partly dispersed by bioturbation over an interval of half a meter is present.

IRD is present only in minor amounts and the number of dropstones is low. The latter rarely exceed 1 cm in size.

Bioturbation is minor to moderate throughout Subunit ID showing only a few identifiable burrows of the Planolites and halo burrow type.

Unit II (Depth 190.0–306.9 mbsf; Age early Pliocene)

Sample 113-695A-23X-3, 80 cm, through Section 113-695A-37X-3; thickness 116.9 m; early Pliocene.

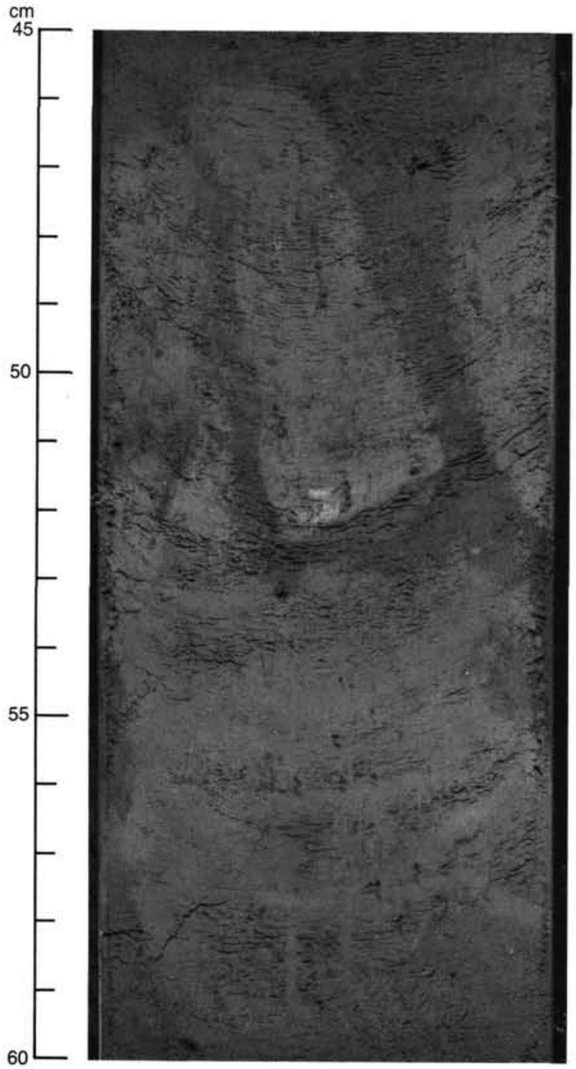

Figure 11. Layer of light olive gray (5Y 6/2) pure carbonate ooze intercalated in a sequence of dark gray (5Y 4/1) muddy diatom ooze. The layer contains abundant dolomite, common Mg-calcite, and rare siderite. Sample 113-695A-14H-3, 45-60 cm.

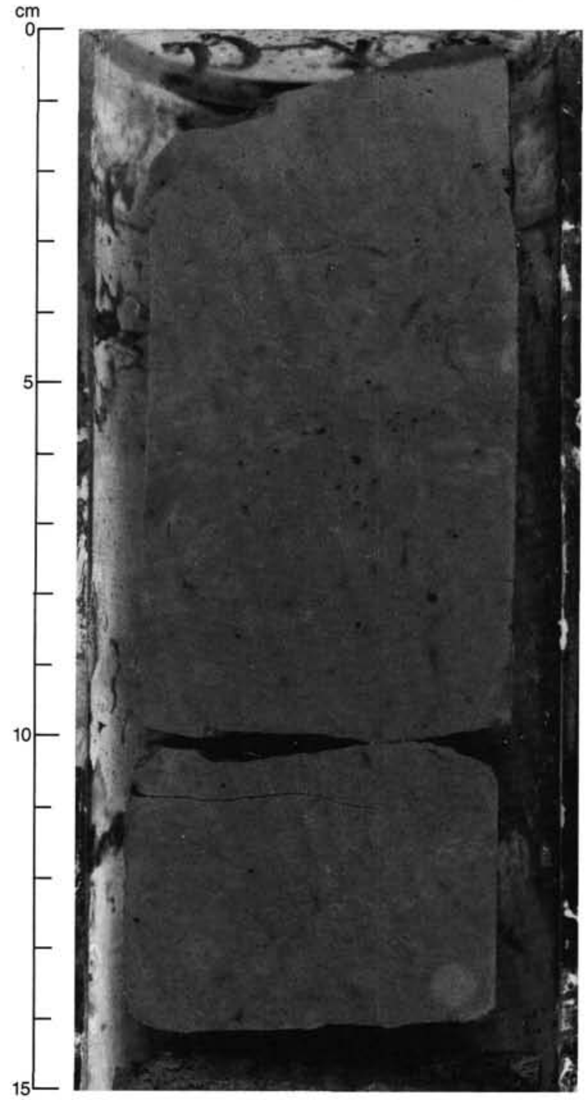

Figure 12. Layer of light gray (5Y 6/1) dolomite-cemented silty mudstone intercalated in olive gray (5Y 4/2) muddy diatom ooze. Sample 113-695A-20X, CC, 0-15 cm.

Sediments of Unit II are characterized by a smaller biosiliceous component than Unit I. The reduction occurs sharply, at the top of the unit.

The predominant lithologies of Unit II are dark greenish gray (5BG 4/1, 5GY 4/1, 5G 4/1) to dark gray (N 4/0) diatom-bearing clayey mud and diatom-bearing silty mud. Both sediment types show the dark gray color in the upper part of Unit II from Cores 113-695A-25X to 113-695A-30X whereas dark gray colors only occur in the lower unit from Core 113-695A-32X to Section 113-695A-37X-3. Other major but less common lithologies in this unit are dark greenish gray (5BG 4/1, 5G 4/1) diatom silty mud (limited to Core 113-695A-23X, at the top of the unit); dark greenish gray (5GY 4/1) diatom clayey mud; dark greenish gray (5BG 4/1) silty mud; and dark gray (N 4/0) clayey mud.

As a minor lithology, a greenish gray (5GY 6/1) carbonate-cemented silty/sandy mudstone occurs in Sample 113-695A-30X-5, 35-50 cm, intercalated with dark greenish gray (5BG 4/1) diatom-bearing clayey mud. The mudstone contains angular detrital grains as large as 2 mm in size. It shows minor bioturbation of Chondrites type, and very closely resembles the mudstone recovered in Core 113-695A-20X in Subunit ID (Fig. 12).

Grayish green (5G 5/2) beds of altered volcanic ash (1-2 cm in thickness) are very common in Unit II (Fig. 13, also see Fig. 6). Several well-defined and coarse-grained volcanic glass layers are also present. In Sample 113-695A-23X-5, 58-68 cm, a dark grayish brown (2.5Y 4/2) volcanic glass layer is present. This layer is slightly dispersed by bioturbation. A similar very dark grayish brown (2.5Y 3/2) layer, strongly bioturbated and dispersed occurs in Sample 113-695A-26X-2, 15-20 cm, whereas laminated or graded layers occur in Samples 113-695A-25X-1, 80-90 cm, and 113-695A-25X-6, 0-10 cm. Moderate amounts (5%-15%) of volcanic glass finely dispersed throughout the sediment occur in Cores 113-695A-27X, 113-695A-28X, and 113-695A-37X.

IRD and dropstones are common throughout the sediments of Unit II but do not show any significant variation in composition and/or distribution.

Discernible bioturbation in Unit II is generally minor or absent. Almost no identifiable burrow patterns are observed. This

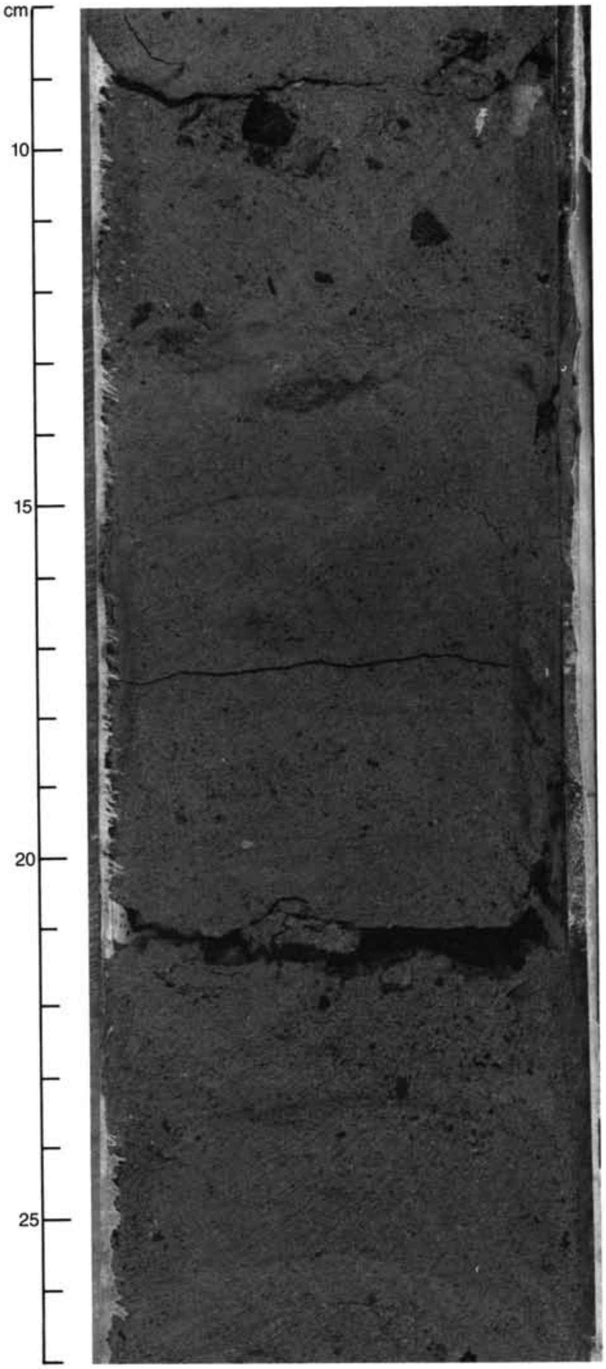

Figure 13. Sequence of grayish green (5G 5/2) beds of altered volcanic ash in a semilithified hemipelagic clayey mudstone. The beds are marked by very faint bands with gradational color contacts at 14–17 cm and 24–26 cm. Sample 113-695A-36X, CC, 8–27 cm.

may be attributed to a lack of color contrast rather than low abundance.

Unit III (Depth 306.9–341.1 mbsf; Age late Miocene to early Pliocene)

Section 113-695A-37X-4 through Core 113-695A-41X; thickness 34.2 m; late Miocene to early Pliocene in age.

Lithostratigraphic Unit III is characterized by a further reduction in and disappearance of biosiliceous components. The boundary with Unit II is defined by a significant drop of sand-sized IRD abundance from Section 113-695A-37X-3 to 113-695A-37X-4.

Sediments of Unit III predominantly consist of dark bluish gray (5B 4/1), dark greenish gray (5BG 4/1, 5G 4/1), and dark gray (N 4/0) silty mud.

A hard, gray (N 5/0) to dark bluish gray (5B 4/1), lithified siltstone occurs in Sample 113-695A-40X, CC (Fig. 14) and near the top of the next core (Sample 113-695A-41X-1, 25–32 cm). It is cemented by dolomite or siderite and intercalated with dark greenish gray (5B 4/1) silty mud. It is likely that one lithified interval has been recovered twice by the drilling process.

The sand-sized IRD content drops remarkably at the top of Unit III to increase again farther downcore but not showing further significant variations. Dropstone content is low throughout the unit. There is no preponderance in the abundance of any rock type or shape (Fig. 15).

Bioturbation is minor to absent in the sediments of Unit III.

Clay Mineralogy

X-ray diffraction analyses were completed on 38 samples from Hole 695A (Fig. 16). The objectives of the clay mineral studies at Site 695 are: (1) to recognize the major paleoenvironmental changes as expressed by the clay associations (using a sampling interval of one per core); (2) to examine cyclical variations of the clay associations, in relation to slight lithological changes expressed by the changing color of the sediment (using a sampling interval of one per color change); (3) to compare the clay associations with those observed at other sites in the Weddell Sea and in the adjacent Falkland Plateau area.

Results

The clay minerals identified include chlorite, illite, kaolinite, and smectite (Fig. 16). Based on the relative abundances of the clay species, four Units (C1–C4) have been recognized for Site 695.

Unit C1 extends from the seafloor to 9 mbsf and has a clay association of illite (abundant), smectite (common to abundant), and kaolinite and chlorite (rare to common). This unit is late Pliocene to Pleistocene.

Unit C2 extends from 9 to 138 mbsf, is early to late Pliocene and consists of illite (abundant), chlorite (common to abundant), kaolinite (rare to common), and smectite (absent to rare).

Figure 14. Layer of gray (N 5/0), lithified siltstone from a silty mud sequence of lithostratigraphic Unit III. Sample 113-695A-40X, CC, 1–7 cm.

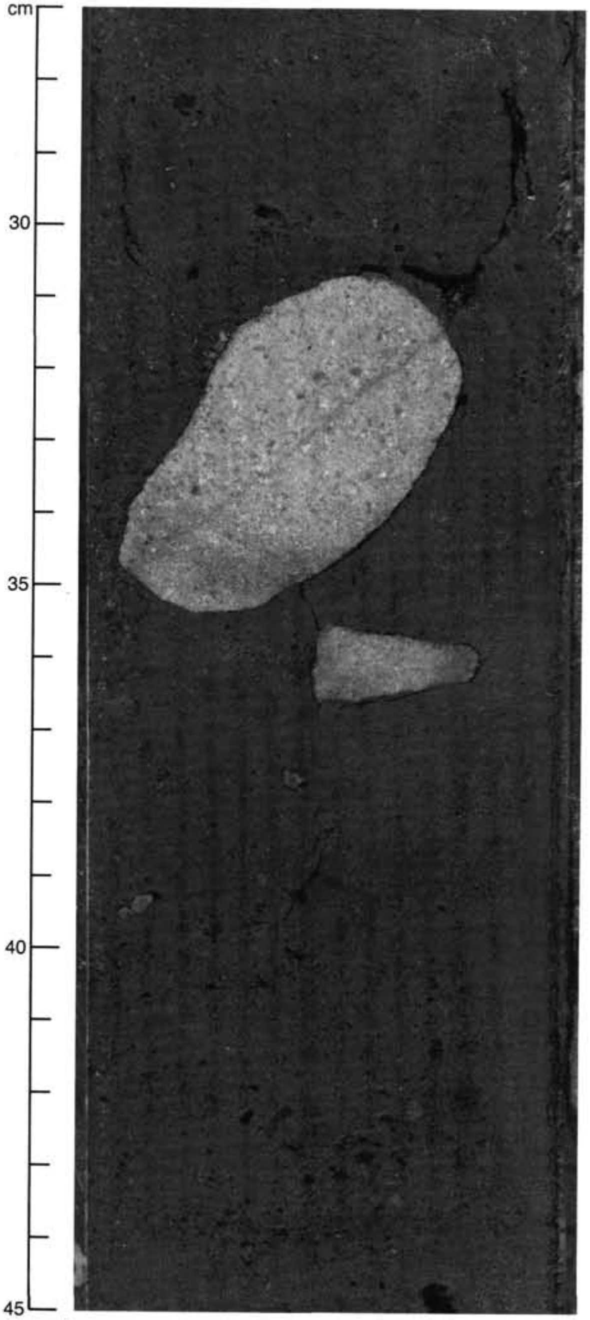

Figure 15. Large quartzite dropstones in hemipelagic glaciomarine silty mud from lithostratigraphic Unit III. Sample 113-695A-39X-5, 27–45 cm.

Unit C3 extends from 138 to 300 mbsf, is early Pliocene, and consists of illite (common to very abundant), chlorite (common to abundant), kaolinite (rare to common), and smectite (absent to abundant).

Unit C4 extends from 300 mbsf to near the bottom of Hole 695A at 339 mbsf, and has a clay association of chlorite (abundant to very abundant), illite (abundant), kaolinite (rare), and smectite (sporadic, rare). This unit ranges from late Miocene to early Pliocene.

Paleoenvironmental History

At Site 695, clay associations consist of abundant chlorite and illite throughout the sedimentary sequence and differ from the clay mineral associations of the adjacent oceanic areas. On the Falkland Plateau (Robert and Maillot, 1983) and Maud Rise (Sites 689 and 690), smectite is more abundant during the Neogene. Moreover, the chlorite content is higher at Site 695 than at either Site 693 on the East Antarctic margin and Site 694 in the Weddell Basin. Similar chlorite contents to those seen at Site 695 have not been reported from adjacent oceanic areas, and hence it is probable that the clay associations at this site are derived mainly from the Antarctic Peninsula.

Unit C4 (late Miocene to early Pliocene) is characterized by abundant to very abundant chlorite and abundant illite. Chemical weathering favors the development of chlorite (and illite) in the modern soils of ice-free Antarctic areas (Ugolini and Jackson, 1982). This unit correlates with Unit C2 at Site 693 where chlorite was generally abundant, and with Unit C2 at Site 694, partially characterized by vermiculite. At these sites, chlorite and vermiculite are derived from a more intense weathering connected with an amelioration of the climate. Increased chemical weathering occurred in both East and West Antarctica during a relatively warm period of the late Miocene around 7–8 Ma ago (Kennett and Von der Borch, 1985). Removal of upper Miocene relict soils locally continued until early Pliocene time (Sites 693 and 695).

Decreasing chlorite and increasing smectite in Unit C3 (lower Pliocene) result from weaker chemical weathering on the Antarctic Peninsula, associated with increased erosion of ancient terrains outcropping on the Antarctic margin. Unit C3 corresponds to Unit C1 at Sites 693 and 694 and suggests that colder conditions and/or increased circulation occurred in Antarctic areas during this interval. The clay association in Unit C3 was probably deposited when the Antarctic ice-sheet began to expand further to a late Neogene maximum (Mercer, 1978).

Unit C2 (early to late Pliocene) is characterized by abundant chlorite and sporadic rare smectite. This mineralogic change suggests that erosion of sediments decreased and that poorly developed soils extended over the partially deglaciated areas. It implies a climate warming, possibly associated with weaker circulation. Unit C2 probably correlates with a relatively warm period of early to middle Gauss age (Mercer, 1978). A similar increase of chlorite (associated with illite and irregular mixed-layers) has been recorded in the Falkland Plateau area at DSDP Sites 513 and 514 in lower Pliocene sediments (Robert and Maillot, 1983).

Unit C1 (late Pliocene to Pleistocene) is characterized by increasing smectite and decreasing chlorite contents. Weak abundances of chlorite probably result from reduced pedogenesis on smaller deglaciated areas of the Antarctic Peninsula, and increased abundances of smectite probably reflect a resumption of erosion of the ancient sediments on the Antarctic margin. The mineralogic change suggests that a cooling associated with enhanced circulation occurred during the early late Pliocene. A similar event has been recorded near the Falkland Plateau at DSDP Site 514 where a decrease of chlorite, illite, and irregular mixed layers, associated with an increase of smectite, occurred above the Gauss-Matuyama boundary (Robert and Maillot, 1983). Increasing smectite and decreasing chlorite in both regions correlate with cooler climatic conditions on Antarctica, resulting in widespread erosion in both deep and shallow waters in the Southern Ocean (Mercer, 1978; Ledbetter and Ciesielski, 1986).

Alternating pale olive, olive, and greenish-gray sediments have been studied in Sections 113-695A-2H-4 and 113-695A-2H-5. Variations of the clay association are not related to the color of the sediment. However, chlorite and/or illite are more abundant in diatom-rich muds, suggesting that these sediments were deposited during warmer periods. Diatom-bearing muds with a higher percentage of diatoms, contain more abundant smectite and were probably deposited during colder periods. Similar variations have been previously described for upper Pleistocene

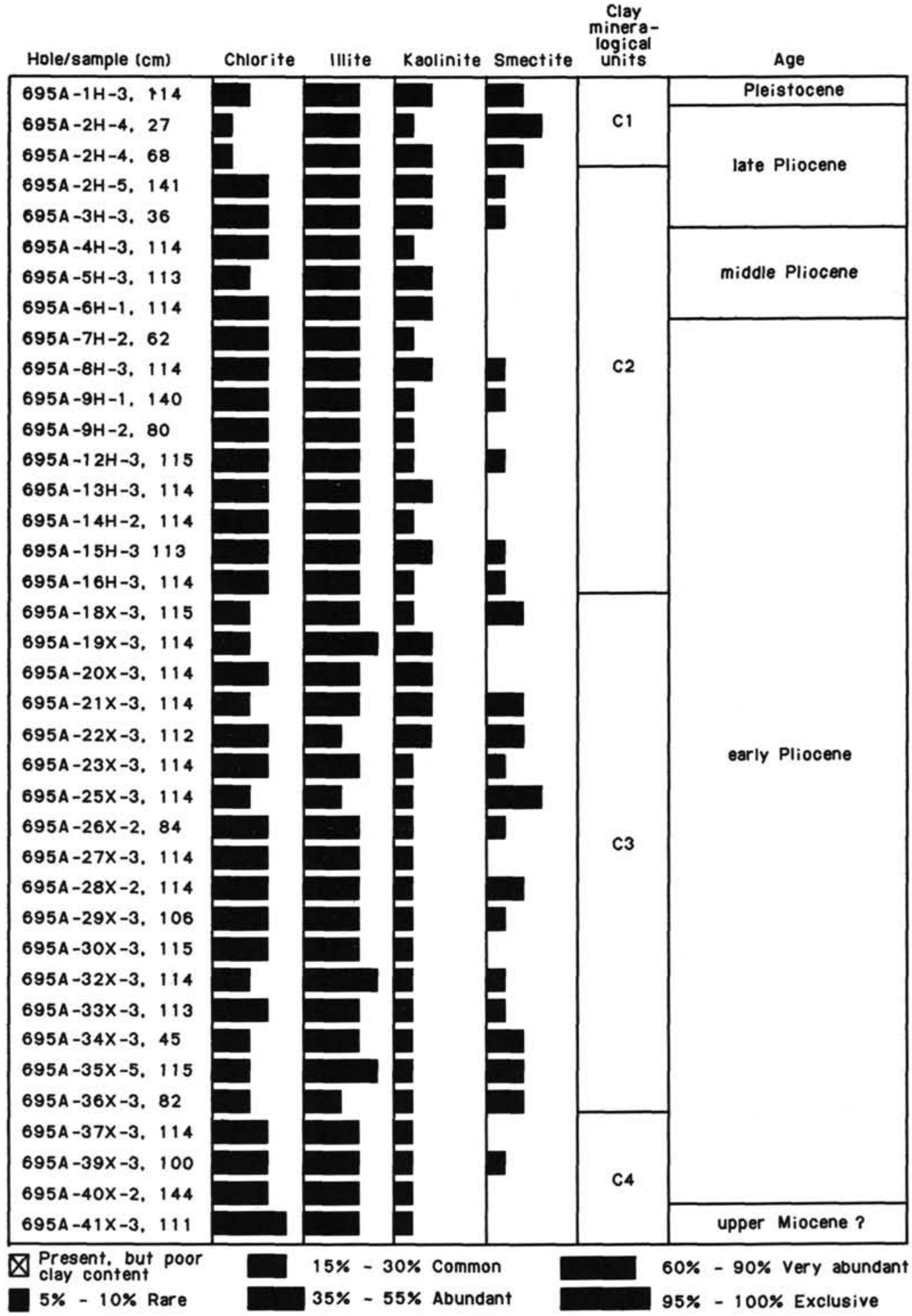

Figure 16. Clay mineralogy, Site 695.

sediments off East Antarctica (Grobe, 1986). Clay mineral data at Site 695 show that these variations occurred also during Pliocene times.

Ice-rafted Dropstones, Site 695A

Five dropstones were examined from Hole 695A. The dropstones range in size from 1 x 1 cm to 3 x 3 cm, are subangular, and do not show signs of weathering. Based on their lithology the rocks are grouped into volcanic, sedimentary, and felsic intrusive rocks. Petrogenetically, the volcanic rocks are tholeiitic basalt and andesite, the sedimentary rocks are sandstone, and the felsic intrusive is a granite. A detailed petrographic description of these dropstones is given in Table 2. They are found throughout the recovered interval.

The basalt has a glomeroporphyritic texture; phenocrysts of olivine and possibly pyroxene have been altered to carbonate. Weathered out phenocrysts have been replaced by quartz. The andesite is an extensively sericitized, porphyritic rock, and the

Table 2. Petrographic description of dropstones from Leg 113, Site 695.[a]

Rock number: 113-695A-1H-4, 137-140 cm
Name: sandstone
Size: 2 × 3 cm
Depth: 5.87 mbsf
Shape: subangular
Weathering: none

Major minerals	%	Accessory minerals	Comments
Quartz	60	Magnetite	Sandstone cemented by chlorite-rich matrix. Green epidote is interstitial to chlorite. Plagioclase and quartz grains are angular and relatively sorted. Feldspars are sericitized. Opaques are oxidized. Very fine-grained rock.
Chlorite	20	Sericite	
Plagioclase	10	Epidote	

Rock number: 113-695A-30X-1, 8-10 cm
Name: olivine tholeiite
Size: 2 × 3 cm
Depth: 244.48 cm
Shape: subangular
Weathering: weathered out phenocrysts

Major minerals	%	Accessory minerals	Comments
Plagioclase	40	Chlorite	Glomeroporphyritic rock, olivine phenocrysts have altered to carbonate. Secondary quartz replaces weathered-out phenocrysts.
Magnetite	20	Quartz	
Carbonate	20	Epidote	
Clinopyroxene	5		

Rock number: 113-695A-34X-4, 61-65 cm
Name: graphic granite
Size: 1 × 1 cm
Depth: 278.61 mbsf
Shape: subangular
Weathering: none

Major minerals	%	Accessory minerals	Comments
Plagioclase	30	Chlorite	Metasomatically altered rock. Graphic texture of quartz often intergrown with feldspars. Some amphibole is recrystallized to blue-green actinolite.
K-feldspar	25	Sphene	
Graphic quartz	20	Magnetite	
Hornblende	20	Zircon	
		Sericite	

Rock number: 113-695A-34X-4, 66-68 cm
Name: andesite
Size: 2 × 3 cm
Depth: 278.66 mbsf
Shape: subrounded
Weathering: none

Major minerals	%	Accessory minerals	Comments
Plagioclase	40	Carbonate	Porphyritic andesite is altered by sericitization. Presence of spherulite indicates andesitic composition.
Quartz	10	Zircon	
Spherulite	30	Sphene	
Orthoclase	5	Epidote	
		Sericite	

Rock number: 113-695A-39X-5, 31-33 cm
Name: sandstone
Size: 3 × 3 cm
Depth: 318.31 mbsf
Shape: subangular
Weathering: none

Major minerals	%	Accessory minerals	Comments
Quartz	90	Sericite	Uneven to even grain boundaries; small grains are interstitial to large ones. Perthite has been altered.
		Feldspars	
		cement	

[a] When the major mineral composition does not equal 100%, the accessory minerals form the remaining component.

matrix contains an abundance of spherulites. The plagioclase feldspars have lost their original An content due to albitization. Graphic granite is the only intrusive rock in this suite of dropstones. It is characterized by extensive hydrothermal alteration (chlorite and sericite). About 20% of the rock is composed of graphic quartz, occasionally intergrown with feldspars. The sandstones are fine to medium grained. One has a chlorite-rich matrix. The grains are poorly sorted, and grain boundaries are relatively uneven. The lithology of dropstones in Hole 695A indicates the Antarctic Peninsula as the source area.

PHYSICAL PROPERTIES

Index properties measured on samples selected from the most intact portions of cores are listed in Table 3. Profiles of bulk density, water content (dry basis), and grain density are illustrated in Figure 17. A profile of porosity is illustrated in Figure 18.

A large number of samples were measured of Site 695 sediments. This allows us to apply the principles of geotechnical stratigraphy to delineate geotechnical units (a segment of sediment of similar geotechnical and acoustic character) and compare these units to lithostratigraphic divisions and seismic horizons. Ten geotechnical units were identified. An examination of index properties (Table 3) shows that the partitioning of these properties into units of similar magnitude is, in most cases, quite obvious. A good example of the partitioning process is geotechnical Unit G3. In Table 3, the water content of Section 113-695A-3H-2 at 78 cm shows a large increase. Subsequent values of water content down to Section 113-695A-7H-1 at 90 cm, are similarly high. Porosity, bulk density, and grain density change within Unit G3, relative to Units G2 and G4, in similar fashion. The ten geotechnical units identified at Site 695 are listed in Table 4, along with their depth range, average water content, porosity, bulk density, grain density, shear strength, acoustic velocity, and thermal conductivity. There are large variations in physical properties between the various geotechnical units.

A description of each geotechnical unit follows:

Geotechnical Unit G1, 0–4 mbsf, has a low water content, low porosity, and high bulk density material with a high grain density. It also has a relatively high velocity and a low shear strength.

Geotechnical Unit G2, 4–11.4 mbsf, has an intermediate to high water content and porosity, low bulk and grain densities, and low velocities.

Geotechnical Unit G3, 11.4–51.8 mbsf, has a very high water content and porosity, very low bulk and grain densities, and an acoustic velocity equal to that of seawater. Shear strength has an intermediate value.

Geotechnical Unit G4, 51.8–94 mbsf, has a normal range of values of its index properties and acoustic velocity for its depth of burial.

Geotechnical Unit G5, 94–112 mbsf, and geotechnical Unit G6, 112–170 mbsf, contain sediments with very high water content and porosity, low bulk and grain densities, and intermediate to low acoustic velocities. These two units are similar except that Unit G5 has a slightly higher water content and porosity and a lower shear strength.

Geotechnical Unit G7, 170–219 mbsf, has low water content, low porosity, high bulk density, and high grain density material with a high acoustic velocity.

Geotechnical Unit G8, 219–286 mbsf, contains material similar to Unit G7 but with a lower water content and a much higher shear strength.

Geotechnical Unit G9, 286–315 mbsf, has very low water content and porosity and a high bulk and grain density with a high acoustic velocity and thermal conductivity.

Table 3. Index properties (water content, porosity, bulk density, and grain density) measured on samples from Site 695.

Core, section, top (cm)	Depth (mbsf)	Water content (% wet weight)	Water content (% dry weight)	Porosity (%)	Bulk density (g/cm³)	Grain density (g/cm³)
113-695A-						
1H-3, 77	3.8	35.84	55.86	62.07	1.77	2.91
1H-4, 90	5.4	54.77	121.08	78.54	1.47	2.97
2H-2, 103	5.4	29.27	41.39	51.83	1.81	2.49
2H-4, 83	8.2	45.95	85.01	70.38	1.57	2.52
2H-6, 90	11.3	47.47	90.37	72.40	1.56	2.49
3H-2, 78	14.6	54.51	119.85	77.71	1.46	2.75
3H-4, 89	17.8	47.33	89.85	75.04	1.62	2.93
3H-6, 80	20.7	58.47	140.80	79.39	1.39	2.42
4H-1, 90	22.9	39.07	64.13	65.13	1.71	2.78
4H-3, 90	25.9	55.58	125.12	79.27	1.46	2.60
4H-5, 90	28.9	58.05	138.36	79.29	1.40	2.71
4H-6, 90	30.4	69.94	232.64	92.47	1.35	1.97
5H-1, 84	32.4	38.35	62.20	63.92	1.71	2.57
5H-2, 84	33.0	55.55	124.98	77.35	1.43	2.41
5H-3, 84	35.4	62.43	166.19	81.99	1.35	2.25
5H-4, 84	36.9	59.80	148.73	80.81	1.38	2.48
5H-5, 84	38.4	33.54	50.46	58.15	1.78	2.75
5H-6, 84	39.9	66.74	200.69	84.04	1.29	2.33
6H-1, 90	42.1	57.00	132.56	78.92	1.42	2.57
6H-2, 90	43.6	47.97	92.21	71.11	1.52	2.41
6H-3, 90	45.1	55.63	125.40	76.28	1.40	2.58
6H-4, 90	46.6	59.78	148.64	78.99	1.35	2.33
6H-5, 90	48.1	50.37	101.50	73.16	1.49	2.63
6H-6, 20	48.9	63.08	170.87	82.51	1.34	2.53
7H-1, 90	51.7	61.10	157.05	82.55	1.38	2.50
7H-2, 90	53.2	46.75	87.78	71.57	1.57	2.73
7H-3, 40	54.2	41.35	70.50	64.81	1.61	2.68
8H-1, 90	61.3	37.67	60.43	62.91	1.71	2.69
8H-2, 90	62.8	32.98	49.22	59.71	1.85	2.90
8H-3, 90	64.3	37.36	59.65	63.32	1.74	2.69
8H-4, 90	65.8	36.44	57.33	61.07	1.72	2.70
8H-5, 90	67.3	46.62	87.35	69.93	1.54	2.52
9H-1, 90	70.9	42.64	74.34	67.54	1.62	2.65
9H-2, 90	72.4	58.04	138.34	79.99	1.41	2.63
9H-3, 90	73.9	47.82	91.65	71.66	1.54	2.66
9H-4, 60	75.1	46.37	86.47	70.24	1.55	2.61
10H-1, 90	80.5	42.69	74.50	68.79	1.65	2.80
10H-2, 90	82.0	38.20	61.81	63.95	1.72	2.71
10H-3, 90	83.5	43.96	78.43	66.49	1.55	2.57
10H-4, 90	85.0	46.73	87.74	70.74	1.55	2.58
10H-5, 90	86.5	42.19	72.99	67.79	1.65	2.84
12H-1, 90	90.1	41.33	70.46	67.04	1.66	2.82
12H-3, 90	93.1	38.12	61.62	62.22	1.67	2.63
12H-5, 90	96.1	55.30	123.72	78.90	1.46	2.55
12H-6, 20	97.6	59.39	146.26	79.27	1.37	2.33
13H-2, 90	101.2	60.09	150.57	80.40	1.37	2.63
13H-3, 90	102.7	43.66	77.50	70.67	1.66	2.88
14H-2, 90	110.9	46.55	87.08	70.83	1.56	2.55
14H-3, 94	112.4	55.29	123.66	78.96	1.46	2.63
15H-2, 90	120.6	62.92	169.70	82.79	1.35	2.26
15H-4, 90	123.6	56.92	132.14	79.58	1.43	2.57
16H-2, 90	130.3	60.76	154.82	78.16	1.32	2.15
16H-4, 89	133.3	47.92	92.01	75.98	1.62	2.73
18X-2, 43	139.5	54.27	118.70	78.44	1.48	2.51
18X-3, 17	140.8	56.21	128.35	78.97	1.44	2.73
19X-2, 82	149.6	50.63	102.56	76.12	1.54	2.69
19X-4, 90	152.7	55.91	126.79	80.23	1.47	2.57
19X-6, 90	155.7	62.70	168.07	80.54	1.32	2.01
20X-2, 90	159.4	42.22	73.07	68.66	1.67	2.56
20X-4, 89	162.4	56.55	130.15	77.38	1.40	2.33
20X-6, 90	165.4	52.34	109.81	76.08	1.49	2.77
21X-2, 91	169.2	48.44	93.94	73.26	1.55	2.72
21X-3, 49	170.3	51.98	108.25	73.90	1.46	2.48
21X-4, 90	172.2	38.26	61.96	64.63	1.73	2.64
22X-3, 80	178.3	51.96	108.16	75.78	1.49	2.61
22X-CC, 15	184.0	28.01	38.91	52.84	1.93	3.13
23X-3, 140	190.6	38.28	62.03	63.93	1.71	2.61
23X-4, 138	192.1	35.36	54.69	64.17	1.86	2.82
25X-1, 67	196.6	33.64	50.69	60.23	1.83	2.79
27X-1, 14	215.4	32.55	48.25	56.49	1.78	2.71
27X-4, 10	219.9	27.73	38.37	51.90	1.92	2.75
29X-4, 12	239.3	30.85	44.61	55.45	1.84	2.76

Table 3 (continued).

Core, section, top (cm)	Depth (mbsf)	Water content (% wet weight)	Water content (% dry weight)	Porosity (%)	Bulk density (g/cm³)	Grain density (g/cm³)
113-695A-						
30X-2, 90	246.8	29.36	41.56	54.90	1.92	2.70
30X-4, 90	249.8	31.07	45.07	55.89	1.84	2.72
32X-2, 87	256.5	36.71	58.00	62.25	1.74	2.72
32X-4, 76	259.4	35.78	55.71	62.27	1.78	2.63
32X-6, 40	262.0	41.15	69.91	67.54	1.68	2.81
33X-2, 95	266.3	33.44	50.24	60.46	1.85	2.83
33X-3, 74	267.6	32.67	48.51	59.63	1.87	2.78
34X-2, 89	275.9	32.32	47.75	58.42	1.85	2.71
34X-5, 75	280.3	32.40	47.92	57.97	1.83	2.78
35X-2, 132	285.9	31.60	46.20	58.48	1.90	3.02
36X-2, 73	295.0	26.01	35.15	57.29	2.26	3.06
36X-4, 38	297.7	28.32	39.52	53.51	1.94	2.69
37X-2, 80	304.7	33.39	50.13	58.98	1.81	2.77
37X-3, 85	306.3	28.74	40.34	52.64	1.88	2.59
39X-1, 111	313.1	34.76	53.28	60.08	1.77	2.74
39X-7, 27	319.7	23.52	30.75	49.68	2.16	2.93
39X-CC, 26	320.2	22.90	29.70	44.68	2.00	2.72
40X-1, 146	323.2	26.46	35.98	51.91	2.01	2.66
40X-CC, 1	325.3	4.89	5.14	12.87	2.69	2.85
41X-1, 29	331.7	14.05	16.34	32.49	2.37	2.79
41X-4, 41	336.3	25.37	33.99	49.89	2.01	2.66
41X-CC, 27	337.3	27.63	38.19	52.89	1.96	2.78

Geotechnical Unit G10, 315 mbsf to the bottom of the hole (341.3 mbsf), has a very low water content (30% lower than Unit G9), very low porosity (17% lower than Unit 9), high bulk density, and an average clay grain density. The acoustic velocity is very high (12% higher than Unit G9), and the thermal conductivity is 24% higher than Unit G9.

The correlation between the geotechnical units and the lithostratigraphic units is shown in Table 5.

Shear Strength

The undrained shear strength of the sediment was determined using the ODP Motorized Vane Shear Device. Standard 1.2-cm equidimensional miniature vanes were used with the device. Its operation and calculations follow procedures outlined in the *Physical Properties Handbook* (used on the ship). Strength measurements were made on the least disturbed sections of the cores.

The shear strengths determined for Site 695 are listed in Table 6 and illustrated in Figure 19. In the interval between 0 and 170 mbsf, the gradient of shear strength (the rate of increase in strength with depth) is 0.476 kPa/m. In the interval from 170 to 350 mbsf, the strength gradient is 0.944 kPa/m. The overall gradient from 0 to 350 mbsf is 0.723 kPa/m. The shear strength profile divides into zones more or less along designated geotechnical units.

Thermal Conductivity

At this site, "normal," "oblique," and "end" insert methods were used to measure the thermal conductivity (Von Herzen and Maxwell, 1959; also see "Physical Properties" section, "Site 694" chapter, this volume). The thermal conductivities are listed in Table 7 and illustrated in Figure 20. Thermal conductivity ranges from 0.886 W/m-K (20.8 mbsf) to 2.321 W/m-K (334 mbsf). The average values of thermal conductivity for each geotechnical unit are listed in Table 4.

Compressional Wave Velocity

Sonic velocity (V_p) in sediments is measured using two methods. First, a continuous measurement of V_p was made through the unsplit core using a *P*-wave logger (PWL) installed next to the Gamma Ray Attenuation Porosity Evaluator (GRAPE) source and detector. Second, measurements were made on individual samples removed from the core with one measurement from every other core section. Velocity was measured in only one direction, usually perpendicular to the long axis of the core.

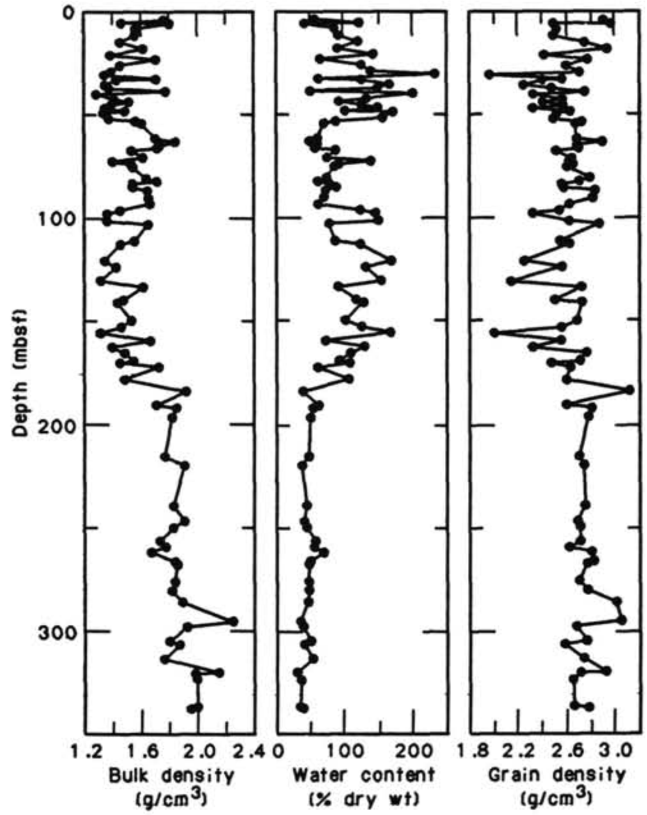

Figure 17. Profile of bulk density, water content, and grain density, Site 695. Data for this profile are given in Table 3.

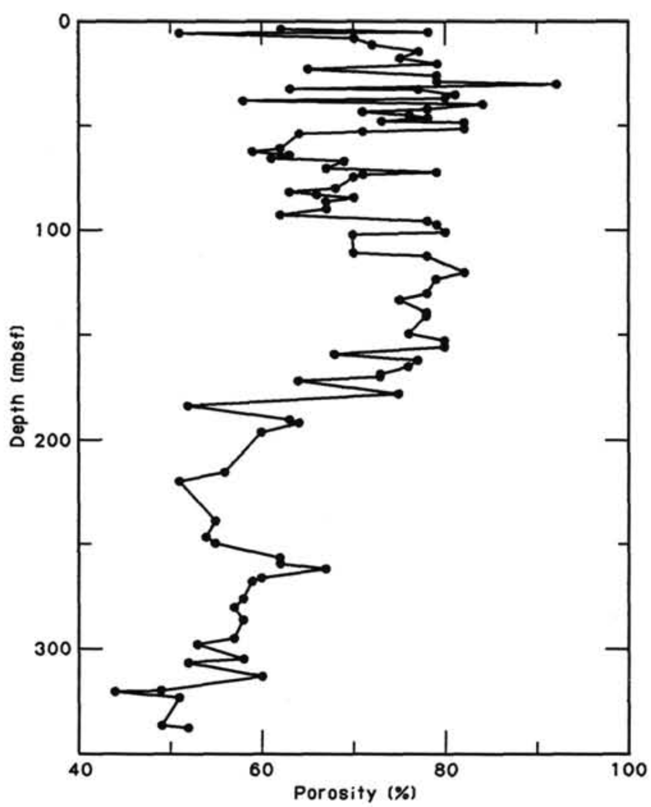

Figure 18. Profile of porosity, Site 695. Data for this profile are given in Table 3.

The results of velocity measurements made on the Hamilton Frame are listed in Table 8 and illustrated in Figure 21. A continuous velocity profile as determined by the PWL is shown in Figure 22. The average velocities of the sediments in the various geotechnical units are listed in Table 4. Velocity increases with depth at a very slow rate. The velocity gradient for the interval 4-170 mbsf is 0.206 m/s/m. The gradient for the interval 170-350 mbsf is 0.14 m/s/m. The overall velocity gradient for Site 695, 0-350 mbsf, is 0.32 m/s/m. The average velocity of the geotechnical units is listed in Table 4. A velocity reversal takes place in Unit G3, 11.4-51.8 mbsf, the velocity dropping to that of seawater. The low velocity in Unit G3 is correlated with an increase in water content and porosity and a decrease in bulk and grain density, reflecting an increase in diatom content. A large increase in velocity takes place between geotechnical Units G9 and G10. Velocities increase on the average by 12% in Unit G10 over those of Unit G9.

The correlation between the Hamilton Frame measured velocities and the velocities determined by the PWL is very good. The PWL registers velocities approximately 2% higher than the Hamilton Frame. The large variations and high velocity values of the sediment in geotechnical Unit G1 (0-4 mbsf) are illustrated in Figure 21.

Each geotechnical unit was assigned an assumed velocity to correlate the geotechnical and lithostratigraphic units with seismic horizons. These assumed velocities were based on the average Hamilton Frame measured velocity which was adjusted to *in-situ* conditions by referring to the difference between Hamilton Frame velocities and downhole logging velocities obtained at Site 693. Table 5 displays the adjusted velocities, the depth in time (one-way traveltime) to the base of each geotechnical unit, and the depth in time (one-way traveltime) to the major seismic horizons (Fig. 23). The agreement between the calculated unit depth and the actual depth to the seismic horizons is very good.

Summary

The characteristics of the physical properties at Site 695 are well defined. Ten geotechnical units are identified and associated with designated lithostratigraphic units and seismic horizons. The very low porosities and water content and the very high velocities of geotechnical Unit G10 would suggest that the top of Unit G10 marks an erosional hiatus or the very rapid onset of diagenetic cementation.

SEISMIC STRATIGRAPHY

Site 695 is located at SP 1720 on multichannel seismic profile AMG845-18 (Birmingham University/British Antarctic Survey; Fig. 3), which runs north-south along the eastern margin of the South Orkney microcontinent. The profile in the vicinity of the site is shown in Figure 2.

The site is the intermediate-depth member of a three-site vertical transect to examine the Neogene history of the Antarctic water masses. It lies above a thick sedimentary sequence (2.8 s two-way traveltime (twt) approximately 4 km), most of which is probably volcanic-arc-derived and of pre-late Oligocene age. However, this phase of deposition ended in the middle Oligocene when Jane Basin opened (see "Background and Objectives" section, this chapter), and the upper sequence was expected to consist largely of pelagic biogenic and ice-rafted sediments. In addition, a prominent BSR at about 700 ms twt had been interpreted as a likely gas hydrate reflection because of its apparent inverse polarity (Shipley et al., 1979; Macleod, 1982). Leg 113 had permission to drill to within 50 m of the BSR.

Hole 695A penetrated 341.1 m of ?upper Miocene to Quaternary siliceous ooze and mud, terminating when the XCB broke, leaving part jammed in the bit. Recovery was high (74.6%) and an extensive set of physical properties measurements was made

Table 4. Average values of the physical properties, acoustic velocity, and thermal conductivity of geotechnical units at Site 695.

Geotechnical Unit	Depth (mbsf)	Water content (% dry weight)	Porosity (%)	Bulk density (g/cm^3)	Grain density (g/cm^3)	Velocity (m/s)	Maximum shear strength (kPa)	Thermal conductivity (W/m-K)
G1	0–4	55.9	62.1	1.77	2.91	1535	12.3	1.21
		(1)	(1)	(1)	(1)	(1)	(1)	(2)
G2	4–11.4	84.5	68.3	1.60	2.62	1510	27.1	1.20
		(4)	(4)	(4)	(4)	(4)	(4)	(3)
G3	11.4–51.8	129.6	76.9	1.46	2.53	1500	40.4	1.05
		(20)	(20)	(20)	(20)	(20)	(16)	(10)
G4	51.8–94	72.5	66.5	1.64	2.69	1520	54.3	1.20
		(17)	(17)	(17)	(17)	(18)	(23)	(9)
G5	94–112	117.0	76.0	1.48	2.59	1520	110.8	1.09
		(5)	(5)	(5)	(5)	(5)	(5)	(4)
G6	112–170	122.1	77.3	1.47	2.51	1520	66.3	1.05
		(15)	(15)	(15)	(15)	(15)	(13)	(12)
G7	170–219	52.8	60.4	1.81	2.78	1590	125.7	1.26
		(6)	(6)	(6)	(6)	(6)	(8)	(10)
G8	219–286	49.5	58.8	1.84	2.77	1590	204.0	1.42
		(12)	(12)	(12)	(12)	(6)	(3)	(15)
G9	286–315	43.7	56.5	1.93	2.77	1610	153.6	1.48
		(5)	(5)	(5)	(5)	(4)	(2)	(6)
G10	315–341.1	30.8	46.9	2.09	2.76	1830	293.2	1.93
		(6)	(6)	(6)	(6)	(3)	(1)	(5)

Note: Number of measurements shown in parentheses.

Table 5. Measured and assumed velocities, depth in time of geotechnical units, and depth in time of seismic horizons, Site 695.

Geotechnical Unit	Litho-stratigraphic Unit	Depth (approximate, mbsf)	Average laboratory velocity (m/s)	Assumed *in-situ* velocity (m/s)	Thickness of interval (m)	Interval transit time (s)	Depth to base of unit (OWT)[a] (s)	Depth of seismic horizons (OWT) (s)
G1		0–4	1535	1540	4	0.003	0.003	
	IA	(0–20)			19.9	(0.025)	(0.025)	
G2		4–11	1510	1550	7	0.009	0.012	
	IB	(11–51)						
G3		20–52	1500	1560	40	0.051	0.063	0.08
G4	IC	52–94	1520	1580	43	0.054	0.117	0.10
G5		94–112	1520	1625	18	0.022	0.139	0.14
G6		112–170	1520	1685	58	0.069	0.201	0.19
	ID	(94–190)			97	(0.128)	(0.245)	0.24
G7		170–219	1590	1700	50	0.059	0.267	0.27
	II	(190–307)						
G8		219–286	1590	1700	65	0.076	0.343	0.33
G9		286–315	1610	1710	30	0.035	0.377	0.375
	III	(307–341)						
G10		315–341	1830	1930	—			

[a] OWT = one-way traveltime.

("Physical Properties" section, this chapter). The hole could not be logged and it was decided not to attempt a second hole at this site.

Extracted PWL velocities measured on cores from Hole 695A are shown in Figure 24, together with the velocity-depth model used for Hole 689B. The model is a reasonable approximation to the Site 695 data down to 200 mbsf, particularly when such factors as core disturbance and changes from *in-situ* conditions are considered. Below 200 mbsf, the Hole 695A velocities are much lower for a given depth. In that the velocity-depth model for Site 689 lay close to the empirical average curves compiled by Carlson et al. (1986), as do data from the other Leg 113 sites, an explanation for the difference should probably be sought at Site 695.

Altogether at Site 695 there were 86 measurements of *P*-wave velocity (by Hamilton frame) and bulk density on the same samples (see "Physical Properties" section, this chapter). This represents a closer average spacing than the spatial equivalent of the seismic sampling interval, and justified generating a synthetic seismogram from them, for comparison with the reflection profile. To produce the seismogram, the data were convolved with a minimum-phase impulse derived from the seabed reflection in the vicinity of the site. The result is shown in Figure 25. The comparison appears successful down to 250 ms (190 mbsf), but at greater depths the correspondence is poorer. In general, the seismic profile is smoother than the synthetic trace, with fewer short-wavelength, impulsive reflections. Probably, matching reflectors occur slightly sooner in the observed seismic profile than in the synthetic seismogram.

At about 190 mbsf, several changes take place downhole: the diatom component decreases while the terrigenous component increases, bulk densities and *P*-wave velocities (Hamilton frame but not PWL) rise, and porosity falls. These changes, however, do not explain directly the poorer correspondence between seismic profile and synthetic seismogram. Also, core recovery is reduced and the sampling interval of physical properties measure-

Table 6. Undrained shear strengths determined for Hole 695A.

Core, section, top (cm)	Depth (mbsf)	Shear strength (kPa)
113-695A-		
1H-3, 82	3.8	12.3
1H-4, 99	5.0	31.4
2H-2, 109	5.5	26.8
2H-4, 87	8.3	22.1
2H-6, 86	11.3	27.9
3H-2, 82	14.7	27.9
3H-4, 92	17.8	37.2
3H-6, 85	20.8	47.7
4H-1, 84	22.8	32.6
4H-3, 94	25.9	32.6
4H-5, 84	28.8	37.2
4H-6, 89	30.4	45.4
5H-2, 90	34.0	25.6
5H-3, 80	35.4	45.4
5H-4, 90	37.0	32.6
5H-5, 80	38.4	29.1
5H-6, 90	40.0	37.2
6H-2, 84	43.5	32.6
6H-4, 84	46.5	81.4
6H-7, 27	50.5	76.8
7H-1, 82	51.6	25.6
7H-2, 54	53.1	23.3
7H-3, 18	55.4	58.2
7H-3, 34	55.5	51.2
8H-1, 94	61.3	32.6
8H-2, 84	62.7	72.1
8H-3, 74	63.1	61.7
8H-3, 84	63.2	55.9
8H-4, 84	65.7	41.9
9H-1, 84	70.8	38.4
9H-2, 84	72.3	62.8
9H-3, 63	73.6	48.9
9H-3, 81	73.8	39.6
9H-3, 84	73.8	44.2
9H-4, 32	74.8	11.6
10H-1, 84	80.4	25.6
10H-2, 84	81.9	65.2
10H-3, 84	83.4	69.8
10H-3, 106	83.7	76.8
10H-4, 104	85.1	72.1
10H-5, 84	86.4	73.3
12H-1, 84	90.0	34.9
12H-3, 58	92.8	81.4
12H-3, 69	92.9	81.4
12H-3, 84	93.0	37.2
12H-5, 84	96.0	83.8
12H-6, 30	97.0	62.8
13H-2, 84	101.1	53.5
13H-3, 84	102.6	65.2
14H-2, 84	110.8	93.1
14H-3, 89	112.4	82.6
15H-2, 81	120.5	55.9
15H-4, 106	123.8	109.4
16H-2, 84	130.2	60.5
16H-4, 82	133.2	100.1
18X-2, 40	139.5	32.6
18X-3, 22	140.8	34.9
19X-4, 82	152.6	32.6
19X-6, 82	155.6	65.2
20X-2, 83	159.3	55.9
20X-4, 68	162.2	39.6
20X-6, 84	165.3	60.5
21X-3, 57	170.4	132.6
21X-4, 84	172.1	102.4
22X-4, 60	181.6	97.7
22X-4, 133	182.2	95.4
22X-5, 90	183.3	160.6
22X-CC, 14	184.0	72.1
23X-3, 100	190.2	128.0
23X-4, 138	192.1	165.2
25X-6, 56	204.0	125.7
27X-7, 25	224.6	148.9
30X-4, 143	250.3	265.3
32X-6, 49	262.1	197.8
39X-2, 52	314.0	153.6
39X-3, 73	315.7	142.0
41X-4, 27	336.2	293.2

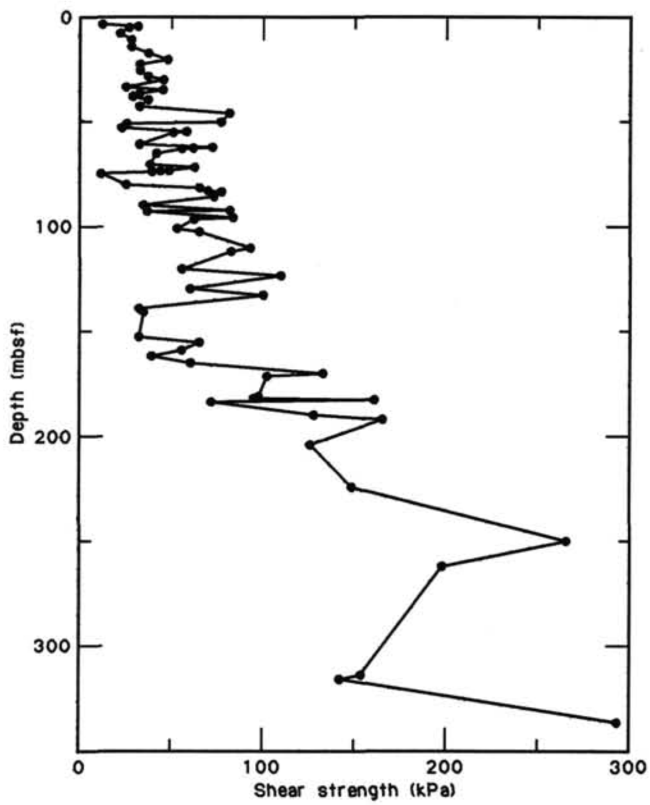

Figure 19. Undrained shear strength profile, Site 695. Data for this profile are given in Table 6.

ments increases (averaging 15 m over the next 60 m). Thus, the *in-situ* changes in sediment physical properties may not be fully described by the measurements. In particular, the *in-situ* changes may be more gradual, or more complex than the measurements suggest, with the effect of producing a smoother profile. Other factors having a similar effect include imperfect stacking of the multichannel data and the existence of nonplanar interfaces away from the site.

Discussion

At Site 695 PWL velocities are lower than at other sites and *in-situ* velocities may be faster. There are many potential causes of such a velocity difference, involving composition, age, core disturbance, and pore fluid state.

Sediments in both Holes 695A and 689B are largely pelagic and biogenic, the main compositional differences being the calcareous component below 70 mbsf at Site 689 and the greater amount of mud and ice-rafted detritus at Site 695. However, the calcareous component was also missing at Site 693, to no effect, and the ice-rafted detritus at the same site did not appear to de-

Certainly core disturbance has depressed the shipboard-measured values of velocity at many of the sites, but recovery at Site 695 was high and core disturbance less than usual. If the observed physical properties provide a reasonable synthetic approximation to the reflection profile, the cores cannot be significantly disturbed. Thus, we are left with age and pore fluid state as possible controlling influences.

The major potential modifier of pore fluid state is the formation of a gas hydrate. If the pore spaces within the sediment were filled with a solid phase, then pore fluid removal and compaction could be prevented or delayed, and some reduction in the normal burial-related gradients in porosity, density, and *P*-

Table 7. Thermal conductivities of sediments from Site 695.

Core, section, top (cm)	Depth (mbsf)	K (W/m-K)	Method
113-695A-			
1H-3, 65	3.7	1.422	Oblique
1H-3, 90	3.9	1.019	Oblique
1H-5, 3	6.0	1.235	Oblique
1H-C, 7	6.2	1.426	Oblique
2H-4, 91	8.3	0.943	Oblique
2H-6, 95	11.4	1.189	Oblique
3H-4, 84	17.7	1.356	Oblique
3H-6, 90	20.8	0.886	Oblique
4H-2, 90	24.4	1.302	
4H-4, 90	27.4	0.964	
4H-CC, 15	31.5	0.854	End
5H-2, 90	34.0	0.941	
5H-4, 91	37.0	0.978	
6H-2, 90	43.6	1.133	
6H-4, 80	46.5	0.959	
7H-2, 90	53.2	1.080	
7H-3, 40	55.6	1.238	
8H-2, 90	62.8	1.541	
8H-4, 90	65.8	1.341	
9H-2, 90	72.4	0.948	
9H-4, 50	75.0	1.106	
10H-2, 90	82.0	1.285	
10H-4, 80	84.9	0.981	
12H-2, 80	91.5	1.345	
12H-4, 80	94.5	1.102	
13H-2, 90	101.2	1.016	
13H-3, 90	102.7	1.167	
14H-2, 90	110.9	1.070	
14H-3, 80	112.3	0.980	
15H-2, 90	120.6	0.927	
15H-3, 90	122.1	1.003	
16H-2, 90	130.3	1.022	
16H-4, 90	133.3	1.108	
18X-3, 20	140.8	1.020	
19X-2, 90	149.7	1.190	
19X-4, 91	152.7	1.083	
20X-2, 90	159.4	1.252	
20X-4, 90	162.4	0.977	
20X-6, 90	165.4	1.113	
21X-2, 90	169.2	0.990	
21X-4, 90	172.2	1.263	
22X-2, 90	178.9	1.058	
22X-4, 90	181.9	1.035	
23X-2, 90	188.6	1.154	
23X-4, 90	191.6	1.328	
25X-2, 90	198.3	1.528	
25X-4, 80	201.2	1.222	
25X-6, 90	204.3	1.113	
26X-2, 60	207.7	1.285	
27X-2, 95	217.8	1.614	
27X-4, 95	220.8	1.795	
27X-6, 35	223.2	1.569	
28X-2, 90	227.4	1.342	
29X-2, 60	236.8	1.518	
29X-4, 40	239.6	1.524	
30X-2, 90	246.8	1.412	
30X-4, 90	249.8	1.522	
32X-2, 90	256.5	1.343	
32X-4, 90	259.5	1.239	
33X-2, 89	266.2	1.264	
33X-3, 90	267.7	1.439	
34X-2, 92	275.9	1.406	
34X-5, 90	280.4	1.341	
35X-2, 112	285.6	1.415	
35X-3, 3	286.0	1.243	Second end
36X-2, 76	295.1	1.622	
36X-4, 36	297.7	1.455	
37X-2, 90	304.8	1.588	
37X-4, 90	307.8	1.411	
39X-2, 92	314.4	1.596	
39X-4, 92	317.4	1.643	
40X-2, 96	324.2	1.604	
40X-3, 33	325.0	2.266	
41X-2, 105	334.0	2.321	
41X-4, 92	336.8	1.838	

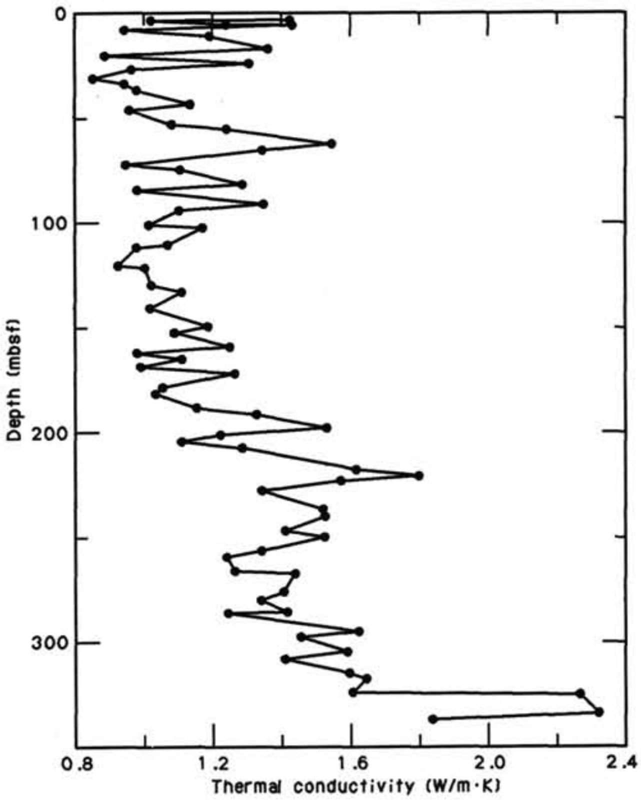

Figure 20. Profile of thermal conductivity, Site 695. Data for this profile are given in Table 7.

wave velocity might be expected. However, the velocity in pure hydrate is high, so it is unlikely that a gas hydrate present in the sediment would produce *in situ* the low velocities observed in shipboard measurements. The strong, inverse-polarity BSR which lies near 700 ms at the site (Fig. 24) was suggested to be the base of a methane gas hydrate, before drilling started. It was thought then that the hydrate layer would be thin, since the gas was considered likely to be thermogenic (the Neogene sediments above the BSR were thought to have been laid down under conditions of vigorous circulation of well-oxygenated water, and thus seemed likely to have been oxidized). The depth of the BSR permitted the estimation of a heat flow value (0.85 to 1.0 HFU, low but not unreasonable) under certain assumptions about its composition, but no heat flow measurements had been made.

Measurements of downhole temperature and thermal conductivity made as the drilling proceeded demonstrated that heat flow was much higher than the BSR had predicted (1.5 HFU; see "Physical Properties" and "Downhole Measurements" sections, this chapter). The base of any gas hydrate layer, computed simply from this value of heat flow, would lie between 310 and 360 mbsf. A sudden increase in methane was observed below about 250 m, and the gas is considered to be forming *in situ* by the action of methanogenic bacteria at the base of a sulfate ion depletion gradient (see "Inorganic Geochemistry" and "Organic Geochemistry" sections, this chapter); the very high lower Pliocene sedimentation rates ("Sedimentation Rates" section, this chapter) probably allowed the burial of unoxidized biogenic matter. Methane forming in these circumstances would be expected to enter the hydrate phase, and the presence of a methane hydrate between, say, 250 and 350 mbsf could produce the slightly faster *in-situ* velocities that the synthetic seismogram suggests. At these depths, core recovery was good, and the cores showed no signs of the presence of a hydrate phase. Also, in

Table 8. Compressional wave velocities (Hamilton Frame) measured on samples from Site 695.

Core, section, top (cm)	Depth (mbsf)	Velocity (m/s)	Core, section, top (cm)	Depth (mbsf)	Velocity (m/s)	
113-695A-			113-695A-			
1H-3, 77	3.8	1608	12H-5, 90	96.1	1514	
1H-4, 90	5.4	1508	12H-6, 20	97.6	1507	
2H-2, 103	5.4	1545	13H-2, 90	101.2	1514	
2H-4, 83	8.2	1460	13H-3, 90	102.7	1531	
2H-6, 90	11.3	1518	14H-2, 90	110.9	1517	
3H-2, 78	14.6	1487	14H-3, 94	112.4	1510	
3H-4, 89	17.8	1497	15H-2, 90	120.6	1509	
3H-6, 80	20.7	1503	15H-4, 90	123.6	1522	
4H-1, 90	22.9	1490	16H-2, 90	130.3	1513	
4H-3, 90	25.9	1480	16H-4, 87	133.3	1526	
4H-5, 90	28.9	1487	18X-2, 43	139.5	1518	
4H-6, 90	30.4	1485	18X-3, 17	140.8	1519	
5H-1, 84	32.4	1533	19X-2, 82	149.6	1507	
5H-2, 84	33.0	1514	19X-4, 90	152.7	1517	
5H-3, 84	35.4	1495	19X-6, 90	155.7	1507	
5H-4, 84	36.9	1490	20X-2, 90	159.4	1530	
5H-5, 84	38.4	1566	20X-4, 89	162.4	1516	
5H-6, 84	39.9	1500	20X-6, 90	165.4	1531	
6H-1, 90	42.1	1494	21X-2, 91	169.2	1512	
6H-2, 90	43.6	1438	21X-3, 49	170.3	1546	
6H-3, 90	45.1	1494	21X-4, 90	172.2	1529	
6H-4, 90	46.6	1504	22X-3, 80	178.3	1536	
6H-5, 90	48.1	1507	22X-CC, 15	184.0	1624	
6H-6, 20	48.9	1494	23X-3, 140	190.6	1643	
7H-1, 90	51.7	1506	25X-1, 67	196.6	1630	
7H-2, 90	53.2	1512	27X-1, 14	215.4	1586	
7H-3, 40	54.2	1525	29X-4, 12	239.3	1574	
8H-1, 90	61.3	1532	30X-4, 90	249.8	1558	
8H-2, 90	62.8	1547	30X-CC, 43	250.6	4616	Limestone
8H-3, 90	64.3	1529	32X-4, 76	259.4	1632	
8H-4, 90	65.8	1538	33X-3, 74	267.6	1548	
8H-5, 90	67.3	1518	34X-5, 75	280.3	1606	
9H-1, 90	70.9	1478	35X-2, 132	285.9	1614	
9H-2, 90	72.4	1504	36X-4, 38	297.9	1643	
9H-3, 90	73.9	1511	37X-2, 80	304.7	1564	
9H-4, 60	75.1	1514	37X-3, 85	306.3	1645	
10H-1, 90	80.5	1540	39X-1, 111	313.1	1583	
10H-2, 90	82.0	1531	39X-7, 27	319.7	1980	Mudstone
10H-3, 90	83.5	1571	40X-1, 146	323.2	1710	Siltstone
10H-4, 90	85.0	1494	40X-CC, 1	325.3	3434	Very hard siltstone
10H-5, 90	86.5	1522	41X-1, 29	331.7	4054	Very hard siltstone
12H-1, 90	90.1	1524	41X-CC, 27	337.3	1809	Mudstone
12H-3, 90	93.1	1534				

these depths in the seismic profile, no seismic reflector resembling a hydrate BSR can be seen. Thus, the presence of a hydrate phase is a possible partial explanation for the low velocity gradient beneath 200 mbsf in Hole 695A, but by no means certain, and the inverse-polarity reflector at 700 ms remains unexplained. Post-cruise reprocessing of the MCS profile is pointing to the possibility that the inverse polarity of the BSR is a processing artifact related to inadequate masking of the far traces.

The remaining possibility for low velocities below 200 mbsf concerns the young age of the sediments cored, and the high concentration of diatoms. Diatom ooze at shallow depth, as at Sites 689 and 690, has very high porosities because of the loose packing of diatoms and diatom fragments. This means that the density of the ooze, and hence its nonhydrostatic load on the underlying sediments, is less than that of the same thickness of sediment of another lithology. Sediment compacts under the nonhydrostatic load of the overlying sediment, so a thick diatomaceous ooze should remain less compacted, depth for depth, than another lithology, and should apply a lesser stress to any sediments beneath. To the extent that Site 695 sediments are diatomaceous, this factor will be operating. Eventually, other factors come into play, such as the strength of the diatom fragments, dissolution and diagenesis (and hence a temperature/time integration), and the pore water chemistry. It may be that the relatively high rate of deposition of lower Pliocene sediments at Site 695 is important: sediments at the base of the hole are only about 5.3 m.y. old.

BIOSTRATIGRAPHY

Site 695 was drilled on the southeastern margin of the the South Orkney microcontinent in 1300 m of water to obtain a hemipelagic record for the Neogene. This site was the intermediate depth component of a three-site transect drilled down the flank of the South Orkney microcontinent to obtain information about changes in water-mass characteristics during the Neogene to late Oligocene. To investigate such changes, a 550-m section overlying a prominent BSR was targeted. Of that 550-m section, 341.1 m were drilled with an average recovery of 74.6%. The recovered section consists of an uppermost 5-m-thick Quaternary planktonic foraminifer-bearing mud overlying about 40 m of upper Pliocene diatom, silty, and clayey mud. This is underlain by an expanded sequence of lower Pliocene and possibly uppermost Miocene diatom silty mud, diatom-bearing mud, and silty mud.

All depths referred to are sub-bottom depths and samples are from the core catcher (CC) unless otherwise specified. On the summary biostratigraphic correlation chart (Fig. 26) the age or biostratigraphic zone assigned to a given core catcher is extrapolated to the midpoint of the overlying and underlying core. The section is described from the top down.

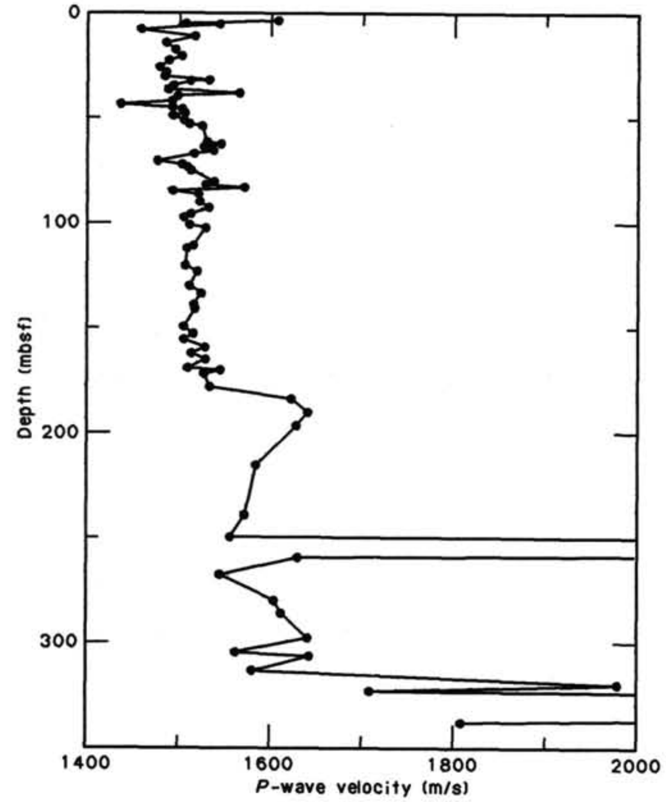

Figure 21. Compressional wave velocities (Hamilton Frame) for Site 695. Velocity data are given in Table 8.

Planktonic Foraminifers

Core catcher samples were examined from each of the 41 cores recovered at Site 695. Two additional samples were examined from the first core (Samples 113-695A-1H-1, 32–35 cm, and 113-695-1H-2, 39–42 cm). All core catcher samples are barren of planktonic foraminifers except Section 113-695A-3H, CC, which contains rare *Neogloboquadrina pachyderma*. The two samples taken from within Core 113-695A-1H contain abundant and well-preserved *Neogloboquadrina pachyderma*. These monospecific assemblages appear to be stratigraphically equivalent to the *N. pachyderma*-rich horizons described from the Quaternary at other Leg 113 sites. The absence of any planktonic, as well as calcareous benthic, foraminiferal pre-Quaternary record, suggests that during the Pliocene the carbonate compensation depth (CCD) in this region of the Weddell Sea was shallower than 1300 m, the present depth of Site 695.

Benthic Foraminifers

Benthic foraminifers were studied in all core catcher samples from Hole 695A and some additional samples (Samples 113-695A-1H-1, 0–2 cm, mud line; 113-695A-1H-1, 32–35 cm, and 113-695A-1H-2, 39–42 cm, *Neogloboquadrina pachyderma*-containing mud). Samples 113-695A-1H-1, 32–35 cm, and 113-695A-1H-2, 39–42 cm, contain low-diversity calcareous faunas. The mud-line sample and Sections 113-695A-1H, CC, through 113-695A-30X, CC, contain low-diversity assemblages of agglutinated foraminifers: specimens are very rare. Lower in the hole, samples are barren or contain very few specimens of *Martinotiella antarctica*. Interpretation of these scarce faunas is difficult, but comparison with Recent faunas from the Scotia Sea (Echols, 1971) suggests that the water depth during deposition of sediments in the lowermost part of the hole may have been greater (about 1500–2000 m) than the present water depth at Site 695 (1300 m). Results from Site 696, however, suggest that depth ranges of species in the Pliocene were different from Recent depth ranges (see "Biostratigraphy" section, "Site 696" chapter, this volume).

Samples 113-695A-1H-1, 32–35 cm,. and 113-695A-1H-2, 39–42 cm, contain low-diversity faunas (18 and 24 species per 200 specimens, compared with 31 to 40 species in samples with *N. pachyderma* at the previously drilled sites of Leg 113). Both samples contain dominant *Angulogerina earlandi* (32.5% and 29.1%) and *Globocassidulina subglobosa* (24.5% and 24.9%). In Sample 113-695A-1H-1, 32–35 cm, *Nonionella* spp. (10.7%), *Cassidulina laevigata* (8.5%), *Eilohedra weddellensis* (7.7%), and *Epistominella exigua* (7.7%) are common. In Sample 113-695A-1H-2, 39–41 cm, *Cassidulinoides parkerianus* (10.8%), *Cassidulina crassa* (10.3%), and *Astrononion* spp. (5.6%) are common. The fauna at Site 695 (shallower than the earlier drilled Sites 689–694) differs from that at the other sites by containing less abundant *E. exigua* and more *A. earlandi* and *G. subglobosa*. The differences between the calcareous benthic foraminiferal faunas in sediments with *N. pachyderma* at Leg 113 sites cannot be evaluated presently because the precise ages of the different samples are not known.

The mud-line sample contains only agglutinated species; *Miliammina arenacea* is dominant (12 out of 33 specimens) and other species (*Psammosphaera fusca*, *Cribrostomoides contortus*, *Haplophragmoides canariensis*, and *Haplophragmoides quadratus*) are rare. These rare species may be absent from lower sediments because they have fragile tests that are not easily preserved. *Miliammina arenacea* and *M. lata* or *Martinotiella antarctica* are dominant in all lower samples. These three species have been reported to use siliceous cement and to occur predominantly in diatomaceous sediments (Echols, 1971; see Fig. 26 in "Site 696" chapter, this volume, for abundances). *Karreriella bradyi*, *Sigmoilina tenuis*, *Eggerella bradyi*, *Trochammina conica*, *Reophax nodulifer*, and *Cystammina pauciloculata* are present as single specimens in a few samples. In Cores 113-695A-1H through 113-695A-6H *M. arenacea* and *M. lata* are dominant and *Martinotiella antarctica* is absent; in Sections 113-695A-7H, CC, through 113-695A-21X, CC, these species occur together at varying absolute and relative abundances, and from Sections 113-695A-22X, CC, through 113-695A-33X, CC, *M. antarctica* is dominant. In Sections 113-695A-34X, CC, through 113-695A-41X, CC, *M. antarctica* is very rare or absent, and no other species were observed.

The environmental significance of the poor assemblages at Site 695 is questionable, especially because depth zonations of benthic faunas in the Antarctic region are not usable from one region to another: faunas at the mud line at the Leg 113 sites are not similar to faunas at equivalent depths in other Antarctic areas (Bandy and Echols, 1964; Theyer, 1971; Milam and Anderson, 1981). Recent faunas dominated by *Miliammina arenacea* occur in the Scotia Sea in water depths of less than 1300 m, whereas faunas dominated by *Martinotiella antarctica* occur in waters deeper than about 2000 m. This suggests that the sediments lower in the hole at Site 695 might have been deposited in deeper water than the sediments higher in the hole. The presence of *M. antarctica* in samples from Site 696 (in much shallower water, see "Biostratigraphy" section, "Site 696" chapter, this volume), however, suggests that water depth was not the major factor controlling the relative abundance of *M. antarctica* and *Milliammina* spp.; the availability of silica in the sediments might have been a controlling factor in the species distribution.

Calcareous Nannofossils

No calcareous nannofossils were recovered at this site.

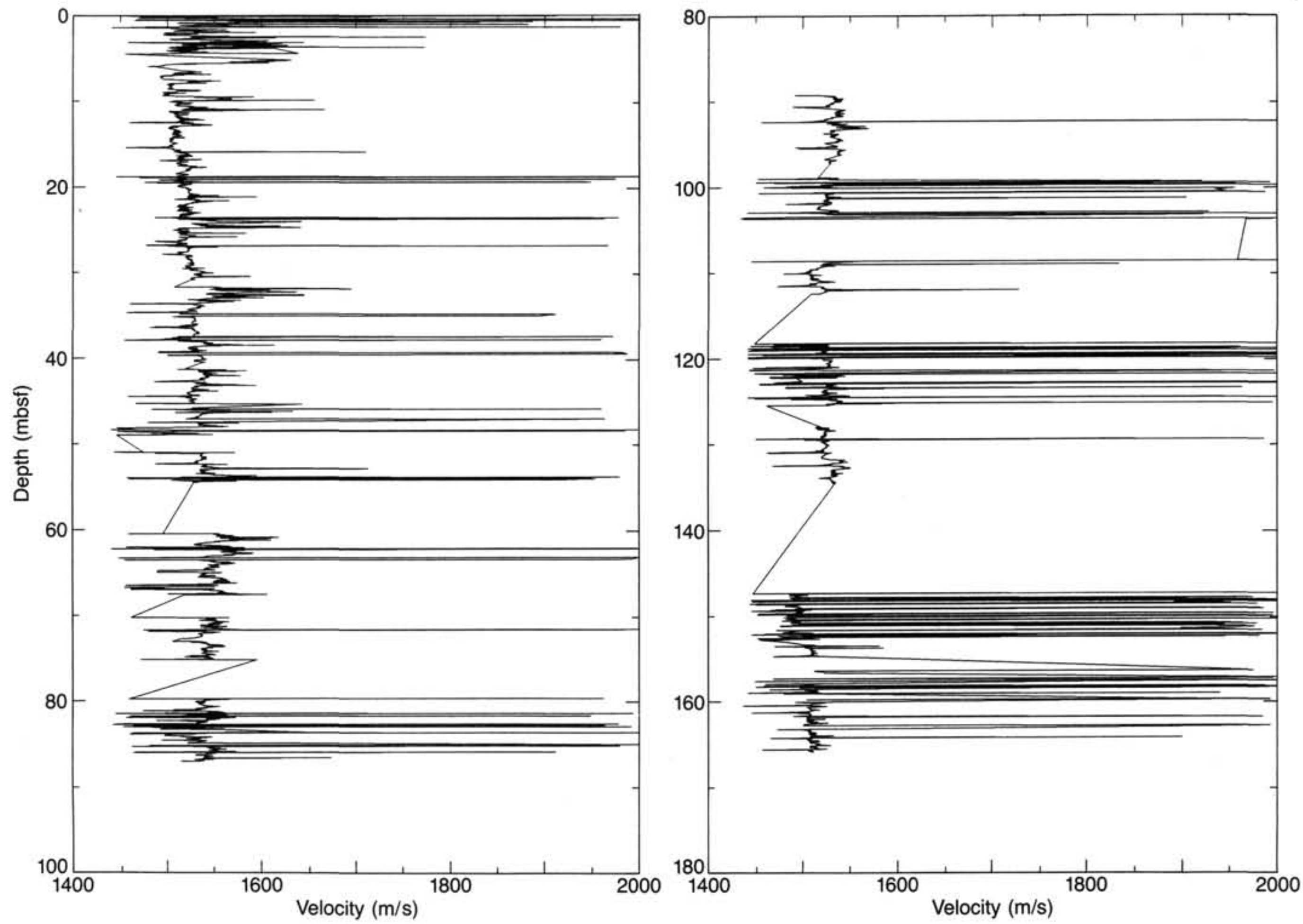

Figure 22. Continuous compressional wave velocity profile as determined by *P*-wave logger for Site 695 sediments.

Silicoflagellates

Silicoflagellates are generally present but of low diversity in Cores 113-695A-1H to -35X (lithostratigraphic Units I and II), and are absent in the clays and glacial marine sediments of lithostratigraphic Unit III (Section 113-695A-37X-4 to Core 113-695A-41X). Overall, silicoflagellates are most common and well preserved where diatoms are well preserved, and are absent or present mostly as fragments where diatom preservation is only moderate or poor. As a group, the silicoflagellates appear to be more sensitive to dissolution than the diatoms.

Short-spined *Distephanus speculum speculum* dominate the assemblages from Cores 113-695A-3H to -7H, and this interval can be assigned to the *D. speculum* B Zone if the zonation of Ciesielski (1975) is used. Silicoflagellates are absent in Cores 113-695A-8H to -12H where diatom preservation is poor. Well-preserved and robust *Distephanus boliviensis* are common in Section 113-695-12H, CC, where diatom preservation is good, and this taxon is present downhole throughout the remaining silicoflagellate-bearing cores. Cores 113-695A-13H to -30X belong to the *D. boliviensis* Zone of Ciesielski (1975). Section 113-695A-16H, CC, contains a single well-preserved specimen of *Distephanus pseudofibula* (reworked?), whereas Cores 113-695A-26X and -27X contain *Distephanus crux*. The top of the *D. boliviensis* Zone is assigned an age of about 3.2 Ma (Shaw and Ciesielski, 1983, Fig. 3), which accords well with the radiolarian assignment for Core 113-695A-12H (middle portion of the Upsilon Zone; see "Radiolarians" discussion below).

Cores 113-695A-32X to -35X are dominated by members of the *Distephanus pseudofibula* plexus, including both symmetric and asymmetric varieties of *D. pseudofibula* and forms often referred to as *D. speculum varians*. These cores belong to the *D. pseudofibula* Zone, which Shaw and Ciesielski (1983) place in the middle Gilbert. This corresponds well to the radiolarian assignment for these cores (upper portion of the lower Tau; see "Radiolarians" discussion below). Core catcher samples below Core 113-695A-35X were barren.

Diatoms

A thin sequence (approximately 5 m) of Quaternary sediments is present at Site 695. Samples from 113-695A-1H-1, 20 cm, and -1H-1, 55 cm, are assigned to the upper Quaternary *Thalassiosira lentiginosa* Zone based on the presence of *T. lentiginosa* and *Nitzschia kerguelensis* and the absence of *Actinocyclus ingens*. Other species include *Nitzschia curta*, *Eucampia antarctica*, and *Actinocyclus actinochilus*. Samples 113-695A-1H-2, 30 cm, and -1H-4, 30 cm, are placed in the lower Pleistocene *Coscinodiscus elliptopora*/*A. ingens* Zone. This assignment is provisional because, of the nominate taxa, only *A. ingens* was observed. Other species include *N. curta*, *A. actinochilus*, *N. kerguelensis*, *E. antarctica*, and *T. lentiginosa*. Diatoms are generally rare to few in Pleistocene sediments and are usually poorly preserved.

Within Sample 113-695-1H-4, 100 cm, and Section 113-695A-1H, CC, diatom abundance and preservation improve consider-

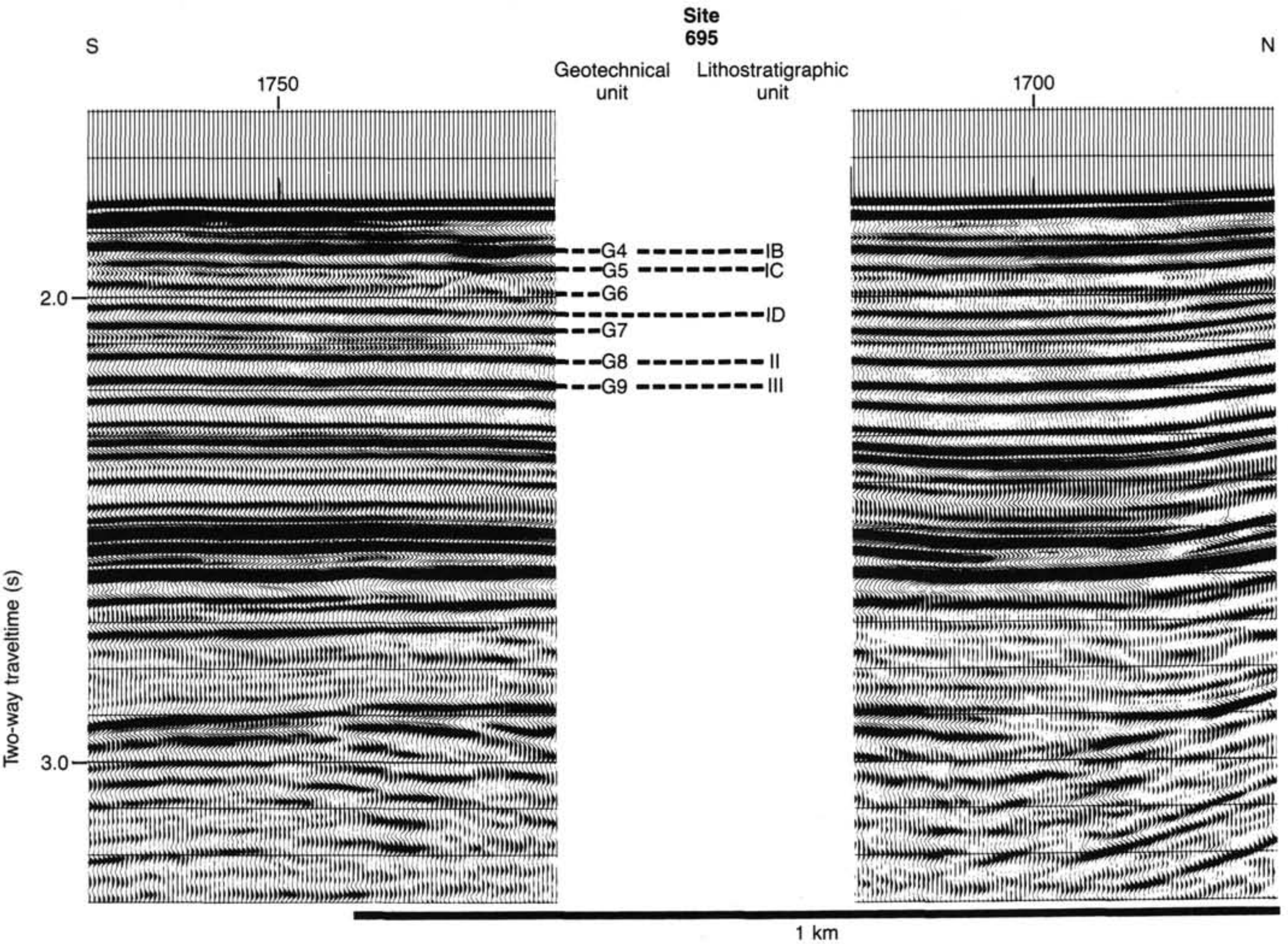

Figure 23. Seismic profile with designated geotechnical and lithostratigraphic units, Site 695.

ably. These samples are placed in the uppermost Pliocene *Coscinodiscus kolbei/Rhizosolenia barboi* Zone. The nominate taxa were not observed, and the age assignment is based on the presence of *Coscinodiscus vulnificus*, which last occurs in the upper part of the *C. kolbei/R. barboi* Zone, and the absence of *Cosmiodiscus insignis*. Considering that this Zone covers the lower third of the Matuyama Chron, there is some indication of a hiatus or truncated section in the uppermost part of the Pliocene of Site 695.

The upper Pliocene *Cosmiodiscus insignis* Zone is present in two samples (Sample 113-695A-2H-6, 70 cm, and Section 113-695A-2H, CC). In addition to the nominate taxon, *N. curta*, *A. ingens*, *E. antarctica*, *C. vulnificus*, and *C. kolbei* were found. The middle Pliocene *N. interfrigidaria* Zone occurs between Sample 113-695A-3H-4, 21 cm, and Section 113-695A-5H, CC. Besides *N. interfrigidaria*, species include *Rouxia antarctica*, *R. naviculoides*, *E. antarctica*, *N. curta*, *T. lentiginosa*, and *Schimperiella antarctica*. Common *N. curta* occur in 113-695A-3H-4, 21 cm, and an acme of *Stephanopyxis turris* occurs in 113-695A-5H-6, 45 cm. In Sample 113-695A-6H-3, 70 cm, we record an acme of *Thalassiosira* cf. *lineata*. At this same level we found common silicoflagellates (*Distephanus* spp.). Invariably, the above-mentioned samples had common to abundant diatoms with moderate to good preservation.

The transition from *Nitzschia praeinterfrigidaria* to *N. interfrigidaria*, which defines the basal boundary of the *N. interfrigidaria* Zone, occurs in Core 113-695A-6H. Preliminary analysis indicates that the transition occurs in Section 113-695A-6H-1, but for now we will regard the core catcher sample as transitional between the *N. interfrigidaria* Zone and the underlying combined *N. angulata/N. reinholdii* Zone (reasons for combining these two zones are given below in the "Summary").

Based on correlations with the paleomagnetic age assignments in Hole 693A and 695A we have tentatively changed the time interval of the transition of *N. praeinterfrigidaria* to *N. interfrigidaria* from within magnetic subchron C3N-1 (3.88–3.97 m.y.) to a time in the lower part of the Gauss Chron (about C2A-2N to C2A-3N, 2.99–3.4 m.y.). Additional evidence for a lesser age assignment for this transition is given in the data on DSDP Site 514 (Ludwig, Krasheninnikov, et al., 1983), Salloway (1983), and Ciesielski (1983) (compare with "Summary", below). Consequently, the age assignment for the boundary between the *N. interfrigidaria* Zone and the underlying combined *N. angulata/N. reinholdii* Zone is changed to the lower part of the Gauss Chron.

Sections 113-695A-7H, CC, through -35X, CC, are placed in the combined *N. angulata/N. reinholdii* Zone (middle to lower Pliocene). In general, diatoms are common to abundant and well preserved in the upper and middle part of this interval (113-695A-7H to -27X) whereas, in the lower part (113-695A-28X to -35X), their abundance and preservation drops to few and poor to moderate, respectively. In addition to *Nitzschia angulata*,

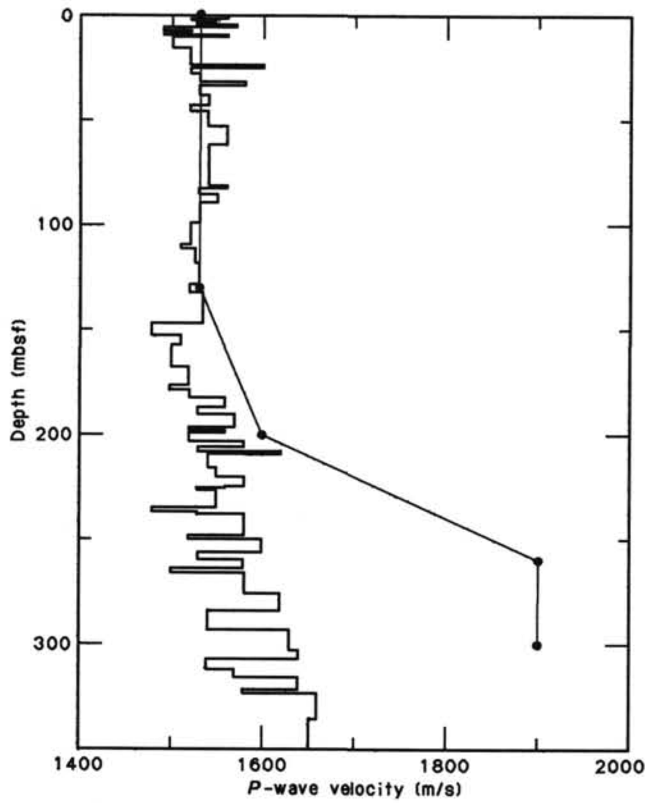

Figure 24. *P*-wave logger velocities from Hole 695A cores (continuous line), compared with velocity-depth model used for Hole 689B (line connecting dots).

such species as *Stellarima microtrias*, *Rouxia* spp., *Cosmiodiscus intersectus*, and *E. balaustium* occur consistently. Specimens which may be attributed to *Nitschia reinholdii* were encountered only in Sections 113-695A-25X, CC, and -35X, CC. Rare to few *N. praeinterfrigidaria* were found in the interval from Cores 113-695A-7H to -22X. Within Core 113-695A-19X to -26X *Thalassiosira torokina*, and *Nitzschia* cf. *vanheurekii occur as well as two species labeled by Schrader (1976) as Nitzschia* sp. 14 and *Cestodiscus* sp. 1. At two levels (Sections 113-695A-10H, CC, and 113-695A-13H, CC), we found an acme of *Stephanodiscus turris*. There were rare but consistent occurrences of *Denticulopsis hustedtii* throughout the interval assigned to the *N. angulata/N. reinholdii* Zone.

From below Section 113-695A-35X, CC, to -41X, CC, only rare and poorly preserved diatoms were found. Species include *D. hustedtii*, *Stellarima microtrias*, and *Cosmiodiscus intersectus*, but their occurrence pattern gives no clear indication that this sediment interval can be placed within the *Denticulopsis hustedtii* Zone, the top of which is defined by the last abundant appearance of the nominate species. Instead, the rare occurrence of *Neobrunia mirabilis* (Section 113-695A-40X, CC) and *Trinacria pileolus* (Section 113-695A-41X, CC) in the two lowermost core catcher samples of Hole 695A may indicate an age near the Miocene/Pliocene boundary or in the uppermost Miocene.

Summary

At Site 695 we recovered a 341-m-thick Quaternary to possibly uppermost Miocene sequence generally rich in biosiliceous components. Diatoms are generally common to abundant and preservation is moderate to good. Exceptions are in the uppermost 5 m of Hole 695A which are assigned to the Quaternary (*Thalassiosira lentiginosa* Zone and *Coscinodiscus elliptopora/*

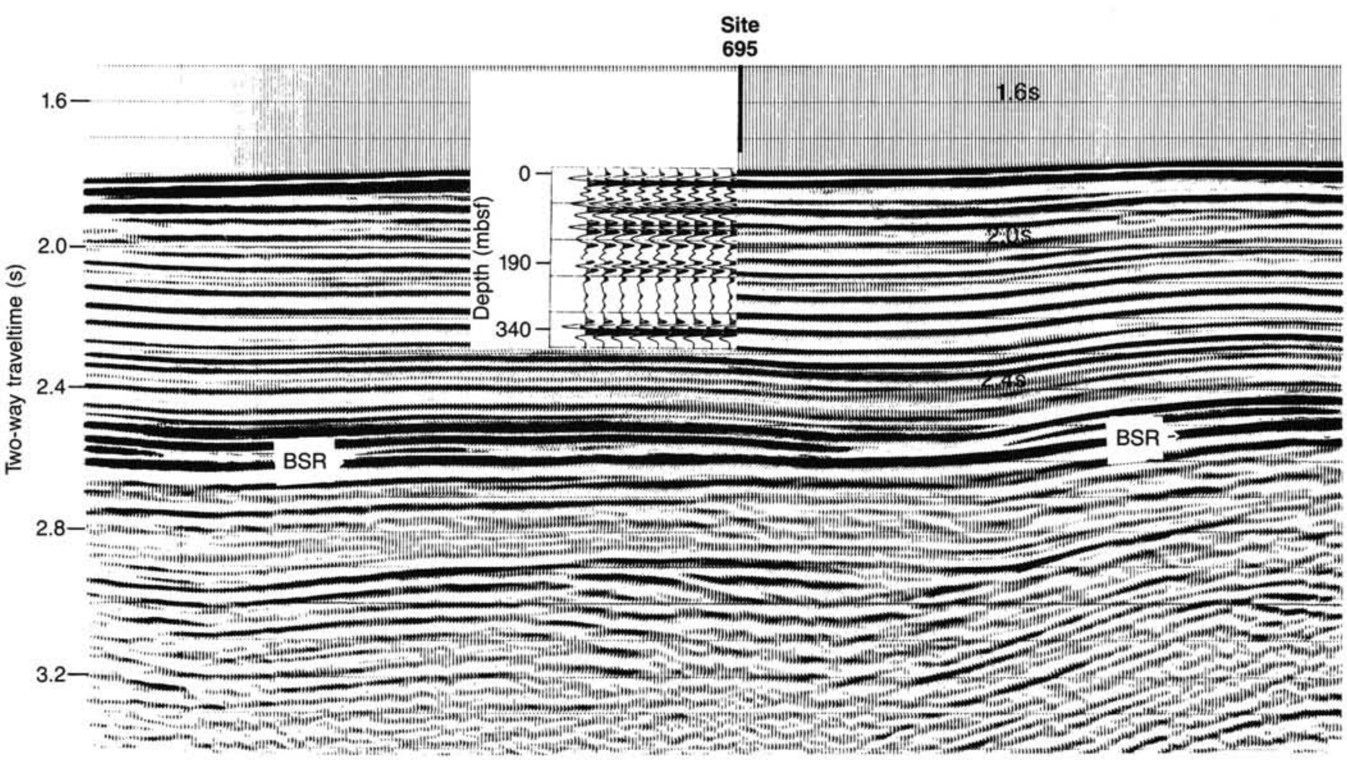

Figure 25. Section of multichannel seismic profile AMG845-18, compared with synthetic seismogram produced from shipboard measurements of velocity and density on the same samples (see "Physical Properties" section, this chapter). BSR = bottom-simulating reflector.

A. ingens Zone) and in the lowermost part of Hole 695A (Cores 113-695A-36X to -41X, approximately 293–341 mbsf), which represents the lowermost Pliocene to possibly uppermost Miocene. In the latter two intervals diatoms are rare to few and preservation is poor.

The biostratigraphic assignment of Site 695 indicates a condensed Quaternary to upper Pliocene sequence which may contain hiatuses. Most of the section cored at Site 695 is assigned to the combined *Nitzschia angulata/N. reinholdii* Zone (middle to lower Pliocene), comprising the interval from Section 113-695A-7H, CC, through -35X, CC. The age assignment for the basal sediments of Site 695 (near the Miocene/Pliocene boundary or in the uppermost Miocene) is tentative because it is based on rare occurrences of species whose stratigraphic ranges are not well known.

It should be noted that we changed the biostratigraphic diatom zonation used in Sites 689–694 and described in the "Explanatory Notes" chapter (this volume). We combined two Pliocene zones of Weaver and Gombos (1981; the *N. angulata* Zone and the *N. reinholdii* Zone) because: (1) we found *N. angulata* sporadically in the upper Miocene, and (2) the first appearance of *N. angulata* in the lower Pliocene is not consistent from site to site. (Also compare taxonomic note regarding *N. angulata* in the diatom discussion in "Site 689" chapter, this volume.)

We also changed the age assignment for the boundary between the *N. interfrigidaria* Zone and the underlying combined *N. angulata/N. reinholdii* Zone, from within the upper Gilbert (C3N-1, 3.88–3.97 Ma) to the lower part of the Gauss Chron (about C2AN-2 to C2AN-3, 2.99–3.4 Ma). The zonal boundary is defined by the presumed evolutionary transition of *N. praeinterfrigidaria* to *N. interfrigidaria* and was placed within C3N-1 at 3.9 Ma (Weaver and Gombos, 1981). McCollum (1975) identified the latest occurrence of *N. praeinterfrigidaria* within C2AR-3 at about 3.65 Ma and used this datum to define the top of his *N. praeinterfrigidaria* Zone. Ciesielski (1983) amended McCollum's poor descriptions of *N. praeinterfrigidaria* and *N. interfrigidaria* and defined a new *N. praeinterfrigidaria* Zone which spans 140,000 yr near and within C3N-1, with its base defined by the first evolutionary transition to *N. interfrigidaria*.

The origin of the paleomagnetic record, however, used by McCollum (1975), Weaver and Gombos (1981), and Ciesielski (1983) is somewhat obscure and not well described. The depths to the paleomagnetic reversals for DSDP Site 514, measured by Salloway (1983), are mislabeled by Ciesielski (1983, his Table 4). Based on the assumption that the transition of *N. praeinterfrigidaria* to *N. interfrigidaria* occurs within C3N-1, Ciesielski (1983) interprets a hiatus at Site 514 in which the lower part of the Gauss and the uppermost Gilbert Chron are missing. This interpretation was made even though the presence of a well-developed Gauss Chron and an undisturbed Gauss/Gilbert boundary based purely on paleomagnetic grounds is noted in the Site Summary for Site 514 (Ludwig, Krasheninnikov, et al., 1983). In addition, the stratigraphic occurrence of the radiolarians in Site 514 gives no indication for a hiatus in the discussed time interval (compare with Table 4 in Weaver, 1983). Based upon our preliminary correlation of the *N. praeinterfrigidaria-N. interfrigidaria* evolutionary transition to the paleomagnetic time scale for Holes 693A and 695A, a time interval for the transition spanning approximately the lower part of the Gauss Chron (about C2A-2N to C2A-3N) is indicated. This new age assignment is in agreement with the paleomagnetic and diatom species distribution data of Salloway (1983) and Ciesielski (1983), respectively, if their interpretation of an early Gauss–late Gilbert hiatus is abandoned. (Additional comments on diatom taxonomy and stratigraphy are given in the "Biostratigraphy" section in "Site 689" and "Site 697" chapters, this volume.)

Radiolarians

Section 113-695A-1H, CC, is assigned to the lower Chi Zone or Phi Zone (basal Pleistocene to uppermost Pliocene) based on the occurrence of *Antarctissa ewingi*, *Clathrocyclas bicornis*, and *Cycladophora davisiana*, and the absence of *Desmospyris spongiosa* and *Helotholus vema*. Section 113-695A-2H, CC, is upper Pliocene (upper Upsilon Zone, about 2.4–2.6 Ma) based on the presence of *D. spongiosa*, *H. vema*, and *C. davisiana*. Other species present in this sample, and throughout the remainder of the Upsilon Zone, include *C. bicornis*, *A. ewingi*, *Antarctissa strelkovi*, *Antarctissa denticulata*, and *Eucyrtidium calvertense*. Sections 113-695A-3H, CC, through -19X, CC, are assigned to the middle part of the Upsilon Zone (about 2.6–3.4 Ma), based on the presence of *H. vema*, *D. spongiosa*, and the absence of *C. davisiana* and *Prunopyle titan*. Sections 113-695A-20X, CC, through -26X, CC, are assigned to the lower part of the Upsilon Zone (about 3.4–4.0 Ma), based on the presence of *H. vema*, *D. spongiosa*, and *P. titan*. *Helotholus vema* populations grow progressively more primitive in morphology with increasing depth in this interval, and begin to resemble an ancestral form (as yet unnamed) seen in upper Miocene through lowermost Pliocene Antarctic sediments. The base of the Upsilon Zone is placed immediately below the lowest occurrence of *H. vema* specimens possessing no more than seven supporting struts in the basal ring, a distinct, subspherical cephalis, and a wide, short, subcylindrical thorax (i.e., between Sections 113-695A-26X, CC, and -27X, CC). Sections 113-695A-27X, CC, through -30X, CC, are placed in the upper part of the Tau Zone (about 4.0–4.4 Ma), based on their stratigraphic position below the Upsilon Zone, the presence of lower Pliocene indicators such as *P. titan* and *Eucyrtidium pseudoinflatum*, and the absence of common *Lychnocanium grande*. Sections 113-695A-32X, CC, through -39X, CC, are assigned to the lower Tau Zone (about 4.4–5.3 Ma), based on the presence of common *L. grande* and the absence of *H. vema* and *Cycladophora spongothorax*. Sections 113-695A-40X, CC, and -41X, CC, contain a poorly preserved, low-diversity assemblage. Species include *A. strelkovi*, *A. denticulata* (early morphs), *L. grande*, *C. bicornis*, *A. ewingi*, *Stylatractus universus*, and (in Section 113-695A-40X, CC) *E. pseudoinflatum*. Subantarctic taxa were also common in these samples (*Pterocanium charybdeum/praetextum*, artostrobid spp., etc). In each sample, very rare, broken specimens of *C. spongothorax* are seen. If it is assumed that these specimens are not reworked, then Sections 113-695A-40X, CC, and -41X, CC, can be assigned to the uppermost part of the *C. spongothorax* Zone (uppermost Miocene).

Discussion

At Site 695 we drilled a single hole, recovering 341 m of Pleistocene through lowermost Pliocene or uppermost Miocene sediments. In the Pleistocene through late Pliocene, sedimentation rates of both terrigenous material and siliceous microfossils were relatively low compared to rates in the early Pliocene, a pattern similar to that at Site 693. The lower Pliocene section at Site 695 was deposited at a very high rate of sedimentation, and the APC and XCB cores recovered from this interval are relatively undisturbed by the drilling process. Radiolarians were common to abundant and well preserved in most samples examined, becoming rare to few and moderate to poorly preserved only in samples near the base of the hole. This site will be an important site for high-resolution radiolarian biostratigraphic, paleoceanographic, and evolutionary studies. Site 695, for example, clearly records the evolutionary origin of the lower Pliocene stratigraphic indicator species *Helotholus vema* from an unnamed ancestor. The evolutionary origin of *H. vema* has not

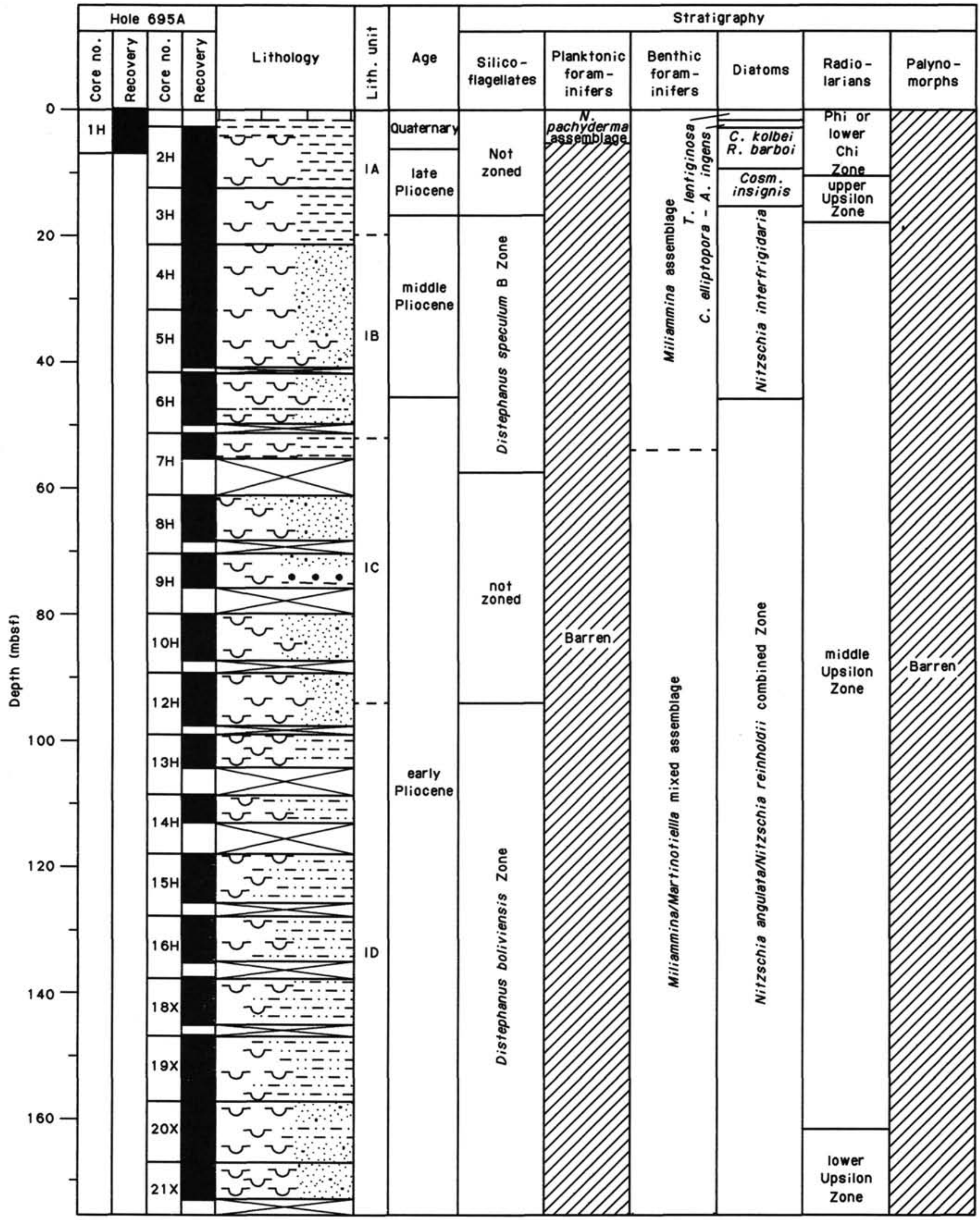

Figure 26. Summary biostratigraphic correlation chart, Site 695.

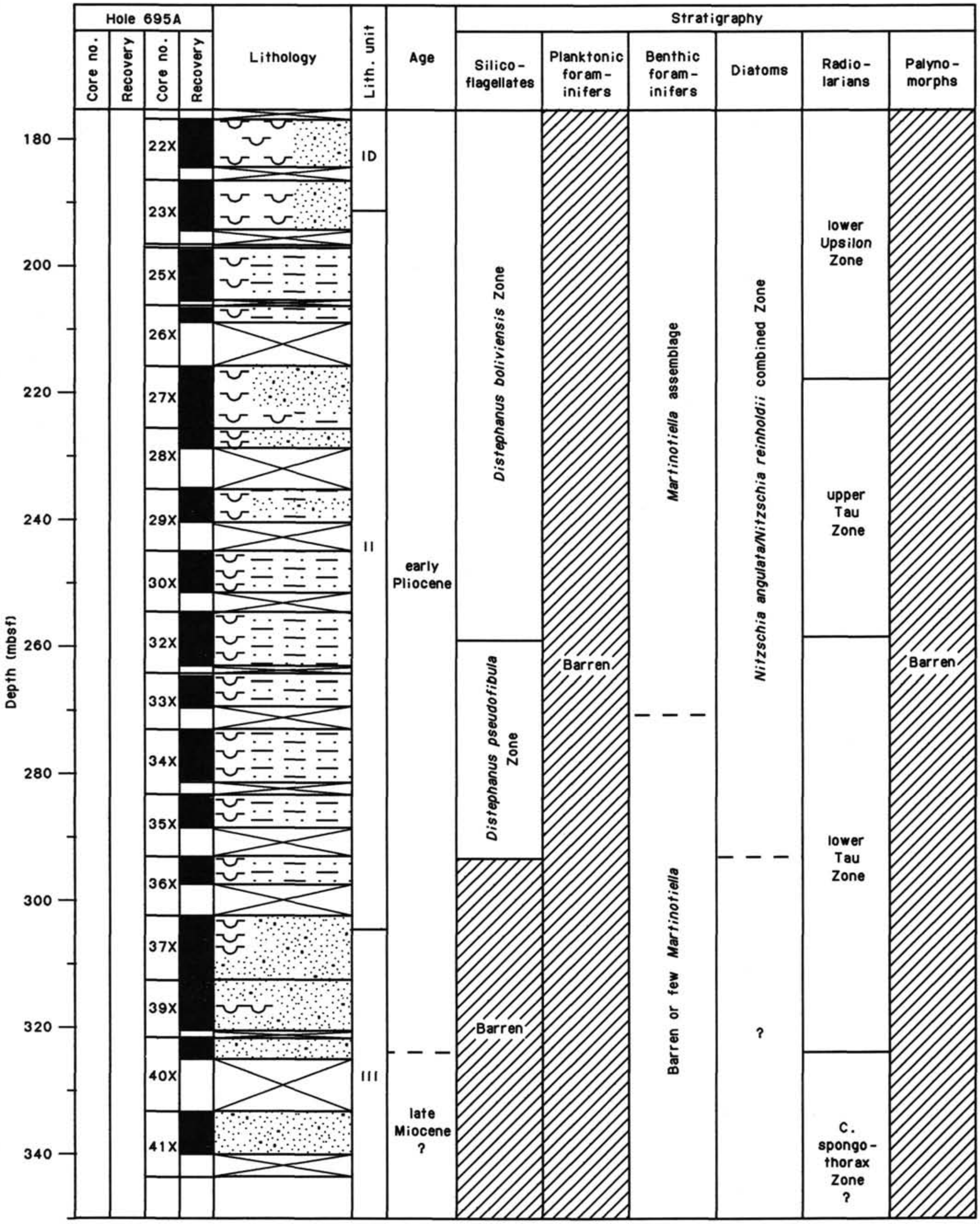

Figure 26 (continued).

been well understood, having been previously studied by Kellogg (1975) at relatively low temporal resolution in a piston core with a much lower sedimentation rate. High lower Pliocene biosiliceous sedimentation rates occur at Site 695 (about 30 m/m.y., based on sedimentation rates during the interval in excess of 100 m/m.y., and an average biogenic silica content of about 30% from smear slide analyses (see "Lithostratigraphy" section, this chapter). This appears to be part of the regional pattern of increased rates of sedimentation of lower Pliocene through upper Miocene biosiliceous sediments, observed during DSDP Leg 71 at Site 514 (Ludwig, Krasheninnikov, et al., 1983), and now encountered by ODP Leg 113 at Sites 689, 690, and 693. At Site 695 the widespread Antarctic basal Pliocene interval of low productivity is also recorded, as is the associated incursion of Subantarctic faunal elements into Antarctic radiolarian assemblages, previously seen in the Indo-Pacific sector of the Antarctic (Keany, 1979) and at Site 693.

Palynology

All smear slides observed from the core catcher samples of Site 695 (113-695A-1H, CC, through 113-695A-37X, CC; Quaternary–lower Pliocene) are barren of palynomorphs.

A small dropstone of organic-rich dark gray shale (Sample 113-695A-37X-2, 125–127 cm) was processed with HNO_3 to lighten the organic material. The organic matter is highly degraded, and therefore no palynomorph taxa or other organic debris were identifiable.

Summary

At Site 695 we sampled a 341-m Quaternary to upper Miocene(?) sequence consisting of predominantly diatom, silty and clayey mud with a thin interval of foraminifer-bearing mud at the top of the section. Core recovery ranged from good to moderate in APC- and XCB-cored sections. Sedimentation rates increase gradually from the Pleistocene to the upper Pliocene, reaching 4–5 m/m.y. in the upper Gauss. Sedimentation rates increase dramatically in the lower Gauss to approximately 130 m/m.y. This increase in sedimentation rate downsection appears to be a function of increased terrigenous and biosiliceous supply. An increase in biosiliceous flux is particularly evident in the lower Pliocene portion of lithostratigraphic Subunits IC and ID where biosiliceous components form an average of 30% of the sediments. This pattern of increased lower Pliocene biosiliceous sedimentation seems to be regional and was also observed at DSDP Site 514 in the South Atlantic as well as at other Leg 113 Sites (see Sites 689, 690, and 693). The expanded nature of this lower Pliocene record should, together with a detailed paleomagnetic record, provide an important reference section for high-resolution Pliocene biosiliceous biostratigraphy. Calcareous fossils, both pelagic and benthic groups, are not observed below the Quaternary. This observation would suggest that through the Pliocene the CCD was shallower than about 1300 m, the present depth of Site 695. The Quaternary and Pliocene are also barren of palynomorphs. Lithostratigraphic subdivisions are therefore made primarily on the basis of variations in the percentage of biosiliceous components.

The Quaternary at the top of lithostratigraphic Subunit IA is a 4–5-m-thick foraminifer-bearing mud containing *Neogloboquadrina pachyderma* as the most conspicuous component. Also present are low-diversity calcareous benthic foraminiferal faunas which differ from similar *N. pachyderma*-bearing horizons at Sites 689 through 693 by containing fewer *Epistominella exigua* and more *Angulogerina earlandi* and *Globocassidulina subglobosa*. Diatoms are rare and in general poorly preserved in Subunit IA. Nonetheless, sufficient numbers occur to allow delineation of the *Coscinodiscus lentiginosus* through *Coscinodiscus elliptopora/Actinocyclus ingens* Zones (Quaternary). Silicoflagellates, although slightly more susceptible to dissolution, exhibit a pattern of diversity and preservation similar to that of the diatoms, although no zonal designations are possible owing to the absence of zonal index species.

The boundary between the Quaternary and the upper Pliocene occurs within lithostratigraphic Subunit IA near the base of Core 113-695A-1H where the siliceous microfossil groups exhibit a marked increase in both diversity and preservation and the calcareous components are no longer present. Diatom evidence, however, suggests that a short hiatus or disconformity exists in the uppermost Pliocene. Thus the boundary between these two epochs may not be completely preserved. Lithostratigraphic Subunits IB–ID and Unit II are composed primarily of diatom, silty, and clayey mud extending to Core 113-695A-37X. These units incorporate all of the upper Pliocene and much of the expanded lower Pliocene. Within the unit, agglutinated benthic foraminiferal assemblages are dominated by *Milliammina* and/or *Martinotiella* species, genera which appear to cement their tests with silica. Their abundant occurrence in the biosiliceous intervals of Hole 695 supports previous observations that these genera are associated primarily with diatomaceous sediments (Echols, 1971). The siliceous microfossil groups, including diatoms, radiolarians, and silicoflagellates, are abundant, and in general, well preserved through this unit, thus allowing delineation of the respective upper and lower Pliocene biozones. As a result, biostratigraphic calibration against a detailed paleomagnetic record should be enhanced. Evolutionary and paleoceanographic studies will also be aided by the expanded nature of this biosiliceous Pliocene record.

The top of lithostratigraphic Unit II is placed in Core 113-695A-23X where the abundance of diatoms drops to approximately half of that of Unit I. Diversity and preservation of siliceous fossils, however, is similar to that of Unit I. Agglutinated benthic foraminiferal assemblages occurring at the top of the unit are dominated by *Martinotiella*, but benthic foraminiferal abundance decreases through the unit.

Lithostratigraphic Unit III occurs between Cores 113-695A-37X and -41X and is composed of silty mud. Here the abundance of siliceous microfossils is very low and preservation poor. Diatoms are represented by only a few rare species which precludes delineation of zonal boundaries. Radiolarians are likewise poorly represented in this interval, and silicoflagellates are absent. This pattern of reduced productivity and poorer preservation in the lowermost Pliocene seems to be widespread, occurring also in the Indo-Pacific sector of the Southern Ocean. During this interval, Subantarctic radiolarians extended their range into the Antarctic region. The poor preservation of radiolarian assemblages at the base of the section precludes precise location assignment of the Miocene/Pliocene boundary. The rare occurrence of *Cycladophora spongothorax* in Cores 113-695A-40X and -41X suggests that the boundary was reached before the hole was terminated at 341 m.

PALEOMAGNETISM

Site 695 is located on the southern part of the South Orkney microcontinent. It lies in the path of Antarctic intermediate water at a depth of 1300 m and was expected to be a site for high-resolution studies of a Neogene sediment sequence. The natural remanent magnetization (NRM) vector from 370 samples was measured to provide a well-constrained magnetostratigraphy although recovery was somewhat less than 50% in the lower half of the hole.

Figure 27A shows a well-defined bimodal distribution of NRM inclination values with two extremes near the expected value for axial dipole field inclination of 75°. Extremely low magnetiza-

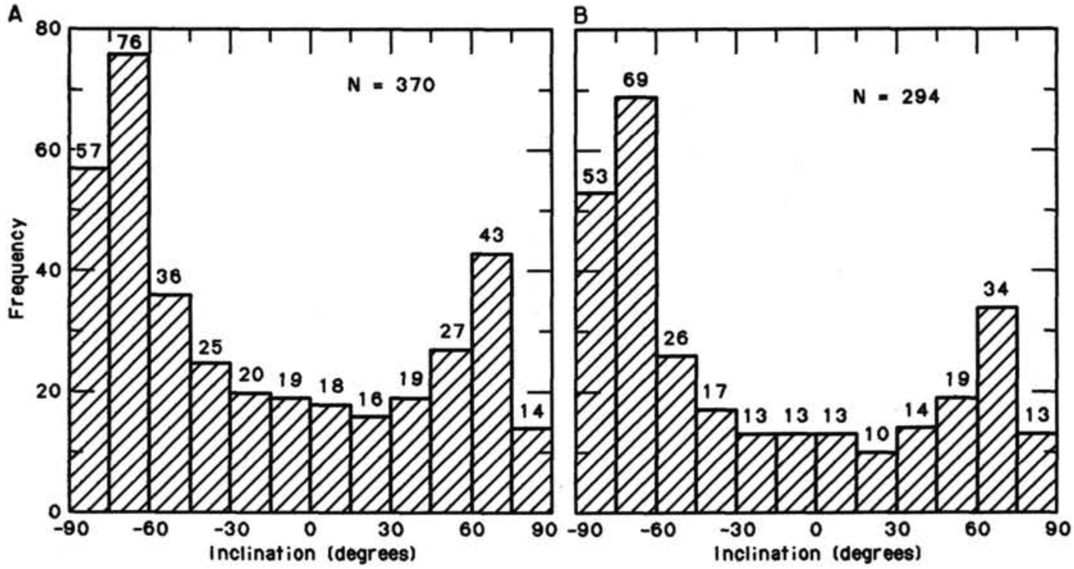

Figure 27. Distribution of NRM inclination values for Hole 695A. A. All samples. B. Samples with intensity higher than 0.1 mA/m.

tion intensities were found at certain depth intervals between 20 and 190 mbsf, which ranged into the noise level of the minispin magnetometer. To evaluate the influence of the weakly magnetized samples, those samples with an NRM intensity below 0.1 mA/m have been excluded from the data set. Figure 27B illustrates the inclination value distribution of the remaining 294 samples. The form of the distribution is not significantly changed, indicating that the sediments at Site 695 preserve a reliable record of the past geomagnetic field behaviour. However, for definition of magnetozones only those samples with intensities greater than 0.1 mA/m were used, except for refining some boundaries where using data from the very weakly magnetized samples was occasionally necessary.

The downhole variation of NRM inclination (Fig. 28) shows a clear polarity pattern, although a straightforward assignment to the Pleistocene and Pliocene part of the geomagnetic polarity time scale is not possible. Using the available biostratigraphic age constraints, most of the sedimentary sequence was deposited during the Pliocene (10–340 mbsf), with a dramatic decrease in sedimentation rate in the upper Pliocene. A high resolution sequence throughout the Gilbert Chron interval reveals more reversals than expected by comparison with the geomagnetic polarity timescale, and for unequivocal assignment, further shore-based demagnetization studies on most of the samples are needed. Our data for the Gilbert Chron suggest that some previously unrecognized short polarity events or magnetic excursions may be preserved in the sedimentary record at Site 695. Figure 29 shows a preliminary interpretation of the inferred downhole polarity pattern with two explanations. Version A assumes a constant sedimentation rate through most of the lower Pliocene (approximately 240 m/m.y. between 89 and 305 mbsf), beginning with an increase in the lowermost Pliocene and a decrease toward the upper lower Pliocene, which slowly changes to a low sedimentation rate in the Pleistocene (4–8 m/m.y.). The alternative, version B, is closer to the biostratigraphic age determinations (see "Sedimentation Rates" section, this chapter) although the variation in sedimentation rate in the lower Pliocene is higher.

The variation in NRM intensity (Fig. 28) shows a remarkable decrease with depth at a level of about 20 mbsf. This effect denotes a dilution of the ferromagnetic sediment component by high biogenic productivity coupled with an increase in the nonmagnetic terrigenous clay fraction. Down to 190 mbsf extremely weak NRM intensities were measured; these samples will have to remeasured with more sensitive cryogenic magnetometers to provide a more reliable NRM magnetostratigraphy for these intervals. Below 190 mbsf a distinct increase in intensity occurs, associated with a higher content of ice-rafted detritus and the coarse-grained sediment fraction. If the sedimentation rate remained constant in the early Pliocene, as suggested by the age-depth relationship (Fig. 29), the input of magnetic material must have changed by as much as a factor of 10.

SEDIMENTATION RATES

Biostratigraphic and Magnetostratigraphic Data

The sedimentation rate curve for Site 695 (Fig. 30) is constructed from two different sources of data. Biostratigraphic ages derived from diatoms, radiolarians, and silicoflagellates provide one source of age information for Site 695. Biostratigraphic data used to construct the age-depth relationship (Table 9) consist of selected datum levels and zonal assignments which have been correlated with the chronostratigraphic scale. The accuracy of the calibration between biostratigraphy and chronostratigraphy varies considerably for different fossil groups and time intervals. In particular, the age given in the literature for the *Distephanus boliviensis* last appearance datum (LAD) (silicoflagellates) ranges from 2.5 to 3.2 Ma. The age-depth curve is constructed as follows. Biostratigraphic data points (boxes, vertical/horizontal lines) are labeled with identifying numbers (Table 9). Magnetostratigraphic data in comparison are shown as line segments with unlabeled datum points (solid boxes). Error boxes for paleomagnetic data represent in depth the distance between two samples of different polarities assigned to different magnetozones. From the preceding and the following magnetozone boundaries a sedimentation rate, and from this a corresponding error in the age determination, is calculated. This age error is represented by the horizontal box size. Biostratigraphic data are of three types. First and last occurrences of species are known only to occur within a finite depth interval, although the age of the datum is generally reported without any associated error estimate. These data thus plot as vertical lines. Age ranges

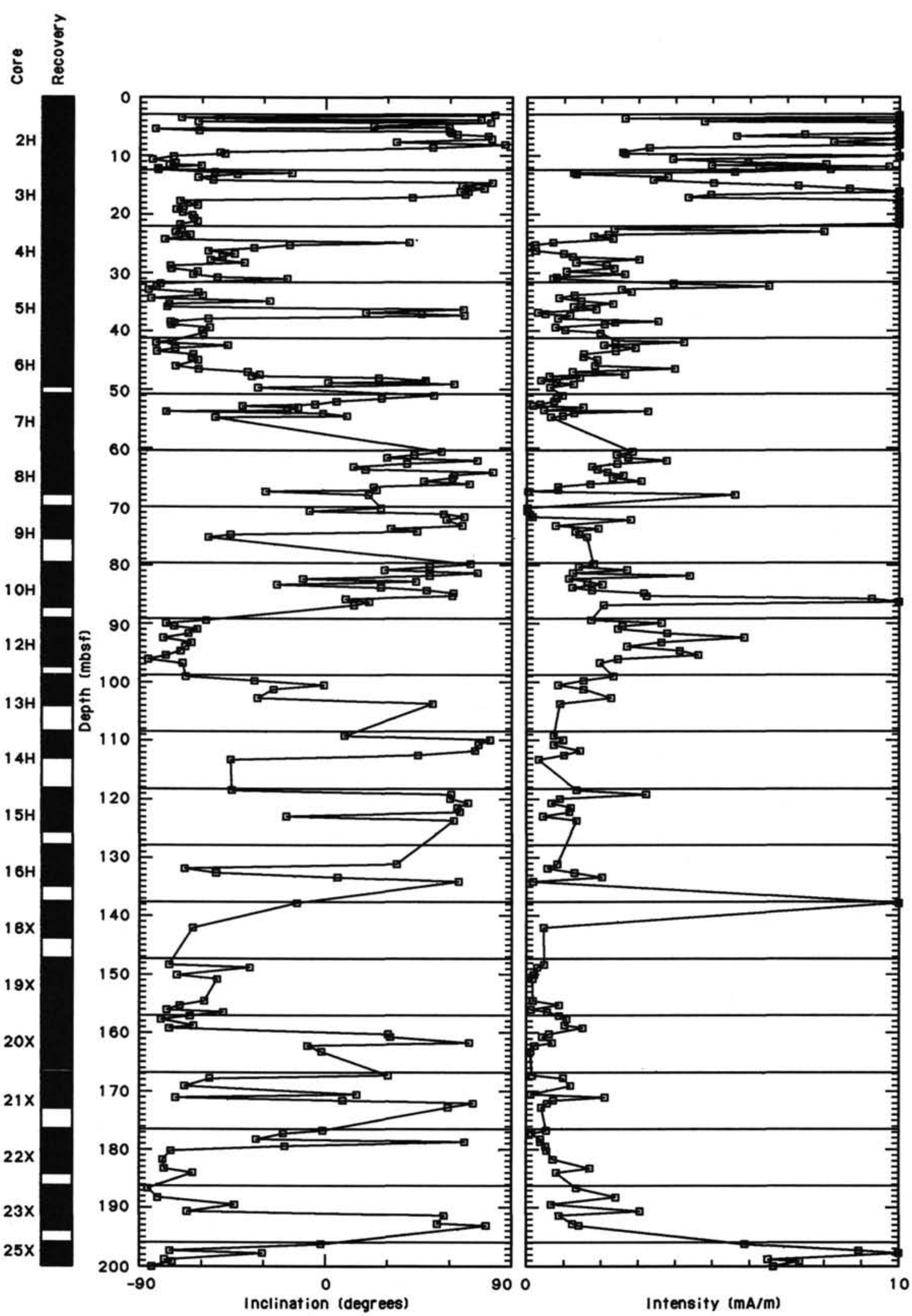

Figure 28. Downhole variation of NRM inclination and intensity for Hole 695A. NRM intensities in the upper three cores range between 1 and 10 mA/m and increase in the lowermost Core 113-695A-41X to 15 mA/m (off chart). Note intensity scale change at 200 mbsf.

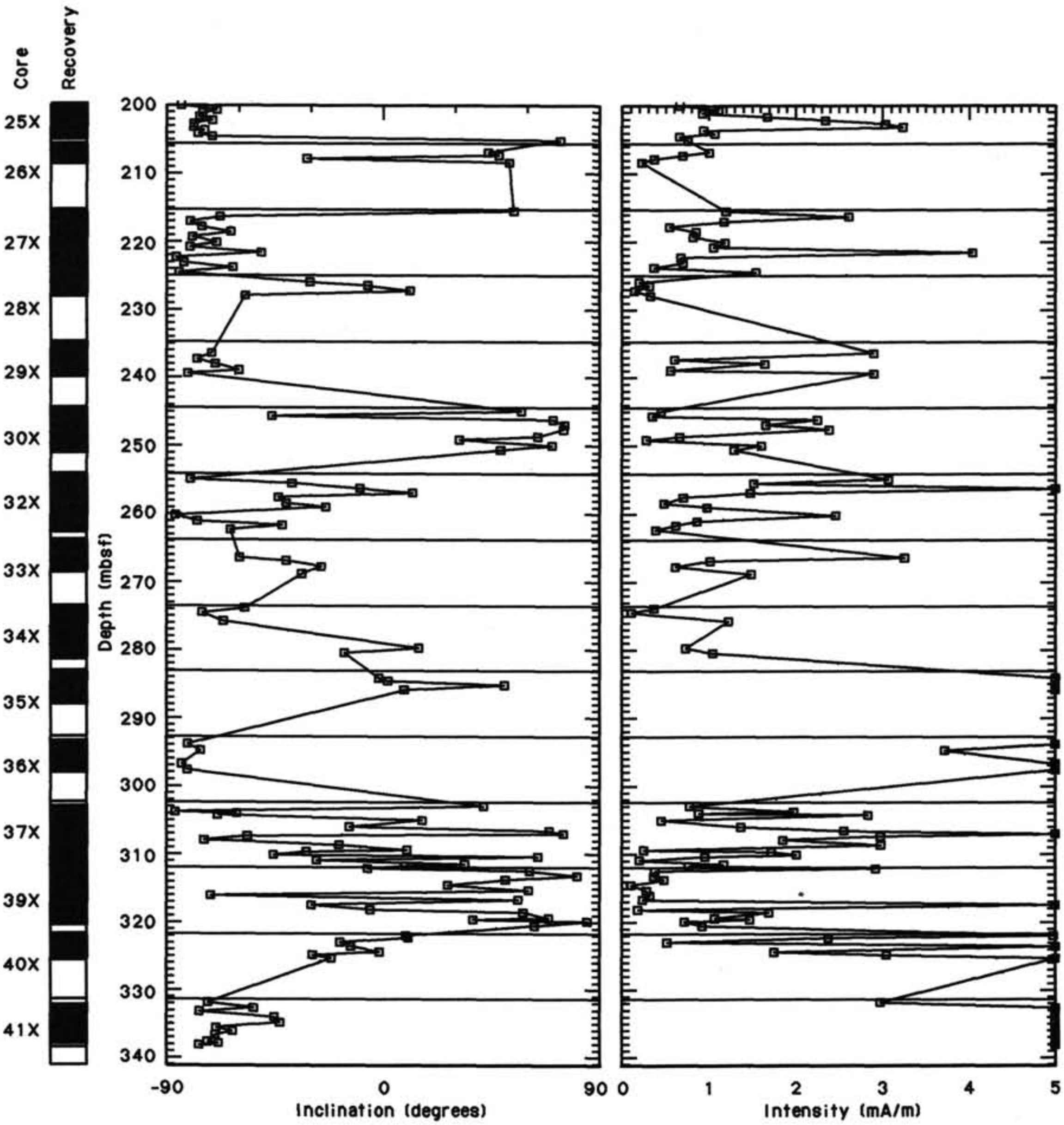

Figure 28 (continued).

for individual samples by contrast have a finite age range but do not have any depth uncertainty, and plot as horizontal lines. Finally, a few first appearance datums (FAD's) and last appearance datums (LAD's) for which uncertainty estimates are available are plotted as boxes. Many samples have more than one age-range estimate from different fossil groups. To make the overlap between multiple dates clear, small solid circles are used to mark the end of each datum which plots as a line. FAD's and LAD's represent, respectively, the oldest and youngest possible ages for a depth interval. Arrows are plotted to indicate datums of this type, with the direction indicating the time direction during which the species occurs.

Magnetostratigraphy provides a second source of age information. Magnetic polarity data were correlated with the geomagnetic polarity reversal time scale of Berggren et al. (1985) (see "Explanatory Notes" chapter, this volume, and "Paleomagnetism" section, this chapter) without recourse to biostratigraphic data. The preliminary interpretation is based on the assumptions of fairly constant sedimentation and a minimum number of hiatuses.

Sedimentation Rates and Hiatuses, Site 695

The Pleistocene and upper Pliocene are marked by lower rates of deposition than most of the section. These rates are on average less than 5 m/m.y. (Fig. 29, version A) for the Pleistocene, based on paleomagnetic data. According to this, the uppermost Pliocene may be absent due to a hiatus or may be present in a condensed section.

Paleomagnetic and biostratigraphic data are generally in close agreement for the remainder of the Pliocene/Pleistocene, where sedimentation rates of 90, 215, and 105 m/m.y. (18–90, 90–245, and 245–330 mbsf) are determined from the magnetostratigraphic assignment (solid line, A) to the geomagnetic polarity time scale (Fig. 30). Although the mean NRM intensity is weak, a clear

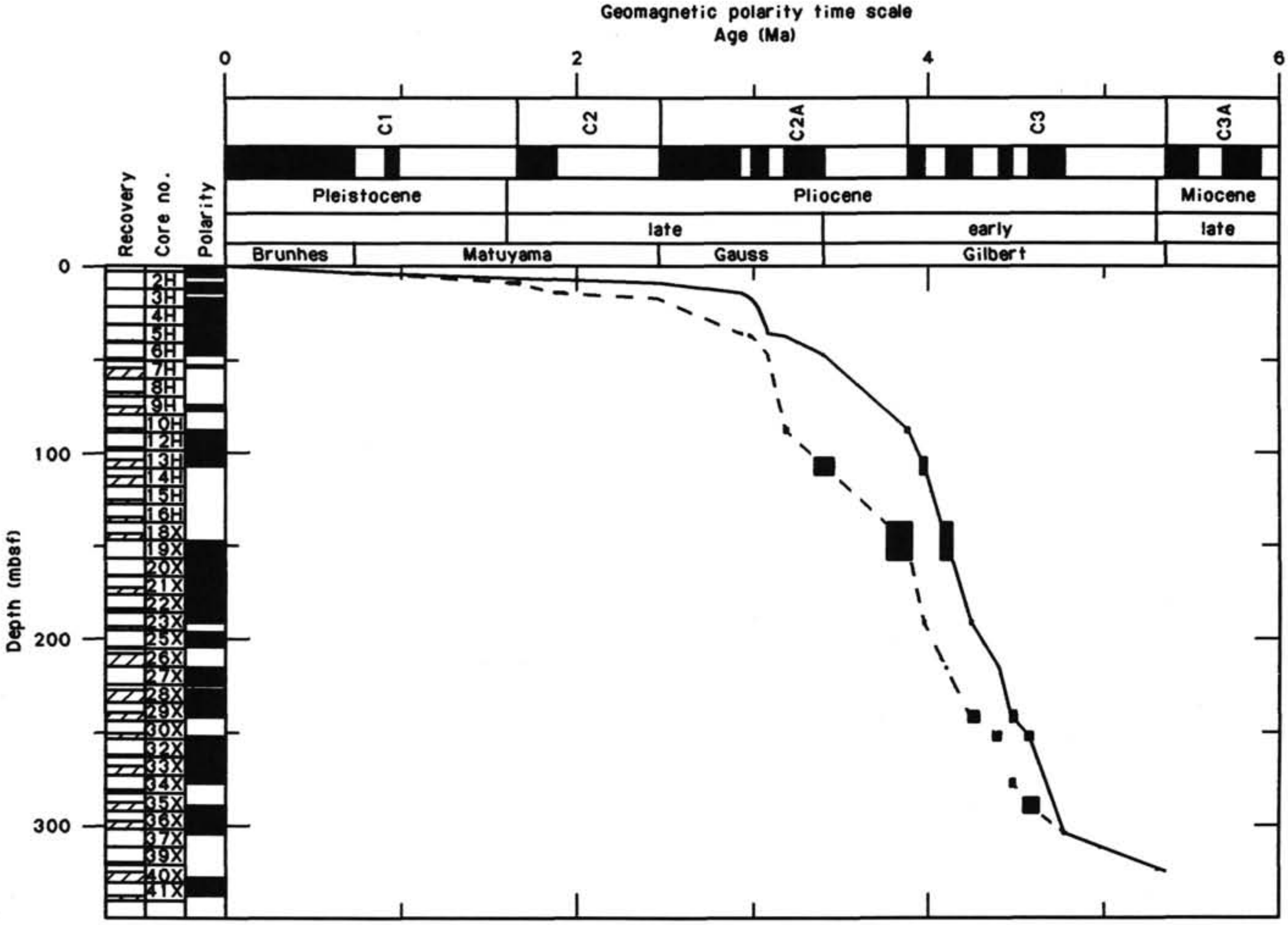

Figure 29. Preliminary assignment of the inferred polarity pattern for Hole 695A. Two interpretations are shown. Version A (solid line) retains a constant sedimentation rate for the whole sequence with abrupt changes at both ends of this interval. Version B (dashed line) is a biostratigraphically-constrained sedimentation rate curve with smoother changes.

polarity pattern could be extracted tentatively from downhole NRM inclination variation. More magnetozones than expected from the geomagnetic polarity time scale are available for assignment of the inferred polarity pattern to the Pliocene reversal sequence. For this reason an unequivocal age assignment is impossible from shipboard paleomagnetic data, and two preliminary magnetostratigraphic interpretations are presented. Version A (solid line) is used to derive sedimentation rates, which remain constant over longer time periods. Version B (dashed line) is in closer agreement to the lower Pliocene biostratigraphic data, although the calibration precision of siliceous microfossil zonation still needs improvement. The sedimentation rates vary considerably for the different interpretations, but generally increase during the lower Pliocene and decrease toward the upper Pliocene with an extremely low sedimentation rate in the Pleistocene. Version B shows two intervals of high sedimentation rate between 3.1 and 3.2 Ma and between 3.9 and 4.3 Ma with a lower rate in the interval between. The high-resolution sequence of the Gilbert Chron might reveal an opportunity for detection of some previously unrecognized short polarity events which cause the problems in magnetostratigraphic interpretation of this sequence. Alternatively a late Miocene age for the lower part of Hole 695A (below 250 mbsf) may be suggested from paleomagnetic data, although it is in conflict with biostratigraphic evidence.

INORGANIC GEOCHEMISTRY

Introduction and Operation

Data on the chemical composition of interstitial water are presented for Hole 695A. Hole 695A was cored with the XCB from 137.6 to 341.1 mbsf following APC coring down to 137.6 mbsf. Fourteen whole-round sediment samples (nine of 5-cm and five of 10-cm thickness) were analyzed. For the potential study of gas hydrates the *in-situ* pore water extractor was run five times. Four samples were recovered and analyzed. Also, the chloride concentration of the seawater used for circulation was monitored. The chemical composition of the drilling-mud filtrate was taken from analyses carried out at Site 693 (see "Inorganic Geochemistry" section, "Site 693" chapter, this volume). Chemical data are summarized in Tables 10 and 11. For details on sampling and analytical procedures see "Explanatory Notes" chapter (this volume).

Evaluation of Data

Data From Whole-Round Samples

For overall evaluation of the data, a charge balance was carried out. As with previous sites this was conducted assuming that the sodium-to-chloride ratio is that of present-day seawater.

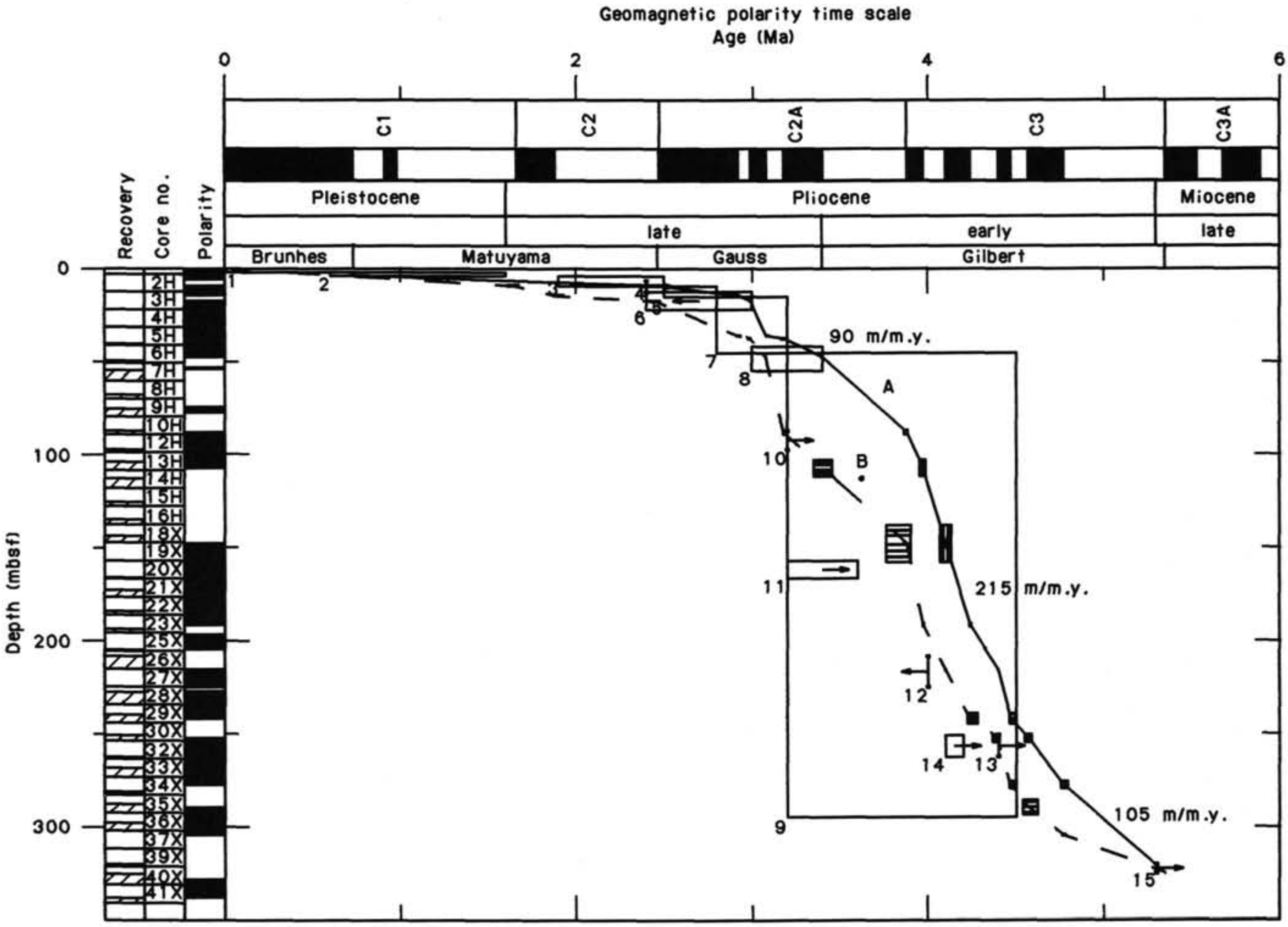

Figure 30. Age-depth interpretation of Site 695. Versions A (solid line) and B (dashed line) and construction of figure are discussed in text.

The calculations reveal a 1.0%–1.5% excess negative charge in all samples. A similar imbalance was detected at the previous sites of Leg 113 and was inferred to indicate variable Na/Cl-ratios, probably brought about by uptake of sodium during formation of clays. No special analytical difficulties were encountered at Hole 695A.

Chloride abundance at Section 113-695A-39X-3 is lower than expected. At Site 693 low chloride concentrations correspond to intervals where drilling mud had been used. Drilling mud was also used during recovery of Core 113-695A-37X. The "core" between 113-695A-37X and 113-695A-39X was the fourth run of the *in-situ* pore water extractor. According to the drilling log the tool penetrated 70 cm of the top of Core 113-695A-39X. On the Visual Core Description form the state of this core is described as moderately disturbed, thus most probably the low chloride level in this core is caused by dilution by drilling-mud filtrate. The data on this sample (Sample 113-695A-39X, 115–125 cm) are corrected using the drilling-mud filtrate composition established at Site 693 (see Table 11 and Fig. 31).

Data for Pore Waters Extracted In Situ

On seismic profiles obtained during the site survey, a BSR interpreted as the base of a gas-hydrate-bearing zone was observed. An *in-situ* pore water extractor was employed to study the mechanisms of clathrate formation.

To prevent leaking during descent and assure proper behavior of the pressure transducers, the tool is filled with distilled water prior to lowering. In cases with incomplete filling of the sample coil, normal procedure has been to use the chloride data to establish the degree of dilution. However, in geological settings where the concentration of chloride is expected to vary (as where clathrates form), the distilled water must be labeled with a tracer. The tracer should meet the following specifications:

1. Zero or constant concentration in natural waters.
2. Stable during sampling.
3. Compatible with the constituents of pore water.
4. Have low affinity for steel surfaces.
5. Be easily and reliably detected in small concentrations.

With the reagents available on board, potassium chromate was used for the following reasons:

1. The chromate ion adsorbs light very strongly at 373 nm, enabling its concentration to be determined with good accuracy down to 1 ppm.
2. Spectrophotometric measurements are fast and reliable.
3. Shipboard measurements show it to be stable in solution for several weeks and that from a 100-ppm solution, absorption to steel surfaces in the sampling coil is undetectable even for 48-hr contact. Futhermore, there is no salt effect at 373 nm, and
4. In these concentrations (less than 100 ppm) chromate is compatible with the constituents of seawater. In organic-rich sediments a possible source of interference involves the presence of other dissolved chromophores absorbing at the actual wavelength. Their presence is established by scanning the sample from the ultraviolet through the visible spectrum.

Table 9. Biostratigraphic data used to construct sedimentation rate, Figure 30.

Datum no.	Depth range (mbsf)	Age (Ma)	Datum or Zone
1	0.0-2.0	0.0-0.6	*C. lentiginosus* Zone—D
2	2.0-4.0	0.6-1.6	*C. elliptopora/A. ingens* Zone—D
3	4.0-9.5	1.9-2.5	*C. kolbei/R. barboi* Zone—D
4	6.4-12.4	2.4	LAD *D. spongiosa* + *H. vema*—R
5	9.5-15.5	2.5-2.8	*C. insignis* Zone—D
6	12.4-22.0	2.4-3.0	FAD *C. davisiana*—R
7	15.5-45.5	2.8-3.2	*N. interfrigidaria* Zone—D
8	42.0-55.0	3.0-3.4	Transition Zone *N. praeinterfrigidaria-N. interfrigidaria*—D
9	45.5-295.0	3.2-4.5	*N. angulata/N. reinholdii* Zone—D
10	87.4-97.4	3.2	LAD *D. boliviensis*—S
11	157.0-166.5	3.2-3.6	LAD *P. titan*—R
12	208.5-225.0	4.0	FAD *H. vema*—R
13	251.0-262.5	4.4	LAD *L. grande*—R
14	251.1-262.7	4.1-4.2	LAD *D. pseudofibula*—S
15	320.5-325.0	5.3	LAD *C. spongothorax*—R

Key to table: Depth range given for first and last appearance datums (FAD's and LAD's). A single value in both depth columns indicates a sample with a zonal or assemblage age assignment. Age range given for zones, and in some instances, for uncertainty in age calibration of a FAD or LAD. Letters following each datum name refer to the fossil group: D = diatom, R = radiolarians, and S = silicoflagellates.

Table 10. Summary of results of *in-situ* pore water sampling program, Site 695.

Core	Depth (mbsf)	Type of water recovered
113-695A-		
11I	80.9	Uncontaminated interstitial water.
17I	138.3	100% labeled water (valve did not open).
24I	196.6	Seawater mixed with some pore water.
31I	254.8	45.7% labeled water, 54.3% pore water.
38I	312.0	Seawater mixed with some pore water.

The *in-situ* pore water extractor was employed at five depths (Table 10). Because of large depths and the potential presence of clathrates, dry formations were expected, and thus small (25 mL) sample coils were used. The sulfate data (Table 11) clearly demonstrate the presence of seawater in Cores 113-695A-24I and 113-695A-38I. This is confirmed by the high magnesium levels (compared with data on neighboring samples). The chloride concentration of the seawater used for circulation (539 mmol/L) is too close to that of pore water to allow a reliable correction to be carried out, also this would not provide any new information.

In order to demonstrate the feasibility of the tracer technique, the measured and corrected concentrations for Core 113-695A-31I are compared in Table 11 and on Figures 31A-31K. Scanning the sample from 300 to 900 nm did not reveal any absorption peaks not present in the standard.

Chlorinity and Salinity

Chloride data are presented in Figure 31A and Table 11. Because the presence of gas hydrates was suspected, varying chloride concentrations were expected (Harrison et al., 1982); thus special attention was paid to the chloride analysis. Chloride was monitored as coring proceeded, and analyses were repeated after completing sampling. The data presented in Figure 31A and Table 11 are the means of four to six replicate runs. Small (less than 2%), but significant, variations in chloride values ranging from 571.9 mmol/L at 72.7 mbsf (Section 113-695A-9H-2) to 560.0 mmol/L at 180.7 mbsf (Section 113-695A-22X-3) are observed (only data from whole-round cores are considered). To accommodate all data, the scale on Figure 31A is too large for these variations to be observed. At present there is no satisfactory interpretation of these variations. However, contamination by distilled water used for rinsing of equipment must be considered. There are no indications of gas hydrate formation.

The chloride data demonstrate how accurately the tracer technique allows the real pore water data to be calculated. By interpolating between the chloride data from Cores 113-695A-36X and 113-695A-41X, a 7% dilution of the sample by drilling-mud filtrate was calculated at Section 113-695A-39X-3. This figure is used to correct the other parameters on this sample.

Using the salinity/chlorinity relation provided by Stumm and Morgan (1981) and assuming constant density equal to that of 35 g/kg seawater, the highest and lowest chloride concentrations correspond to 35.4 and 34.6 g/kg, respectively.

The average salinity measured using the optical refractometer is 0.9 g/kg units lower than values calculated from the chloride data. There is a significant ($n = 8$, $P = 0.95$) correlation between salinity and chloride concentration. This correlation, however, breaks down when the single low (18 g/kg) reading on the diluted downhole sample (Core 113-695A-31I) is excluded.

pH

The pH (Fig. 31B and Table 11) exhibits systematic variations peaking at pH 8.40 and 8.30 at 122.4 and 259.9 mbsf, respectively (Cores 113-695A-15H and 113-695A-32X). These variations are not related to any changes in the major lithology (as observed from smear slides). The average pH (8.0) is similar (within experimental accuracy) to the average pH measured at Site 694 (pH = 8.1) and Site 693 (pH = 8.0) and higher than the average pH measured in carbonate-rich sediments at Sites 689 and 690 (pH = 7.7).

Alkalinity, Sulfate

The alkalinity data are presented in Figure 31C. The alkalinity increases steadily from 3.72 meq/L at 4.45 mbsf (Section 113-695A-1H-3) to 12.37 meq/L in the deepest sample (Core 113-695A-41X) at 335.8 mbsf. Due to small sample volumes, alkalinity was not titrated on samples obtained with the *in-situ* pore water tool. The high alkalinity reflects the high (relative to the other sites at Leg 113) bacterial activity, but is also exaggerated by the very high rates of sedimentation (see "Sedimentation Rates" section, this chapter). High rates of sedimentation render diffusive exchange with the seawater less efficient, making the pore water evolve more like a closed system. Below 50 mbsf most of the alkalinity is probably produced by sulfate-reducing bacteria. Assuming stoichiometric oxidation and diffusion coefficients of a similar order of magnitude, the alkalinity is lower than expected from the sulfate profile, indicating that substantial amounts of alkalinity have been removed (see "Calcium" and "Magnesium" discussions below).

The sulfate profile is presented in Figure 31D. The concentration of sulfate is constant at about sea water values (29 mmol/L) in the upper 50 mbsf and decreases linearly to zero at 340 mbsf (extrapolated). This is the most extensive sulfate reduction encountered during Leg 113 and is related to the shallower water of the site (more organic matter escapes oxidation in the water column), high primary productivity, and high sedimentation rates. At this site, the classical transition from sulfate reduction to methane production is observed (see "Organic Geochemistry" section, this chapter), demonstrating that even below 300 mbsf there is ample organic matter to sustain microbial activity. Smear slide inspection revealed the presence of considerable amounts of opaque minerals, many of which are likely to be sulfides.

Table 11. Summary of shipboard interstitial water data, Site 695.

Core, section, interval (cm)	Depth (mbsf)	Vol (mL)	pH	Alk. (meq/L)	Sal. (g/kg)	Mg (mmol/L)	Ca (mmol/L)	Cl (mmol/L)	SO_4 (mmol/L)	PO_4 (μmol/L)	K (mmol/L)	NH_4 (mmol/L)	SiO_2 (μmol/L)	Mg/Ca
113-695A-														
1H-3, 145–150	4.45	63	7.86	3.72	34.2	52.15	10.66	557.0	29.7	3.5	12.0	0.04	527	4.9
3H-4, 120–125	18.10	46	7.92	3.78	34.4	52.02	10.75	561.7	29.4	4.2	11.5	0.11	760	4.8
6H-3, 120–125	45.40	57	8.00	5.23	34.4	51.27	10.97	564.0	28.3	7.9	10.3	0.34	727	4.7
9H-2, 120–125	72.70	80	8.00	7.07	35.6	49.56	11.39	571.9	24.1	9.0	9.3	0.61	875	4.4
12H-4, 120–125	94.90	55	8.11	7.95	34.6	45.33	11.38	562.5	21.9	8.3	8.8	0.86	1035	4.0
15H-3, 120–125	122.40	60	8.40	8.14	34.2	44.79	11.27	568.3	19.0	5.1	7.7	0.97	950	4.0
19X-4, 120–125	153.00	76	7.78	9.35	34.0	42.56	11.48	566.0	17.6	5.8	9.2	1.17	921	3.7
22X-3, 120–125	180.70	53	7.78	9.62	33.9	39.45	11.35	560.0	14.1	4.1	8.0	1.31	975	3.4
25X-3, 120–121	200.10	50	7.84	9.86	33.9	38.66	11.46	561.6	13.8	4.0	7.8	1.33	1117	3.4
29X-2, 115–125	237.35	50	8.17	10.99	33.6	34.06	11.86	561.0	9.3	4.0	7.8	1.64	1125	2.9
32X-4, 115–125	259.75		8.30	11.10	33.7	32.41	11.97	565.5	7.7	3.6	7.7	1.76	1073	2.7
36X-2, 115–125	295.45	50	7.91	12.32	33.1	30.29	12.43	566.5	5.3	2.4	7.4	1.61	1108	2.4
39X-3, 115–125	316.15	60	7.75	12.17	31.8	26.83	11.89	539.6	2.6	2.2	6.0	1.56	1117	2.3
41X-3, 140–150	335.80	45	8.08	12.37	32.6	26.39	12.81	571.4	1.2	3.1	5.5	1.57	994	2.1
11I	89.90				34.6	46.09	11.16	563.0	23.1	2.8	8.4	0.68	1079	4.1
24I	196.60				34.0	44.30	11.32	552.7	20.5	2.2	6.3	0.97	748	3.9
31I	254.80				18.0	22.24	6.17	305.8	5.6	1.3	4.5	0.71	408	3.9
38I	312.70				33.9	43.80	11.30	544.1	20.9	0.4	8.1	0.65	410	3.9
[a]31I	254.80				33.2	40.99	11.38	563.5	10.3	2.4	8.3	1.31	752	3.9
[b]39X-3, 115–125	316.15	60				28.68	12.53	569.6	1.8	1.7	6.3	1.64	1161	2.3
Drilling-mud filtrate			9			2.14	3.37	141.2	13.1	8.9	1.6	0.52	529	0.6

[a] Corrected for dilution by water initially in the sampler.
[b] Corrected for dilution by drilling-mud filtrate.

Phosphate and Ammonia

The concentration profile for phosphate is presented in Figure 31E and Table 11. The concentration of phosphate increases from 3.5 μmol/L in the upper section (Section 113-695A-1H-3), peaks at 9.0 μmol/L at 72.7 mbsf (Section 113-695A-9H-2), and drops to a level of about 3 μmol/L below 300 mbsf. The concentrations of phosphate at Site 695 are the highest encountered during Leg 113, again attributed to high bacterial activity and high rates of sedimentation. The pronounced subsurface maximum (Section 113-695A-9H-2) is probably caused partly by desorption of phosphate from ferric hydroxides and oxyhydroxides (Stumm and Leckie, 1970) as these get buried beneath the redox boundary.

Phosphate is the parameter for which the discrepancy between samples obtained by the two different sampling techniques is greatest. This is caused by the large surface-area-to-volume ratio of the sampling coil, and the high affinity of phosphate for steel surfaces.

The concentration of ammonia (Fig. 31F and Table 11) increases from 0.04 mmol/L in the shallower section (Section 113-695A-1H-3) and peaks at 1.76 mmol/L at 259.75 mbsf (Section 113-695A-32X-4) below which only minor variations take place. The concentration of ammonia is higher than observed at any of the previous sites during Leg 113. This is in keeping with the observations of alkalinity, phosphate, and sulfate. The almost stable level below 260 mbsf represents the depth where the rate of processes removing ammonia from the pore water (mainly absorption and ion exchange processes; Berner, 1974) equals or exceeds the rate by which ammonia is generated microbially.

The cause of the poor correlation between the ammonia analyses of the water collected downhole and the water squeezed from whole rounds is not immediately obvious. However, as the labeled water was not deoxygenated, it is possible that some ammonia has been oxidized to nitrite or nitrate.

Calcium and Magnesium

Calcium and magnesium data are presented in Figures 31G and 31H, respectively. The concentration of calcium increases linearly from close to the seawater value (10.66 mmol/L) at 4.45 mbsf (Section 113-695A-1H-3) to 12.81 mmol/L in the deepest sample (Section 113-695A-41X-3). The increase in calcium concentration with depth is lower than that recorded at any of the previous sites on Leg 113, and is related to the high production of alkalinity. The bicarbonate released during sulfate reduction precipitates calcium released from inorganic sources.

The concentration of magnesium decreases from 52.15 mmol/L in the shallower section (Section 113-695A-1H-3) to 26.39 mmol/L at the base of the drilled sequence (Section 113-695A-41X-3). The removal of magnesium from the pore water is more extensive than observed on any previous site in Leg 113. This could be brought about either by higher reaction rates or slower downward fluxes. The magnesium/calcium ratio vs. depth is shown in Figure 31I.

The correction procedure applied to the sample from Core 113-695A-31I gives a poor result for magnesium. It is possible that the labeled water with which the downhole tool was initially filled has become contaminated by an alloy in the high-pressure pump used for filling the tool.

Potassium

The concentration profile for potassium is shown in Figure 31J. The concentration of potassium decreases erratically from 12.0 mmol/L at 4.45 mbsf (Section 113-695A-1H-3) to 5.5 mmol/L in the lower sample (Section 113-695A-41X-3). This trend is commonly observed in marine sediments and was observed at all previous Leg 113 sites. The decrease in potassium is probably related to reversed weathering processes (Mackenzie and Garrels, 1966; Manheim and Sayles, 1974).

Dissolved Silica

The concentration of dissolved silica (Fig. 31K) varies between 527 μmol/L in the shallower section (Section 113-695A-1H-3) and 1125 μmol/L at 237.35 mbsf (Section 113-695A-29X-2). As observed at Site 693 below 100 mbsf there is a plateau of about 1000 μmol/L (1060 and 1050 μmol/L at Site 693 and Site 695 respectively). At both sites diatoms and quartz are abundant, yet the concentrations of dissolved silica fall within that predicted (with the thermodynamic data provided by Stumm and Morgan, 1981) for saturation with respect to quartz and amorphous silica. However, the concentration plateaus are remarkably similar to that predicted for cristobalite saturation (1.0 mmol/L, Stoeber, 1967). Data on dissolved silica are not sufficient alone to determine which phase controls its concentration.

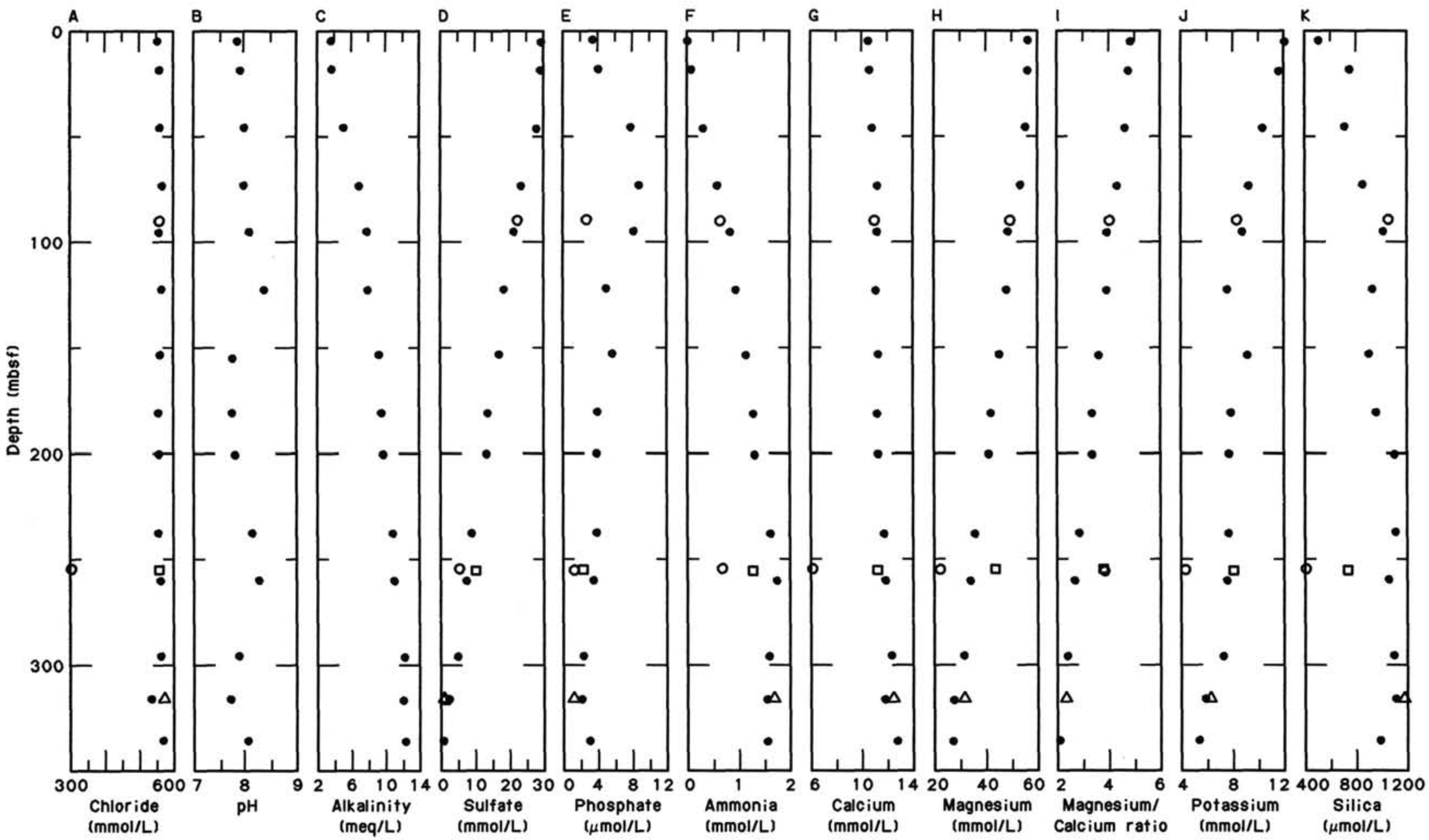

Figure 31. Concentrations vs. depth for Hole 695A. A. Chloride. B. pH. C. Alkalinity. D. Sulfate. E. Phosphate. F. Ammonia. G. Calcium. H. Magnesium. I. Magnesium/calcium-ratio. J. Potassium. K. Silica. Circles are for measurements made from *in-situ* water samples. Squares are for measurements corrected for dilution by water, and triangles are for measurements corrected for drilling-mud filtrate. Data are given in Table 11.

ORGANIC GEOCHEMISTRY

Light Hydrocarbons

At Site 695, light hydrocarbon levels in and above the 238.85 mbsf sample are extremely low, not exceeding 12.8 μL of methane per liter of moist sediment. However, methane levels increase dramatically, commencing with the 259.75 mbsf sample, as described below. Analytical data are presented in Table 12. Methane/ethane ratios are low at all depths (Table 13). No partings in the core, suggestive of gas pressure within the liner, were observed.

An unusual increase in occluded methane began with the 259.75 mbsf sample. Concentrations increased exponentially (Fig. 32) to the final observed level at 335.8 mbsf, just below which, tool failure terminated drilling. Data are presented in linear format in Figure 33. The build-up in methane was closely monitored. It was unaccompanied by increases in ethane or propane (both of which were close to the lower detection limit), therefore a thermogenic source of gas was considered improbable. Nevertheless, a potential hazard could have been present due to accumulated biogenic gas. Increases of two orders of magnitude over a 100-m depth range are comparable to those developed above gas and oil accumulations.

An explanation of the increase in methane was provided by analytical data pertaining to interstitial waters. Sulfate concentration decreases linearly with depth to approximately zero close to 350 mbsf (see Fig. 31C). Decrease in sulfate is a necessary precursor to the activity of methanogenic bacteria.

An analogous case was described by Presley and Kaplan (1970) at DSDP Site 27, Leg 4, Southwest Atlantic, where sulfate decreases linearly with depth to 249 mbsf. As shown by Goldhaber and Kaplan (1974), the decrease was caused by progressive sulfate reduction during burial, with concomitant change in the sulfur isotope ratio of the residual sulfate, also to 249 mbsf. This infers a process of long duration; in the case of Site 27, from early Miocene to the present. In the case of Site 695 it is inferred that methane generation began when sulfate concentration was reduced below an approximate level of 7 mmol/L at 260 mbsf, in sediments of Miocene age. The methane appears to be geologically young.

Kerogens at Site 695

Rock-Eval and organic carbon data are detailed in Table 14. Carbon is low in the first two samples, 1.45 and 8.85 mbsf, but a few relatively high values are found in deeper samples, compared to other Weddell Sea Cenozoic sections. The average of 19 analyses from 18.35 to 355.80 mbsf is 0.40% organic carbon. At Site 694 the average is 0.34%, at Site 693, 0.17%.

Kerogens at Site 695 are also more reactive upon pyrolysis: numerous samples exhibit hydrogen index (HI) values between 100 and 250 mg of hydrocarbons per gram of carbon, in contrast to the mode at Site 694, 75 HI units, and the average at Site 693, 100 units, (excluding those cases with 0.1% or less organic carbon).

However, the data are difficult to interpret in terms of conventional Rock-Eval criteria. For example, sediments with high values of T_{max}, evidently highly mature, are expected to plot close to the origin of the key diagram (Fig. 34). Here samples with high values plot in the position of immature sediments (triangular symbols, Fig. 34). This phenomenon also occurred at Sites 689 and 690 where unrealistically high values of HI were observed.

A further anomaly is evident in the remaining data. T_{max} measurements are instrumental temperature values which indicate natural thermal exposure in accordance with the following scale:

400°C Immature	(lignite equivalent)	(square, Fig. 34)
440°C Mature	(high-volume bituminous coal)	(dot, Fig. 34)
480°C Highly mature	(low-volume bituminous coal, anthracite)	(triangle, Fig. 34)

Below 8.85 mbsf at Site 695, values average 447°C, though with a substantial range (385°–543°C), representing a wide range of maturities. The corresponding HI and OI values would be expected to be scattered along the evolutionary paths for Types 1 and 2, or Type 3 kerogen. Howevever, observed combinations of HI and OI values are clustered between the two principal pathways. This might be explicable in terms of the rationale of Deroo et al. (1983). They found that the oxidation of planktonic

Table 12. Headspace analyses of light hydrocarbon, Site 695.

Core, section, interval (cm)	Depth (mbsf)	Methane	Ethane	Propane	iC_4	n-C_4	iC_5	n-C_5	iC^6	n-C^6
		Microliters (gas)/liter (sediment)								
113-695A-										
1H-3, 145–150	1.45	3.0	—	—	—	—	—	—	—	4.1
2H-4, 145–150	8.85	4.9	0.8	—	—	—	—	—	—	1.7
3H-4, 145–150	18.35	5.1	—	—	—	—	—	—	—	12.2
4H-4, 145–150	27.95	11.7	1.3	—	—	0.8	—	—	—	31.7
5H-5, 145–150	39.05	8.2	1.6	—	—	1.5	—	—	—	44.0
6H-3, 125–129	45.45	9.8	2.0	—	—	—	—	—	—	39.4
7H-1, 145–150	52.25	10.1	2.0	—	—	2.2		—	—	42.2
8H-3, 145–150	64.85	7.8	2.3	—	—	—	—	—	—	32.3
9H-2, 120–125	72.70	12.8	1.4	—	—	—	—	—	—	33.1
12H-4, 120–125	94.90	6.0	2.0	—	—	—	—	—	—	43.1
15H-3, 120–125	122.40	7.8	1.6	—	—	—	—	—	—	31.9
19X-4, 120–125	153.00	11.4	2.8	—	—	—	—	0.5	—	30.2
20X-4, 147–150	162.97	4.8	1.9	—	—	—	—	—	—	34.4
21X-4, 145–150	172.75	9.0	—	—	—	2.4	—	—	—	—
22X-3, 120–125	180.70	9.4	1.4	0.84	—	1.2	—	0.5	—	32.3
23X-3, 145–150	190.65	7.8	—	—	—	2.1	—	7.5	—	6.4
25X-3, 120–125	200.10	7.1	—	—	—	—	—	—	—	5.6
29X-2, 115–125	237.35	9.1	1.3	—	—	—	—	—	—	18.1
32X-4, 115–125	259.75	19.4	2.4	—	—	—	—	—	—	44.1
36X-2, 115–125	295.45	496.3	1.5	0.9	—	1.0	—	—	—	12.6
39X-3, 115–125	316.15	979.3	0.8	0.7	—	0.7	—	—	—	10.9
41X-3, 140–150	335.8	1640.2	0.9	0.3	—	0.4	—	—	—	11.7

Table 13. Methane/ethane ratios, Site 695.

Depth (mbsf)	Methane/ethane ratio	Depth (mbsf)	Methane/ethane ratio
8.85	6.1	153.00	4.1
27.95	9.0	162.97	2.5
39.05	5.1	180.70	6.7
45.45	4.9	237.35	7.0
52.25	5.1	259.75	8.1
64.85	3.4	295.45	330.9
72.70	9.1	316.15	1224.1
94.90	3.0	335.80	1822.4
122.40	4.9		

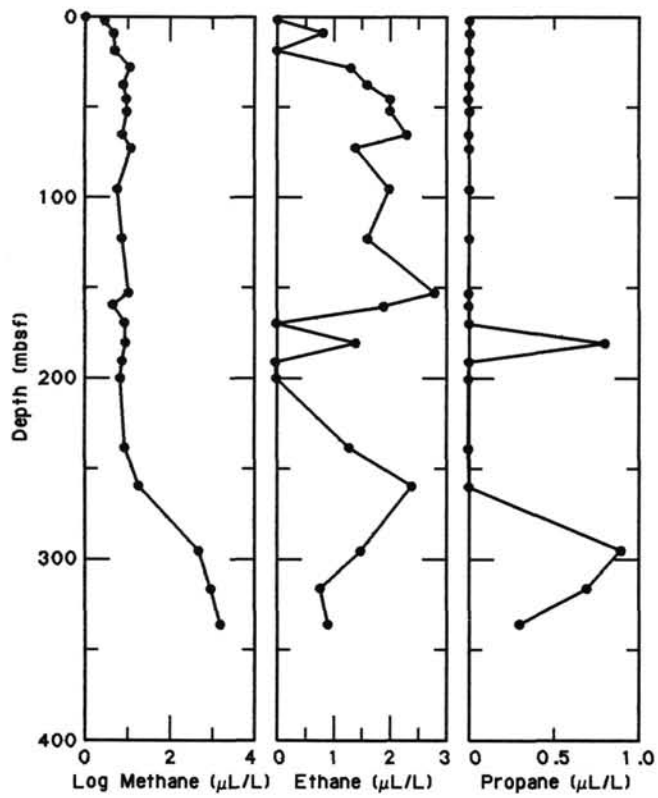

Figure 32. Light hydrocarbon data, Site 695. Methane concentrations plotted on a logarithmic scale.

kerogens, originally of Type 2, caused diminution in both hydrogen and oxygen indices such that data points occurred between pathways, as in the case at Site 695. The lower T_{max} values (<430°C) at Site 695 could represent Cenozoic, first cycle, diatomaceous kerogen. Kerogens of intermediate T_{max} values (>430°C, <480°C), such as occur at 39.05, 52.25, and 259.75 mbsf, could speculatively be assigned a Mesozoic provenance. The highly mature kerogens (T_{max} >480°C) could be of Paleozoic origin. Both of the latter types would clearly be recycled.

DOWNHOLE MEASUREMENTS

Introduction

One of the main objectives of heat flow measurements at Site 695, east of the South Orkney microcontinent, was to learn about the origin of a prominent BSR, considered to represent the presence of a gas hydrate. Drilling this site was expected to provide the chance for further geophysical and geochemical investigations of gas hydrate characteristics.

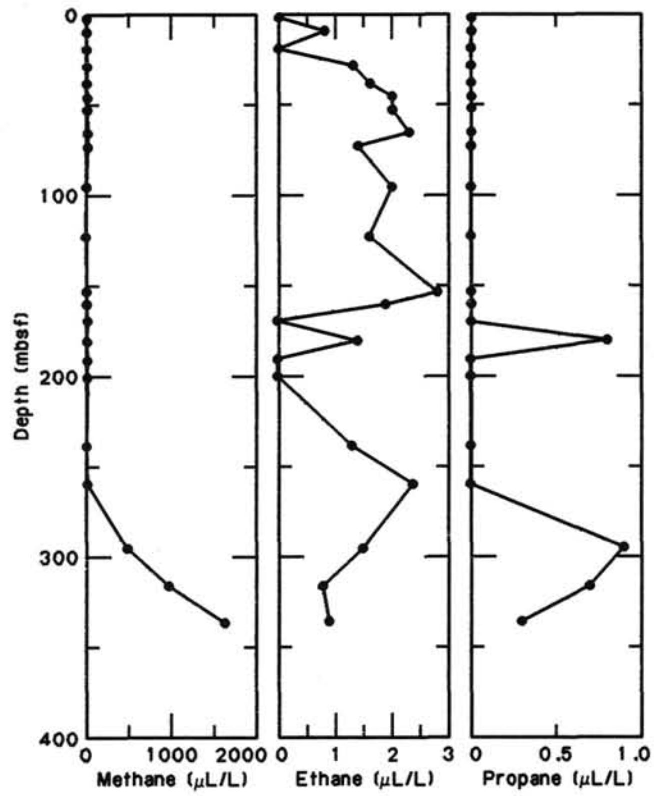

Figure 33. Light hydrocarbon data (Table 12), Site 695. Methane concentrations plotted on a linear scale.

Temperature Measurements

At Hole 695A, the Von Herzen APC temperature recording device #1 (VH-probe #1) and the temperature recording instruments for the pore water sampler (Uyeda/Kinoshita probe, T-probe) #12 and #14 were used eight times (Cores 113-695A-5H, -8H, -11I, -14H, -17I, -24I, -31I, and -38I). The results are described as follows:

Core 113-695A-5H (41.2 mbsf)

We used VH-probe #1 with Core 113-695A-5H. Figure 35 shows the temperature record at the Core 113-695A-5H. The temperature reached 5.88°C just after penetration due to frictional heat production, and just before pull out, the temperature was 3.65°C. The temperature data were gradually approaching the true formation temperature. The temperature data can be extrapolated to equilibrium following Horai and Von Herzen (1986). The estimated formation temperature, using the "DECAY3" and "FITTING3" computer programs (see "Explanatory Notes" chapter, this volume), is 2.4°–2.6°C at 41.2 mbsf. We think that this is a reliable temperature estimate.

Core 113-695A-8H (70.0 mbsf)

We used VH-probe #1 with Core 113-695A-8H. Figure 36 shows the temperature record. The temperature reached 4.97°C just after penetration. However, a few minutes after penetration, the temperature records showed two values (4.425° and 4.435°C). This difference corresponds to 1 Least Significant Bit (LSB). Something may have happened to the tool in the sediments, however, frictional heating of pull out was observed and the data in the mud line were well recorded. The cause of this behavior is unknown. Accordingly, this temperature record is treated as only a reference value.

Table 14. Rock-Eval data, Site 695.

Core, section interval (cm)	Depth (mbsf)	S_1 mg(HC)/g(rock)	S_2 mg(HC)/g(rock)	S_3 mg(HC)/g(rock)	TOC (%)	HI $mg(CO_2)/g/(C)$	OI mg(HC)/g(C)	T_{max} (°C)
113-695A-								
1H-3, 145–150	1.45	0.02	0.61	0.00	0.10	[a]610	0	543
2H-4, 145–150	8.85	0.08	0.58	0.02	0.13	446	15	551
3H-4, 145–150	18.35	0.10	0.76	0.12	0.43	176	27	428
4H-4, 145–150	27.95	0.34	1.70	0.05	0.47	361	10	511
5H-4, 145–150	39.05	0.17	1.01	0.13	0.54	187	24	445
6H-3, 125–129	45.45	0.02	0.19	0.00	0.16	118	0	478
7H-1, 145–150	52.25	0.23	1.14	0.17	0.47	242	34	445
8H-3, 145–150	64.85	0.06	0.42	0.10	0.39	107	25	431
9H-2, 120–125	72.70	0.19	1.08	0.34	0.44	245	77	508
15H-3, 120–125	122.40	0.11	0.70	0.14	0.40	175	35	501
19X-4, 120–125	153.00	0.25	1.06	0.32	0.56	189	57	386
20X-4, 145–150	162.97	0.27	1.25	0.52	0.67	186	77	388
21X-2, 145–150	172.75	0.18	0.79	0.16	0.35	225	45	385
22X-3, 120–125	180.70	0.06	0.65	0.08	0.35	185	22	467
23X-3, 145–150	190.65	0.03	0.66	0.01	0.25	264	4	512
25X-3, 120–125	200.10	0.04	0.47	0.28	0.48	97	58	434
29X-2, 115–125	237.35	0.04	0.37	0.35	0.37	100	94	432
32X-4, 115–125	259.75	0.06	0.54	0.09	0.32	168	28	429
36X-2, 115–120	295.45	0.04	0.42	0.12	0.39	107	30	438
39X-3, 115–120	316.15	0.04	0.36	0.17	0.39	92	43	421
41X-3, 140–145	335.80	0.01	0.15	0.16	0.24	62	66	462
Standard (observed)		0.15	10.44	1.51	2.86	365	52	404
Standard (known values)		0.10	8.62	1.00	2.86	340	33	419

[a] Dubious value, in view of high T_{max}.

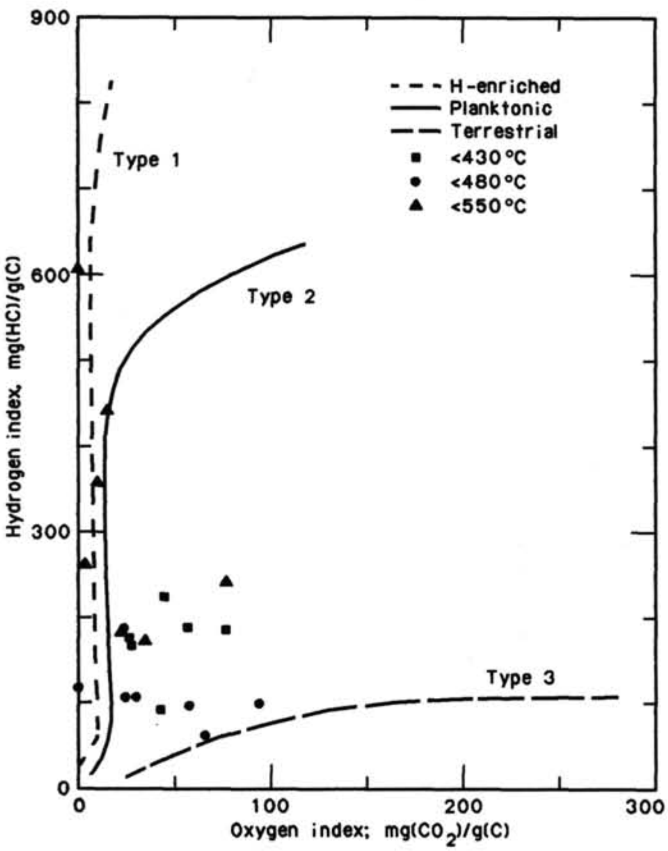

Figure 34. Kerogens, Site 695, subdivided by thermal maturity based on T_{max}. Data given in Table 14.

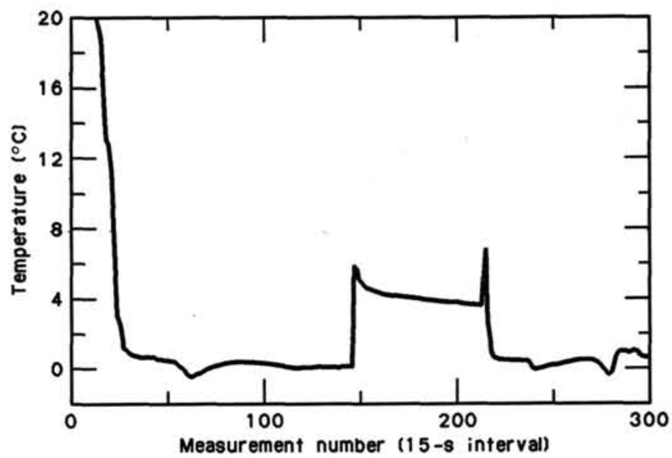

Figure 35. Temperatures measured with the Von Herzen APC tool #1 (VH-probe #1) during Core 113-695A-5H at 41.2 mbsf.

Core 113-695A-11I (89.2 mbsf)

This core was taken to obtain a pore water sample. We used VH-probe #1 and T-probe #12, simultaneously. Figure 37 shows the temperature record for Core 113-695A-11I. Solid and dashed lines depict the records of VH-probe #1 and T-probe #12, respectively. The closely parallel lines indicate that both temperature recording devices worked well. However, temperature records were unstable. This might be produced by sensor movement which was caused by ship's motion or by some unknown phenomenon.

Core 113-695A-14H (118.2 mbsf)

We used VH-probe #1 with Core 113-695A-14H. Figure 38 shows the temperature record for this core. The temperature reached 12.76°C just after penetration. Just before pull out, the

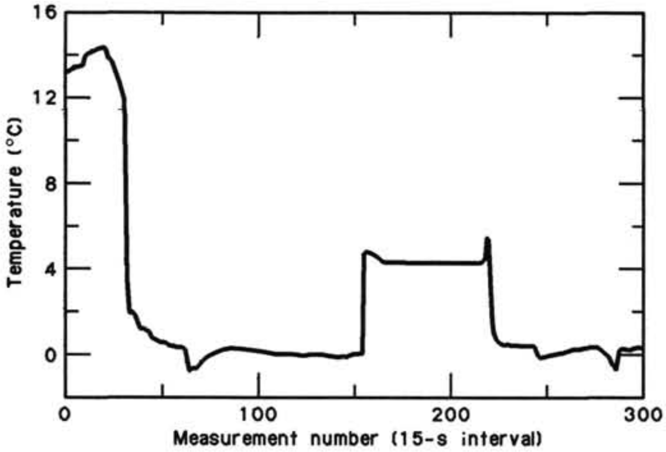

Figure 36. Temperatures measured with the VH-probe #1 during Core 113-695A-8H at 70.0 mbsf.

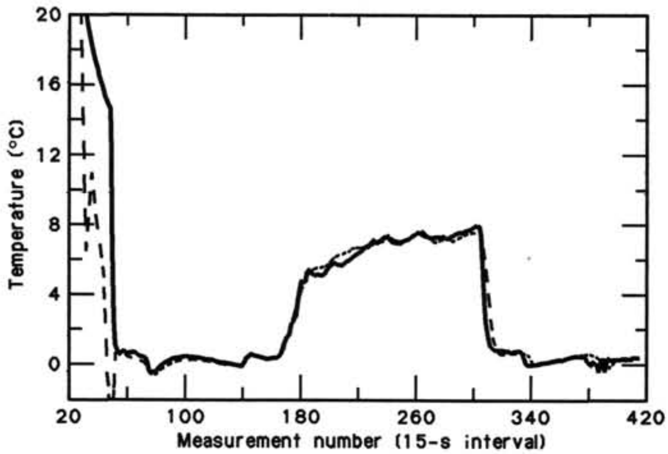

Figure 37. Temperatured measured with the VH-probe #1 (solid line) and the temperature recording instruments for pore water sampler (Uyeda/Kinoshita probe, T-probe) #12 (dashed line) during Core 113-695A-11I at 89.2 mbsf.

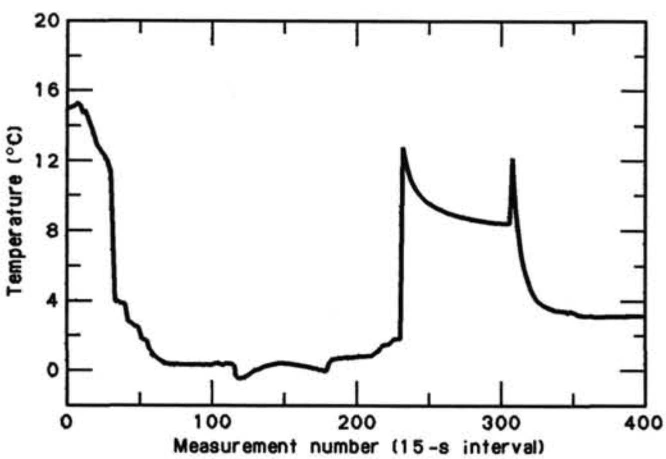

Figure 38. Temperatures measured with the VH-probe #1 during Core 113-695A-14H at 118.2 mbsf.

temperature was 8.43°C. The estimated true formation temperature is 6.8°–7.0°C at 118.2 mbsf. We consider that this is a high-quality temperature estimate.

Core 113-695A-17I (137.6 mbsf)

This core was taken to obtain a pore water sample. We used VH-probe #1 and T-probe #14. However, T-probe #14 did not work. Figure 39 only shows the temperature record of VH-probe #1. Just before pull-out, the temperature was 7.21°C, and the temperature was still increasing. Thus, this provides only a minimum temperature.

Core 113-695A-24I (196.6 mbsf)

This core was also taken to obtain a pore water sample. We used VH-probe #1 and T-probe #14. However, T-probe #14 did not work. Figure 40 shows only the temperature record of VH-probe #1. Just before pull out, the temperature was 4.26°C, and the temperature was still increasing. Thus, this provides only a minimum temperature.

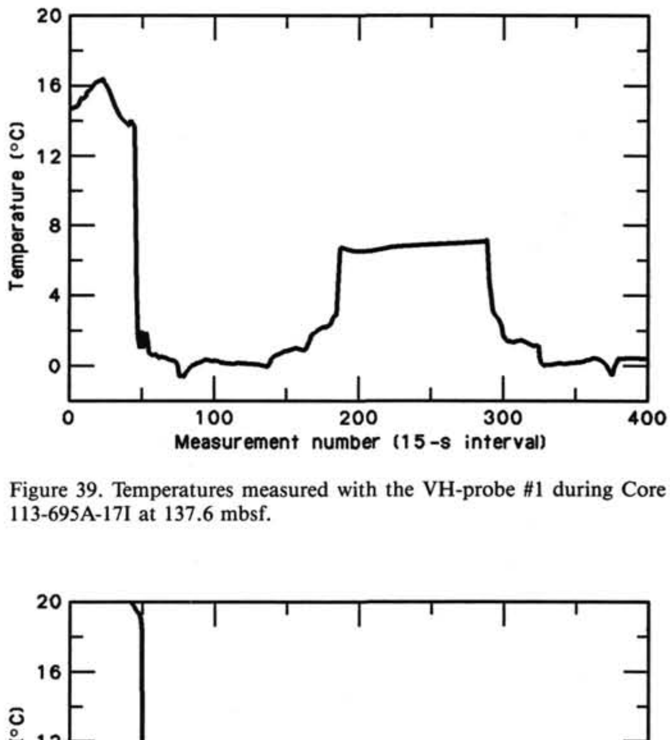

Figure 39. Temperatures measured with the VH-probe #1 during Core 113-695A-17I at 137.6 mbsf.

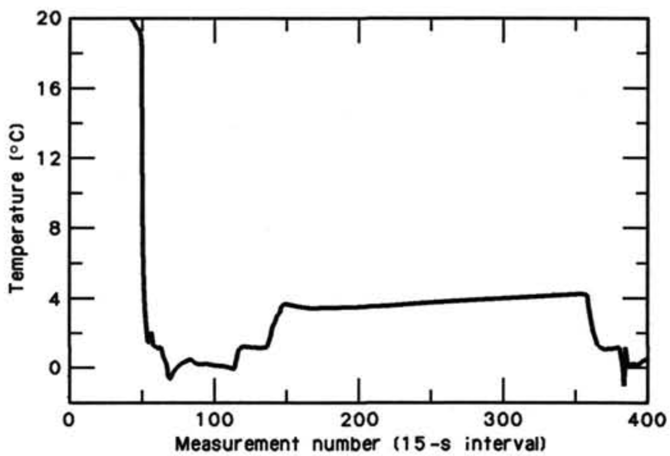

Figure 40. Temperatures measured with the VH-probe #1 during Core 113-695A-24I at 196.6 mbsf.

Core 113-695A-31I (254.4 mbsf)

The VH-probe #1 and T-probe #14 were used in conjunction with the pore water sampler. Figure 41 gives the temperature record. Solid and dashed lines show records of the VH-probe #1 and the T-probe #14, respectively. Both temperature recording devices worked well. Just before pull out, VH-probe showed a temperature of 10.44°C, and was still increasing. On the other hand, the T-probe showed 16.94°C, and was still decreasing. This large temperature difference may be attributed to the sensor position. For pore water sampling, the *in-situ* sediments were already removed by the previous coring operation. The VH-probe is located in a wall of the APC cutting shoe. Inside the APC cutting shoe, there is probably drilling fluid, not true sediment. In contrast, the pore-water sampling needle and the sensor part of the T-probe are located 15–30 cm lower than the APC cutting shoe, and are inserted into the sediments. In this interval, the true formation temperature was between 16.94° and 10.44°C.

Core 113-695A-38I (312.7 mbsf)

The VH-probe #1 and T-probe #14 were used again with the pore water sampler. Figure 42 shows the temperature record. Solid and dashed lines present records of the VH-probe #1 and T-probe #14, respectively. In this case, both temperature recording devices worked well. Just before pull out, the VH-probe gave a temperature of 8.69°C, and still increasing. The T-probe #14 showed almost constant temperatures of 17.00°C, although it might be seen as increasing slightly in contrast to the result of Core 113-695A-31I. We consider that the decreasing or increasing temperature records just before pull out were related to the degree of frictional heating, the difference between a true formation temperature and cutting shoe temperature, the thermal diffusivities of cutting shoe and sediments (including specific heat), and the degree of cutting shoe penetration. In this case, we can conclude that the true formation temperature was at least 17.00°C.

Discussion

At this site, we used two kinds of temperature recording devices (VH-probe and T-probe). Therefore, calibration of the temperature sensors is very important. Unfortunately, no cryostat was available on board the ship; because of this, the data obtained by the VH-probe and the T-probe cannot be exactly compared. However, the data obtained at the mud line show that the T-probe #12 data is consistent with the VH-probe #1 (Fig. 37). In contrast, the T-probe #14 always gives 0.7° to 0.9°C higher temperature measurements than the VH-probe #1 (Figs. 41 and 42). We cannot compare these two devices, because the T-probe #14 was lost at Hole 696B. Therefore, in this section, we assume that the T-probe #14 had always shown a temperature value 0.8°C higher than the VH-probe #1. Thus, we have subtracted 0.8°C from the observed T-probe values.

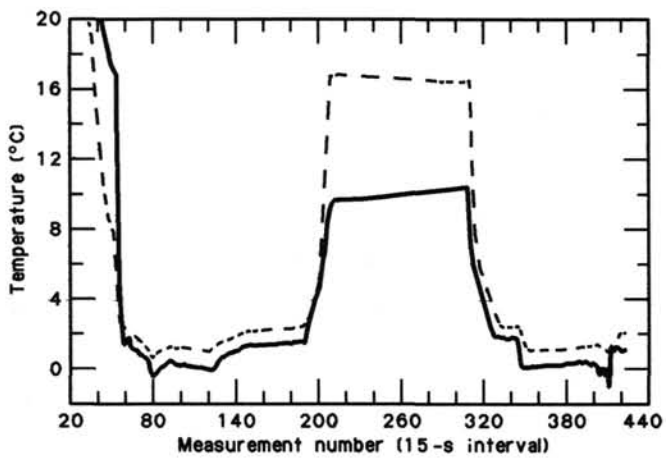

Figure 41. Temperatures measured with the VH-probe #1 (solid line) and T-probe #14 (dashed line) during Core 113-695A-31I at 254.4 mbsf.

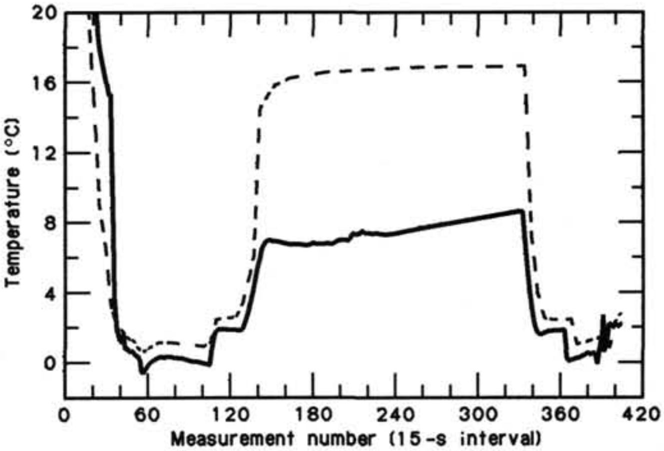

Figure 42. Temperatures measured with the VH-probe #1 (solid line) and T-probe #14 (dashed line) during Core 113-695A-38I at 312.7 mbsf.

Figure 43 shows results of all of the temperature measurements. Crosses show the observed temperature values just before pull out, and arrows show the direction of temperature record change. Dots show the estimated true formation temperatures for Cores 113-695A-5H (41.2 mbsf) and -14H (118.2 mbsf). At this site, a temperature gradient was calculated as 57.1 mK/m by using values at these two depths.

Thermal conductivity measurements were made on 16 samples (Fig. 20), between 40 mbsf and 120 mbsf, yielding an average value of 1.14W/m-K. Corrections for temperature (Ratcliffe, 1960) and pressure effects are not yet finished; however, these effects never exceeded 3% (e.g., Morin and Von Herzen, 1986).

Heat flow is defined as the product of temperature gradient and thermal conductivity. As a preliminary result we can conclude an estimated heat flow value at Site 695 of 65.1 mW/m^2 by using 57.1 mK/m for the temperature gradient and 1.14 W/m-K for the thermal conductivity. This value is not a final value. However, the final value will probably not change by more than 5%.

The average thermal conductivity between 0 and 40 mbsf and between 120 and 200 mbsf is 1.12 W/m-K in both intervals. These results indicate that the thermal conductivity structure from 0 to 200 mbsf is essentially the same. Therefore, we extrapolate the 57.1 mK/m gradient to 0 mbsf and to 200 mbsf. The extrapolated data are shown by the dashed line in Figure 43. According to this extrapolation, the temperature at 0 mbsf is 0.15°C. This value is consistent with the data obtained at the mud line. Furthermore, the thermal conductivity structure changed below 200 mbsf. The average thermal conductivity value from 200 mbsf to 315 mbsf was 1.42 W/m-K. If basal heat flux at this site, considered to be constant, is postulated as 65.1 mW/m^2, then the 1.42 W/m-K thermal conductivity value produces a 45.8 mK/m temperature gradient in this depth range. The dashed line below 200 mbsf was calculated in this manner. This estimated temperature profile is consistent with actual measurements.

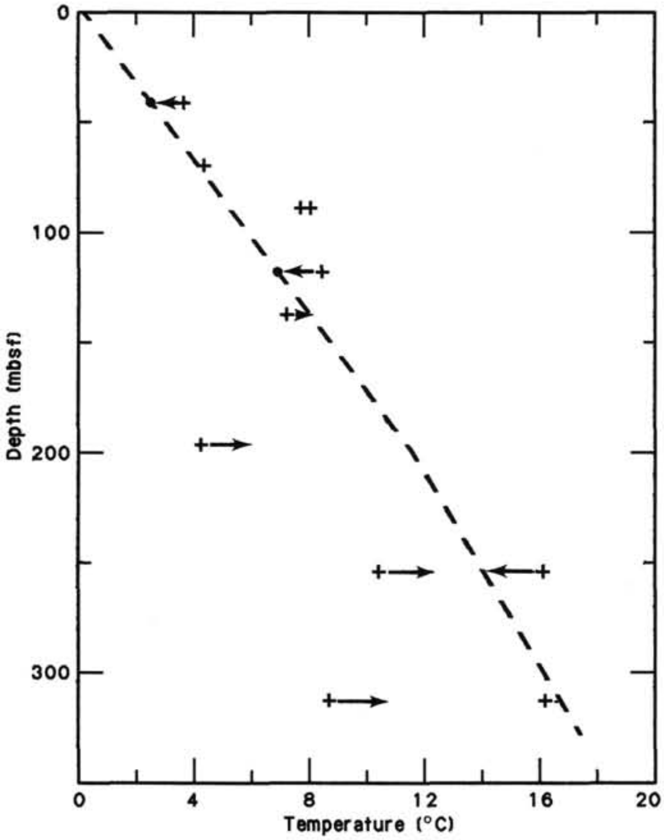

Figure 43. Observed temperature measurements just before pull out (crosses) and estimated true formation temperatures (dots). Dashed line shows an estimated temperature structure, assuming a constant thermal conductivity of 1.12 W/m-K and a thermal gradient of 57.1 mK/m above 200 mbsf, and 1.42 W/m-k and 45.8 mK/m, respectively, between 200 and 315 mbsf. Arrows show direction of temperature record change.

Conclusion

The heat flow value at Site 695 is 65.1 mW/m^2. At this site, a prominent BSR at about 600 mbsf was postulated to be a gas hydrate. We observed large thermal conductivity values greater than 2.3 W/m-K below 300 mbsf. If we adopt a thermal conductivity structure below 300 mbsf of 2.5 W/m-K (this is the maximum thermal conductivity value of the sedimentary rocks), the temperature at 600 mbsf is estimated to be 25.5°C. This is the minimum temperature value. Therefore, it is difficult to believe that the inferred BSR at 600 mbsf is a gas hydrate, because hydrates are not stable at such high temperatures. The nature of the BSR remains a mystery.

SUMMARY AND CONCLUSIONS

Site 695 is the intermediate site of three on a depth transect through the circum-Antarctic water masses on the northern edge of the Weddell Gyre, and was the first of the three to be drilled. It lies on the southeastern edge of the South Orkney microcontinent (SOM) on the northern margin of the Weddell Sea, at 62°23.48′S, 43°27.10′W in 1300 m water depth. The site falls at SP 1720 on multichannel reflection profile AMG845-18 (Birmingham University/British Antarctic Survey).

The South Orkney microcontinent separated from the Antarctic Peninsula to the west at about 30–35 Ma ago, and from the then-active island arc of Jane Bank in the east at about 25–30 Ma ago (Barker et al., 1984; King and Barker, 1988; Lawver et al., 1986). The microcontinent was pervasively block-faulted by these events, which thus provide an effective older limit to the period for which the SOM can be used as a passive indicator for the paleocean. In addition to the largely pelagic Neogene and uppermost Oligocene section which was predicted to be present at this site, the reflection profiles showed a BSR at about 600 mbsf, which was thought to be a methane gas hydrate. Drilling was required to stop 50 m above the BSR for safety reasons.

One hole was drilled at Site 695 in three days and one-half hour, between 20 and 23 February 1987. It penetrated to 341.1 mbsf and we recovered 254.4 m (74.6%) in 15 APC and 21 XCB cores. Also, 5 *in-situ* pore water samples were taken, and 8 downhole temperature measurements were made. Hole 695A had to be abandoned without being logged when the XCB corer sheared, leaving its lower part in the hole and the upper part jammed in the base of the pipe.

The section at Site 695 consists of 341.1 m of Quaternary to uppermost Miocene or lowermost Pliocene sediment, essentially of mixed siliceous biogenic, hemipelagic and ice-rafted terrigenous, and air-fall volcanic origin. Core disturbance is minor. Three lithostratigraphic units are recognised, the first of which has four subunits.

Unit I: 0–190.0 mbsf, comprises a range of diatom-rich sediments (as much as 80%). Subunit IA is 19.9 m thick, Quaternary to middle Pliocene, mainly diatom-bearing silty and clayey muds with minor foraminifers above 4 mbsf. This is the only certain, *in-situ* occurrence of calcareous microfossils in Hole 695A. Subunit IB is 32.4 m thick, middle to lower Pliocene muddy diatom oozes. Subunit IC is 41.4 m thick, upper lower Pliocene mainly silty and muddy diatom oozes. Subunit ID is 96.3 m thick, lower Pliocene diatom oozes to diatom silty muds.

Unit II: 190.0–306.9 mbsf, with a much smaller biosiliceous component (10%–25%) than Unit I, consists of lower Pliocene diatom-bearing silty and clayey muds.

Unit III: 306.9–341.1 mbsf, consists of lower Pliocene and possibly uppermost Miocene silty mud with 0%–10% diatoms.

Ice-rafted detritus occurs throughout the sequence in varying amounts. It is common in Subunit IA and Unit II, and minor elsewhere; dropstones (>3 mm) show isolated maxima from 0 to 20 mbsf (IA), 150–165 mbsf, and 293–306 mbsf. The sequence contains volcanic material throughout. All units contain 1- to 2-cm-thick devitrified ash beds, particularly Subunit IC and Unit II. Glass-rich horizons occur in Subunits IC and ID, and Unit II, and Unit II also contains a large amount of finely-dispersed glass. An anomalous minor lithology comprises four occurrences of authigenic carbonate or carbonate-cemented sediment, each about 15 cm thick, at 112, 166, 254, and 321 mbsf. Graded beds are rare, and the bulk of the terrigenous component is probably ice-rafted or hemipelagic.

Illite and chlorite dominate the clay mineral assemblages at Site 695: both are abundant in the majority of samples. Kaolinite is rare to common in Unit I but uniformly rare beneath. Smectite abundance is variable, but is greatest above 9 mbsf (where chlorite is less abundant) and in some parts of Unit II.

The biogenic component of the sediments is almost completely siliceous, dominantly diatoms with minor silicoflagellates, radiolarians, and sponge spicules. Calcareous fossils, found *in situ* at only two thin horizons, both in the uppermost 4 m, are *Neogloboquadrina pachyderma* and a low-diversity assemblage of benthic foraminifers. Agglutinated benthic foraminifers occur as rare, low-diversity assemblages in the uppermost 252 mbsf. They indicate paleodepths slightly deeper than the present 1300 m depth at Site 695, but the species could be responding to the abundance of biogenic opal rather than to water depth alone (see "Site 696" chapter, this volume). Diatoms are generally common to abundant, and moderately to well-preserved, except in the uppermost 5 mbsf (Pleistocene) and below 293 mbsf (uppermost Miocene(?) and lowermost Pliocene), where they are rare to few, and poorly preserved. Radiolarians are less abundant but also well preserved. Silicoflagellates are less abundant and consistently less well preserved than diatoms.

The high recovery and low core disturbance that characterize Site 695 should provide a detailed magnetostratigraphic record, but low intensities of magnetization meant that the complete sample suite could not be measured aboard the ship. Sedimentation rates were moderate (less than 30 m/m.y.) in the latest Miocene and earliest Pliocene (early Gilbert), becoming very high (up to about 200 m/m.y.) in the early Pliocene (late Gilbert). Rates decreased markedly through the late Pliocene (Gauss), to 2.5–8 m/m.y. in the latest Pliocene and Quaternary (Brunhes and Matuyama). This pattern of enhanced lower Pliocene biosiliceous productivity and preservation was encountered at other ODP Leg 113 sites (689, 690, and particularly 693), and has been seen also in the Subantarctic South Atlantic (Site 514, Ludwig, Krashenninikov, et al., 1983). In the warmer Southwest Pacific, Kennett, Von der Borch, et al. (1986) report a parallel enhancement of calcareous productivity.

The high sedimentation rates and generally good preservation in the lower Pliocene make the section at Site 695 of great potential value for correlation of magnetostratigraphy and siliceous biostratigraphy. For example, a revision of the *N. praeinterfrigidaria* to *N. interfrigidaria* diatom zonal transition has already been proposed. The presence of layers of fresh volcanic glass could strengthen chronostratigraphic links and aid regional correlation between sites. Evolutionary and paleoceanographic studies should also benefit from the expanded lower Pliocene section. In the lowermost Pliocene, where siliceous preservation is poor, there is a short-lived invasion of Subantarctic forms, seen previously in the Indo-Pacific sector and at Site 693.

An inverse-polarity BSR at about 700 ms twt had been tentatively identified during the site survey as the base of a methane gas hydrate. This provided an additional focus for studies of sediment physical properties, heat flow, pore water chemistry, and organic geochemistry. A well-constrained heat flow of 1.5 HFU was determined, almost twice that predicted from the presence of the BSR, and sufficient to show that the BSR could not be the base of a methane hydrate stability zone. If such a zone existed around Site 695 its base would lie at 310–360 mbsf (400–450 ms), where no BSR was visible on the reflection profile. Methane concentrations increased sharply below 250 mbsf, near the base of a pore water sulfate ion depletion curve, suggesting that the methane was biogenic. Presumably the exceptionally high lower Pliocene sedimentation rates allowed organic matter to be buried without complete oxidation and effectively isolated the pore water from seabed sulfate replenishment. At and directly below 250 mbsf, methane should occur *in situ* in the hydrate phase, but no signs of hydrate were visible in the cores.

The nature of the BSR at 700 ms is unexplained: its presence, however, limited the permitted depth of drilling. The high sedimentation rates in the section already penetrated suggested that the sequence above the BSR would not extend far below the upper Miocene. When XCB failure prevented further drilling in Hole 695A, caused the abandonment of the hole without logging, and dictated a pipe trip, it was decided to move to the shallower Site 696 where the older section was accessible and where a more calcareous section remained a possibility, rather than start another hole at Site 695.

REFERENCES

Bandy, O. L., and Echols, R. J., 1964. Antarctic foraminiferal zonation. *Antarct. Res. Ser.*, Am. Geophys. Union, 1:73–91.

Barker, P. F., Barber, P. L., and King, E. C., 1984. An early Miocene ridge crest-trench collision on the South Scotia Ridge near 36°W. *Tectonophysics*, 102:315–322.

Berggren, W. A., Kent, D. V., Flynn, J. J., and Van Couvering, J. A., 1985. Cenozoic geochronology. *Geol. Soc. Am. Bull.*, 96:1407–1418.

Berner, R. A., 1974. Kinetic models for the early diagenesis of nitrogen, sulfur, phosphorus, and silicon in anoxic marine sediments. *In* Goldberg, E. D. (Ed.), *The Sea* (Vol. 5): New York (Wiley), 427–450.

Carlson, R. L., Gangi, A. F., and Snow, K. R., 1986. Empirical reflection travel time versus depth and velocity versus depth functions for the deep-sea sediment column. *J. Geophys. Res.*, 91:8249–8266.

Ciesielski, P. F., 1975. Biostratigraphy and paleoecology of Neogene and Oligocene silicoflagellates from cores recovered during Antarctic Leg 28, Deep Sea Drilling Project. *In* Hayes, D. E., Frakes, L. A., et al., *Init. Repts. DSDP*, 28: Washington (U.S. Govt. Prinitng Office), 625–691.

———, 1983. The Neogene and Quaternary diatom biostratigraphy of subantarctic sediments, Deep Sea Drilling Project Leg 71. *In* Ludwig, W. J., Krasheninnikov, V. A., et al., *Init. Repts. DSDP*, 71, Pt. 2: Washington (U.S. Govt. Printing Office), 635–665.

Ciesielski, P. F., Ledbetter, M. T., and Ellwood, B. B., 1982. The development of Antarctic glaciation and the Neogene paleo-environment of the Maurice Ewing Bank. *Mar. Geol.*, 46:1–51.

Deroo, G., Herbin, J. P., and Roucaché, J., 1983. Organic geochemistry of Upper Jurassic-Cretaceous sediments from Site 511, Leg 71, western south Atlantic. *In* Ludwig, W. J., Krasheninnikov, V. A., et al., *Init. Repts. DSDP*, 71: Washington (U.S. Govt. Printing Office), 1001–1013.

Echols, R. J., 1971. Distribution of Foraminifera in sediments of the Scotia Sea area, Antarctic waters. *In* Reid, J. L., *Antarctic Oceanology*, Am. Geophys. Union, *Antarct. Res. Ser.*, 15:93–168.

Goldhaber, M. B., and Kaplan, I. R., 1974. The sulfur cycle. *In* Goldberg, E. D. (Ed.), *The Sea* (Vol. 5): New York (Wiley), 569–655.

Grobe, H., 1986. Sedimentation processes on the Antarctic continental margin at Kapp Norvegia during the Late Pleistocene. *Geol. Rundschau*, 75:97–104.

Harrison, W. E., Hesse, R., and Gieskes, J. M., 1982. Relationship between sedimentary facies and interstitial water chemistry of slope, trench, and Cocos plate sites from the Middle America trench transect, active margin off Guatemala, Deep Sea Drilling Project Leg 67. *In* Aubouin, J., von Huene, R., et al., *Init. Repts. DSDP*, 67: Washington (U.S. Govt. Printing Office), 603–616.

Horai, K., and Von Herzen, R. P., 1986. Measurement of heat flow on Leg 86 of the Deep Sea Drilling Project. *In* Heath, G. R., Burckle, L. H., et al., *Init. Repts. DSDP*, 86: Washington (U.S. Govt. Printing Office), 759–777.

Keany, J., 1979. Early Pliocene radiolarian taxonomy and biostratigraphy in the Antarctic region. *Micropaleontology*, 25:50–74.

Kellogg, D. E., 1975. The role of phyletic change in the evolution of *Pseudocubus vema* (Radiolaria). *Paleobiology* 1:359–370.

Kennett, J. P., and Von der Borch, C. C., 1985. Southwest Pacific Cenozoic paleoceanography. *In* Kennett, J. P., Von der Borch, C. C., et al, *Init. Repts. DSDP*, 90: Washington (U.S. Govt. Printing Office), 1493–1517.

King, E. C., and Barker, P. F., 1988. The margins of the South Orkney Microcontinent. *J. Geol. Soc. Lond.*, 145:317–331.

Lawver, L. A., Della Vedova, B., and Von Herzen, R.P., 1986. Heat flow in Jane Basin, South Scotia Ridge, a small back-arc basin. *Antarct. J. U.S.*, 19:87–88.

Ledbetter, M. T., and Ciesielski, P. F., 1986. Post-Miocene disconformities and paleoceanography in the Atlantic sector of the Southern Ocean. *Palaeogeogr. Palaeoclimatol. Palaeoecol.*, 52:185–214.

Ludwig, W. J., Krasheninnikov, V. A., et al., 1983. Init. Repts. DSDP, 71, Pt. 1: Washington (U.S. Govt. Printing Office).

MacKenzie, F. T., and Garrels, R. M., 1966. Chemical mass balance between rivers and oceans. *Am. J. Sci.*, 264:507–525.

Macleod, M. K., 1982. Gas hydrates in ocean bottom sediments. *Am. Assoc. Pet. Geol. Bull.*, 66:2649–62.

Manheim, F. T., and Sayles, F. L., 1974. Composition and origin of inter- stitial waters of marine sediments. *In* Goldberg, E. D. (Ed.), *The Sea* (Vol. 5): New York (Wiley), 527–568.

McCollum, D. W., 1975. Diatom stratigraphy of the Southern Ocean. *In* Hayes, D. E., Frakes, L. A., et al., *Init. Repts. DSDP*, 28: Washington (U.S. Govt. Printing Office), 515–571.

Mercer, J. H., 1978. Glacial development and temperature trends in the Antarctic and in South America. *In* Van Zinderen Bakker, E. M. (Ed.), *Antarctic Glacial History and World Paleoenvironments*: Rotterdam (A.A. Balkema), 73–93.

Milam, R. W., and Anderson, J. B., 1981. Distribution and ecology of Recent benthic Foraminifera of the Adelie-George V continental shelf and slope, Antarctica. *Mar. Micropaleontol.*, 6:297-325.

Miller, K. G., and Fairbanks, R. G., 1985. Cainozoic ^{18}O record of climate and sea level. *S. Afr. J. Science*, 81:248-249.

Morin, R. H., and Von Herzen, R. B., 1986. Geothermal measurements at Deep Sea Drilling Project Site 587. *In* Kennett, J. P., von der Borch, C. C., et al., *Init. Repts. DSDP*, 90: Washington (U.S. Govt. Printing Office), 1317-1324.

Murphy, M. G., and Kennett, J. P., 1986. Development of latitudinal thermal gradients during the Oligocene: oxygen-isotope evidence from the southwest Pacific. *In* Kennett, J. P., von der Borch, C. C., et al., *Init. Repts. DSDP*, 90: Washington (U.S. Govt. Printing Office), 1347-1360.

Presley, B. J., and Kaplan, I. R., 1970. Interstitial water chemistry: DSDP Leg 4. *In* Bader, R. G., Gerard, R. D., et al., *Init. Repts. DSDP*, 4: Washington (U.S. Govt. Printing Office), 415-430. Ratcliffe, E. H., 1960. The thermal conductivities of ocean sediments. *J. Geophys. Res.*, 65:1535-1541.

Robert, C., and Maillot, H., 1983. Paleoenvironmental significance of clay mineralogical and geochemical data, Southwest Atlantic, DSDP Legs 36 and 71. *In* Ludwig, W. J., Krasheninnikov, V., et al, *Init. Repts. DSDP*, 71: Washington (U.S Govt. Printing Office), 317-343.

Salloway, J. C., 1983. Paleomagnetism of sediments from Deep Sea Drilling Project Leg 71. *In* Ludwig, W. J., Krasheninnikov, V. A., et al., *Init. Repts. DSDP*, 71, Pt. 1: Washington (U.S. Govt. Printing Office), 1073-1092.

Schrader, H. J., 1976. Cenozoic planktonic diatom biostratigraphy of the Southern Pacific Ocean. *In* Hollister, C. D., Craddock, C., et al., *Init. Repts. DSDP*, 35: Washington (U.S. Govt. Printing Office), 605-672.

Shackleton, N. J., and Kennett, J. P., 1975. Paleotemperature history of the Cenozoic and the initiation of Antarctic glaciation: oxygen and carbon isotope analyses in DSDP Sites 277, 279 and 281. *In* Kennett, J. P., Houtz, R. E., et al., *Init. Repts. DSDP*, 29: Washington (U.S. Govt. Printing Office), 801-806.

Shaw, C. A., and Ciesielski, P. F., 1983. Silicoflagellate biostratigraphy of middle Eocene to Holocene subantarctic sediments recovered by Deep Sea Drilling Project Leg 71. *In* Ludwig, W. J., Krasheninnikov, V. A., et al., *Init. Repts. DSDP*, 71: Washington (U.S. Govt. Printing Office), 687-737.

Shipley, T. H., Houston, M. H., Buffler, R. T., Shaub, F. J., McMillen, K. J., Ladd, J. W., and Worzel, J. L., 1979. Seismic reflection evidence for widespread possible gas hydrate horizons on continental slopes and rises. *Am. Assoc. Pet. Geol. Bull.*, 63:2204-2213.

Stumm, W., and Morgan J.J., (Eds.), 1981. *Aquatic Chemistry* (2nd Ed.). New York (Wiley).

Stumm, W., and Leckie, Z. O., 1970. Phosphate exchange with sediments, its role in the productivity of surface waters. *Advances in Water Pollution Research* (Vol. 2): New York (Pergamon), III:26/1-26/16.

Theyer, F., 1971. Benthic foraminiferal trends, Pacific-Antarctic Basin. *Deep Sea Res.*, 18:723-738.

Ugolini, F. C., and Jackson, M. L., 1982. Weathering and mineral synthesis in Antarctic soils. *In* Craddock, C. (Ed.), *Antarct. Geosci., I.U.G.S. Ser. B*, 4:1101-1108.

Vail, P. R., and Hardenbol, J., 1979. Sea level changes during the Tertiary. *Oceanus*, 22:71-79.

Von Herzen, R. P., and Maxwell, A. E., 1959. The measurement of thermal conductivity of deep-sea sediments by a needle probe method. *J. Geophys. Res.*, 65:1535-1541.

Weaver, F. M., 1983. Cenozoic radiolarians from the southwest Atlantic, Falkland Plateau region, Deep Sea Drilling Project Leg 71. *In* Ludwig, W. J., Krasheninnikov, V. A., et al., *Init. Repts. DSDP*, 71, Pt. 2: Washington (U.S. Govt. Printing Office), 667-686.

Weaver, F. M., and Gombos, A. M., 1981. Southern high-latitude diatom biostratigraphy. *Soc. Econ. Paleontol. Mineral. Spec. Publ.*, 32:445-470.

Ms 113A-111

SITE 695 HOLE A CORE 1H CORED INTERVAL 1300.0-1306.4 mbsl; 0-6.4 mbsf

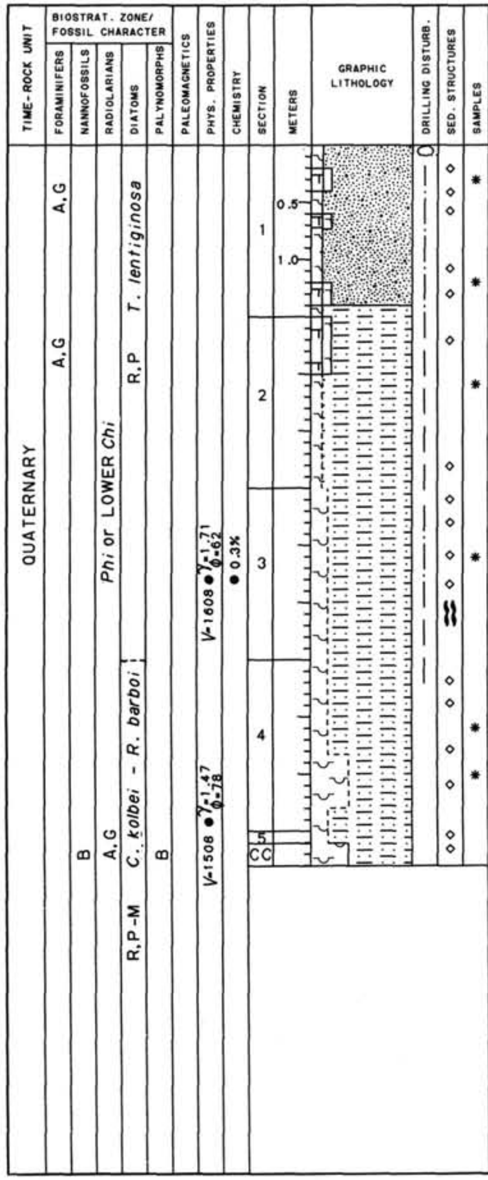

LITHOLOGIC DESCRIPTION

DIATOM-BEARING CLAYEY MUD

Major lithology: Diatom-bearing clayey mud, olive gray (5Y 5/2) and olive (5Y 5/3). *Color changes are cyclic, and most are gradational. In Section 4, 85 cm,* there is a sharp color break between pale olive (5Y 6/3) below and olive gray (5Y 5/2) above.

Minor lithologies:

a. Foraminifer-bearing clayey mud, gray (5Y 5/1), Section 1, 22-41, 59-76, and 118-140 cm.
b. Diatom-bearing silty mud, olive gray (5Y 5/2), Section 1.
c. Diatom clayey mud, Section 4, 84-130 cm.

Sand-sized *ice-rafted detritus occurs throughout core* and is most abundant in Section 1, 0-22, 38-50, 75-79, 100-109, and 129-140 cm; Section 2, 85-126 and 140-150 cm; Section 3, 0-14, 30-55, and 75-90 cm; and Section 4, 0-84 and 140-150 cm. Ice-rafted detritus is most abundant in the grayest sediment at the base of the cycles. Identifiable dropstones are predominantly subrounded sedimentary rocks.

SMEAR SLIDE SUMMARY (%):

	1, 30 M	1, 120 D	2, 60 D	3, 60 D	4, 60 D	4, 100 D
TEXTURE:						
Sand	10	20	10	10	7	2
Silt	30	54	49	48	44	45
Clay	60	26	41	42	49	53
COMPOSITION:						
Quartz	20	30	25	20	15	7
Feldspar	2	3	2	2	—	—
Mica	—	—	2	3	5	3
Clay	60	26	41	42	49	53
Accessory minerals:						
Amphibole	2	5	5	5	5	2
Glauconite	Tr	—	—	—	—	—
Garnet	—	2	1	1	1	—
Heavy minerals	3	7	7	5	3	1
Opaque minerals	1	2	2	2	1	2
Foraminifers	7	10	2	—	—	—
Diatoms	3	10	10	15	15	30
Radiolarians	—	2	—	2	3	2
Sponge spicules	2	3	3	3	3	Tr

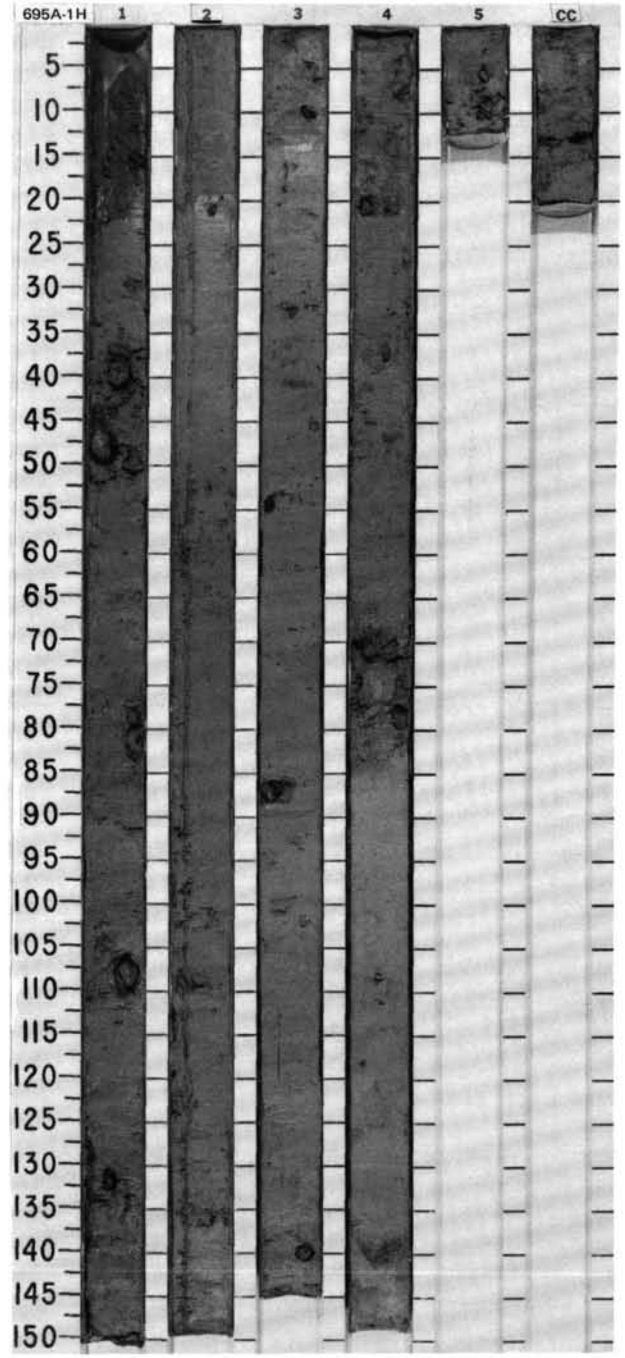

SITE 695 HOLE A CORE 2H CORED INTERVAL 1302.9-1312.4 mbsl; 2.9-12.4 mbsf

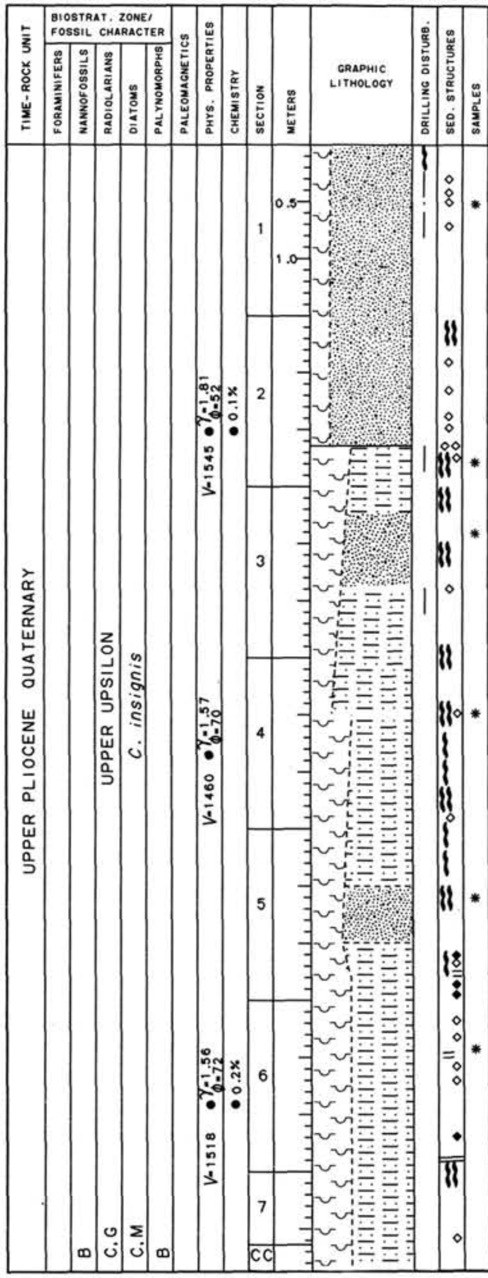

LITHOLOGIC DESCRIPTION

DIATOM-BEARING SILTY MUD, DIATOM CLAYEY MUD, and DIATOM SILTY MUD

Major lithologies: Diatom-bearing silty mud, olive gray (5Y 5/2) in Section 1 and Section 2, 0-115 cm; diatom clayey mud and diatom silty mud, pale olive (5Y 6/3), grading down to diatom-bearing silty mud from Section 2, 115 cm, to Section 4, 52 cm; diatom clayey mud and diatom silty mud, pale olive (5Y 6/3), gradually changing to olive gray (5Y 5/2) from Section 4, 52 cm, to Section 5, 127 cm. Diatom clayey mud, greenish gray (5G 5/1), with thin darker layers in Section 5, 127-145 cm, and Section 7, 30-32 cm.

Minor lithology: Sand, gray (5Y 5/1), as rounded clasts 1-2 cm across in Sections 5 and 6. Fine-grained, poorly sorted; contains diatoms and a few radiolarians, many heavy minerals, fresh feldspar, and about 50% quartz.

Dropstones up to 2 cm across occur in all sections and are subangular to subrounded; mostly sedimentary rocks, one diorite. Concentrations of ice-rafted sand occur throughout Section 1; Section 2, 0-6 and 23-116 cm; Section 3, 25-110 cm; Section 4, 5-52 and 120-150 cm; Section 5, 55-105 cm; and Section 6, 61-75 cm.

SMEAR SLIDE SUMMARY (%):

	1, 50 D	2, 130 D	3, 50 D	4, 50 D	5, 65 D	6, 40 D
TEXTURE:						
Sand	15	2	25	15	10	3
Silt	50	64	61	48	60	55
Clay	35	34	14	37	30	42
COMPOSITION:						
Quartz	30	20	30	20	20	10
Feldspar	1	—	3	—	2	—
Mica	5	2	7	5	3	3
Clay	35	34	14	37	30	42
Accessory minerals:						
Amphibole	5	1	5	3	3	3
Glauconite	—	—	Tr	—	—	Tr
Garnet	1	—	1	Tr	Tr	—
Opaque minerals	1	1	3	2	3	1
Heavy minerals	3	1	5	3	2	2
Diatoms	15	40	30	25	30	30
Radiolarians	2	—	—	2	5	5
Sponge spicules	2	1	2	3	2	2
Silicoflagellates	—	Tr	Tr	—	Tr	2

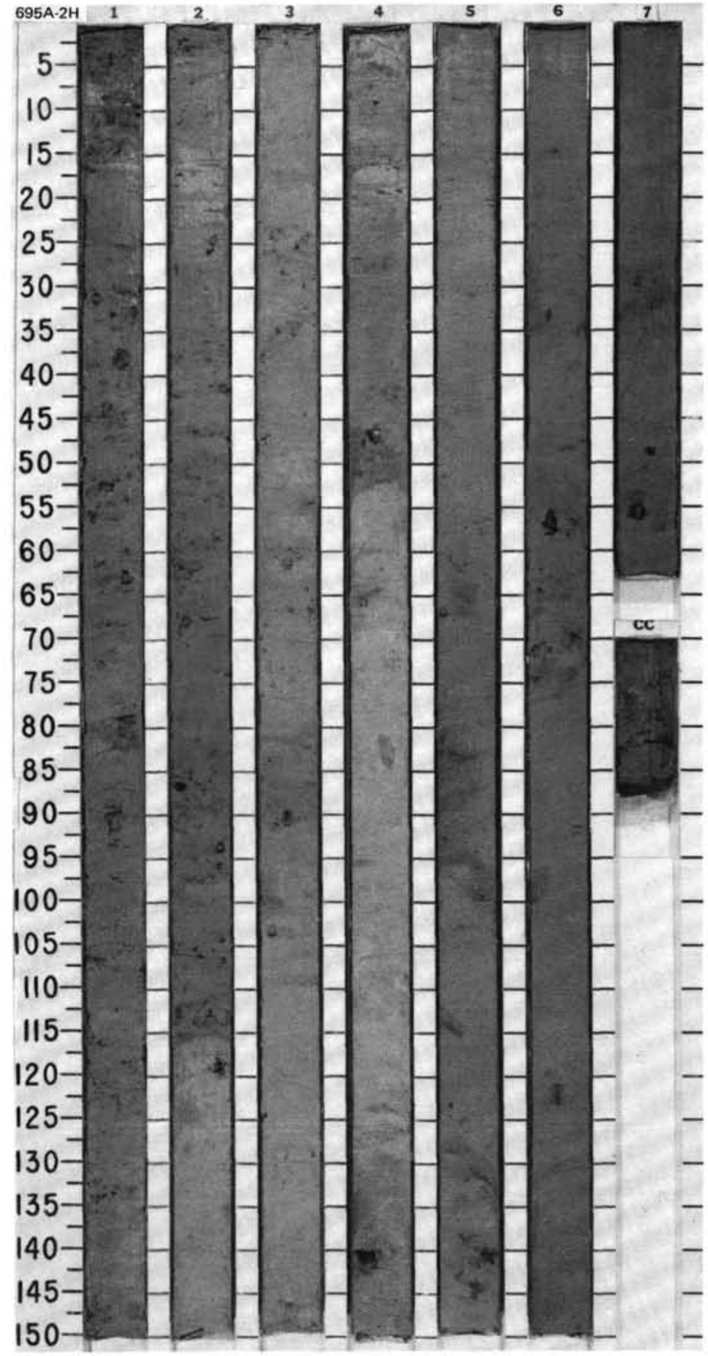

SITE 695 HOLE A CORE 3H CORED INTERVAL 1312.4-1322.0 mbsl; 12.4-22.0 mbsf

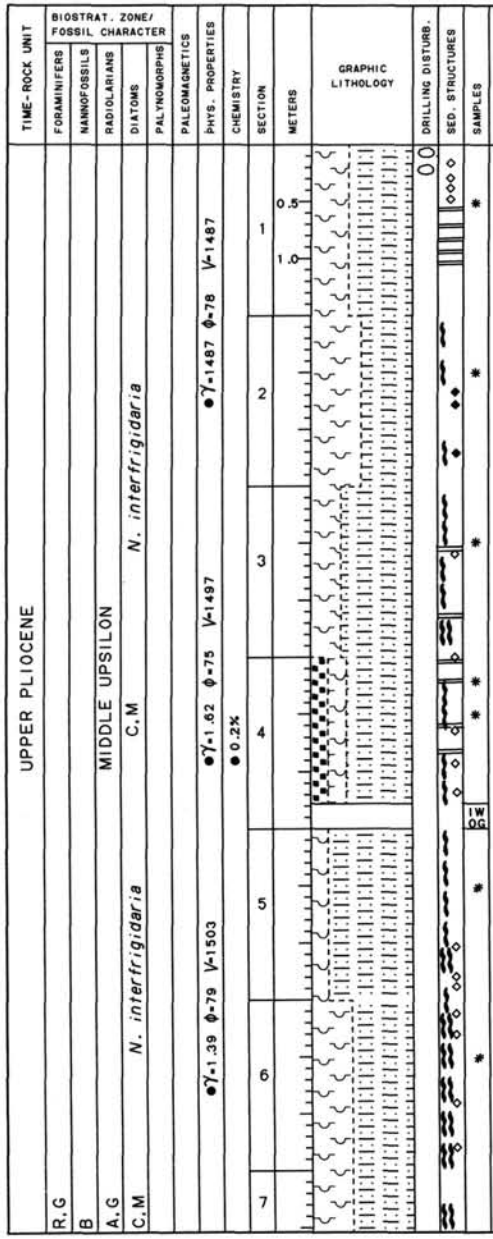

LITHOLOGIC DESCRIPTION

DIATOM CLAYEY MUD, DIATOM-BEARING CLAYEY MUD, and DIATOM- AND SILICOFLAGELLATE-BEARING CLAYEY MUD

Major lithologies: Diatom clayey mud in Sections 1–3 and 6–7, dark greenish gray (5GY 4/1) and dark gray (5Y 4/1), with greenish gray (5G 5/1) and dark gray (N 4/0) laminae. Diatom-bearing clayey mud in Section 5, dark greenish gray (5GY 4/1). Diatom- and silicoflagellate-bearing clayey mud in Section 4, dark greenish gray (5GY 4/1). Minor to moderate bioturbation, Sections 2 to 7; includes *Chondrites* and halo, vertical, and diffuse burrows. Few scattered sand grains, Sections 1 to 4. Dropstones, up to 3.5 cm in size, in Sections 1 and 3–6. Mud clasts in Section 2. No CC.

SMEAR SLIDE SUMMARY (%):

	1, 50 D	2, 50 D	3, 50 D	4, 22 M	4, 50 D	5, 50 D	6, 50 D
TEXTURE:							
Sand	2	3	2	—	3	2	—
Silt	59	65	64	—	59	34	52
Clay	39	32	34	—	38	64	48
COMPOSITION:							
Quartz	12	6	27	7	23	11	7
Feldspar	2	—	—	—	—	2	Tr
Mica	2	2	3	1	Tr	Tr	2
Clay	39	32	34	19	38	64	48
Volcanic glass	—	—	—	—	—	—	Tr
Accessory minerals:							
Amphibole	2	1	1	Tr	2	1	Tr
Glauconite	—	Tr	1	—	Tr	Tr	—
Heavy minerals	1	1	2	Tr	—	Tr	Tr
Opaque minerals	3	2	3	1	2	3	1
Diatoms	35	49	28	60	18	14	40
Radiolarians	1	2	Tr	1	2	Tr	—
Sponge spicules	2	2	—	1	—	2	1
Silicoflagellates	1	3	1	10	15	3	1

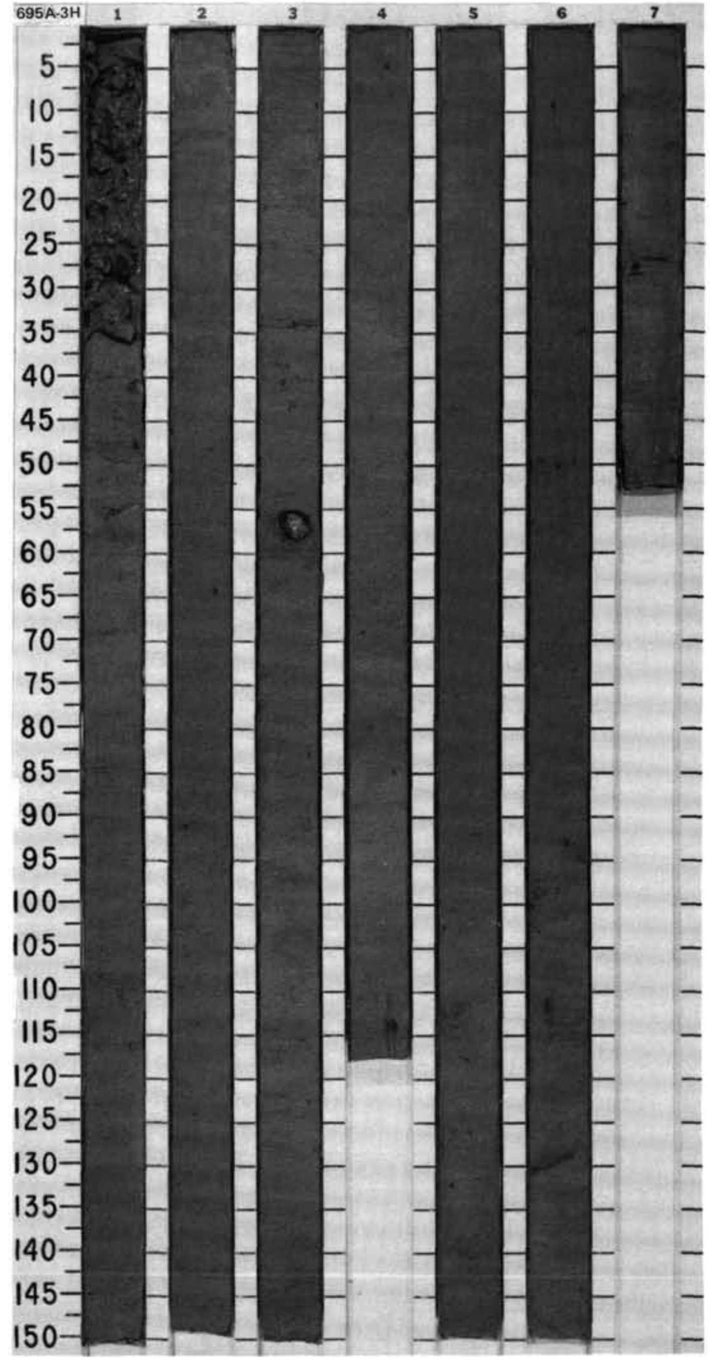

SITE 695 HOLE A CORE 4H CORED INTERVAL 1322.0-1331.6 mbsl; 22.0-31.6 mbsf

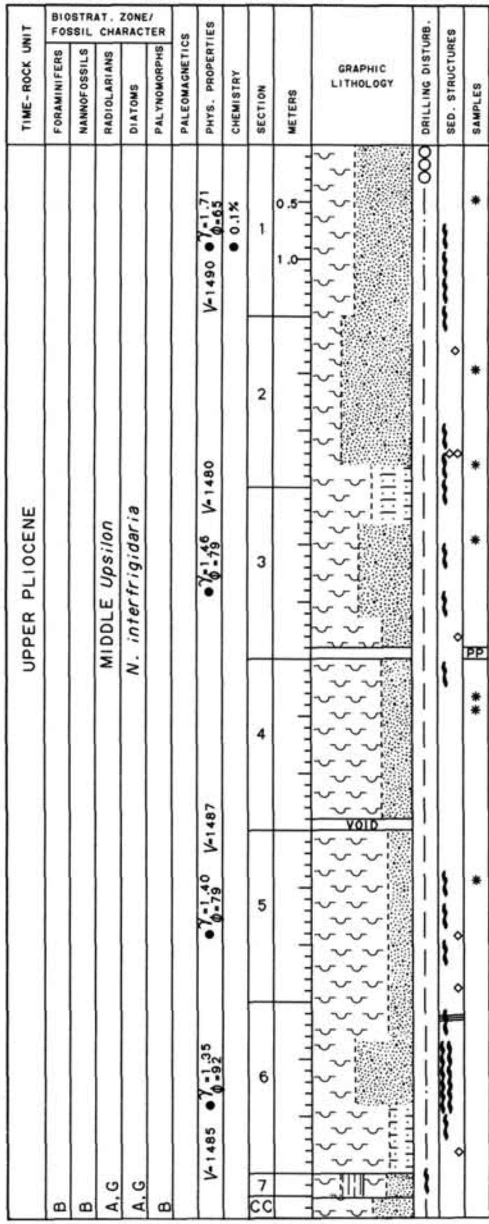

LITHOLOGIC DESCRIPTION

DIATOM SILTY MUD and MUDDY DIATOM OOZE

Major lithologies: Diatom silty mud in Section 1; Section 2, 0–130 cm; Section 3, 30–115 cm; and Section 6, 30-90 cm. Predominantly greenish gray (5GY 5/1 to 5G 5/1). Muddy diatom ooze in Section 2, 130 cm, to Section 3, 30 cm; Section 3, 115 cm, to Section 6, 30 cm; and Section 6, 90–150 cm), predominantly olive gray (5Y 5/2) with some grayish green (5G 5/2) layers when in or adjacent to the silty mud. Ooze layers are more common in the mud than mud layers in the ooze.

Minor lithology: Diatom-bearing silty mud, dark greenish gray (5GY 4/1), as irregular (disturbed?), thin layers and as clasts up to 8 cm long. Layers are present in Section 3, 40-43 and 80-84 cm, and Section 4, 53-56 cm.

Dropstones greater than mm-size are shown in the graphic column and include, with location and diameter: Section 2, 17 cm (0.5 cm); Section 2, 123 cm (1-2 cm, two); Section 3, 140 cm (1 cm); Section 5, 85 cm (1 cm); Section 5, 129 cm (1 cm); and Section 6, 120 cm (0.3 cm). These dropstones are subangular. Sand to mm-sized dropstones are present throughout. In the diatom silty muds, irregular "clasts" of white sand are also observed. Dominant color changes are gradual and a cyclicity is observed. Minor to moderate bioturbation is present in about 50-60% of the core.

SMEAR SLIDE SUMMARY (%):

	1, 50 D	2, 50 D	2, 130 M	3, 50 D	4, 40 M	4, 50 D	5, 50 D
TEXTURE:							
Sand	Tr	10	—	2	35	—	—
Silt	85	80	—	88	55	—	—
Clay	15	10	—	10	10	—	—
COMPOSITION:							
Quartz	33	30	12	30	45	15	12
Feldspar	—	2	—	—	5	—	—
Rock fragments	4	12	—	3	20	—	—
Mica	1	Tr	—	1	—	3	2
Clay	15	10	20	10	—	10	10
Volcanic glass	—	—	—	—	2	—	—
Accessory minerals	—	8	6	7	8	7	6
Amphibole	Tr	5	—	—	5	—	—
Glauconite	Tr	—	—	—	—	—	—
Opaque minerals	2	—	—	2	—	—	—
Diatoms	42	30	60	45	15	65	70
Radiolarians	1	1	—	Tr	—	—	—
Sponge spicules	—	Tr	Tr	Tr	—	—	—
Silicoflagellates	2	2	2	2	—	—	—

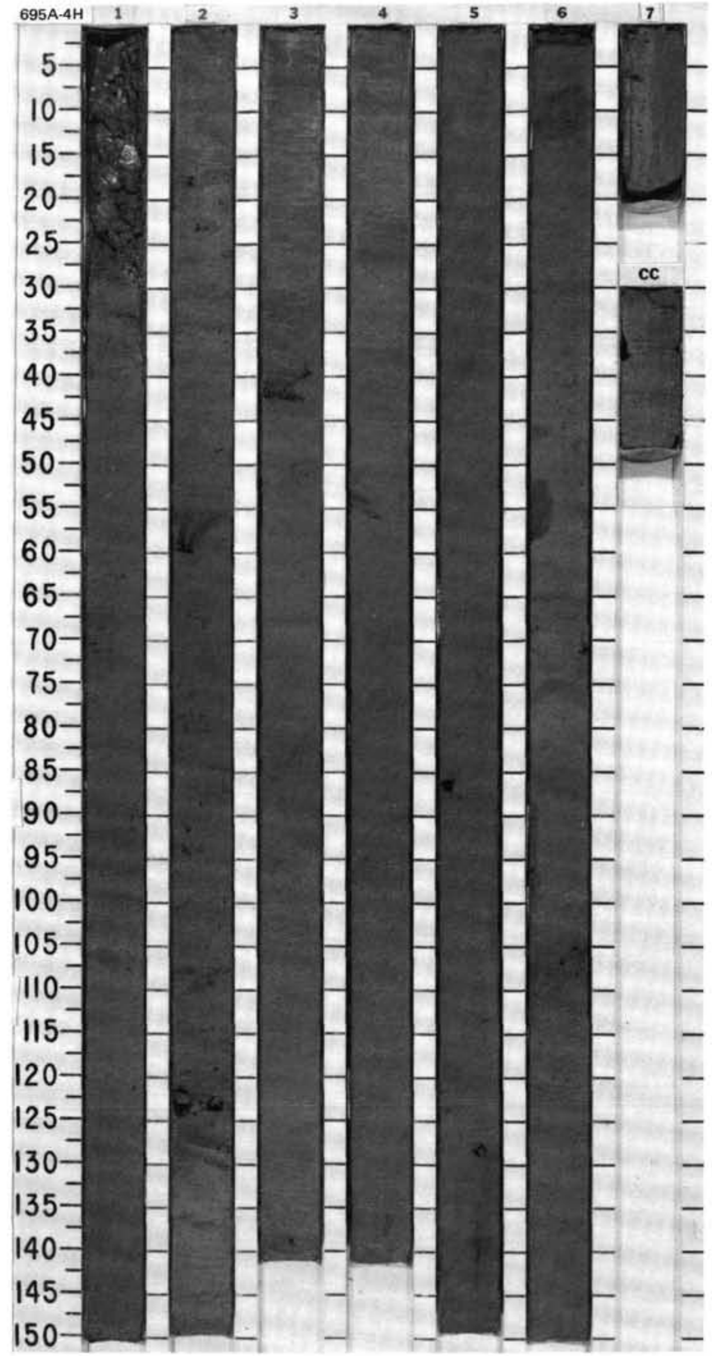

SITE 695 HOLE A CORE 5H CORED INTERVAL 1331.6-1341.2 mbsl; 31.6-41.2 mbsf

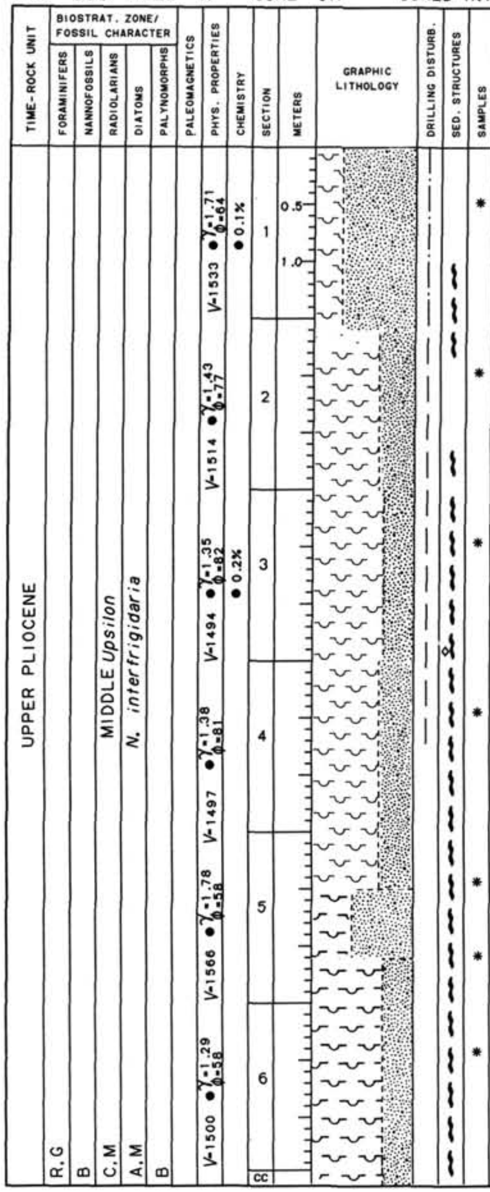

LITHOLOGIC DESCRIPTION

DIATOM SILTY MUD and MUDDY DIATOM OOZE

Major lithologies: Diatom silty mud from Section 1, 0 cm, to Section 2, 10 cm, and Section 5, 50-110 cm, greenish gray (5BG 5/1), grading at the base of Section 1 into grayish green (5G 5/1). Muddy diatom ooze from Section 2, 10 cm, to Section 5, 50 cm, and Section 5, 110 cm, through CC, olive gray (5Y 5/2).

Minor lithologies: Silty mud, as irregular layers, is present in Section 3, 29-40 and 57-73 cm. Muddy diatom ooze, that may be altered volcanic ash layers, grayish green (5G 5/2), 1-4 cm thick, are present in Section 1, 24-26, 50-52, 96-99, and 104-106 cm.

Dropstones are minor. A 22-mm dropstone occurs at Section 1, 141 cm. In Section 5, 80-92 cm, sand-sized dropstones are present. Color and lithologic changes show clear cyclicity. Minor bioturbation throughout.

SMEAR SLIDE SUMMARY (%):

	1, 45 D	2, 45 D	3, 45 D	4, 45 D	5, 45 D	5, 105 M	6, 45 D
TEXTURE:							
Sand	15	—	—	—	—	12	—
Silt	80	—	—	—	—	68	—
Clay	5	—	—	—	—	20	—
COMPOSITION:							
Quartz	49	27	13	15	24	26	8
Feldspar	5	2	5	3	5	3	4
Rock fragments	10	—	—	—	2	2	—
Mica	4	4	2	2	4	3	5
Clay	—	—	10	12	10	20	12
Accessory minerals	—	—	—	6	—	—	—
Amphiboles	Tr	—	—	—	—	2	—
Glauconite	Tr	—	—	Tr	—	—	—
Opaque minerals	2	1	Tr	2	Tr	4	Tr
Diatoms	30	65	70	60	55	40	70
Radiolarians	Tr	1	Tr	—	—	—	—
Sponge spicules	—	—	—	Tr	—	—	—
Silicoflagellates	—	—	—	Tr	—	—	—

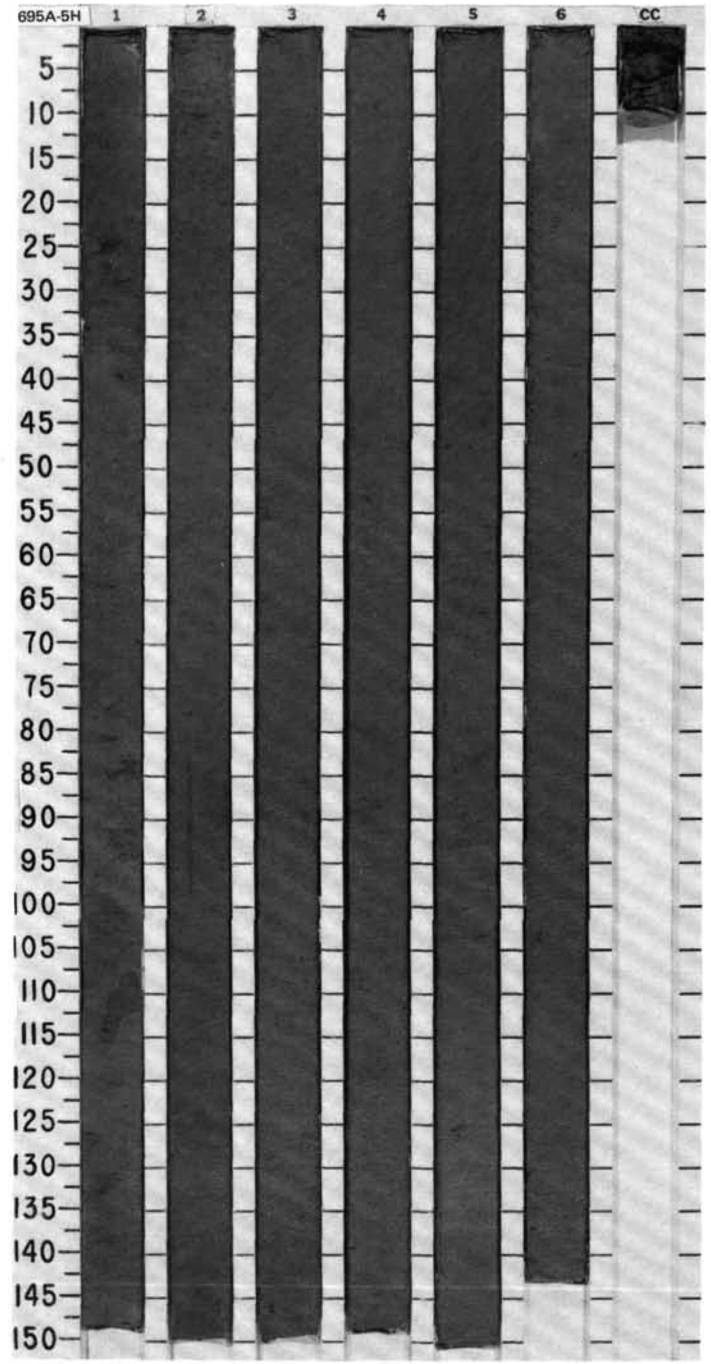

SITE 695 HOLE A CORE 6H CORED INTERVAL 1341.2-1350.8 mbsl; 41.2-50.8 mbsf

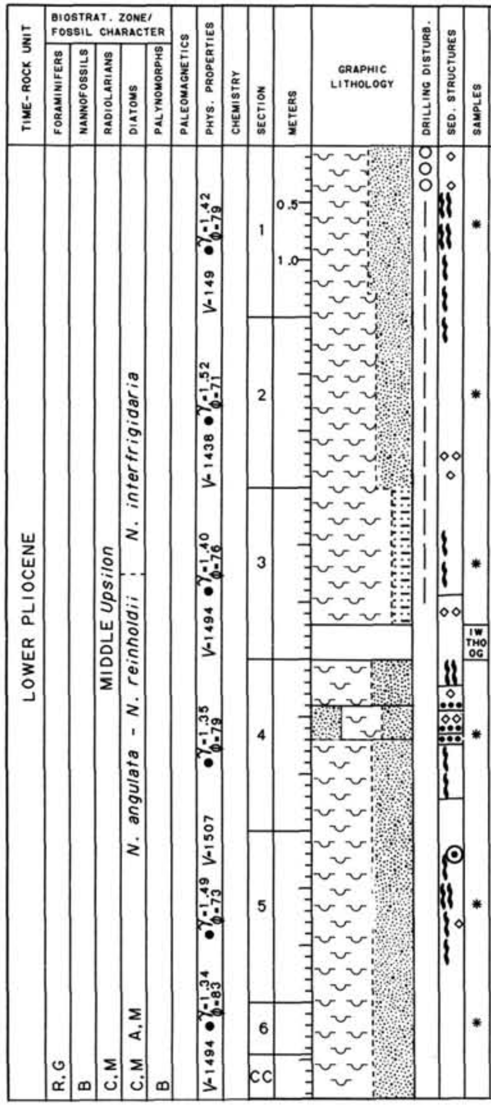

LITHOLOGIC DESCRIPTION

MUDDY DIATOM OOZE

Major lithology: Muddy diatom ooze, predominantly greenish gray (5GY 5/1) and olive gray (5Y 5/2), with minor amounts of grayish green (5G 5/2). Like the cores above, the color changes in this core parallel lithologic changes, but at the level of smear slide resolution and because the sequence is becoming more diatom-rich, lithologic boundary changes are not detectable.

Minor lithologies: Silty and sandy mud (turbidites), possibly in all of the coarser layers, which include Section 2, 47-51 cm, 96-97 cm (clast), and 113-114 cm; Section 3, 78 cm (clast) and 108 cm; and Section 4, 20 and 40-70 cm (many layers show sharp bases and graded bedding), and 125 cm. The silt-sized quartz grains are angular to very angular, whereas the sand-sized grains tend to be rounded to subrounded. Muddy diatom ooze, possibly altered volcanic ash, grayish green (5G 5/2), in layers in Section 1, 37-38 cm; Section 2, 46-47 and 70 cm; and Section 4, 40-70 cm.

Dropstones are common throughout and tend to be angular to subangular. Greater than mm-sized dropstones are present in Section 1, 4 cm (2 cm in size), black and angular; Section 1, 22 cm, (0.8 cm), rounded, black, very weathered; Section 1, 27 cm (0.8 cm), black and angular; Section 2, 119 cm (two, 1 cm), angular, metamorphic; Section 2, 138 cm (2 mm), angular, black; Section 3, 103 cm (two, 0.3-0.5 cm), angular; Section 4, 25 cm (0.3 cm); Section 4, 49 cm (0.8 cm); Section 4, 57 cm (0.6 cm); Section 5, 83 cm (0.8 cm), subrounded; there is also a Mn concretion at Section 5, 17 cm. Abundant sand-sized dropstone "clasts" are also present in Section 4, 40-70 cm, and Section 5. Color changes are gradual and cyclic.

SMEAR SLIDE SUMMARY (%):

	1, 70 D	2, 70 D	3, 70 D	4, 70 D	5, 70 D	6, 30 D
TEXTURE:						
Sand	—	—	—	—	—	—
Silt	—	—	—	—	—	—
COMPOSITION:						
Quartz	19	14	6	15	19	15
Feldspar	2	2	—	2	—	2
Mica	4	4	2	—	6	—
Clay	10	12	6	20	12	20
Volcanic glass	2	2	—	Tr	2	Tr
Accessory minerals	6	—	2	1	—	1
Opaque minerals	2	Tr	—	1	1	1
Diatoms	55	65	80	60	60	60
Radiolarians	—	1	—	—	Tr	—
Sponge spicules	—	—	4	1	1	1
Silicoflagellates	—	—	—	—	-1	—

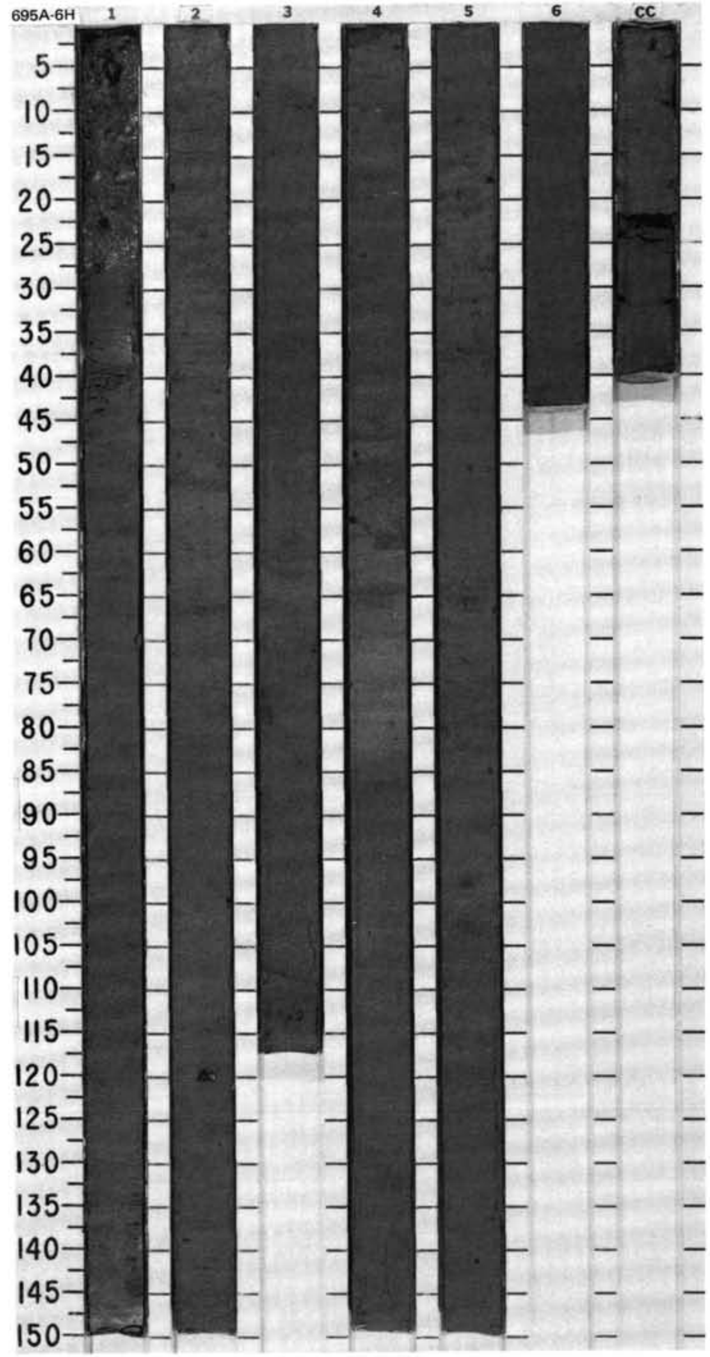

SITE 695 HOLE A CORE 7H CORED INTERVAL 1350.8-1360.4 mbsl; 50.8-60.4 mbsf

TIME-ROCK UNIT	BIOSTRAT. ZONE/ FOSSIL CHARACTER: FORAMINIFERS	NANNOFOSSILS	RADIOLARIANS	DIATOMS	PALYNOMORPHS	PALEOMAGNETICS	PHYS. PROPERTIES	CHEMISTRY	SECTION
LOWER PLIOCENE	B	B	MIDDLE *Upsilon* A,G	*N. angulata* - *N. reinholdii* F,M	B		V=1506 ● γ=1.38 ϕ=83; V=1512 ● γ=1.57 ϕ=72; γ=1.61 ϕ=65 ●; V=1525		1, 2, 3, CC

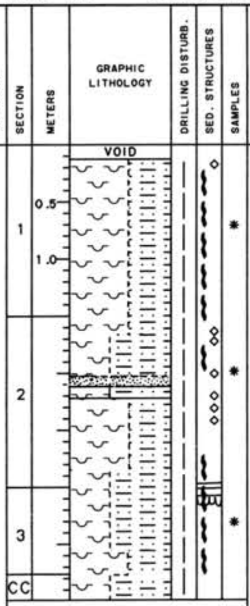

LITHOLOGIC DESCRIPTION

MUDDY DIATOM OOZE and DIATOM CLAYEY MUD

Major lithologies: Muddy diatom ooze, olive gray (5Y 5/2). Diatom clayey mud, greenish gray (5G 5/1) with minor bluish gray (5B 5/1) and gray (5Y 5/1). Silty mud layer is present in Section 2, 53–63 cm. Color changes are cyclic and gradual.

Bioturbation is minor throughout. *Planolites* burrows occur in Section 3, 7 cm. Sand-sized dropstones throughout, 7-mm-sized dropstones in Section 1, 15 cm, and Section 2, 10, 27, 52, 74, 82, and 86 cm.

SMEAR SLIDE SUMMARY (%):

	1, 70 D	2, 47 D	3, 30 D
TEXTURE:			
Sand	—	2	2
Silt	—	68	59
Clay	—	30	39
COMPOSITION:			
Quartz	20	23	20
Feldspar	5	2	—
Rock fragments	—	1	—
Clay	15	30	39
Volcanic glass	—	2	—
Accessory minerals	2	1	2
Opaque minerals	1	1	2
Hornblende	—	—	2
Diatoms	56	40	35
Radiolarians	Tr	Tr	Tr
Sponge spicules	1	Tr	—

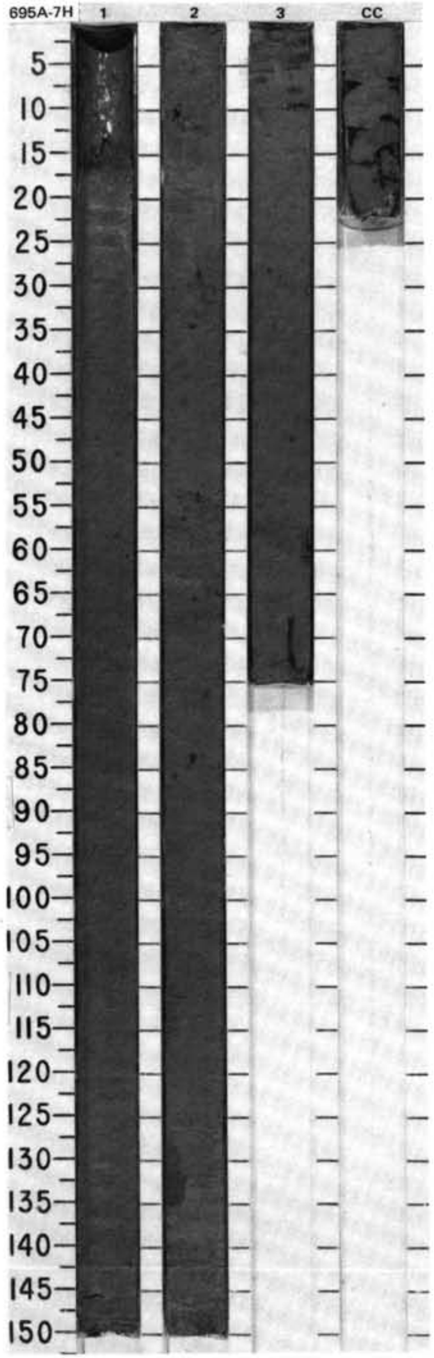

SITE 695 HOLE A CORE 8H CORED INTERVAL 1360.4-1370.0 mbsl; 60.4-70.0 mbsf

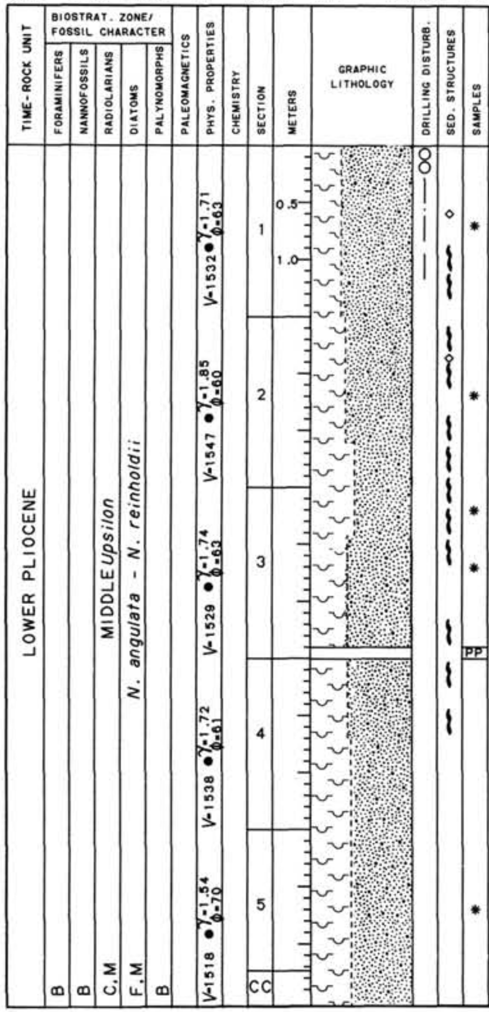

LITHOLOGIC DESCRIPTION

DIATOM SILTY MUD

Major lithology: Diatom silty mud, greenish gray (5GY 5/1) and dark greenish gray (5GY 4/1), alternating on the scale of 100 cm.

Minor lithologies: Altered volcanic ash(?), in faint grayish green (5G 5/2) layers, occurs in Section 1, 33-34, 41-42, 55-56, 65-66, and 71-72 cm; Section 2, 2, 4-5, 8-13, 21-22, 42-43, 44-45, and 51-52 cm; Section 3, 54-55 and 63-65 cm; Section 4, 102-103, 105-106, and 126-127 cm; and as disturbed layers in Section 5. Silt in Section 2, 56-58 cm, dark gray (5Y 4/1), with sharp boundaries. At Section 1, 30 cm, one of the dropstones is pumice. At Section 2, 55 cm, there is a possible layer of mud pebbles.

Sand-sized dropstones observed throughout. Bioturbation varies from absent to minor. Drilling disturbance is severe (soupy) at the top of Section 1, but is otherwise minor.

SMEAR SLIDE SUMMARY (%):

	1, 70 D	2, 70 D	3, 24 D	3, 70 D	5, 70 D
TEXTURE:					
Sand	10	2	Tr	5	5
Silt	75	70	85	85	80
Clay	15	28	15	10	15
COMPOSITION:					
Quartz	40	30	30	47	32
Feldspar	—	—	—	2	—
Rock fragments	—	—	—	—	2
Mica	5	1	4	4	4
Clay	15	28	15	10	15
Volcanic glass	2	2	—	—	2
Accessory minerals	5	—	6	—	—
Opaque minerals	2	2	—	2	4
Amphiboles	1	1	Tr	—	Tr
Diatoms	30	35	45	35	40
Radiolarians	—	Tr	Tr	—	—
Sponge spicules	—	1	—	—	1
Silicoflagellates	—	Tr	—	—	—

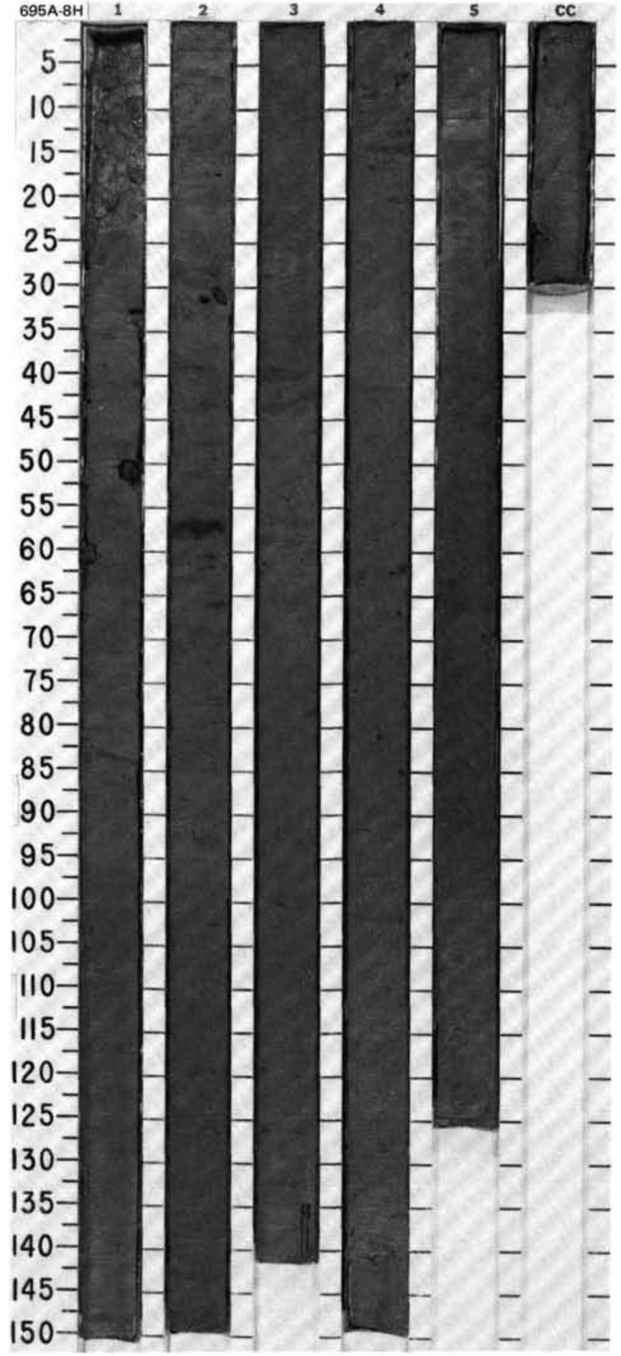

SITE 695 HOLE A CORE 9H CORED INTERVAL 1370.0-1379.6 mbsl; 70.0-79.6 mbsf

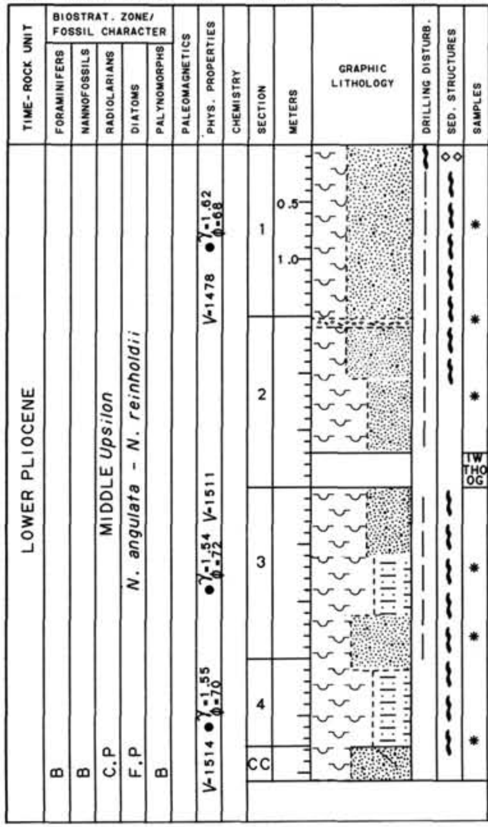

LITHOLOGIC DESCRIPTION

DIATOM SILTY MUD and MUDDY DIATOM OOZE

Major lithologies: Diatom silty mud, dark greenish gray (5G 4/1) and greenish gray (5G 5/1). Muddy diatom ooze, olive gray (5Y 5/2). Lithologic and color transitions are gradual, occuring over 2-10 cm intervals.

Minor lithologies: Sandy mud/volcanic ash, in Section 2, 5-12 cm, and Section 3, 5-12 cm, black (5Y 2.5/1). Altered volcanic ash(?) as thin (1-3 cm) layers of greenish gray (5G 5/2) which occur in Section 1, 135-136 and 143-144 cm; Section 2, 35-36 and 42-43 cm; and Section 3, 7-8, 19-20, 36-37, 54-55, 122-123, 127-128, and 131-132 cm.

Sand-sized dropstones occur throughout. Two larger dropstones are present in Section 1, 10 cm, subrounded and rounded, 3 cm in size, possibly from uphole contamination. Minor bioturbation throughout.

SMEAR SLIDE SUMMARY (%):

	1, 70 D	2, 5 M	2, 70 D	3, 70 D	3, 130 D	4, 70 D
TEXTURE:						
Sand	12	50	—	—	10	—
Silt	72	35	—	—	75	—
Clay	16	15	—	—	15	—
COMPOSITION:						
Quartz	34	5	17	14	34	12
Feldspar	—	—	2	—	2	—
Mica	4	—	—	4	—	6
Clay	16	15	20	20	15	15
Volcanic glass	—	72	3	2	Tr	1
Accessory minerals	8	8	—	—	8	—
Glauconite	Tr	—	—	Tr	Tr	—
Amphibole	Tr	—	—	Tr	Tr	—
Opaque minerals	4	—	3	—	1	1
Diatoms	34	Tr	55	60	40	65
Radiolarians	Tr	—	—	Tr	—	—
Sponge spicules	Tr	—	—	Tr	—	—

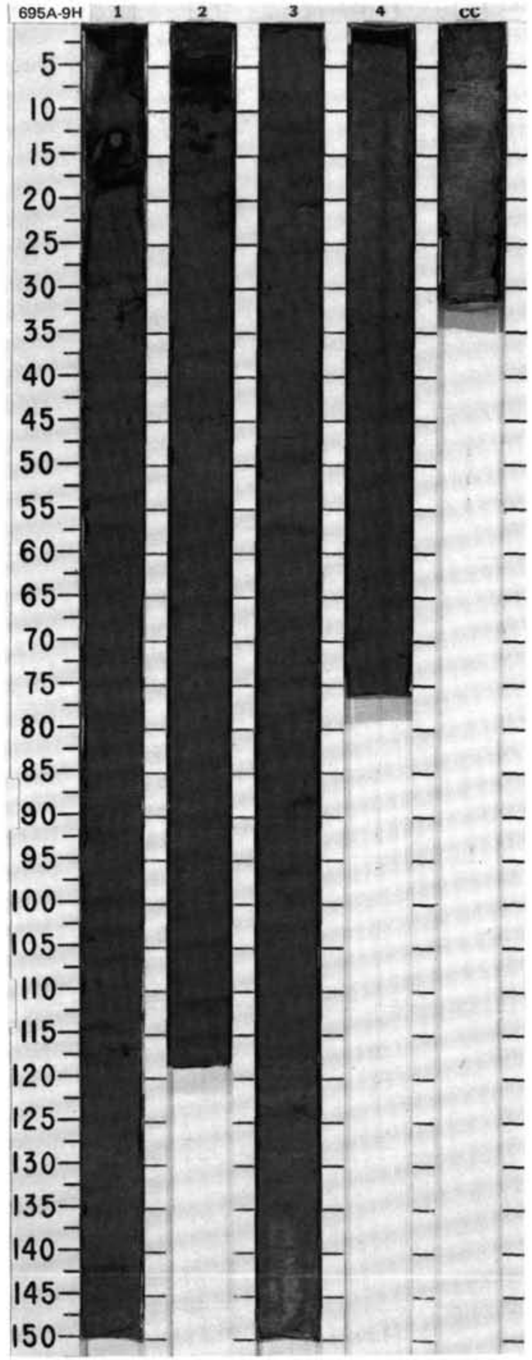

SITE 695 HOLE A CORE 10H CORED INTERVAL 1379.6-1389.2 mbsl; 79.6-89.2 mbsf

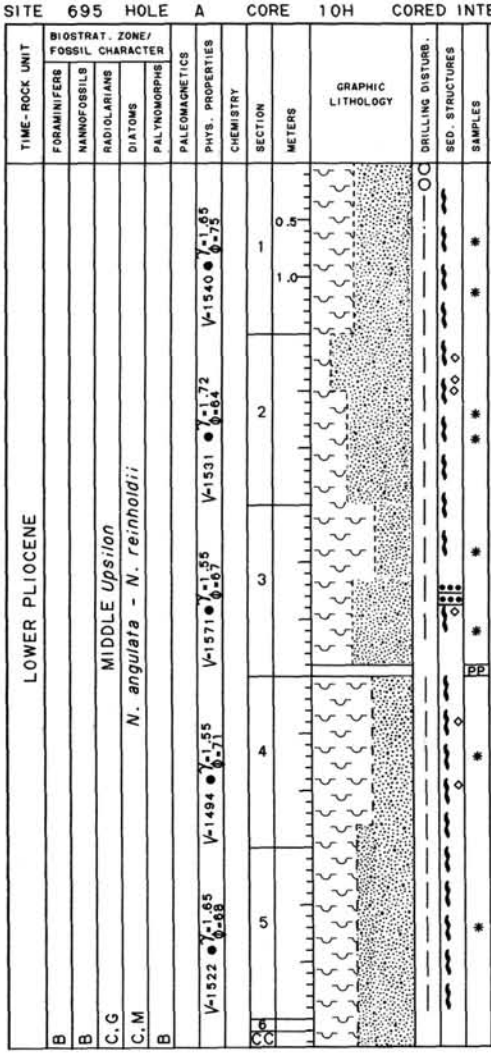

LITHOLOGIC DESCRIPTION

DIATOM-BEARING SILTY MUD, DIATOM SILTY MUD, and MUDDY DIATOM OOZE

Major lithologies: Diatom silty mud, dark greenish gray (5G 4/1). White 1–3 mm, diatom-bearing, sandy mud "clasts" are dispersed throughout the unit. In Section 3, 65–70 cm, there are two graded beds with sharp basal contacts (possibly scoured). Muddy diatom ooze, gray (5Y 5/1).

Minor lithologies: Diatom-bearing sandy mud, grayish green (5G 5/2), with up to 10% volcanic ash present throughout the core in 1-5-cm-thick layers; clasts occur in Section 1, 35–36, 44–45, 66–67, 90–91, and 134–135 cm; Section 2, approximately 15% of the core in 15 layers; Section 3, 73–140 cm, approximately 30% of the core in 12 layers; and Section 5, approximately 15% of the core in 16 layers.

Minor bioturbation present throughout. Sand-sized dropstones are present throughout. Larger dropstones are present in Section 2, 15, 28, and 44 cm, all approximately 0.5 cm in size and angular; in Section 3, 91 cm, 1 cm in size and angular; and in Section 4, 45 and 91 cm, mm size.

SMEAR SLIDE SUMMARY (%):

	1, 70 D	2, 72 M	2, 85 D	3, 40 D	3, 110 D	4, 70 D	5, 70 D
TEXTURE:							
Sand	12	64	16	—	2	—	2
Silt	78	28	72	—	74	—	74
Clay	10	8	12	—	24	—	24
COMPOSITION:							
Quartz	22	38	32	17	17	17	27
Feldspar	4	8	2	—	2	—	—
Rock fragments	—	14	4	—	—	—	—
Mica	6	—	4	4	8	4	6
Clay	10	8	12	12	24	10	14
Volcanic glass	—	4	—	Tr	4	Tr	Tr
Accessory minerals	8	6	8	—	—	8	8
Opaque minerals	3	—	2	2	1	1	Tr
Amphiboles	—	2	Tr	Tr	—	—	—
Glauconite	—	Tr	—	—	—	—	—
Diatoms	45	20	34	65	42	60	45
Radiolarians	—	—	1	—	—	—	—
Sponge spicules	2	—	1	—	2	—	—

CORE 113-695A-11I NO RECOVERY

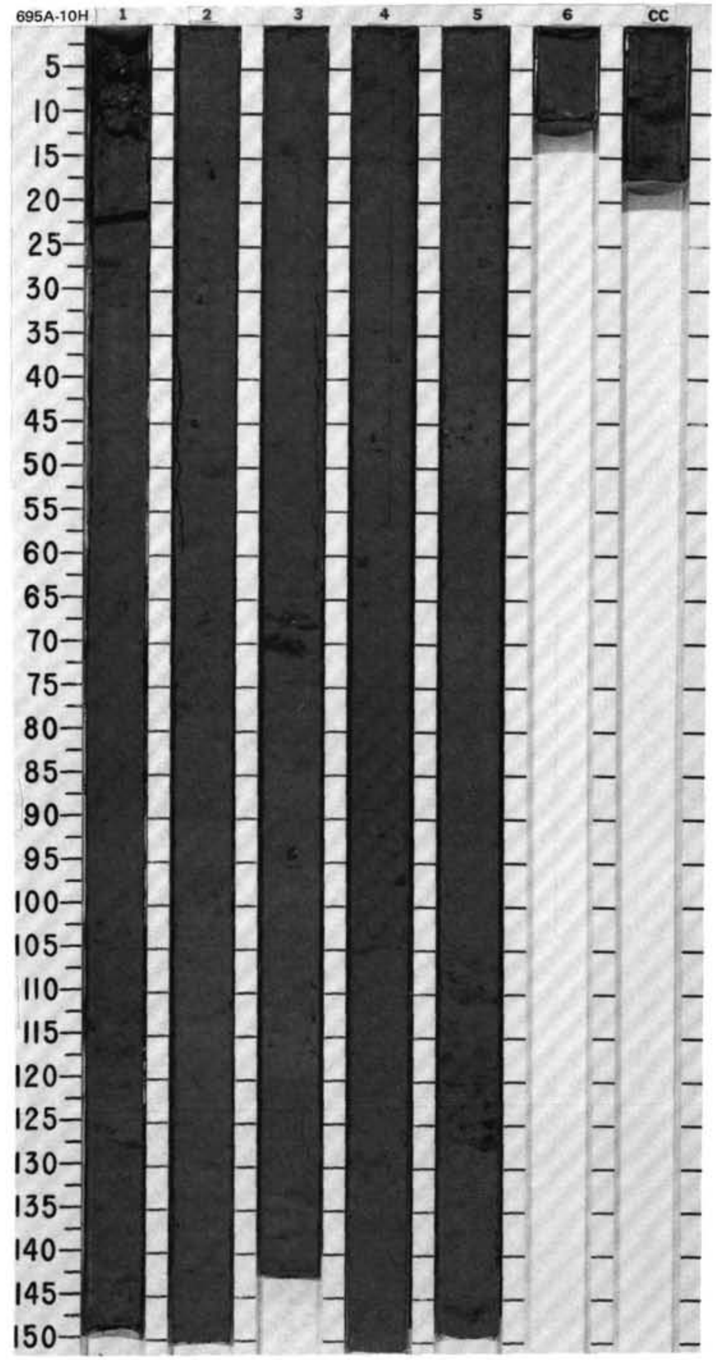

SITE 695 HOLE A CORE 12H CORED INTERVAL 1389.2-1398.8 mbsl; 89.2-98.8 mbsf

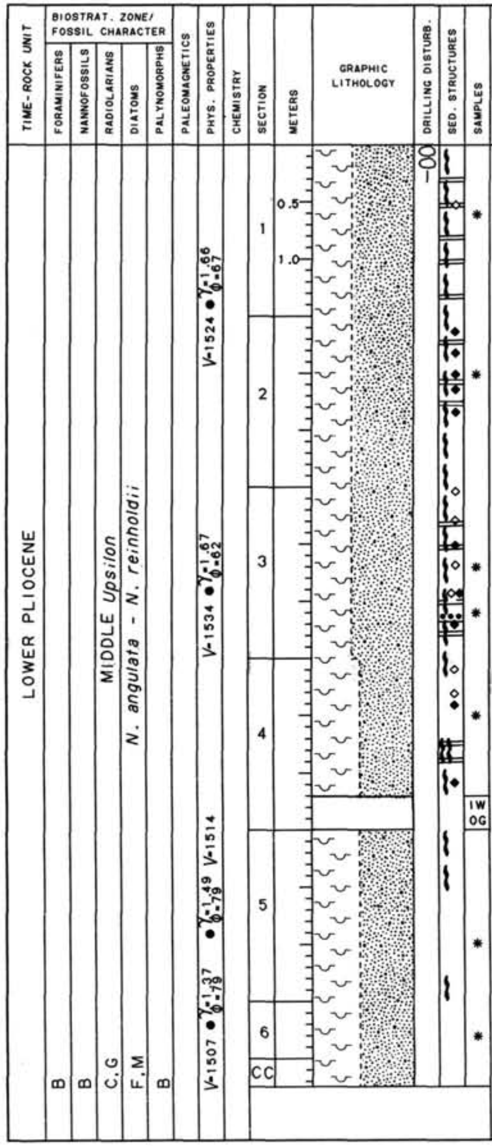

LITHOLOGIC DESCRIPTION

DIATOM SILTY MUD and MUDDY DIATOM OOZE

Major lithologies: Diatom silty mud, dark greenish gray (5G 4/1). Muddy diatom ooze, olive gray (5Y 4/2).

Minor lithology: Muddy diatom ooze, greenish gray (5G 5/2); laminae and beds of devitrified ash occur in Sections 1-4.

Slight bioturbation in Sections 1-5; dark gray (N 4/0) mottles and laminae in Section 2, 23-81 cm. Dropstones occur in Sections 1-4; clasts of white sand are especially abundant in Section 2.

SMEAR SLIDE SUMMARY (%):

	1, 69 D	2, 50 D	3, 70 D	3, 113 M	4, 50 D	5, 101 D	5, 126 M
TEXTURE:							
Sand	Tr	3	3	15	2	—	4
Silt	84	74	67	73	79	—	77
Clay	16	23	30	12	19	—	19
COMPOSITION:							
Quartz	18	20	20	25	12	10	12
Feldspar	—	—	2	2	—	Tr	1
Mica	10	3	7	2	12	2	7
Clay	16	23	30	12	19	20	19
Volcanic glass	4	—	3	—	3	—	—
Calcite	—	—	—	—	—	—	Tr
Accessory minerals	12	—	—	—	—	—	—
Garnet	—	Tr	—	2	—	—	—
Amphibole	—	2	1	3	1	2	1
Glauconite	Tr	—	1	Tr	Tr	Tr	2
Micronodules	—	2	—	—	2	—	7
Heavy minerals	—	3	1	2	—	Tr	—
Opaque minerals	—	—	2	3	1	3	3
Diatoms	40	40	39	40	47	54	45
Radiolarians	Tr	5	2	7	2	5	2
Sponge spicules	—	2	—	2	Tr	2	Tr
Silicoflagellates	—	—	2	—	1	2	1

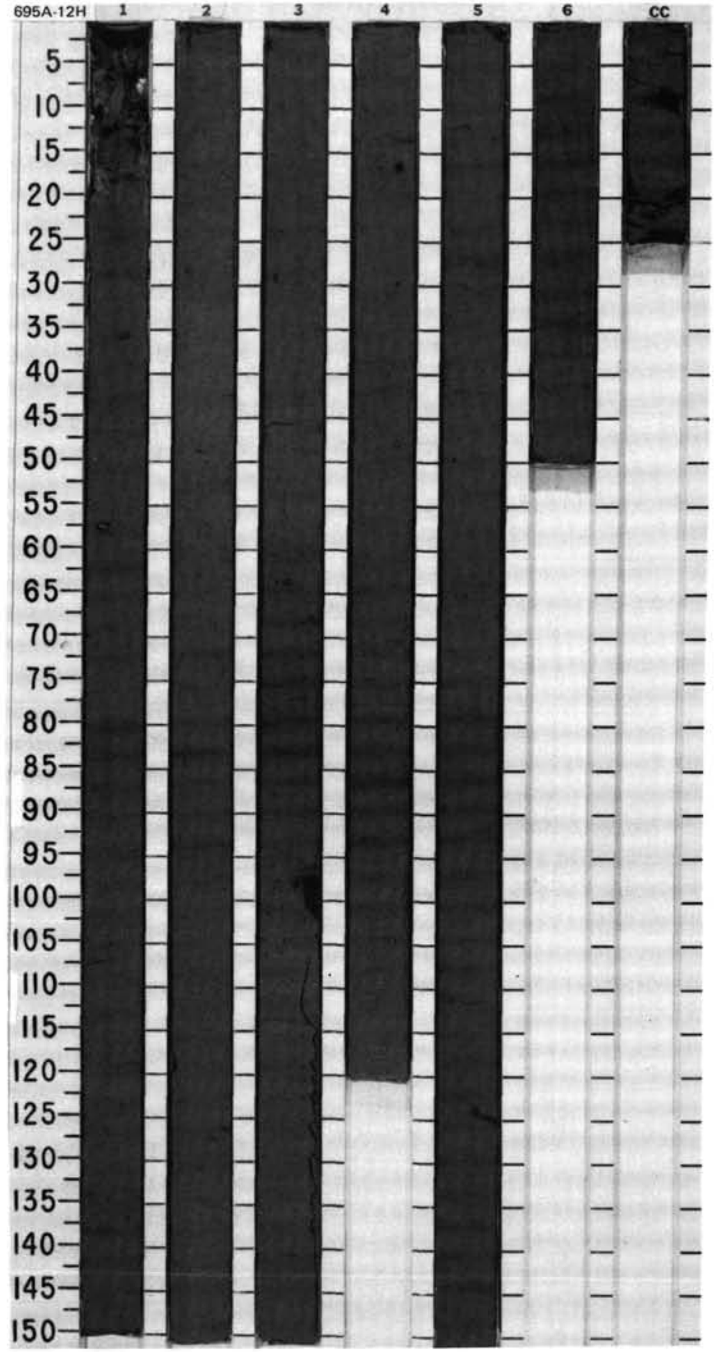

SITE 695 HOLE A CORE 13H CORED INTERVAL 1398.8-1408.5 mbsl; 98.8-108.5 mbsf

TIME-ROCK UNIT	FORAMINIFERS	NANNOFOSSILS	RADIOLARIANS	DIATOMS	PALYNOMORPHS	PALEOMAGNETICS	PHYS. PROPERTIES	CHEMISTRY	SECTION	METERS	GRAPHIC LITHOLOGY	DRILLING DISTURB.	SED. STRUCTURES	SAMPLES
LOWER PLIOCENE	B	B		*N. angulata - N. reinholdii* C,M	B				1, 2, 3, 4, CC	0.5, 1.0				

Biostrat. zone/fossil character

LITHOLOGIC DESCRIPTION

MUDDY DIATOM OOZE and DIATOM CLAYEY MUD

Major lithologies: Muddy diatom ooze in Section 1, grading to diatom clayey mud in Section 2, dark gray (5Y 4/1) and olive gray (5Y 4/2). Color boundaries are gradational over about 10 cm with color changes at 40-120 cm intervals.

Minor lithology: Diatom-bearing silty mud, as clasts up to 3 cm across in Section 1, 101 cm, and Section 2, 82 cm, dark gray (5Y 4/1), with about 10% opaque grains/Mn micronodules.

Minor to moderate bioturbation. A few ice-rafted(?) sand grains occur in Section 1, 0-30 cm; Section 2, 60-83 and 140-143 cm; Section 3, 85-150 cm; and Section 4, 0-25 cm. Tiny clasts (1-2 mm) of white silty mud also occur rarely.

SMEAR SLIDE SUMMARY (%):

	1, 50 D	2, 50 D	3, 50 D	4, 50 D
TEXTURE:				
Sand	—	2	4	—
Silt	—	68	81	—
Clay	—	30	15	—
COMPOSITION:				
Quartz	10	12	12	8
Mica	2	5	2	1
Clay	25	30	15	12
Volcanic glass	—	3	3	3
Calcite/dolomite	—	3	10	8
Accessory minerals:				
Heavy minerals	1	—	2	2
Micronodules	3	Tr	—	—
Amphibole	1	1	—	—
Opaque minerals	—	1	2	3
Diatoms	50	43	49	59
Radiolarians	5	Tr	3	2
Sponge spicules	2	Tr	—	Tr
Silicoflagellates	1	1	2	2

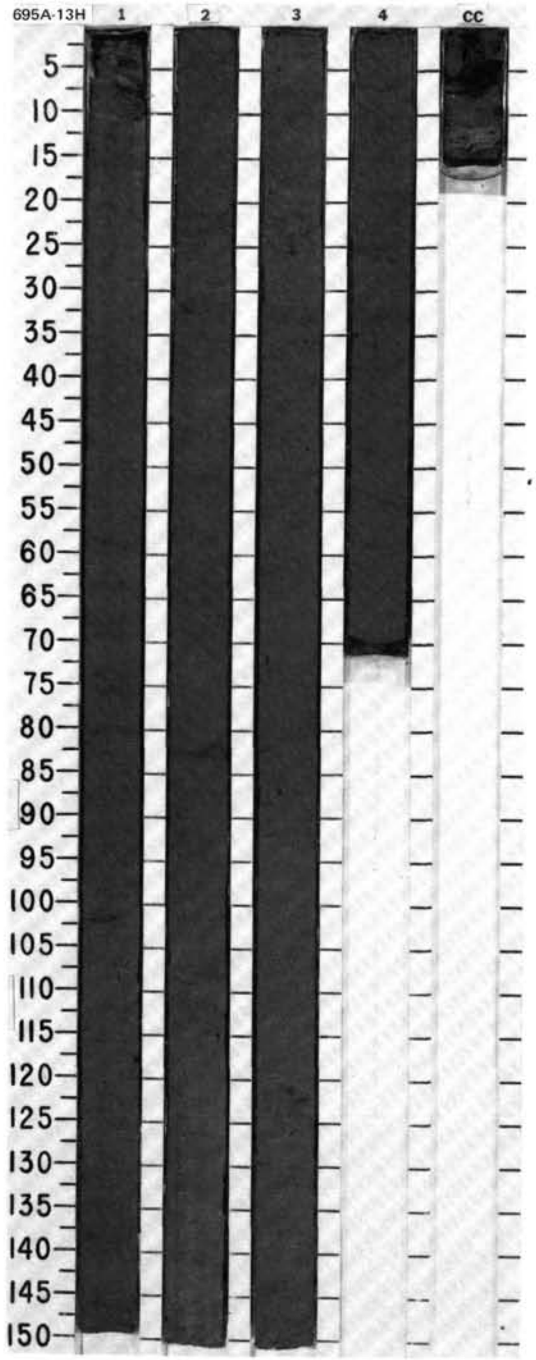

SITE 695 HOLE A CORE 14H CORED INTERVAL 1408.5-1418.2 mbsl; 108.5-118.2 mbsf

TIME-ROCK UNIT	FORAMINIFERS	NANNOFOSSILS	RADIOLARIANS	DIATOMS	PALYNOMORPHS	PALEOMAGNETICS	PHYS. PROPERTIES	CHEMISTRY	SECTION	METERS
LOWER PLIOCENE	B	B	MIDDLE *Upsilon* A,G	*N. angulata - N. reinholdii* F,P	B		V-1510 ● γ=1.46 φ=79; ● γ=1.56 φ=71 V-1517	● 0.3%	1, 2, 3, CC	0.5, 1.0

GRAPHIC LITHOLOGY / DRILLING DISTURB. / SED. STRUCTURES / SAMPLES

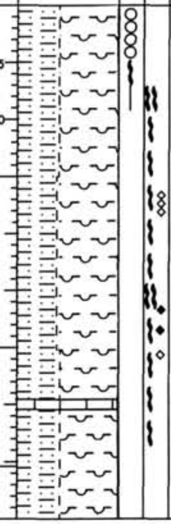

LITHOLOGIC DESCRIPTION

MUDDY DIATOM OOZE

Major lithology: Muddy diatom ooze, olive gray (5Y 4/2) to dark gray (5Y 4/1), slightly lighter toward base (5Y 4.5/1).

Minor lithologies:

a. Carbonate layer, light olive gray (5Y 6/2), Section 3, 46-60 cm; burrowed top, gradational base. XRD analysis of this layer shows a mixture of carbonate minerals. Dolomite is the dominant phase, Mg-calcite is common, and siderite is rare.

b. Diatom and glass-bearing silty mud, very dark gray (5Y 3/1), 4 cm layer at top of CC and base of Section 3; ash bed. Grades up into muddy diatom ooze.

Very few scattered sand grains and small dropstones, predominantly angular and sedimentary.

SMEAR SLIDE SUMMARY (%):

	1, 50 D	2, 50 D	3, 50 M	3, 70 D	CC, 2 M
TEXTURE:					
Sand	—	—	—	—	20
Silt	—	—	—	—	66
Clay	—	—	—	—	14
COMPOSITION:					
Quartz	8	7	2	8	15
Feldspar	—	—	—	—	3
Mica	3	Tr	—	12	2
Clay	23	18	—	11	14
Volcanic glass	1	2	—	—	25
Calcite/dolomite	3	4	89	5	—
Accessory minerals:					
Opaque minerals	Tr	3	1	4	—
Micronodules	2	2	—	—	15
Glauconite	1	Tr	—	—	1
Amphibole	1	Tr	1	2	3
Diatoms	56	62	7	55	20
Radiolarians	2	1	Tr	1	—
Sponge spicules	Tr	—	—	Tr	1
Silicoflagellates	Tr	1	—	2	1

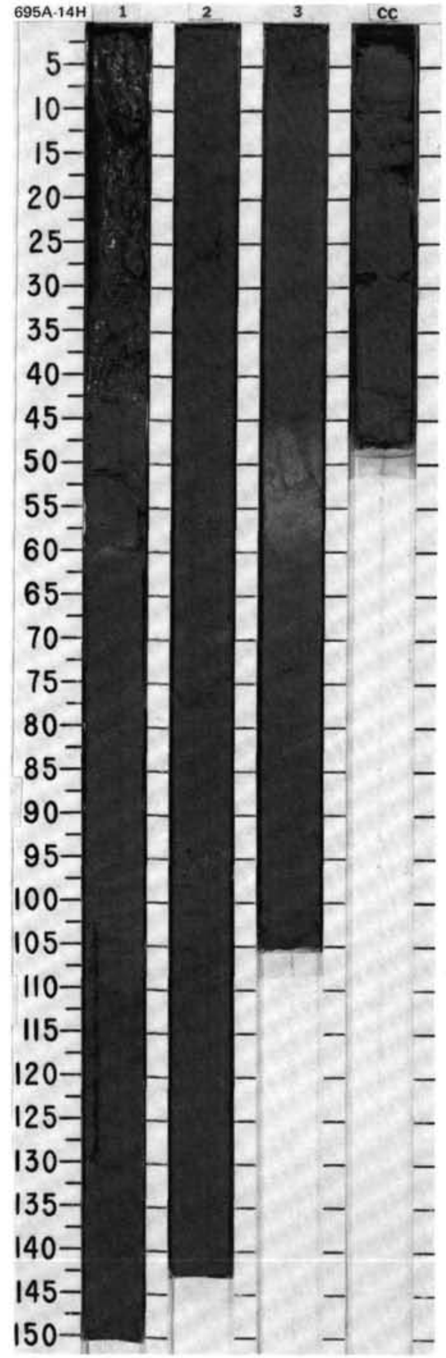

SITE 695 HOLE A CORE 15H CORED INTERVAL 1418.2-1427.9 mbsl; 118.2-127.9 mbsf

TIME-ROCK UNIT	BIOSTRAT. ZONE/ FOSSIL CHARACTER: FORAMINIFERS	NANNOFOSSILS	RADIOLARIANS	DIATOMS	PALYNOMORPHS	PALEOMAGNETICS	PHYS. PROPERTIES	CHEMISTRY	SECTION	METERS	GRAPHIC LITHOLOGY	DRILLING DISTURB.	SED. STRUCTURES	SAMPLES
LOWER PLIOCENE	B	B		*N. angulata - N. reinholdii* C,M	B		V-1509 ● γ=1.35 φ=83; V-1522 ● γ=1.43 φ=80		1, 2, 3, 4, 5, CC	0.5, 1.0				* * * IW OG * *

LITHOLOGIC DESCRIPTION

MUDDY DIATOM OOZE and DIATOM SILTY MUD

Major lithologies: Muddy diatom ooze, mainly dark gray (5Y 4.5/1 grading to 5Y 4/1) and olive gray (5Y 4/2), in Section 1, 0 cm, through Section 2, 150 cm. Diatom silty mud, olive gray (5Y 4/2), grading to and interlayered with dark gray (5Y 4/1).

Slight to moderate bioturbation occurs throughout the core, with mottles and very dark gray (5Y 3/) streaks, and a halo burrow in Section 5, 60 cm. A few dropstones are present in Sections 1-4, mud and sand clasts in Sections 4 and 5. Coarse sand grains (often white) are scattered throughout Sections 1, 4, and 5, principally in the dark gray mud.

SMEAR SLIDE SUMMARY (%):

	1, 50 D	2, 50 D	3, 50 D	4, 50 D	5, 50 D
TEXTURE:					
Sand	—	—	2	—	—
Silt	—	—	70	—	—
Clay	—	—	28	—	—
COMPOSITION:					
Quartz	8	7	15	8	6
Feldspar	—	—	2	—	—
Mica	2	4	2	1	—
Clay	15	19	28	30	24
Volcanic glass	3	3	3	3	3
Calcite	12	9	2	—	8
Accessory minerals:					
Amphibole	1	—	—	1	2
Glauconite	1	Tr	Tr	Tr	—
Garnet	Tr	—	—	—	—
Opaque minerals	3	2	3	2	2
Heavy minerals	2	2	—	2	2
Rutile	—	—	—	Tr	—
Diatoms	45	49	44	49	48
Radiolarians	2	2	1	2	2
Sponge spicules	2	—	Tr	Tr	Tr
Silicoflagellates	4	3	—	2	3

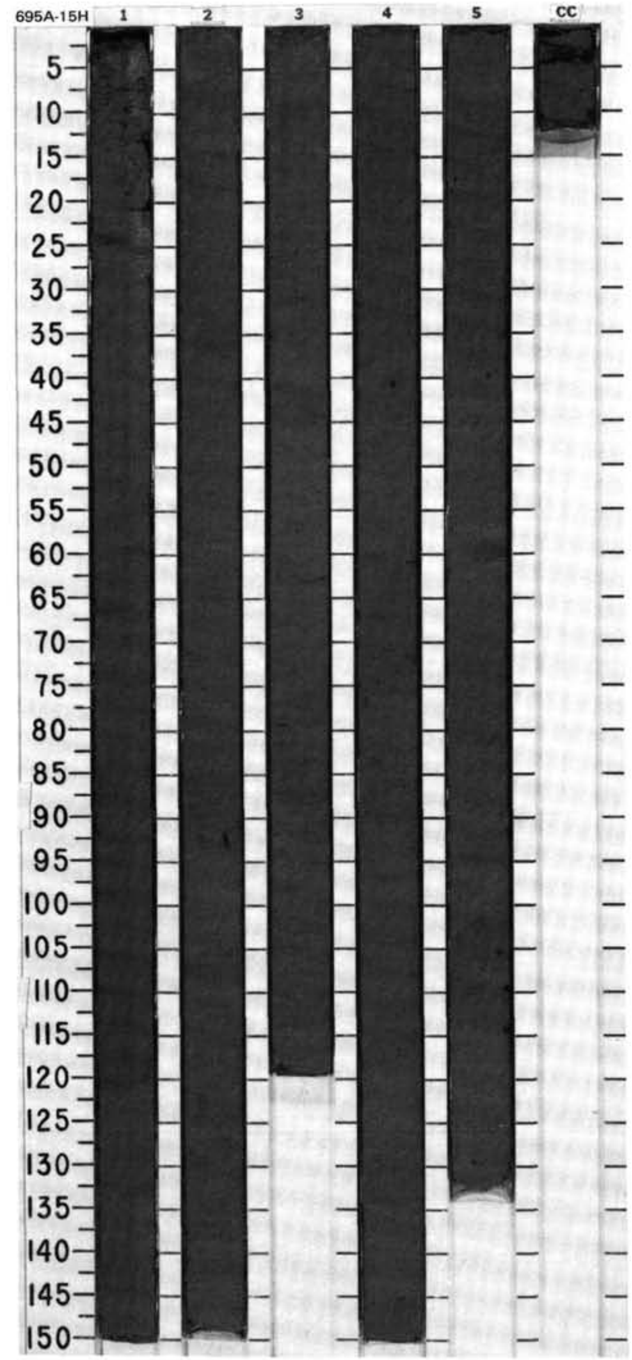

SITE 695 HOLE A CORE 16H CORED INTERVAL 1427.9-1437.6 mbsl; 127.9-137.6 mbsf

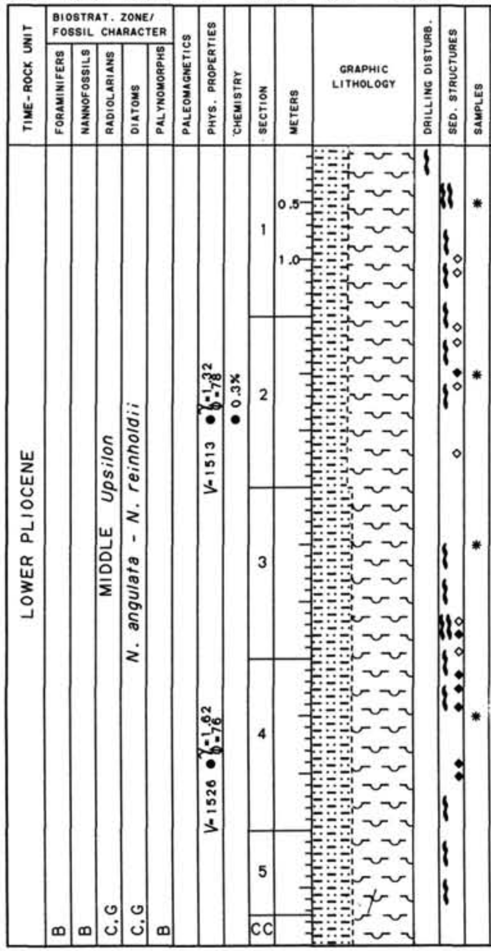

LITHOLOGIC DESCRIPTION

MUDDY DIATOM OOZE

Major lithologies: Muddy diatom ooze, gray (5Y 5/1) to dark gray (5Y 4.5/1 and N 4/0), color changes are gradational.

Slight to moderate bioturbation throughout the core. Ice-rafted detritus is present along the core; dropstones are less than 10 mm in size, occur mainly *in Sections 1 and 3, and include granodiorite and sandstone fragments.* Mudclasts consist mainly of white silty mud and occur mainly in Section 4.

SMEAR SLIDE SUMMARY (%):

	1, 50 D	2, 50 D	3, 50 D	4, 50 D
COMPOSITION:				
Quartz	5	7	10	7
Mica	1	3	3	5
Clay	20	15	20	25
Accessory minerals:				
Amphibole	1	Tr	1	Tr
Glauconite	—	Tr	Tr	—
Micronodules	2	1	2	1
Heavy minerals	1	Tr	1	Tr
Opaque minerals	—	—	Tr	1
Diatoms	63	70	59	59
Radiolarians	5	3	3	1
Sponge spicules	1	Tr	Tr	1
Silicoflagellates	1	1	1	Tr

CORE 113-695A-17I NO RECOVERY

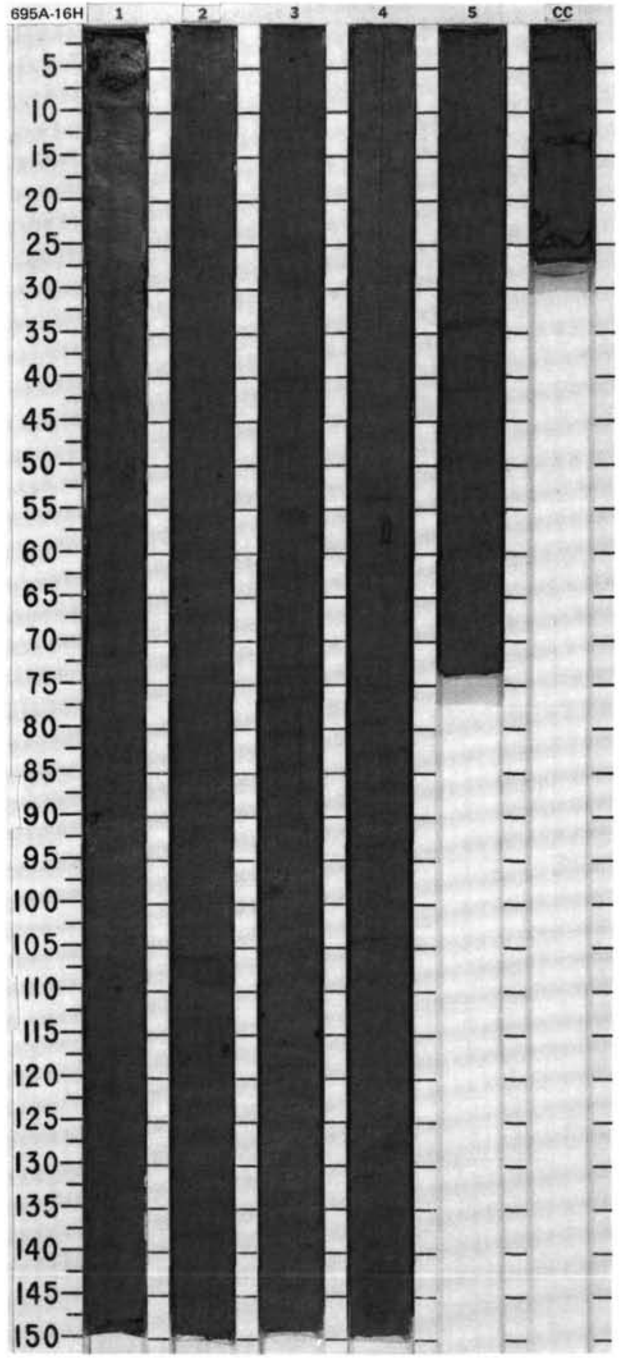

SITE 695 HOLE A CORE 18X CORED INTERVAL 1437.6-1447.3 mbsl; 137.6-147.3 mbsf

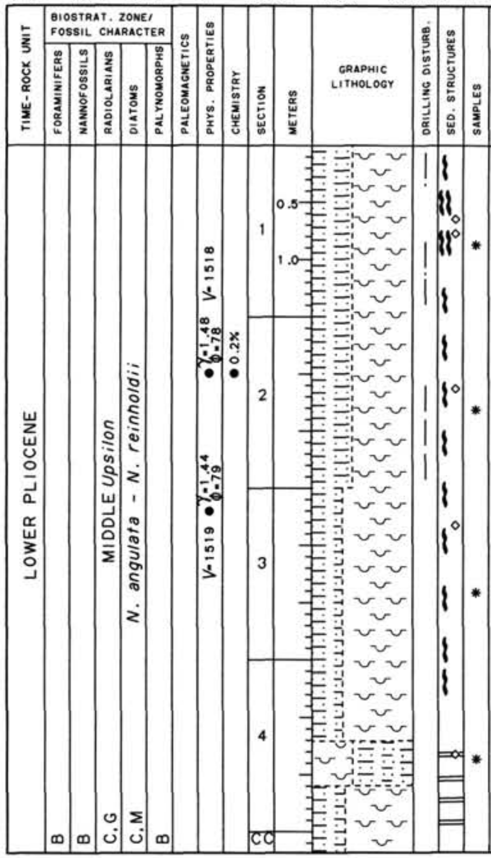

LITHOLOGIC DESCRIPTION

MUDDY DIATOM OOZE

Major lithology: Muddy diatom ooze, dark gray (5Y 4/1) with gradual transitions to olive gray (5Y 4/2).

Minor lithology: Diatom silty mud in Section 4, 70-110 cm, dark gray (N 4/0). Greenish gray (5G 5/1) laminae of devitrified volcanic ash, Section 4, 80 and 100 cm. Black volcanic ash-rich layer, Section 4, 120-125 cm.

Slight to moderate bioturbation in Sections 1-3; faint streaky laminations in Section 4, 130-147 cm. Dropstones are present, and scattered coarse sand grains occur in Section 2, 30-60 cm.

SMEAR SLIDE SUMMARY (%):

	1, 85 D	2, 85 D	3, 85 D	4, 85 M
TEXTURE:				
Sand	—	—	—	4
Silt	—	—	—	61
Clay	—	—	—	35
COMPOSITION:				
Quartz	7	5	5	15
Feldspar	Tr	—	—	—
Mica	3	2	3	5
Clay	24	25	15	35
Volcanic glass	—	—	Tr	—
Accessory minerals:				
Amphibole	Tr	Tr	Tr	Tr
Glauconite	Tr	—	—	Tr
Garnet	Tr	Tr	—	—
Micronodules	3	2	2	3
Heavy minerals	Tr	Tr	Tr	Tr
Opaque minerals	—	—	—	Tr
Diatoms	60	65	69	40
Radiolarians	3	1	2	2
Sponge spicules	—	Tr	1	Tr
Silicoflagellates	Tr	Tr	3	—

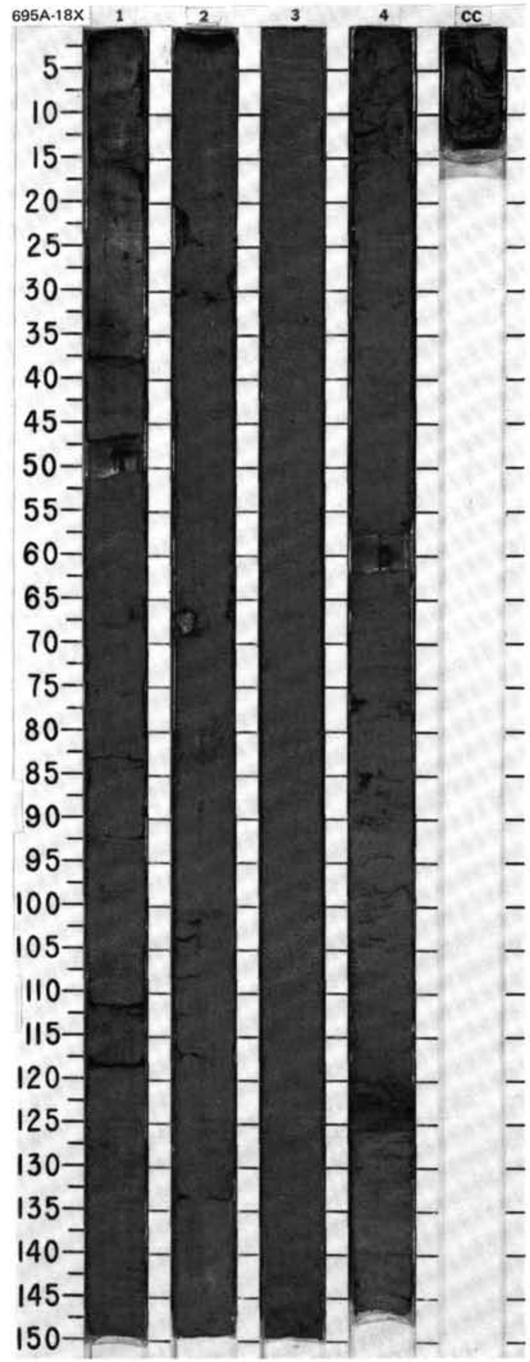

SITE 695 HOLE A CORE 19X CORED INTERVAL 1447.3-1457.0 mbsl; 147.3-157.0 mbsf

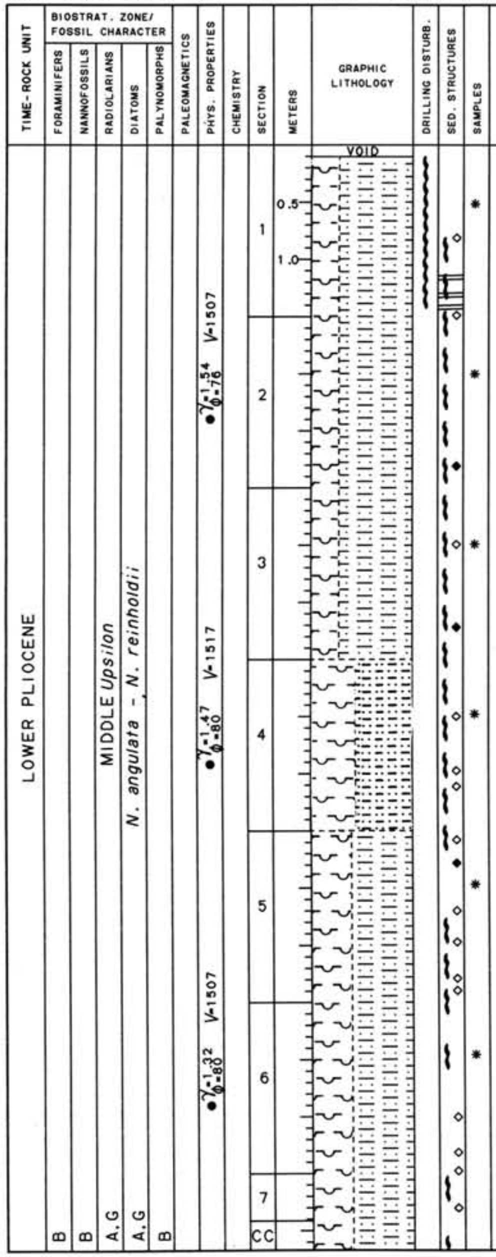

LITHOLOGIC DESCRIPTION

DIATOM SILTY MUD and MUDDY DIATOM OOZE

Major lithologies: Diatom silty mud, predominantly dark gray (5Y 4/1) and olive gray (5Y 4/2), in parts of Section 6. Muddy diatom ooze in Section 4, dark gray (5Y 4/1).

Minor lithology: Greenish gray laminae of devitrified ash in Section 1, 115-135 cm. Volcanic glass "clast", probably associated with manganese concretions, in black pocket at Section 2, 65 cm. :m.

Slight bioturbation, mainly dark gray (N 4/0) streaks and mottles, throughout the core. Dropstones, up to 50 mm but generally 3-10 mm in size, throughout the core. Sand clasts in Sections 2, 3, and 5.

SMEAR SLIDE SUMMARY (%):

	1, 50 D	2, 50 D	3, 50 D	4, 50 D	5, 50 D	6, 50 D
TEXTURE:						
Sand	2	1	2	—	3	2
Silt	68	65	63	—	60	65
Clay	30	34	35	—	37	33
COMPOSITION:						
Quartz	18	19	15	14	15	3
Feldspar	1	—	—	—	—	—
Mica	3	3	Tr	2	—	2
Clay	30	34	35	23	37	33
Volcanic glass	2	2	—	Tr	2	3
Calcite	3	—	2	—	—	7
Accessory minerals:						
Amphibole	—	1	1	Tr	—	Tr
Glauconite	Tr	1	Tr	—	—	Tr
Garnet	Tr	—	—	—	Tr	—
Opaque minerals	2	5	4	1	3	—
Heavy minerals	3	2	1	1	—	3
Diatoms	35	30	39	55	40	46
Radiolarians	1	Tr	Tr	—	Tr	Tr
Sponge spicules	Tr	2	—	Tr	Tr	Tr
Silicoflagellates	2	1	3	4	3	3

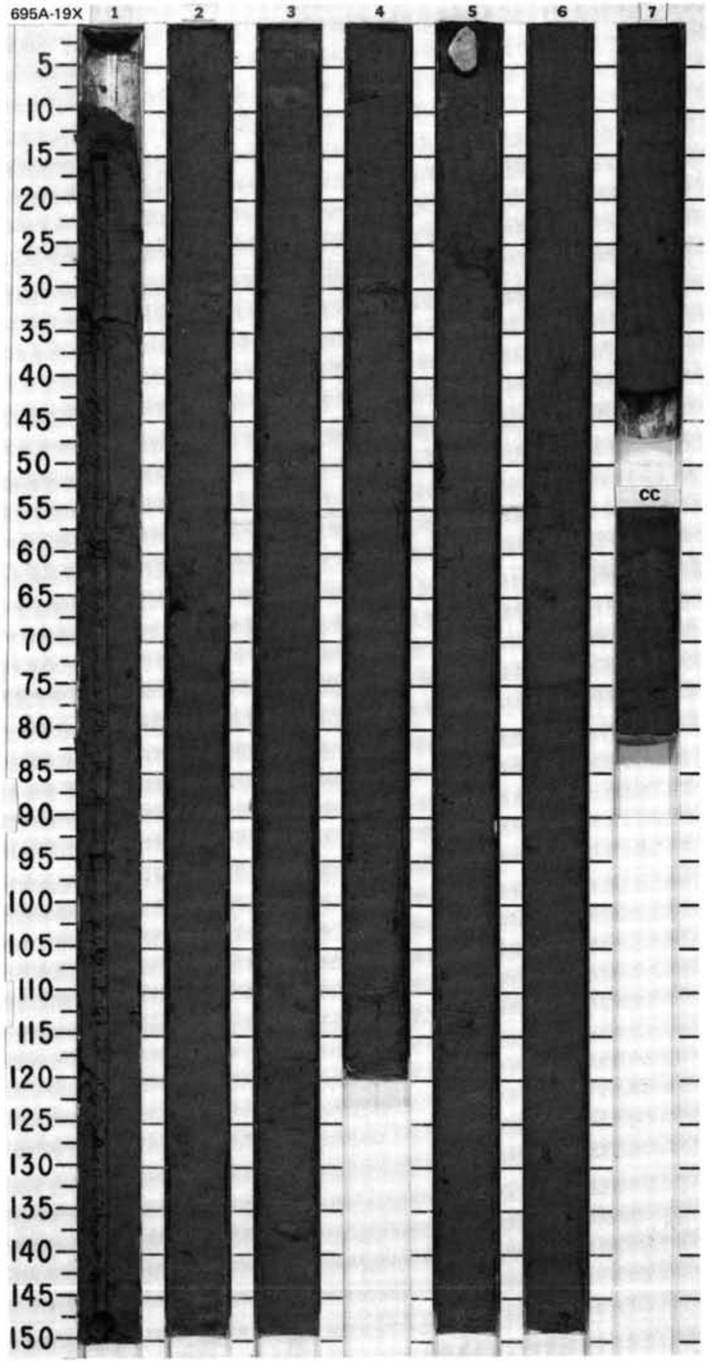

SITE 695 HOLE A CORE 20X CORED INTERVAL 1457.0-1466.8 mbsl; 157.0-166.8 mbsf

TIME-ROCK UNIT	BIOSTRAT. ZONE/FOSSIL CHARACTER: FORAMINIFERS	NANNOFOSSILS	RADIOLARIANS	DIATOMS	PALYNOMORPHS	PALEOMAGNETICS	PHYS. PROPERTIES	CHEMISTRY	SECTION	METERS
LOWER PLIOCENE	B	B	LOWER *Upsilon* A,G	*N. angulata - N. reinholdii* A,M	B		V-1530 ●γ=1.67 φ=69; V-1530 ●γ=1.67 φ=69; V-1531 ●γ=1.49 φ=76		1, 2, 3, 4, 5, 6, CC	0.5, 1.0

GRAPHIC LITHOLOGY / DRILLING DISTURB. / SED. STRUCTURES / SAMPLES

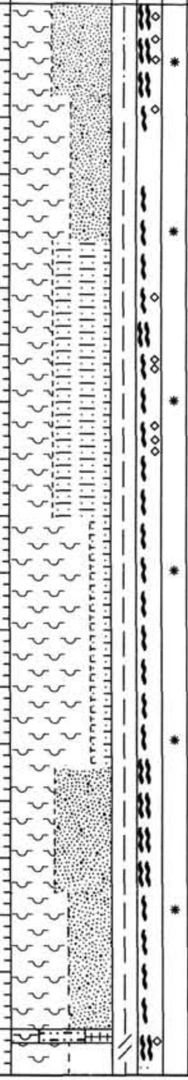

LITHOLOGIC DESCRIPTION

MUDDY DIATOM OOZE and DIATOM SILTY MUD

Major lithologies: Muddy diatom ooze, dark gray (N 4/0, 5Y 4/1) in Section 2, to olive gray (5Y 4/2) in Section 5, to almost uniform dark gray (5Y 4/1) in Section 6. Diatom silty mud, dark gray (N 4/0), gradually changing to dark gray (5Y 4/1) after passing through streaky olive-ish and greenish colors.

Minor lithologies: Mud-bearing diatom ooze, almost uniform olive gray (5Y 4/2), firm layering in Section 4, 23, 54, 67, and 103 cm. Carbonate-cemented greenish gray (5G 5/1) laminae in Section 2, 86, 88, 96, and 119 cm.

Minor to moderate bioturbation throughout the core. Large 4 cm quartzite dropstone in Section 1, 10 cm; smaller mm-sized dropstones in Section 3; and few scattered sand grains in Sections 1 and 2.

SMEAR SLIDE SUMMARY (%):

	1, 50 D	2, 50 D	3, 50 D	4, 50 D	5, 50 D	6, 50 D
TEXTURE:						
Sand	3	—	Tr	—	—	—
Silt	72	—	66	—	—	—
Clay	25	—	34	—	—	—
COMPOSITION:						
Quartz	20	10	8	5	25	20
Feldspar	Tr	—	—	—	Tr	1
Mica	2	2	1	2	1	2
Clay	25	20	34	10	15	15
Volcanic glass	Tr	—	2	—	1	—
Calcite/dolomite	—	—	2	—	Tr	—
Accessory minerals:						
Amphibole	1	Tr	—	—	1	1
Glauconite	Tr	Tr	Tr	Tr	Tr	Tr
Garnet	Tr	—	Tr	—	—	—
Micronodules	3	3	Tr	2	—	2
Heavy minerals	1	1	1	Tr	3	1
Opaque minerals	—	—	3	—	1	—
Diatoms	45	61	44	80	52	54
Radiolarians	2	3	2	1	Tr	1
Sponge spicules	Tr	Tr	Tr	—	Tr	3
Silicoflagellates	1	Tr	3	Tr	1	—

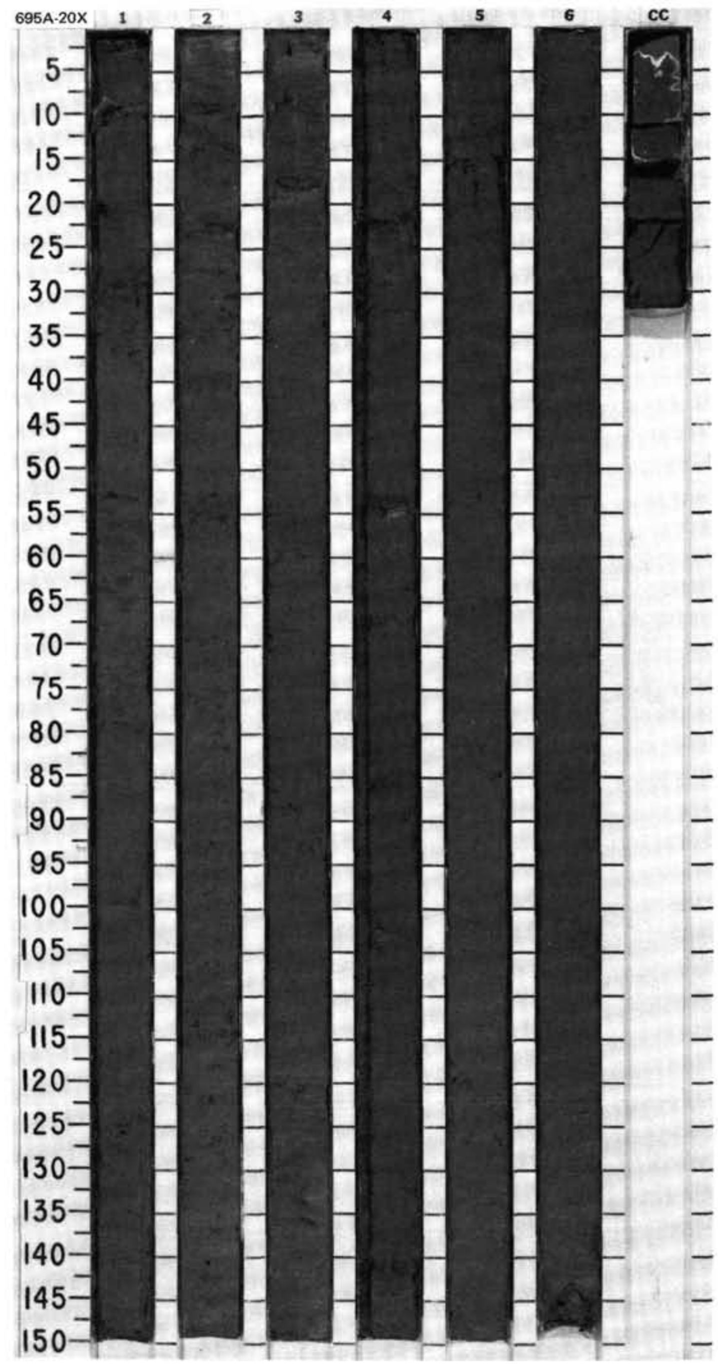

SITE 695 HOLE A CORE 21X CORED INTERVAL 1466.8-1476.5 mbsl; 166.8-176.5 mbsf

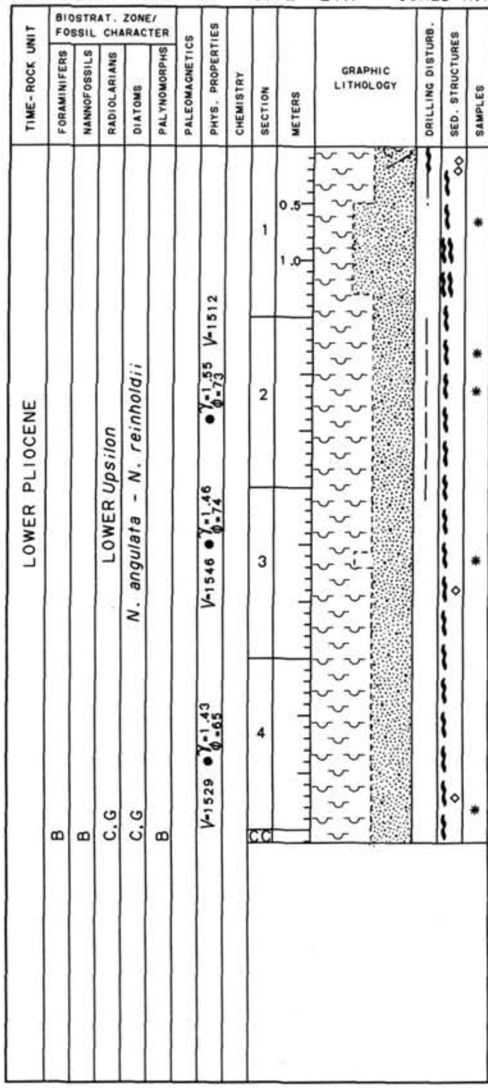

LITHOLOGIC DESCRIPTION

DIATOM SILTY MUD and MUDDY DIATOM OOZE

Major lithologies: Muddy diatom ooze, greenish gray (5G 5/1), changing to olive gray (5Y 5/2) in the lower half. Dropstones at top of Section 1 probably fell down during drilling. Bioturbation varies from minor to moderate. Top of Section 1 is very disturbed by drilling.

Minor lithologies: Diatom silty mud in Section 2, 50-135 cm, and Section 3, 50-60 cm, greenish gray (5BG 5/1). Altered volcanic ash, greenish gray (5G 5/2), as layers within diatom silty mud in Section 1, 74-75, 89-90, 124-125, 128-129, and 134 cm. Sandy mud occurs as a very dark gray (5Y 3/1) bed consisting of 60% volcanic matter in Section 2, 70 cm.

Bioturbation varies from minor to moderate. Identifiable structures include *Planolites*.

SMEAR SLIDE SUMMARY (%):

	1, 68 D	2, 30 D	2, 70 M	3, 60 D	4, 131 D
TEXTURE:					
Sand	10	—	80	8	—
Silt	75	—	15	77	—
Clay	15	—	5	15	—
COMPOSITION:					
Quartz	31	15	17	27	12
Feldspar	—	—	—	Tr	—
Mica	8	2	6	6	6
Clay	15	15	5	15	10
Volcanic glass	Tr	—	60	Tr	—
Accessory minerals	—	6	12	5	6
Opaque minerals	6	2	Tr	2	1
Glauconite	Tr	—	Tr	Tr	—
Zeolites	Tr	Tr	Tr	Tr	—
Diatoms	40	60	—	45	65
Radiolarians	Tr	—	—	Tr	—

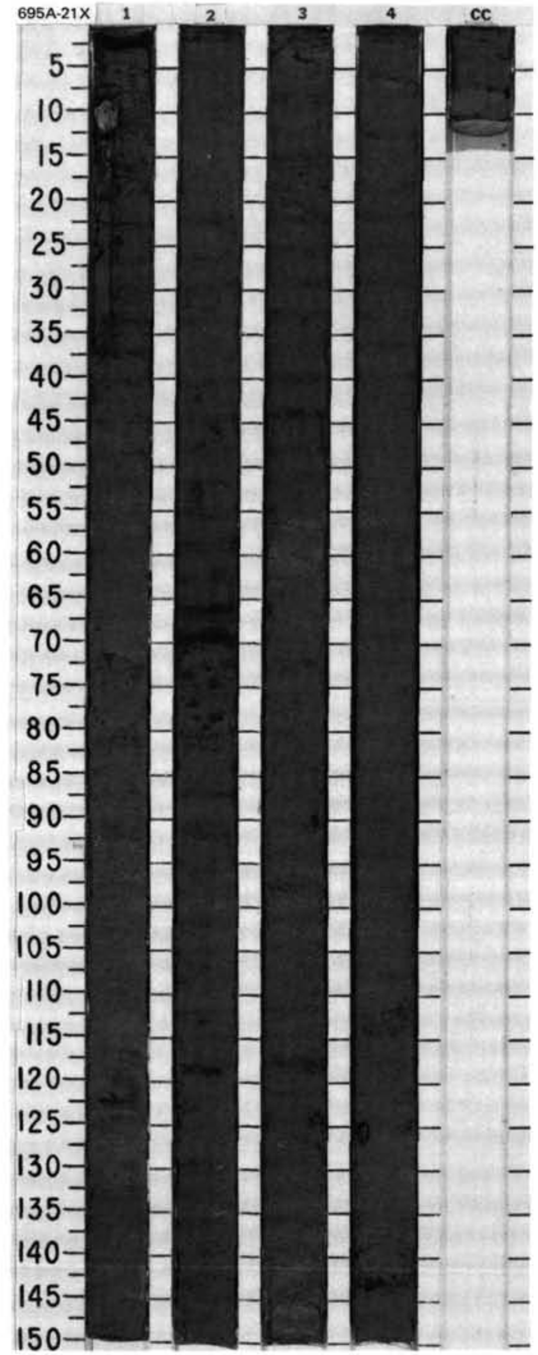

SITE 695 HOLE A CORE 22X CORED INTERVAL 1476.5-1486.2 mbsl; 176.5-186.2 mbsf

TIME-ROCK UNIT	FORAMINIFERS	NANNOFOSSILS	RADIOLARIANS	DIATOMS	PALYNOMORPHS	PALEOMAGNETICS	PHYS. PROPERTIES	CHEMISTRY	SECTION	METERS	GRAPHIC LITHOLOGY	DRILLING DISTURB.	SED. STRUCTURES	SAMPLES
LOWER PLIOCENE	B	B	LOWER *Upsilon*; A, G	*N. angulata - N. reinholdii*; C, G	B		V=1536 ● γ=1.73 φ=65; V=1624 ● γ=1.93 φ=53		1, 2, 3, 4, 5, CC	0.5, 1.0				IW TH OG

BIOSTRAT. ZONE/ FOSSIL CHARACTER

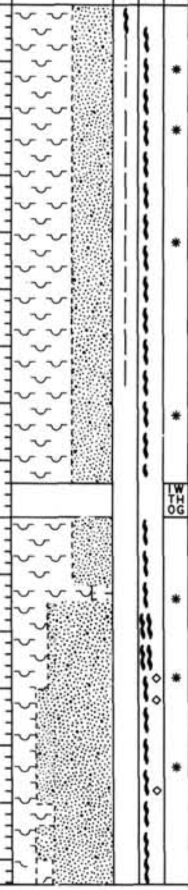

LITHOLOGIC DESCRIPTION

MUDDY DIATOM OOZE and DIATOM SILTY MUD

Major lithologies: Muddy diatom ooze, greenish gray (5GY 5/1) (a slightly olive shade), contains dark blotches of volcanic glass-rich silt. Diatom silty mud, greenish gray (5G 5/1) (although a more bluish shade), glass present throughout.

Minor lithologies: Diatom ooze, as clasts in Section 4, 70-80 cm, olive (5Y 5/3). Volcanic glass-rich silt, in dark blotches, in Section 1, 60, 78, 106, and 138 cm; Section 3, 15, 43, 75, and 112 cm; Section 5, 19 cm; and CC, 22-26 cm. Altered volcanic ash is present as diffuse, more greenish layers, in Section 4, 92, 110, and 131-132 cm.

Minor to moderate bioturbation throughout. Sand-sized dropstones present, but are difficult to distinguish from the volcanic glass. Larger dropstones are present in the less diatom-rich material in Section 4, 138 cm (1 cm), subangular; and in Section 5, 9 cm (1.5 cm), subangular, black metamorphic with pyrite, and Section 5, 81 cm (0.5 cm), subrounded, black shale.

SMEAR SLIDE SUMMARY (%):

	1, 60 D	1, 106 M	2, 60 D	3, 60 D	4, 74 M	4, 135 M	5, 60 D
TEXTURE:							
Sand	—	30	—	—	—	Tr	—
Silt	—	55	—	—	—	85	—
Clay	—	15	—	—	—	15	—
COMPOSITION:							
Quartz	16	5	20	15	—	32	31
Feldspar	—	—	—	—	—	—	2
Mica	8	6	2	6	6	12	4
Clay	12	15	15	15	11	15	20
Volcanic glass	—	40	—	—	—	2	2
Accessory minerals	2	—	3	3	2	—	7
Opaque minerals	2	4	2	1	—	4	4
Diatoms	60	30	58	60	81	35	30
Radiolarians	—	—	—	—	—	—	Tr
Silicoflagellates	—	Tr	—	Tr	—	—	Tr

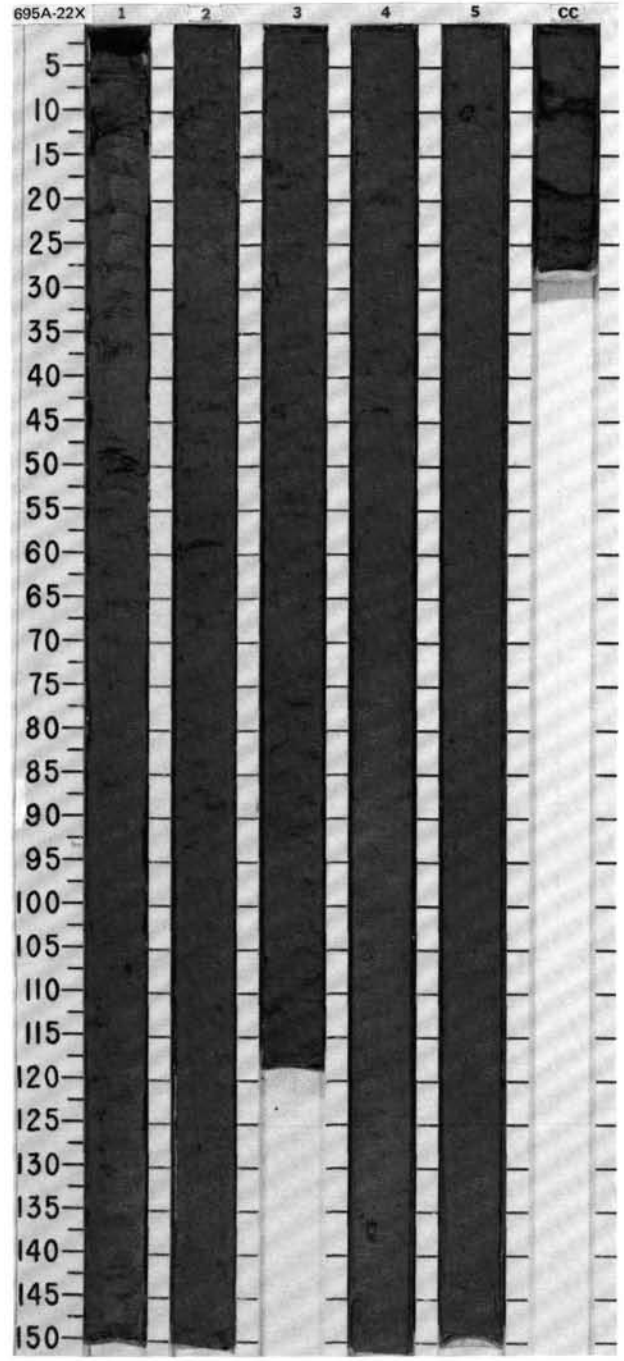

SITE 695 HOLE A CORE 23X CORED INTERVAL 1486.2-1495.9 mbsl; 186.2-195.9 mbsf

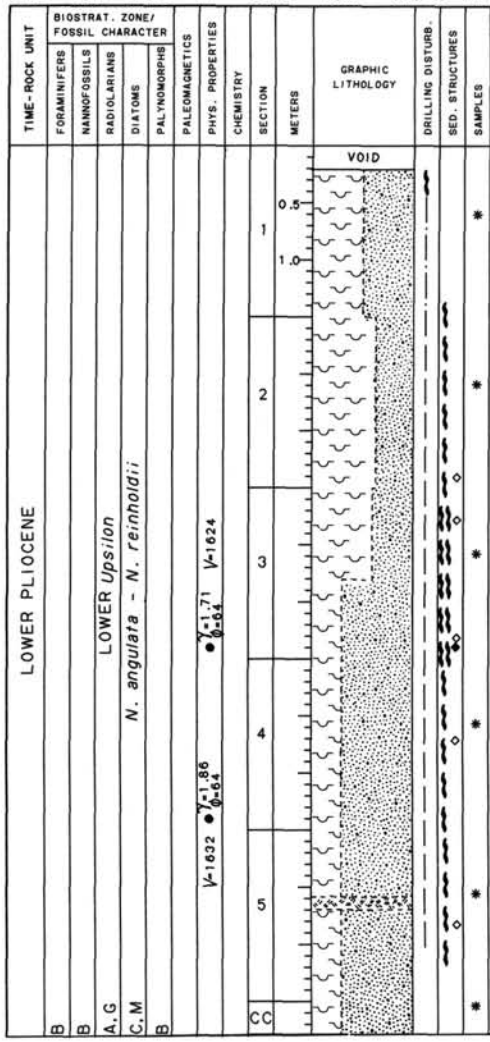

LITHOLOGIC DESCRIPTION

MUDDY DIATOM OOZE and DIATOM SILTY MUD

Major lithologies: Muddy diatom ooze, dark greenish gray (5GY 4/1) and greenish gray (5GY 5/1). In Section 1, below 72 cm, the greenish gray sediments lie adjacent to the core barrel with discontinuous dark grayish green sediments in the center. Coarser material (volcanic glass) is present throughout. A particularly abundant accumulation occurs in Section 2, 63–75 cm. Diatom silty mud, dark greenish gray (5BG 4/1) and greenish gray (5BG 5/1), contains thin diffuse layers of grayish green (5G 5/2), probably more volcanic rich, throughout.

Minor lithologies: Volcanic glass in Section 2, 63–75 cm, and Section 5, 58–68 cm, dark brown (2.5Y 4/2), mm sized, plus as thin laminae and dispersed grains. Altered volcanic ash(?), grayish green (5G 5/2), as thin diffuse layers (21) in Section 4, 19 cm, through Section 5, 35 cm.

Dropstones occur in Section 2, 138 cm (1.1 cm), subangular, black metamorphic; Section 3, 26 cm (3.5 cm diameter), subangular on flat side and subrounded on rounded side, black; Section 3, 131 cm (0.8 cm), subangular, black; Section 4, 80 cm (1 cm), subrounded, metasediment; and Section 5, 70 cm (1 cm), subrounded.

SMEAR SLIDE SUMMARY (%):

	1, 60 D	2, 60 D	3, 60 D	4, 60 D	5, 60 D	CC, 1 M
TEXTURE:						
Sand	—	—	—	5	2	4
Silt	—	—	—	65	66	39
Clay	—	—	—	30	32	57
COMPOSITION:						
Quartz	13	18	12	25	20	20
Feldspar	—	—	—	—	—	3
Rock fragments	—	—	—	—	—	4
Mica	2	1	Tr	4	2	1
Clay	16	10	16	30	32	57
Volcanic glass	—	Tr	Tr	—	—	1
Accessory minerals	5	—	10	7	12	—
Zeolites	8	2	—	2	4	2
Opaque minerals	4	4	—	2	—	1
Glauconite	—	—	Tr	—	—	—
Diatoms	52	65	60	30	30	10
Radiolarians	—	—	—	—	—	Tr
Sponge spicules	—	—	—	Tr	—	1
Silicoflagellates	Tr	—	—	Tr	—	—

CORE 113-695A-24I NO RECOVERY

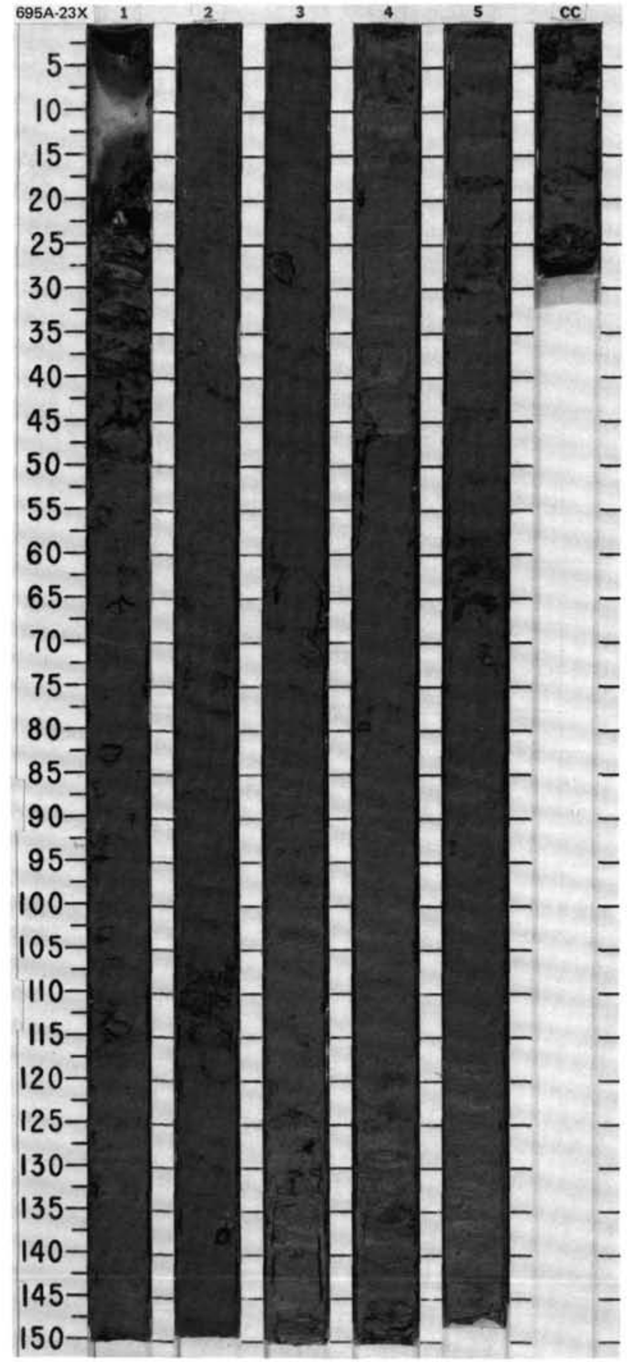

SITE 695 HOLE A CORE 25X CORED INTERVAL 1495.9-1505.6 mbsl; 195.9-205.6 mbsf

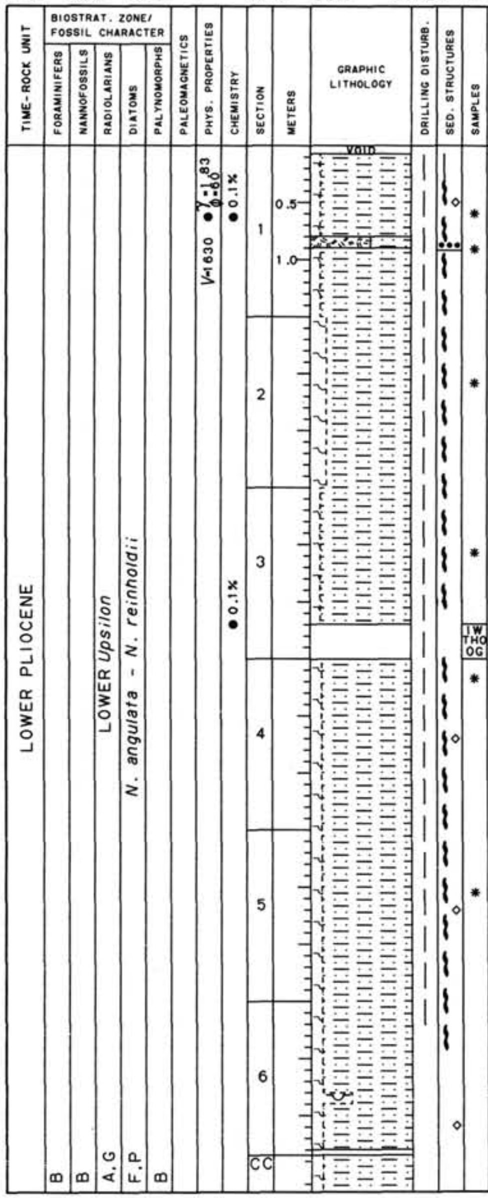

LITHOLOGIC DESCRIPTION

DIATOM-BEARING CLAYEY MUD and DIATOM-BEARING SILTY MUD

Major lithologies: Diatom-bearing clayey mud and diatom-bearing silty mud, dark greenish gray (5G 4/1) and greenish gray (5GY 5/1). In Section 5, 30 cm, through Section 6, 130 cm, dark greenish gray (5BG 7/1) is the dominant color.

Minor lithologies: Silty mud, dark grayish brown (2.5Y 3/2) graded layer, and as a thicker concentration in Section 4, toward base; clasts are present in Section 5, 110-115 cm. Silts and sands, as dispersed clasts throughout and as a thin layer in Section 3, 100 cm. Diatom clayey mud as faint dispersed beds in Section 6, 80-90 cm, olive gray (5Y 5/2). Altered volcanic ash(?), grayish green (5G 5/2), as thin layers in Section 1, 10-66 cm (6 layers); Section 2, 58-136 cm (5 layers); Section 3 (3 layers); Section 4, 5-43 cm (5 layers); Section 6 (15 layers); and CC (2 layers).

Dropstones are present in Section 1, 49 cm (1 cm diameter); Section 4, 78 cm (1.5 cm), angular; Section 5, 75 cm (2 cm), rounded; and Section 6, 100-105 cm (5-6 cm), well rounded.

SMEAR SLIDE SUMMARY (%):

	1, 66 M	1, 91 M	2, 60 D	3, 60 D	4, 18 D	5, 60 D
TEXTURE:						
Sand	4	20	20	—	1	8
Silt	39	70	2	58	55	40
Clay	57	10	3	42	44	52
COMPOSITION:						
Quartz	20	4	—	35	30	20
Feldspar	3	—	—	3	2	2
Rock fragments	4	—	—	1	2	3
Mica	1	—	—	—	—	—
Clay	57	10	53	42	44	52
Volcanic glass	1	73	1	2	2	3
Accessory minerals	—	—	2	4	2	2
Opaque minerals	1	10	1	2	2	2
Zeolites	2	—	—	—	—	Tr
Glauconite	—	Tr	—	—	—	Tr
Diatoms	10	3	14	10	15	15
Radiolarians	Tr	—	Tr	—	—	—
Sponge spicules	1	Tr	—	1	1	1

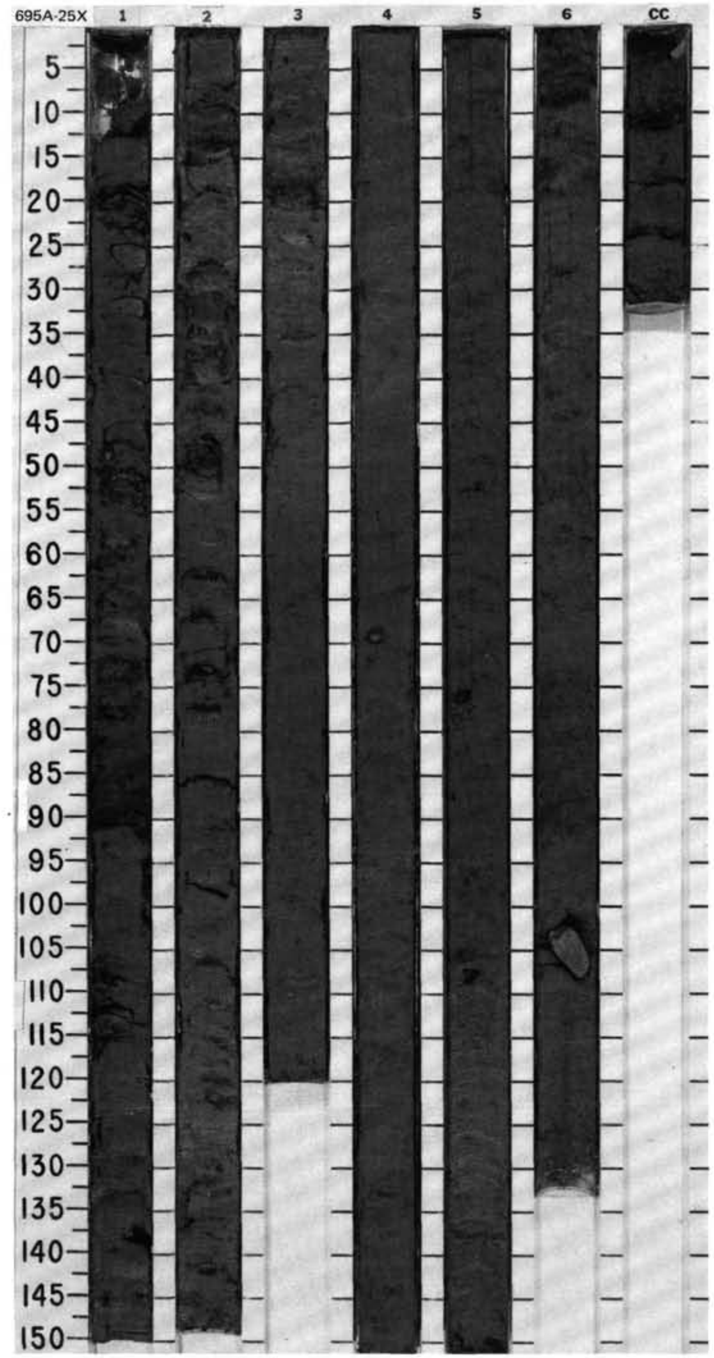

SITE 695 HOLE A CORE 26X CORED INTERVAL 1505.6-1515.3 mbsl; 205.6-215.3 mbsf

TIME-ROCK UNIT	FORAMINIFERS	NANNOFOSSILS	RADIOLARIANS	DIATOMS	PALYNOMORPHS	PALEOMAGNETICS	PHYS. PROPERTIES	CHEMISTRY	SECTION	METERS	GRAPHIC LITHOLOGY	DRILLING DISTURB.	SED. STRUCTURES	SAMPLES	LITHOLOGIC DESCRIPTION
LOWER PLIOCENE	B	B	C.P LOWER *Upsilon*	F.M *N. angulata-N. reinholdii*	B				1, 2, CC	0.5, 1.0				* *	

BIOSTRAT. ZONE/ FOSSIL CHARACTER

DIATOM-BEARING CLAYEY MUD and DIATOM CLAYEY MUD

Major lithologies: Diatom-bearing clayey mud and diatom clayey mud, dark greenish gray (5G 4/1).

Minor lithologies: Silty mud/volcanic glass in Section 2, 15-20 cm, very dark grayish brown (5Y 3/2), and as small patches downcore in Section 2, 70-72 and 85-87 cm. Altered volcanic ash(?), grayish green (5G 5/2), thin layers in Section 2, 7 cm, and CC, 2 cm.

Section 1, 0-130 cm, is totally disturbed by coring. Minor bioturbation in less disturbed part of core.

SMEAR SLIDE SUMMARY (%):

	1, 45 D	2, 45 D
TEXTURE:		
Sand	—	Tr
Silt	38	65
Clay	62	35
COMPOSITION:		
Quartz	10	15
Clay	62	35
Volcanic glass	5	4
Accessory minerals	5	—
Opaque minerals	—	2
Hornblende	2	—
Diatoms	15	44
Radiolarians	Tr	—
Sponge spicules	1	Tr

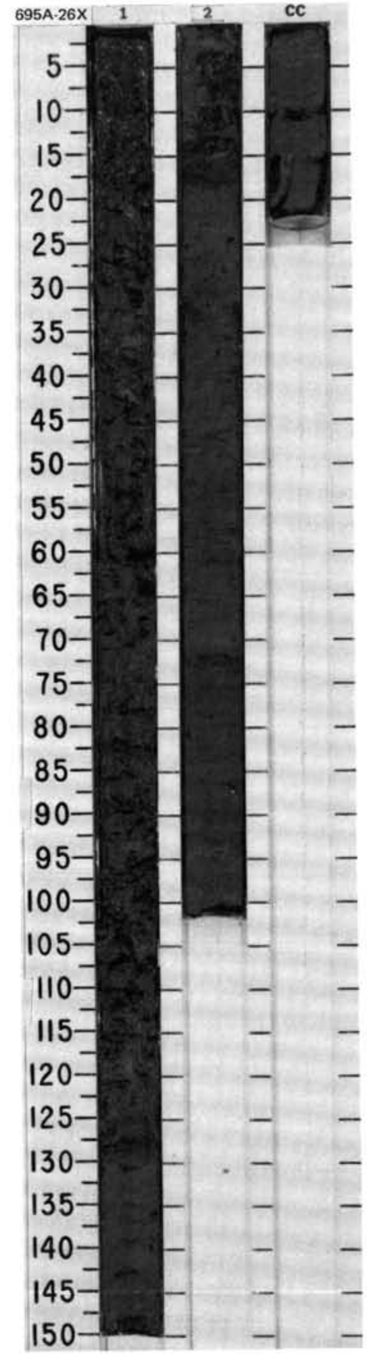

SITE 695 HOLE A CORE 27X CORED INTERVAL 1515.3-1525.0 mbsl; 215.3-225.0 mbsf

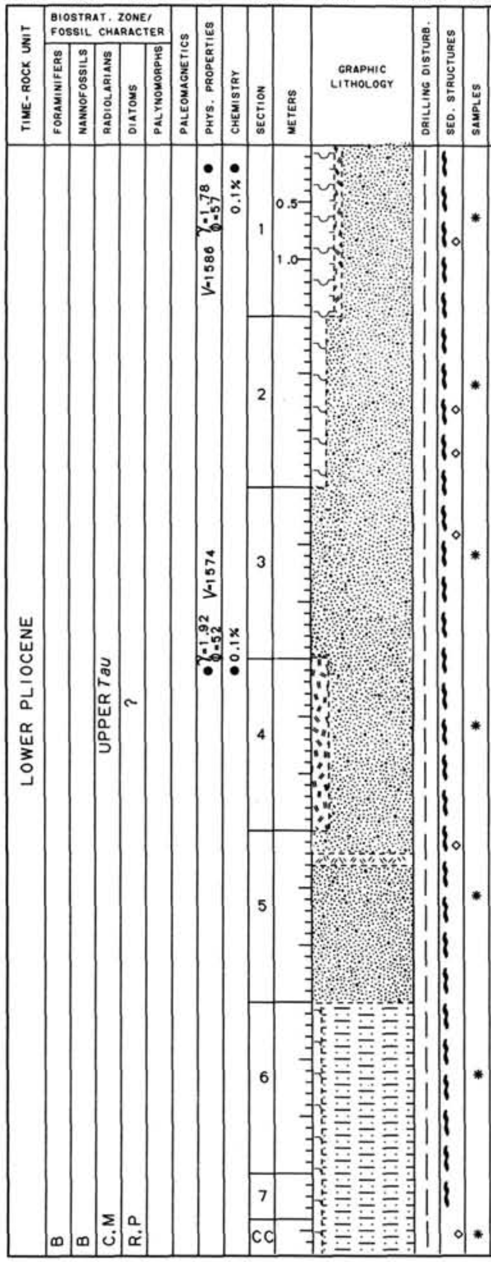

LITHOLOGIC DESCRIPTION

GLASS AND DIATOM-BEARING SILTY MUD, DIATOM-BEARING SILTY MUD, DIATOM-BEARING CLAYEY MUD, SILTY MUD, and GLASS-BEARING SILTY MUD

Major lithologies: Glass and diatom-bearing silty mud, diatom-bearing silty mud, and diatom-bearing clayey mud, dark greenish gray (5BG 4/1), contains diffuse patches of brownish volcanic ash dispersed throughout. Silty mud and glass-bearing silty mud, dark greenish gray (5BG 4/1).

Minor lithologies: Silty mud/sandy mud (volcanic glass) in Section 1, 95–110 cm, 130 cm; Section 3, 15–20 cm; Section 5, 20–32 cm; Section 6, 50–80 cm, fining upwards), very dark grayish brown (2.5Y 3/4), as patches, laminae, and as a higher concentration within the surrounding sediment. Altered volcanic ash(?), grayish green (5G 5/2), in thin layers in Section 2, 81 and 84 cm; Section 4, 3–4, 27–28, and 29–31 cm; Section 5, 57–58, 64–65, 99–100, 121–122, and 124–125 cm; Section 6, 22–23, 31–32, 47, 53, 80–81, 87–89, 104–105, 108–109, and 129–130 cm; and Section 7, 21–22 cm.

Sand-sized dropstones are common. Larger dropstones are angular and subangular and occur in Section 1, 80 cm (0.5 cm diameter); Section 2, 80 and 124 cm (1 cm); Section 3, 45 cm (1.5 cm); and CC, 14 cm (0.8 cm). Minor bioturbation throughout.

SMEAR SLIDE SUMMARY (%):

	1, 60 D	2, 60 D	3, 60 D	4, 60 D	5, 60 D	6, 60 D	CC, 13 M
TEXTURE:							
Sand	12	10	6	4	16	Tr	30
Silt	64	70	62	70	46	48	70
Clay	24	20	32	26	38	52	—
COMPOSITION:							
Quartz	25	45	45	42	43	17	70
Feldspar	—	—	2	2	—	Tr	12
Rock fragments	4	2	—	—	—	—	14
Mica	2	4	4	4	4	4	—
Clay	24	20	32	26	38	52	—
Volcanic glass	12	6	6	18	6	7	—
Accessory minerals	6	7	—	6	—	6	4
Opaque minerals	3	2	1	Tr	3	1	Tr
Zeolites	2	Tr	2	Tr	2	1	—
Diatoms	22	14	8	2	4	12	Tr
Radiolarians	—	Tr	—	—	—	—	—

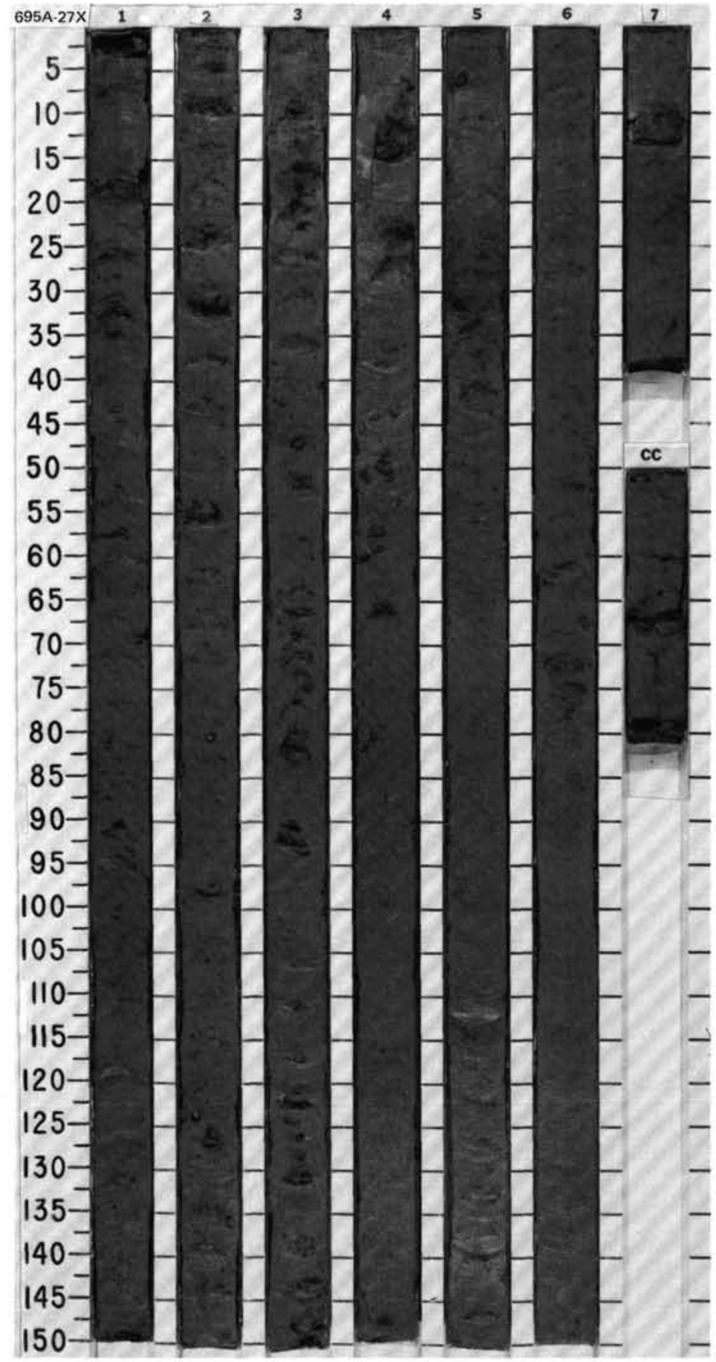

SITE 695 HOLE A CORE 28X CORED INTERVAL 1525.0-1534.7 mbsl; 225.0-234.7 mbsf

TIME-ROCK UNIT	BIOSTRAT. ZONE/ FOSSIL CHARACTER: FORAMINIFERS	NANNOFOSSILS	RADIOLARIANS	DIATOMS	PALYNOMORPHS	PALEOMAGNETICS	PHYS. PROPERTIES	CHEMISTRY	SECTION	METERS	GRAPHIC LITHOLOGY	DRILLING DISTURB.	SED. STRUCTURES	SAMPLES
LOWER PLIOCENE	B	B	UPPER *Tau* C,M	*N. angulata - N. reinholdii* F,M	B				1 2 CC	0.5 1.0	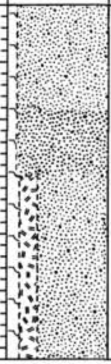			* *

LITHOLOGIC DESCRIPTION

DIATOM-BEARING SILTY MUD and DIATOM- AND GLASS-BEARING SILTY MUD

Major lithologies: Diatom-bearing silty mud, dark greenish gray (5BG 4/1). Diatom- and glass-bearing silty mud, dark greenish gray (5BG 4/1).

Minor lithologies: Silty/sandy mud (volcanic glass), very dark brown (5Y 3/2), dispersed patch, in Section 2, 88 cm. Altered volcanic ash(?), grayish green (5G 5/2), thin layers and laminae, in Section 1, 50–53 and 77–79 cm; and Section 2, 18–20, 26–27, 123–124, and 126–127 cm.

Dropstones are present in Section 2, 28 cm (1 cm diameter), subangular; Section 2, 50 cm (1 cm), rounded; and Section 2, 70 cm (1 cm), rounded. Core soupy and very disturbed, Section 1, 0–45 cm; in remainder of core disturbance minor to moderate.

SMEAR SLIDE SUMMARY (%):

	1, 70 D	2, 70 D
TEXTURE:		
Sand	8	Tr
Silt	54	68
Clay	36	32
COMPOSITION:		
Quartz	29	20
Mica	4	4
Clay	36	32
Volcanic glass	8	18
Accessory minerals	6	5
Zeolites	2	4
Opaque minerals	3	1
Diatoms	12	16
Radiolarians	Tr	—
Sponge spicules	Tr	—

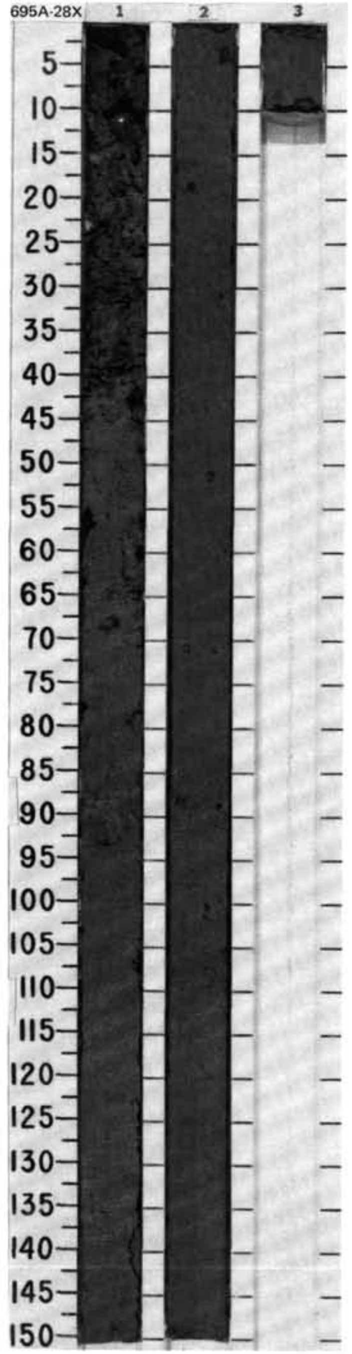

SITE 695 HOLE A CORE 29X CORED INTERVAL 1534.7-1544.4 mbsl; 234.7-244.4 mbsf

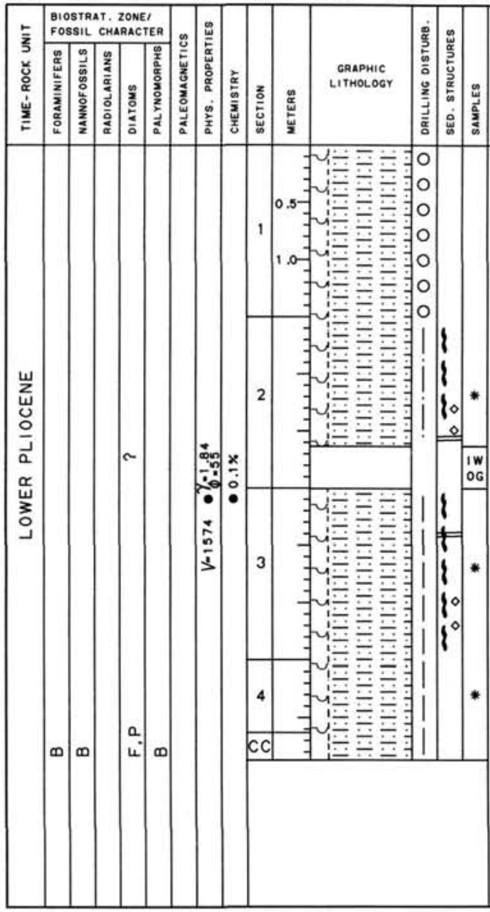

LITHOLOGIC DESCRIPTION

DIATOM-BEARING CLAYEY MUD

Major lithology: Diatom-bearing clayey mud, dark greenish gray (5BG 4/1, 5G 4/1).

Minor lithology: Grayish green (5G 5/2) layers of devitrified volcanic ash, Section 2, 102-105 cm,and Section 3, 30-34 cm; faint ash-rich lenses in Section 4.

Slight bioturbation in Sections 2 and 3. Dropstones up to 5 cm in size in Section 2, 78 and 93 cm (0.5 cm diameter), both subangular; Section 3,90 cm (4 cm), rounded; and Section 3, 115 cm (5 cm), rounded. Section 1 is completely disturbed; minor biscuiting in Section 4.

SMEAR SLIDE SUMMARY (%):

	2, 70 D	3, 70 D	4, 31 D
TEXTURE:			
Sand	1	3	7
Silt	38	51	35
Clay	61	46	58
COMPOSITION:			
Quartz	20	20	10
Feldspar	Tr	2	—
Mica	1	1	2
Clay	61	46	58
Accessory minerals:			
Zeolites	—	—	2
Amphibole	Tr	2	Tr
Glauconite	—	Tr	—
Garnet	—	—	Tr
Opaque minerals	Tr	—	—
Heavy minerals	Tr	1	Tr
Micronodules	1	2	2
Diatoms	15	25	25
Radiolarians	1	Tr	1
Sponge spicules	1	1	—
Silicoflagellates	Tr	Tr	Tr

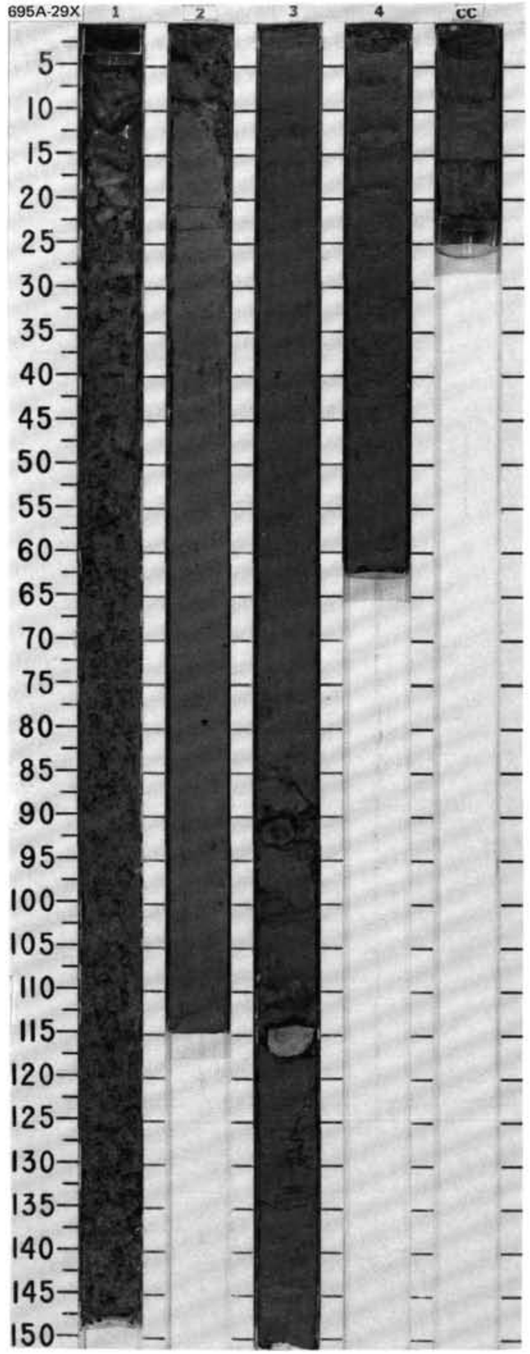

SITE 695 HOLE A CORE 30X CORED INTERVAL 1544.4-1554.1 mbsl; 244.4-254.1 mbsf

TIME-ROCK UNIT: LOWER PLIOCENE

BIOSTRAT. ZONE/FOSSIL CHARACTER: FORAMINIFERS, NANNOFOSSILS, RADIOLARIANS, DIATOMS, PALYNOMORPHS

RADIOLARIANS: UPPER Tau

DIATOMS: N. angulata - N. reinholdii

FORAMINIFERS: B; NANNOFOSSILS: B; RADIOLARIANS: C,M; DIATOMS: F,M; PALYNOMORPHS: B

PALEOMAGNETICS | PHYS. PROPERTIES | CHEMISTRY | SECTION | METERS | GRAPHIC LITHOLOGY | DRILLING DISTURB. | SED. STRUCTURES | SAMPLES

PHYS. PROPERTIES: ● γ=1.92 φ=55; V=1558; ● γ=1.84 φ=56

CHEMISTRY: ● 0.1%

SECTION: 1, 2, 3, 4, 5, CC

METERS: 0.5, 1.0

SAMPLES: TSB

LITHOLOGIC DESCRIPTION

DIATOM-BEARING CLAYEY MUD

Major lithology: Diatom-bearing clayey mud, dark greenish gray (5BG 4/1), minor bioturbation. Firm and biscuited.

Minor lithologies: Slightly ashy (altered) diatom-bearing clayey mud, grayish green (5G 5/2), in Section 1, 132-134 cm; Section 2, 52-54 cm; Section 3, 10-14 and 30-31 cm; and Section 4, 0-5, 44-48, 82-83, 133-134, and 138-139 cm. Diatom clayey mud, dark gray (5Y 4/1), in Section 3, 90-122 cm. Top gradational over 2 cm; base gradational over 15 cm. Carbonate-cemented sandy mud, dark olive gray (5Y 3/2), sand grains up to 2 mm, minor bioturbation (*Chondrites*) at Section 5, 35-50 cm.

Dropstones in Sections 1, 2, and 4 include sandstone, 0. 8 cm, subrounded (Section 1, 17 cm); quartzite, 3 cm, subrounded (Section 4, 33 cm); granodiorite, 15 mm, very angular (Section 4, 74 cm). Other dropstones are less than 0.5 cm. Whitish silty clasts 1 cm across occur in Section 1 and abundantly in Section 4.

SMEAR SLIDE SUMMARY (%):

	1, 50 D	2, 50 D	3, 50 D	4, 50 D
TEXTURE:				
Sand	1	3	3	1
Silt	49	37	30	39
Clay	50	60	67	60
COMPOSITION:				
Quartz	18	20	15	10
Feldspar	—	2	—	—
Mica	6	1	1	2
Clay	50	60	67	60
Volcanic glass	2	Tr	—	2
Accessory minerals:				
Zeolites	—	2	2	—
Heavy minerals	—	2	2	—
Opaque minerals	3	—	—	3
Glauconite	1	—	—	Tr
Micronodules	1	2	1	—
Amphibole	2	1	—	1
Diatoms	15	10	10	18
Radiolarians	2	1	1	1
Sponge spicules	Tr	—	1	3

CORE 113-695A-31I NO RECOVERY

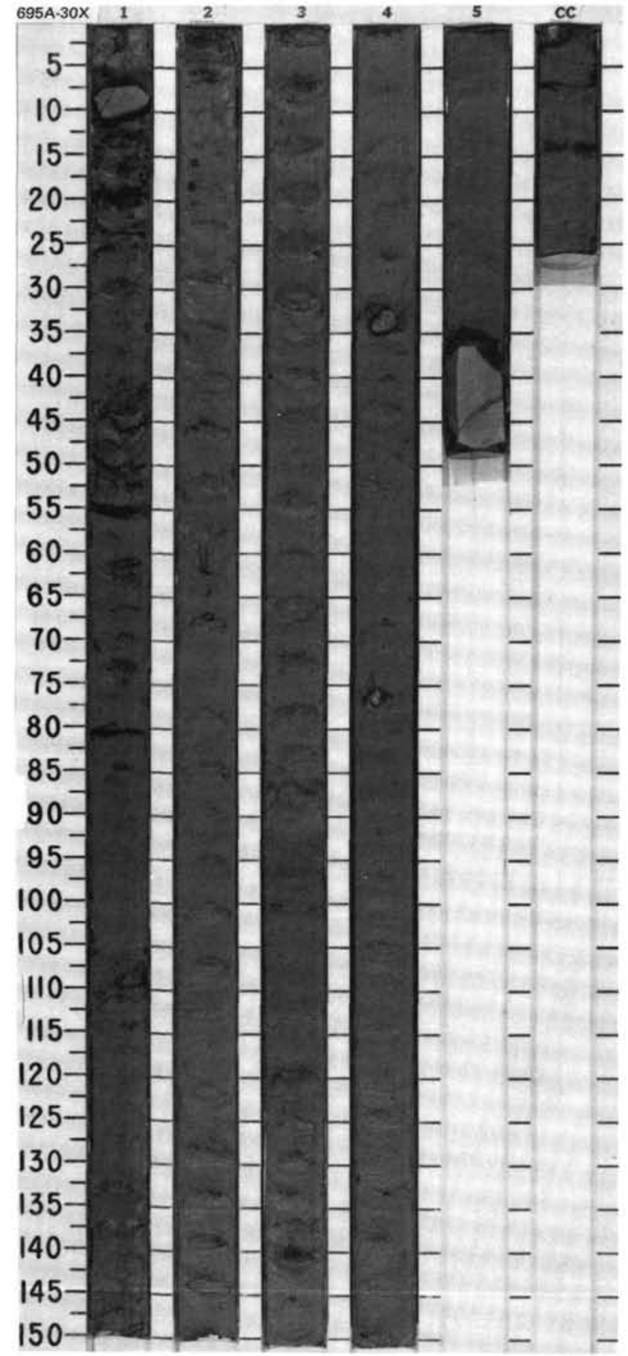

SITE 695 HOLE A CORE 32X CORED INTERVAL 1554.1 -1563.8 mbsl; 254.1-263.8 mbsf

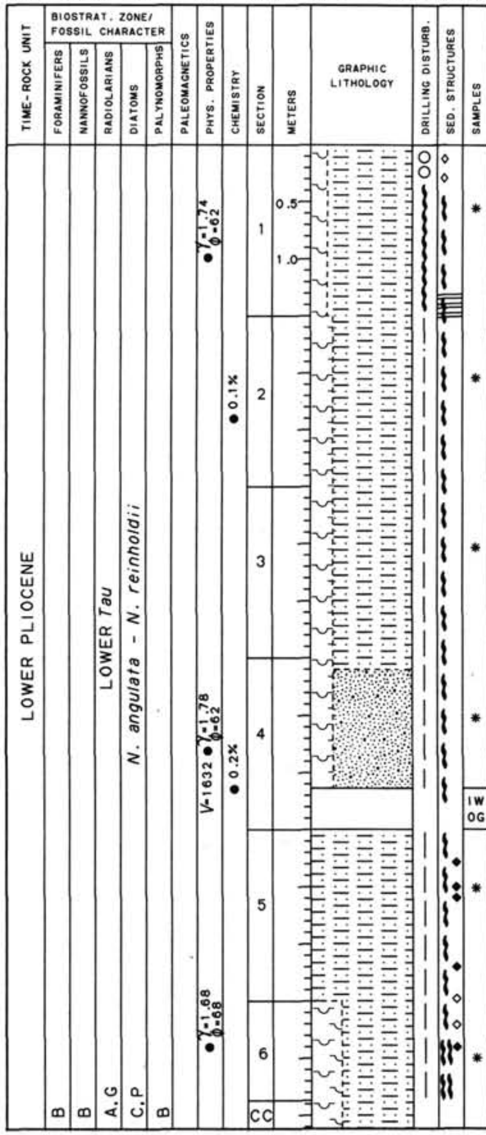

LITHOLOGIC DESCRIPTION

DIATOM-BEARING CLAYEY MUD, DIATOM SILTY MUD, and CLAYEY MUD

Major lithologies: Diatom-bearing clayey mud in Sections 1, 2, and 3, dark greenish gray (5BG 4/1) to dark gray (N 4/0, 5Y 4/1). Diatom silty mud in Section 4, dark gray (N4 /0). Clayey mud in Section 5, dark gray (N 4/0).

Minor lithologies: Diatom clayey mud in Section 6, dark gray (N 4/0, 5Y 4/1). Ash layers, primarily grayish green (5G 5/2) when altered and very dark gray (5Y 3/1) when fresher, in Section 1, 125, 140, and 146 cm; Section 2, 3-5, 8-9, 41-42, 45-47, 64-65, 69-70, and 129-130 cm; Section 4, 24-25 and 26-27 cm (very dark gray), 84-86, and 92-94 cm; and Section 5, 65-67, 77-78, 84-85, and 97-100.

Dropstones in Sections 1, 5, and 6 include quartzite, 5 cm, subangular (Section 1, 50 cm); and shale, subrounded, 1 cm (Section 6, 22 cm). Other white silt mm-sized mud clasts in Section 5, 43 and 55 cm; sandgrains in Section 6, 70 cm, to base. Minor bioturbation throughout. Core disturbed by extensive biscuiting.

SMEAR SLIDE SUMMARY (%):

	1, 50 D	2, 50 D	3, 50 D	4, 50 D	5, 50 D	6, 50 D
TEXTURE:						
Sand	1	2	Tr	2	3	2
Silt	38	49	47	64	24	52
Clay	61	49	53	34	73	46
COMPOSITION:						
Quartz	8	9	8	25	12	15
Feldspar	Tr	—	Tr	—	—	Tr
Mica	7	10	2	6	4	3
Clay	61	49	53	34	73	46
Volcanic glass	Tr	Tr	1	Tr	—	1
Calcite/dolomite	—	—	Tr	—	—	—
Accessory minerals:						
Amphibole	1	Tr	Tr	1	—	—
Glauconite	Tr	2	1	Tr	Tr	Tr
Garnet	—	—	—	—	—	Tr
Heavy minerals	1	3	2	1	—	1
Opaque minerals	2	2	3	3	3	2
Micronodules	—	—	—	—	2	1
Diatoms	17	24	25	26	6	28
Radiolarians	Tr	Tr	Tr	1	Tr	2
Sponge spicules	1	Tr	1	1	Tr	—
Silicoflagellates	2	1	1	2	—	1

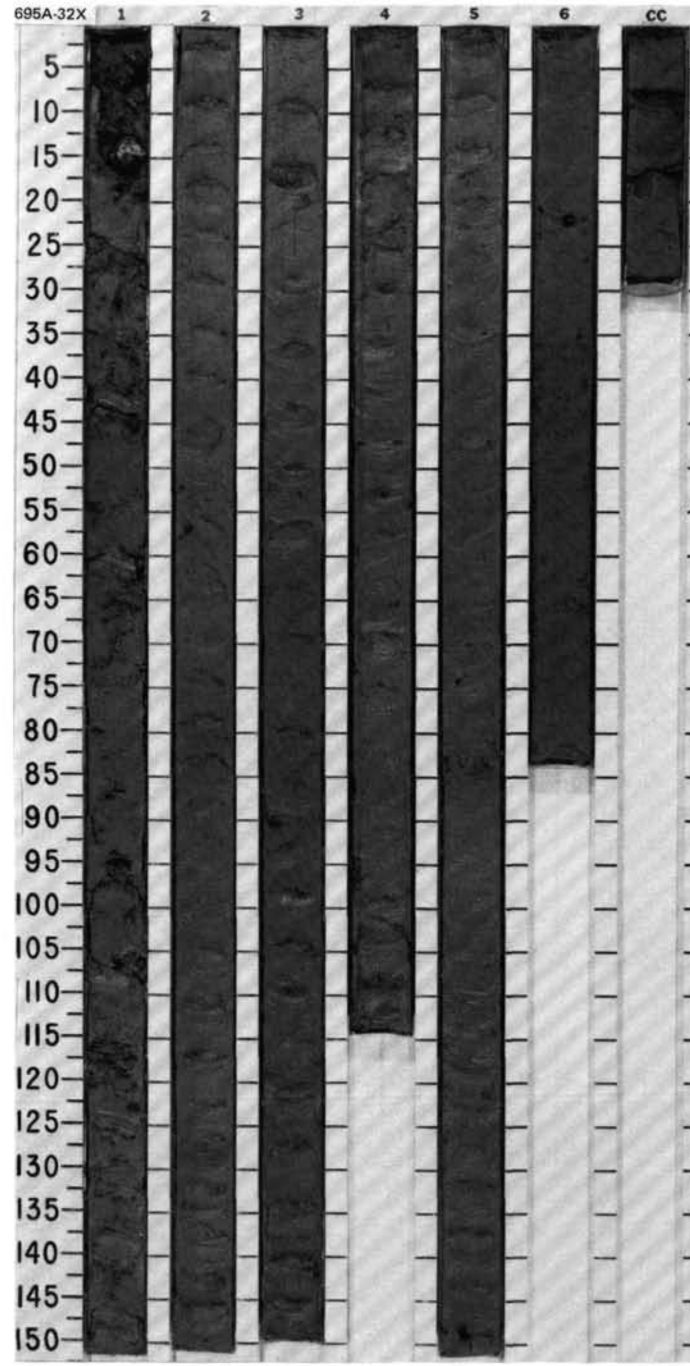

SITE 695 HOLE A CORE 33X CORED INTERVAL 1563.8-1573.5 mbsl; 263.8-273.5 mbsf

TIME-ROCK UNIT	BIOSTRAT. ZONE/ FOSSIL CHARACTER: FORAMINIFERS	NANNOFOSSILS	RADIOLARIANS	DIATOMS	PALYNOMORPHS	PALEOMAGNETICS	PHYS. PROPERTIES	CHEMISTRY	SECTION	METERS
LOWER PLIOCENE	B	B	LOWER *Tau* C,M	*N. angulata* - *N. reinholdii* C,P	B		●γ=1.68 φ=68 ●γ=1.87 φ=60 V=1548 ●γ=1.85 φ=60	● 0.2%	1, 2, 3, CC	0.5, 1.0

GRAPHIC LITHOLOGY / DRILLING DISTURB. / SED. STRUCTURES / SAMPLES

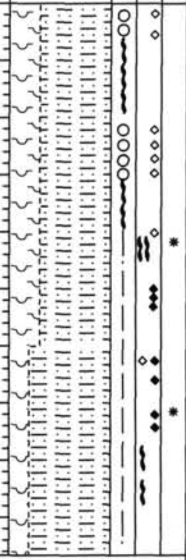

LITHOLOGIC DESCRIPTION

DIATOM CLAYEY MUD and DIATOM-BEARING CLAYEY MUD

Major lithologies: Diatom clayey mud, dark gray (N 4/0 to 5Y 4/1). Diatom-bearing clayey mud, dark gray (N 4/0, gradually changing to 5Y 4/1).

Minor bioturbation occurs in Section 3, 85–150 cm, and moderate bioturbation (*Chondrites*) in Section 2, 60–70 cm. Angular to rounded lithified dropstones up to 5 cm in size, include granodiorite, mafic schist, quartzite, sandstone, and siltstone. Dropstones occur mainly in Sections 1 and 2 (although this may be an effect of downhole contamination), especially in Section 1, 110–150 cm; very small sand and silt clasts Sections 2 and 3; sand grains scattered throughout Section 3. Sediment lithified in Section 2, 42–82 cm. Core very disturbed in Section 1, 0 cm, through Section 2, 90 cm.

SMEAR SLIDE SUMMARY (%):

	2, 62 D	3, 62 D
TEXTURE:		
Sand	2	1
Silt	57	47
Clay	41	52
COMPOSITION:		
Quartz	18	10
Mica	4	12
Clay	41	52
Volcanic glass	2	—
Accessory minerals:		
Amphibole	1	Tr
Glauconite	—	1
Opaque minerals	4	3
Heavy minerals	—	1
Micronodules	—	1
Diatoms	28	20
Radiolarians	2	Tr
Sponge spicules	Tr	Tr

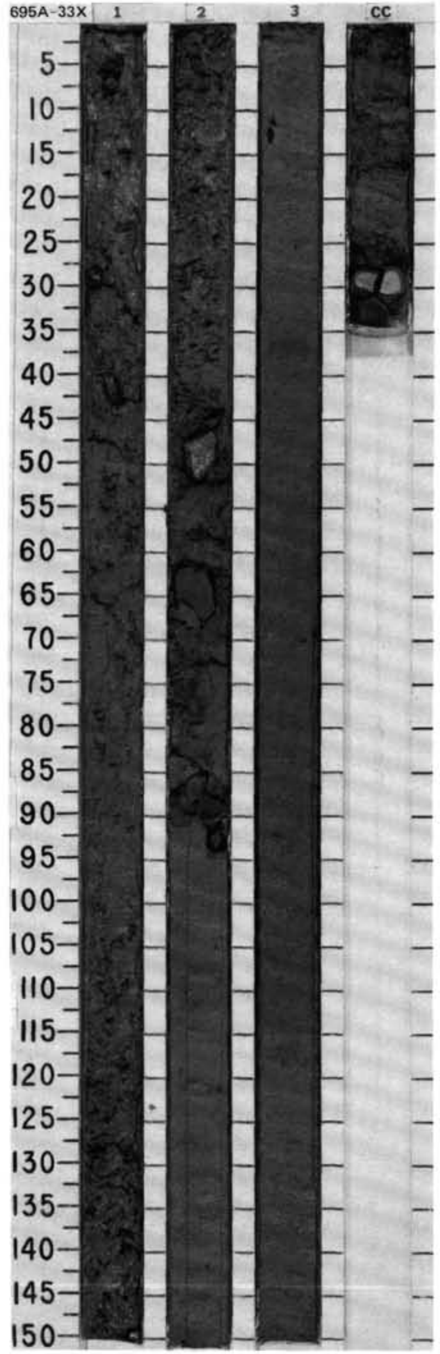

SITE 695 HOLE A CORE 34X CORED INTERVAL 1573.5-1583.1 mbsl; 273.5-283.1 mbsf

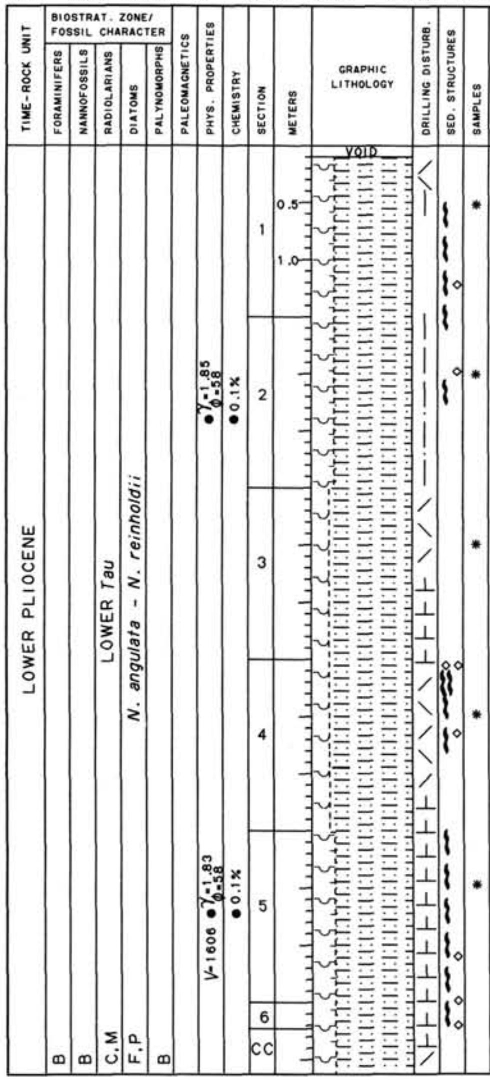

LITHOLOGIC DESCRIPTION

DIATOM-BEARING CLAYEY MUD/MUDSTONE

Major lithology: Diatom-bearing clayey mud/mudstone (wire-saw transition), mainly dark gray (N 4/0); dark gray (5Y 4/1) from Section 1, 120 cm, to Section 2, 70 cm. Abundant drilling biscuits throughout; hard mudstone layers in Section 4, 0-60 cm. Also moderately to very disturbed by splitting, particularly Section 3, 0-70 cm, and Section 4, 0-70 cm.

Minor lithology: Ashy bed in Section 2, 84-85 cm, very dark gray (5Y 3/1).

Sand-sized dropstones throughout core. Larger dropstones include: Section 1, 122 cm (1 cm diameter), quartzite, rounded; Section 2, 44 cm (7 cm), diabase, rounded; Section 3, 136 cm (2 cm), quartzite, subangular; Section 3, 141 cm (1 cm), shale, subrounded; Section 4, 63 cm (4 cm), granodiorite, very angular; Section 4, 68 cm (3 cm), granite, angular; and Section 5, 113 cm (2.5 cm), sandstone, subrounded.

SMEAR SLIDE SUMMARY (%):

	1, 50 D	2, 50 D	3, 50 D	4, 50 D	5, 50 D
TEXTURE:					
Sand	3	2	3	2	3
Silt	49	52	43	34	46
Clay	48	46	54	64	51
COMPOSITION:					
Quartz	15	22	25	15	15
Feldspar	1	—	2	—	1
Mica	3	2	3	2	1
Clay	48	46	54	64	51
Volcanic glass	—	1	—	—	—
Accessory minerals:					
Amphibole	1	Tr	—	Tr	1
Glauconite	1	Tr	Tr	Tr	Tr
Heavy minerals	2	1	—	1	1
Opaque minerals	4	3	1	—	—
Micronodules	—	Tr	—	2	2
Diatoms	24	22	15	15	25
Radiolarians	1	2	Tr	1	2
Sponge spicules	Tr	1	Tr	Tr	1
Silicoflagellates	—	Tr	—	—	—

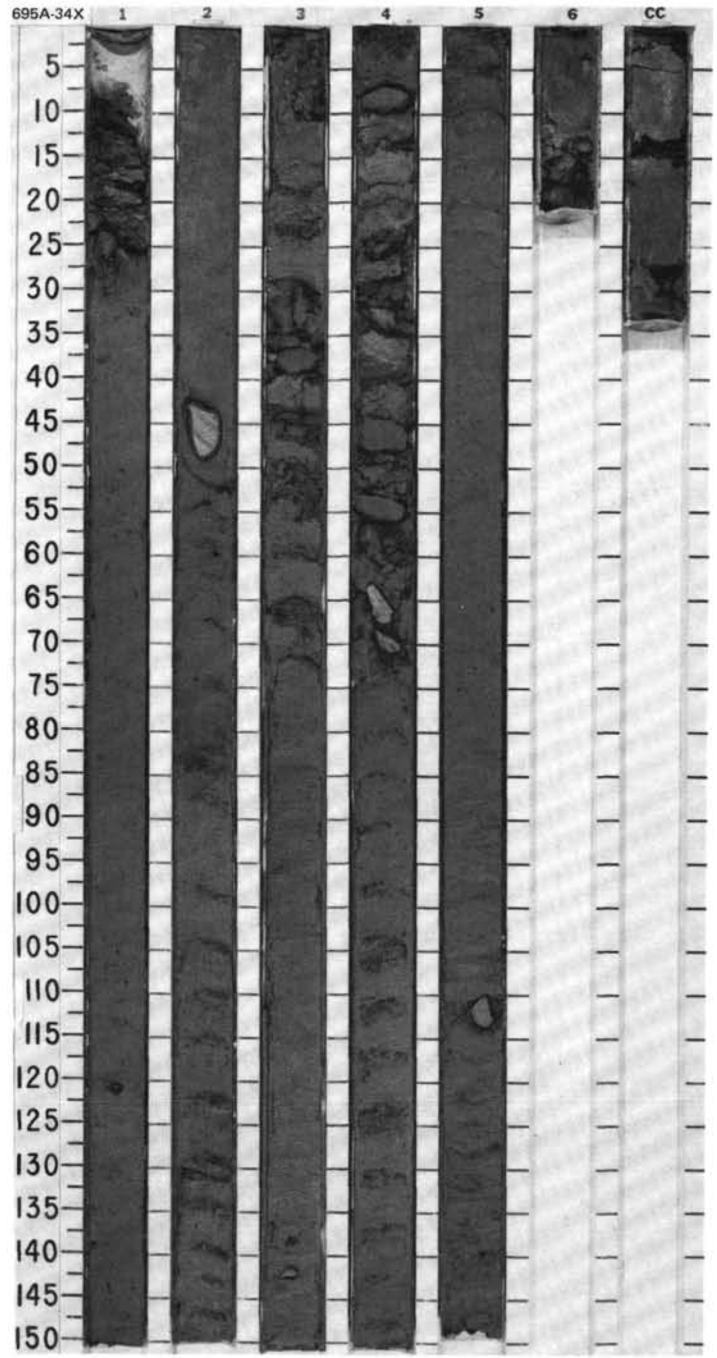

SITE 695 HOLE A CORE 35X CORED INTERVAL 1583.1-1592.8 mbsl; 283.1-292.8 mbsf

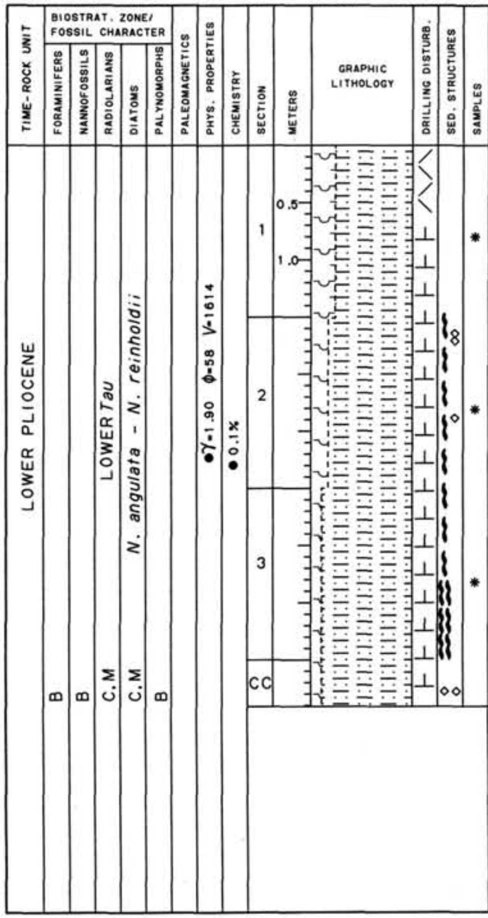

LITHOLOGIC DESCRIPTION

DIATOM-BEARING CLAYEY MUDSTONE

Major lithology: Diatom-bearing clayey mudstone, dark gray (N 4/0) to dark greenish gray (5BG 4/1, 5G 4/1). Some biscuits preserve thick laminations between these colors.

Minor lithology: Dark greenish gray (5G 4/1) ashy layers in Section 1, 142-144 cm, and Section 3, 67-70 and 93-94 cm.

Minor to moderate bioturbation in Sections 2 and 3. Ice-rafted sand grains and granules abundant throughout core. Dropstones in Section 2, 84 cm (2 cm diameter), mafic fine-grained igneous rock, subrounded; CC, 28 cm (3 cm), slate, rounded; and CC, 32 cm (2 cm), granodiorite, subrounded.

SMEAR SLIDE SUMMARY (%):

	1, 75 D	2, 75 D	3, 75 D
TEXTURE:			
Sand	3	3	3
Silt	46	34	45
Clay	51	64	52
COMPOSITION:			
Quartz	15	15	20
Feldspar	1	1	3
Mica	2	1	8
Clay	51	64	52
Volcanic glass	—	—	Tr
Calcite/dolomite	Tr	—	—
Accessory minerals:			
Heavy minerals	1	1	2
Micronodules	3	2	—
Amphibole	Tr	Tr	1
Opaque minerals	—	—	3
Diatoms	25	15	10
Radiolarians	2	1	1
Sponge spicules	—	Tr	Tr
Silicoflagellates	Tr	Tr	Tr

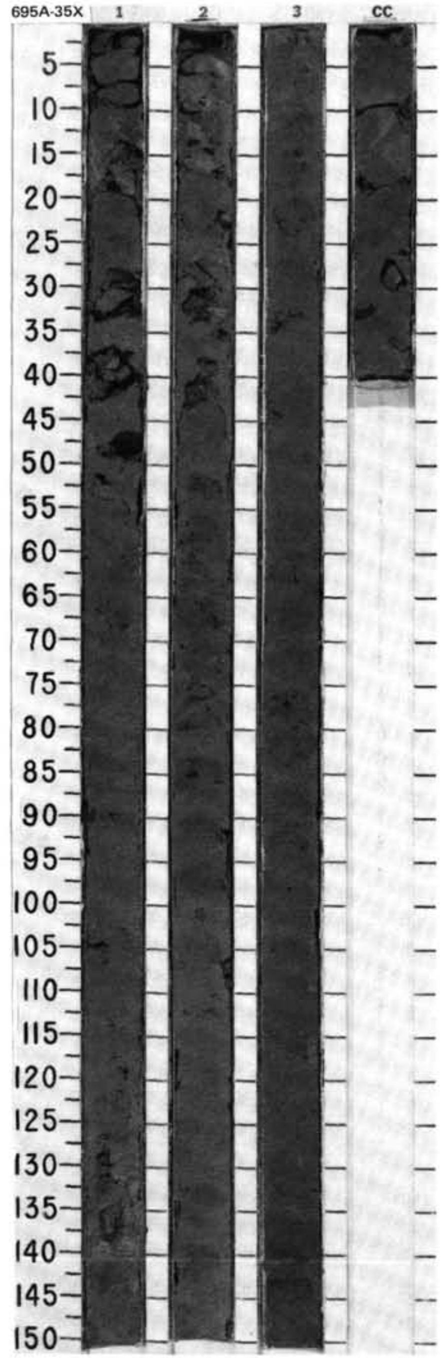

SITE 695 HOLE A CORE 36X CORED INTERVAL 1592.8-1602.4 mbsl; 292.8-302.4 mbsf

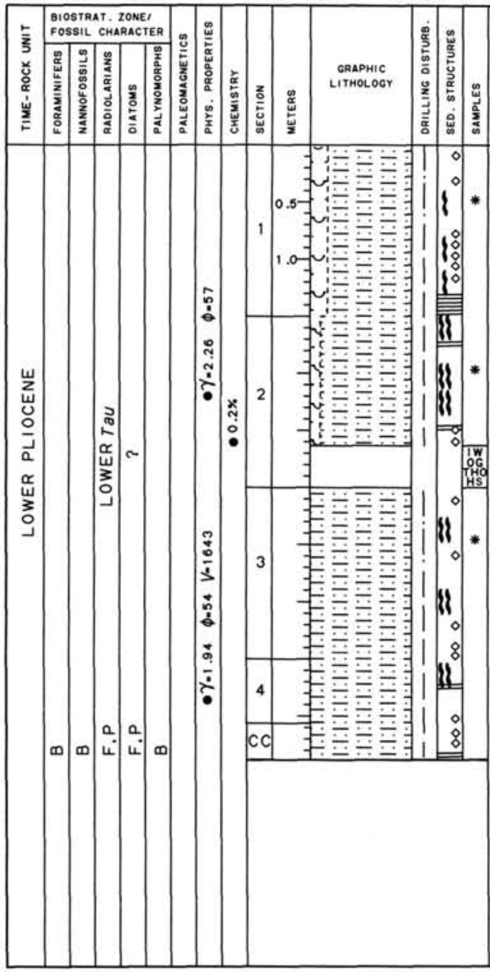

LITHOLOGIC DESCRIPTION

DIATOM-BEARING CLAYEY MUDSTONE and CLAYEY MUDSTONE

Major lithologies: Diatom-bearing clayey mudstone, dark gray (N 4/0) to dark grayish green (5BG 4/1). Clayey mudstone, dark gray (N 4/0).

Minor lithologies: Altered volcanic ash(?), grayish green (5G 4/1), thin layers in Section 1, 120-125 cm; Section 2, 12-14, 16-17, 37-38, 60-61, 92-93, and 99-100 cm; and Section 3, 14-15, 17-18, 108-109, 118-119, 125-126, and 133-134 cm.

Dropstones are common to abundant throughout and are rounded to subrounded. The largest ones are up to 5 cm; dropstones greater than 0.5 cm are shown in the graphic column. They also occur in concentrated areas. Concentrations of dropstones occur in Section 1, 30-120 cm; Section 3, 6-20, 45-70, and 130-150 cm; and CC, 5-15 cm. Drilling disturbance, primarily biscuiting, is minor to moderate.

SMEAR SLIDE SUMMARY (%):

	1, 41 D	2, 48 D	3, 55 D
TEXTURE:			
Sand	2	1	2
Silt	50	33	37
Clay	48	66	61
COMPOSITION:			
Quartz	23	15	25
Feldspar	2	2	2
Mica	2	1	2
Clay	48	66	61
Volcanic glass	3	—	2
Accessory minerals:			
Amphibole	1	—	Tr
Opaque minerals	5	3	3
Glauconite	Tr	Tr	1
Heavy minerals	—	1	2
Diatoms	15	10	2
Radiolarians	Tr	Tr	Tr
Sponge spicules	Tr	Tr	—
Silicoflagellates	1	Tr	—

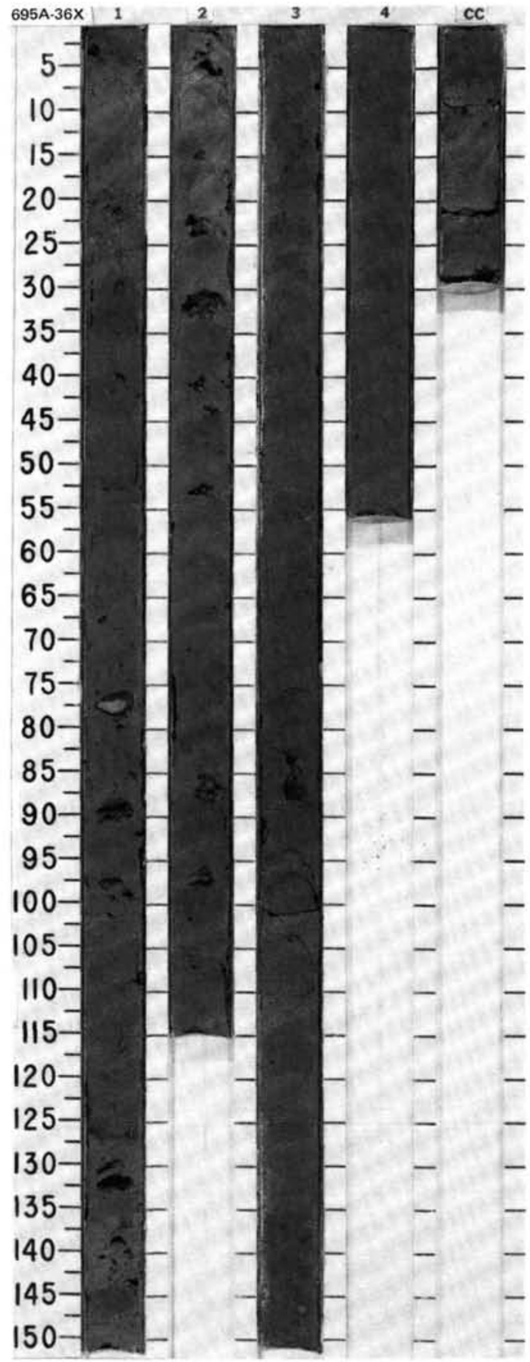

SITE 695 HOLE A CORE 37X CORED INTERVAL 1602.4-1612.0 mbsl; 302.4-312.0 mbsf

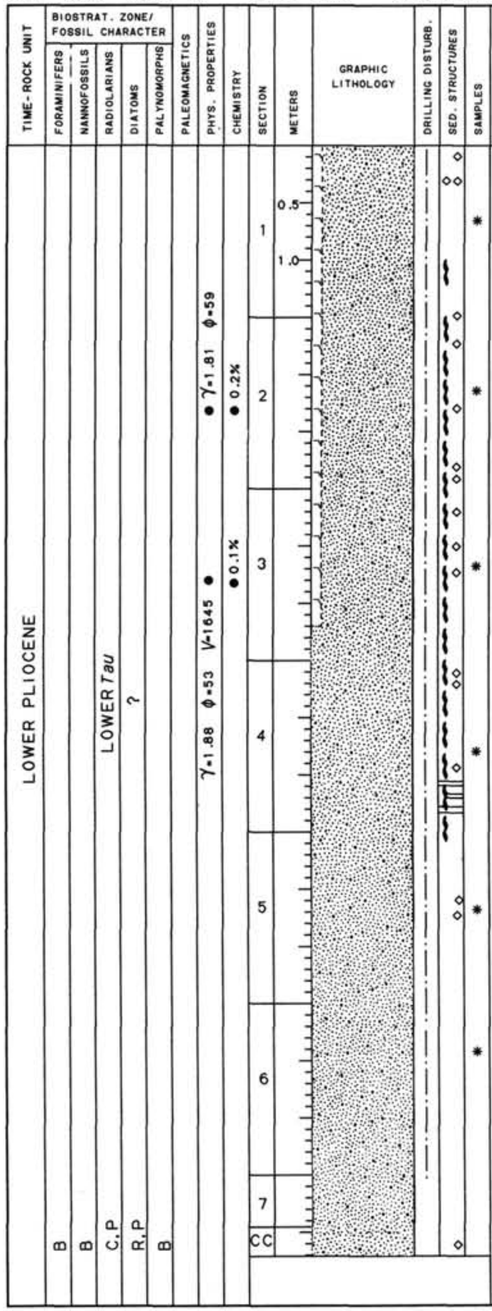

LITHOLOGIC DESCRIPTION

DIATOM-BEARING SILTY MUD, DIATOM-BEARING CLAYEY MUD, and SILTY MUD

Major lithologies: Diatom-bearing silty mud and diatom-bearing clayey mud, gray (5Y 5/0, Section 1, 0–45 cm) and dark gray (Section 1, 45 cm, through Section 3). Abundant sand-sized ice-rafted detritus and larger dropstones are present. Silty mud, dark bluish gray (5B 4/1); ice-rafted detritus is less abundant.

Minor lithologies: Silt/sand in Section 4, 110–130 cm, as parallel laminae. Other parallel laminae may be present, but destroyed by coring. Altered volcanic ash, grayish green (5G 5/2), as thin layers in Section 1, 50–51, 64–65, 66–67, 79–80, 94–95, and 128–129 cm; Section 2, 29–30, 32–33, 74–75, 84–85, 104–105, 115–116, 129–130, and 137–138 cm; Section 3, 7–8, 28–29, 44–45, 46–47, 65–66, 67–68, and 87–88 cm; Section 4, 24–25, 67–68, 69–70, 80–82, 99–100, 129–130, and 135–136 cm; Section 5, 4–5, 11-12, 35-37, 94–95, 104–105, and 134–135; Section 6, 2–4, 30-31, 50–51, 66–67, 85–86, 90–91, and 143–144 cm; and Section 7, 30–31 and 40–42 cm.

Sand-sized dropstones are abundant throughout; dropstones >0.5 cm are predominantly rounded and shown in lithology column. Moderately disturbed by drilling, primarily biscuiting.

SMEAR SLIDE SUMMARY (%):

	1, 60 D	2, 61 D	3, 60 D	4, 81 M	5, 60 D	6, 37 M
TEXTURE:						
Sand	8	3	1	4	Tr	—
Silt	58	59	55	58	58	68
Clay	34	38	44	38	42	32
COMPOSITION:						
Quartz	51	36	25	33	23	34
Feldspar	1	Tr	—	Tr	—	1
Mica	4	4	2	6	2	1
Clay	34	38	44	38	42	32
Volcanic glass	8	6	2	4	18	14
Accessory minerals	—	Tr	4	—	—	4
Zeolites	—	2	3	3	Tr	2
Glauconite	—	Tr	4	—	—	4
Amphibole	Tr	—	—	Tr	—	—
Opaque minerals	2	4	4	4	1	Tr
Diatoms	10	10	16	12	8	8
Sponge spicules	Tr	—	—	Tr	—	—

CORE 113-695A-38 NO RECOVERY

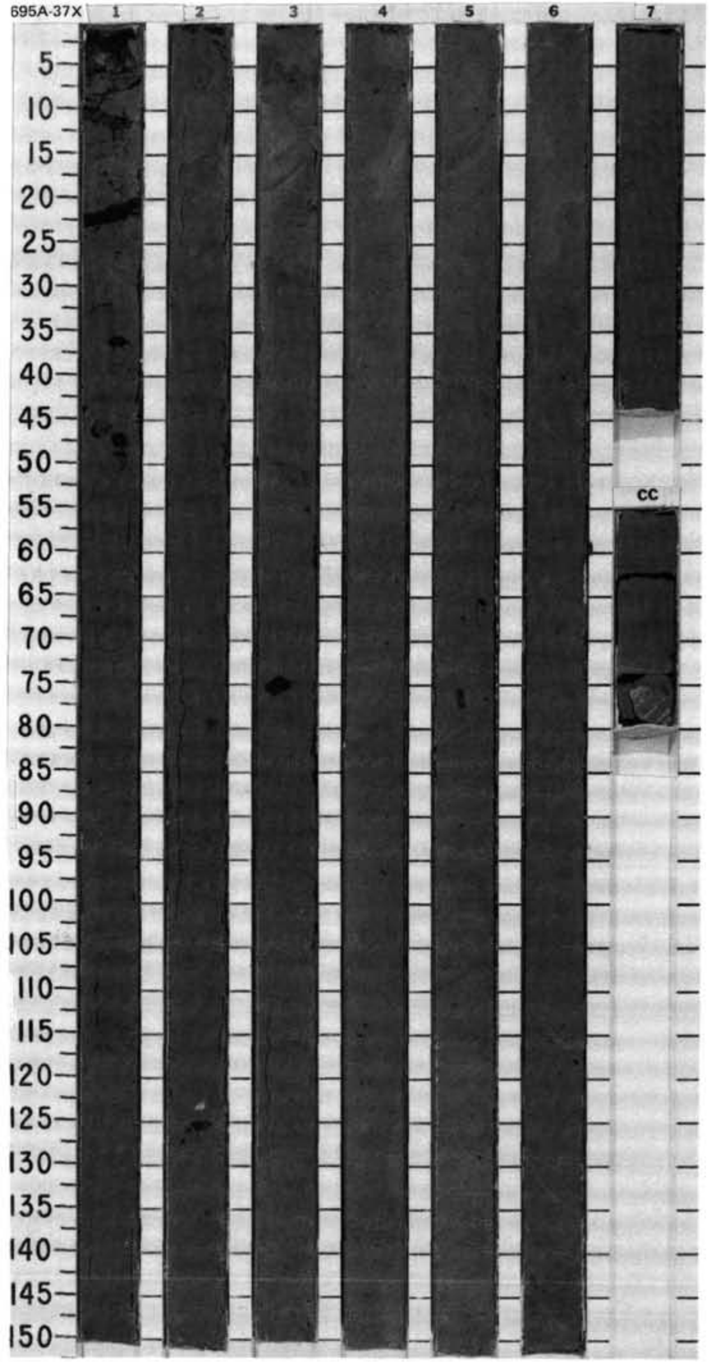

SITE 695 HOLE A CORE 39X CORED INTERVAL 1612.0-1621.7 mbsl; 312.0-321.7 mbsf

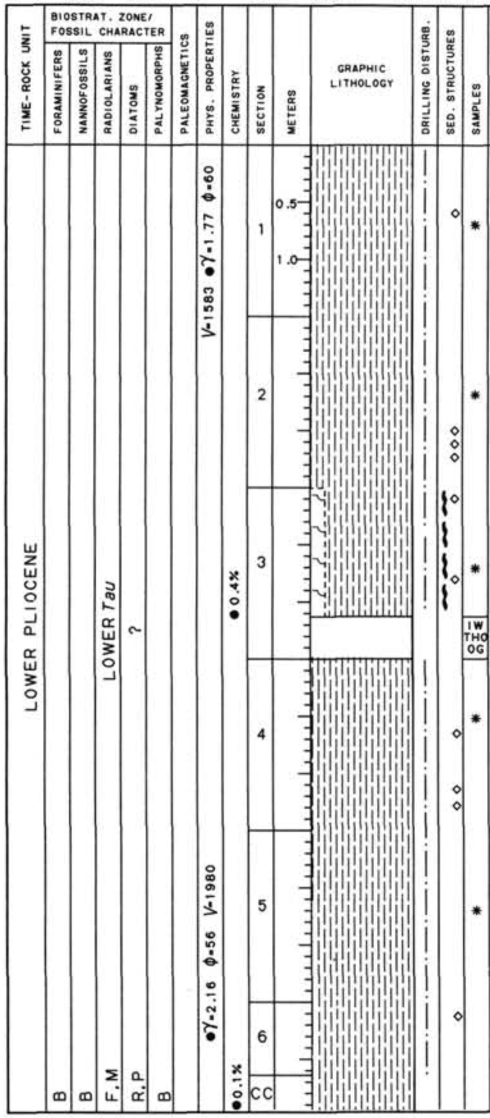

LITHOLOGIC DESCRIPTION

SILTY MUD and DIATOM-BEARING SILTY MUD

Major lithologies: Silty mud, dark greenish gray (5G 4/1, 5BG 4/1). The dark greenish gray appears to be more common where there are higher concentrations of ice-rafted detritus. Diatom-bearing silty mud, dark greenish gray (5G 4/1).

Minor lithology: Altered volcanic ash(?), grayish green (5G 5/2), is less abundant than in the previous core, and occurs as thin layers in Section 4, 6-7, 12-13, 20-21, and 125-126 cm; Section 5, between 90 and 120 cm; Section 6, 36 and 48 cm; and CC, 17-18 cm.

The heaviest concentration of dropstones and sand-sized ice-rafted detritus occurs in Section 2. Dropstones range from rounded to subangular, but rounded ones predominate.

SMEAR SLIDE SUMMARY (%):

	1, 70 D	2, 70 D	3, 70 D	4, 70 D	5, 70 D
TEXTURE:					
Sand	15	16	12	4	3
Silt	50	48	56	54	53
Clay	35	36	32	42	44
COMPOSITION:					
Quartz	37	37	36	34	35
Feldspar	—	Tr	2	4	4
Rock fragments	6	8	12	8	3
Mica	2	6	2	4	—
Clay	35	36	32	42	44
Volcanic glass	3	3	2	Tr	3
Accessory minerals	7	—	—	—	—
Amphibole	Tr	Tr	Tr	Tr	2
Zeolites	2	4	Tr	3	2
Opaque minerals	4	2	2	1	3
Glauconite	—	—	Tr	Tr	—
Diatoms	4	4	12	—	4
Radiolarians	Tr	Tr	—	—	—

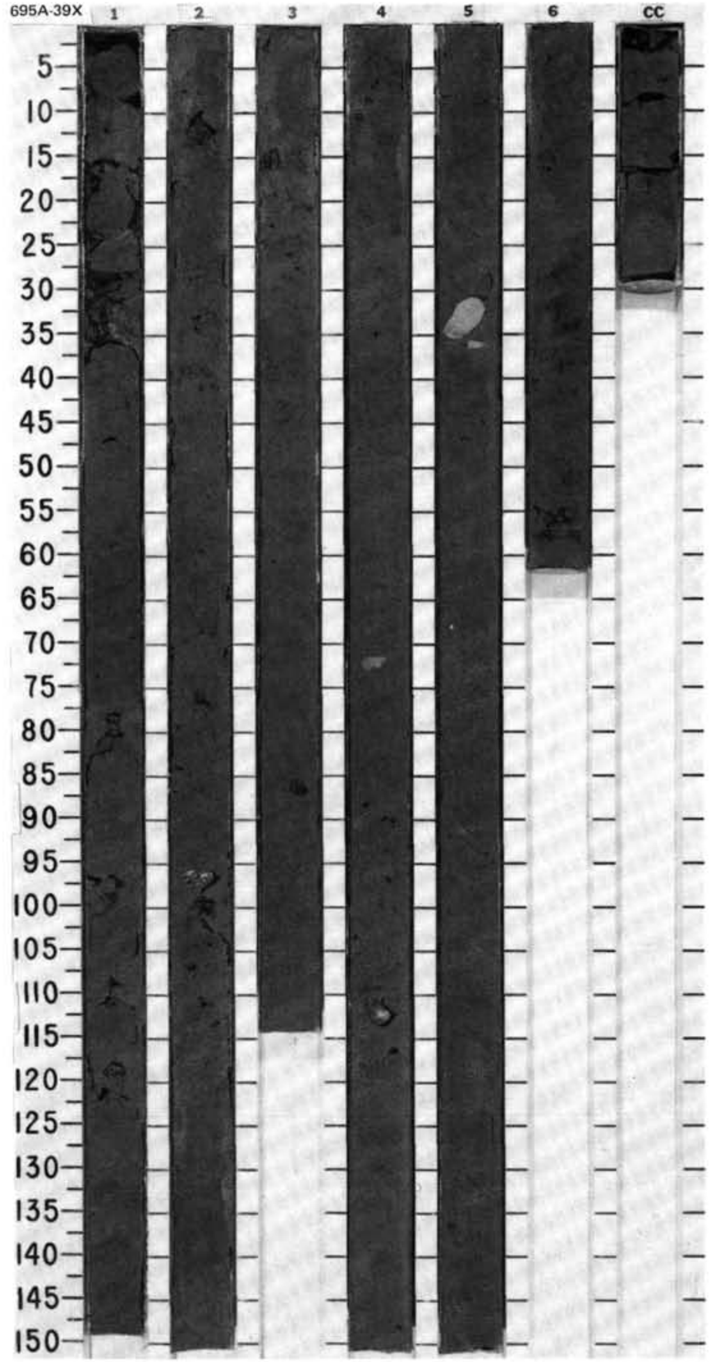

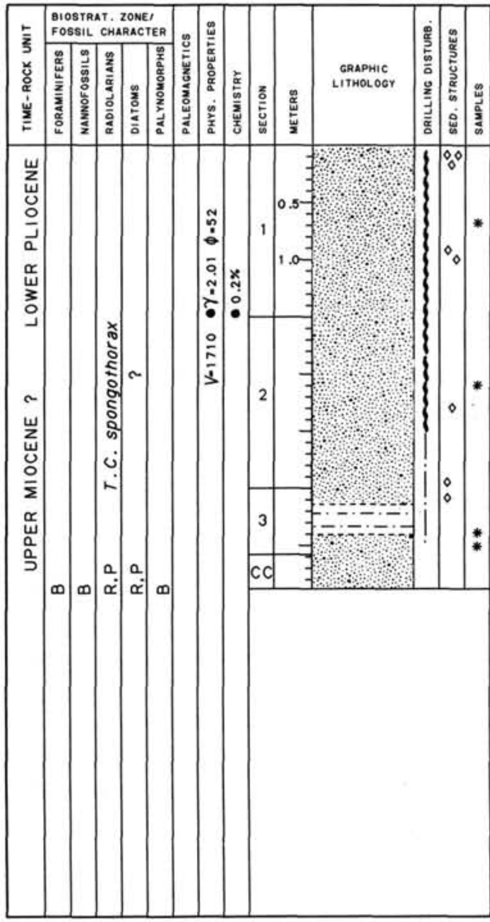

LITHOLOGIC DESCRIPTION

SILTY MUD

Major lithology: Silty mud, dark bluish gray (5B 4/1) in Sections 1-2 and dark gray (N 4/0) in Section 3-CC.

Minor lithologies: Sandy mud, Section 3, 18-42 cm, dark gray (N 4/1), contains many black sand-sized dropstones. Altered volcanic ash(?), grayish green (5G 5/2), thin layers, in Section 2, 3-5 and 85-86 cm; Section 3, 13-14 cm; Section 4, 2-3, 7-9, 34, 35-36, 63-64, 104-105, and 123-124 cm; and Section 5, 49-50 and 74-75 cm. Lithified carbonate(?) in Section 1, 25-32 cm, with small (<1 mm), subrounded, sedimentary clasts.

Sand-sized ice-rafted detritus common throughout. Larger dropstones are rounded, and those at the top of the core are probably in place. Moderate to strong drilling disturbance.

SMEAR SLIDE SUMMARY (%):

	1, 61 D	2, 61 D	3, 38 M	3, 98 D
TEXTURE:				
Sand	3	10	20	2
Silt	64	50	47	48
Clay	33	40	33	50
COMPOSITION:				
Quartz	47	46	44	35
Feldspar	—	3	2	1
Rock fragments	5	5	10	5
Mica	—	—	1	1
Clay	33	40	33	50
Volcanic glass	4	2	2	2
Accessory minerals	4	—	5	3
Zeolites	1	1	1	—
Opaque minerals	1	1	2	2
Glauconite	Tr	—	—	—
Diatoms	—	—	—	1
Sponge spicules	—	—	—	Tr

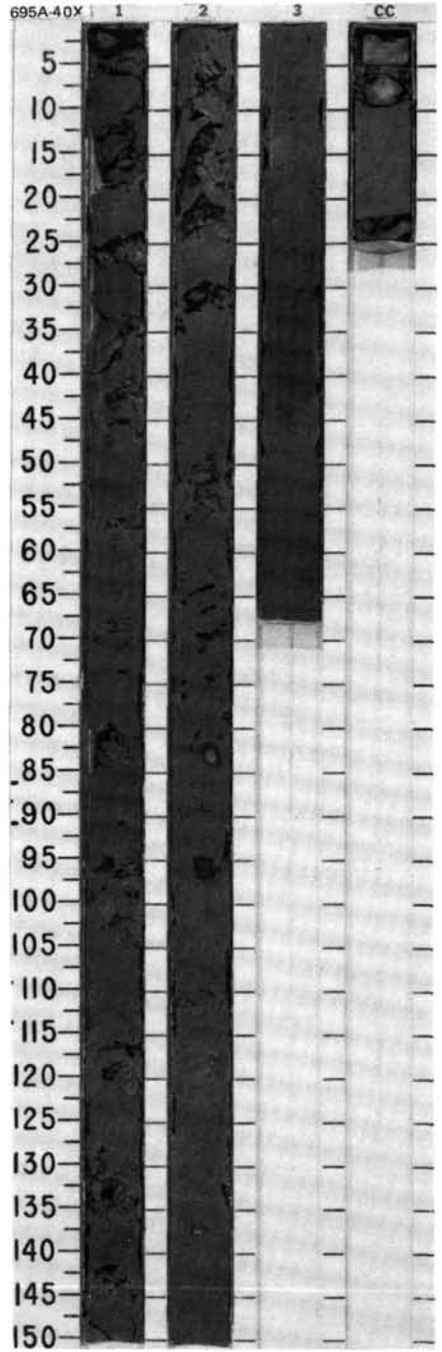

SITE 695 HOLE A CORE 41X CORED INTERVAL 1631.4-1641.1 mbsl; 331.4-341.1 mbsf

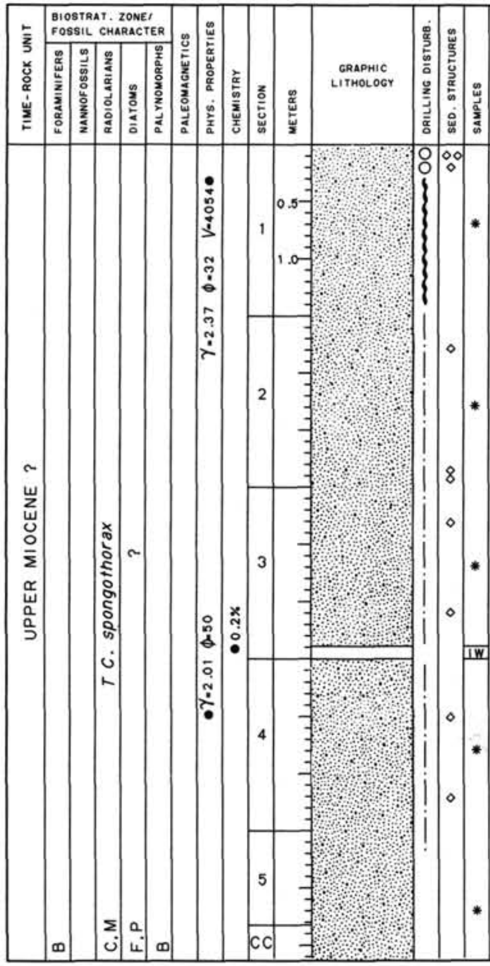

LITHOLOGIC DESCRIPTION

SILTY MUD

Major lithology: Silty mud, dark greenish gray (5BG 4/1) and dark gray (N 4/1), containing abundant ice-rafted detritus, which is more concentrated in darker areas.

Minor lithologies: Altered volcanic ash(?), greenish gray (5G 5/2), thin layers, occur in Section 1, 95-96 cm; Section 2, 5-7, 85-86, and 130-131 cm; Section 3, 16-17 cm; Section 4, 2-3, 8-11, 35, 37, 63-64, 104-105, and 123-124 cm; and Section 5, 48-50 and 75-76 cm. Lithified carbonate in CC, 0-5 cm.

Drilling disturbance ranges from strong at the top of the core to moderate throughout most of the core.

SMEAR SLIDE SUMMARY (%):

	1, 70 D	2, 70 D	3, 70 D	4, 70 D	5, 70 D
TEXTURE:					
Sand	10	5	6	2	2
Silt	50	55	49	58	53
Clay	40	40	45	40	45
COMPOSITION:					
Quartz	42	43	43	40	44
Feldspar	6	4	2	8	3
Rock fragments	5	5	2	6	2
Mica	—	2	2	2	1
Clay	—	40	45	40	45
Volcanic glass	—	3	2	1	1
Accessory minerals	3	3	3	2	2
Opaque minerals	1	1	1	1	Tr
Glauconite	—	Tr	Tr	Tr	Tr
Amphibole	Tr	Tr	—	—	Tr
Diatoms	Tr	Tr	Tr	—	Tr
Sponge spicules	—	—	—	—	1